iScience

CellPress
OPEN ACCESS

Article

Catalytic Asymmetric *trans*-Selective Hydrosilylation of Bisalkynes to Access AIE and CPL-Active Silicon-Stereogenic Benzosiloles

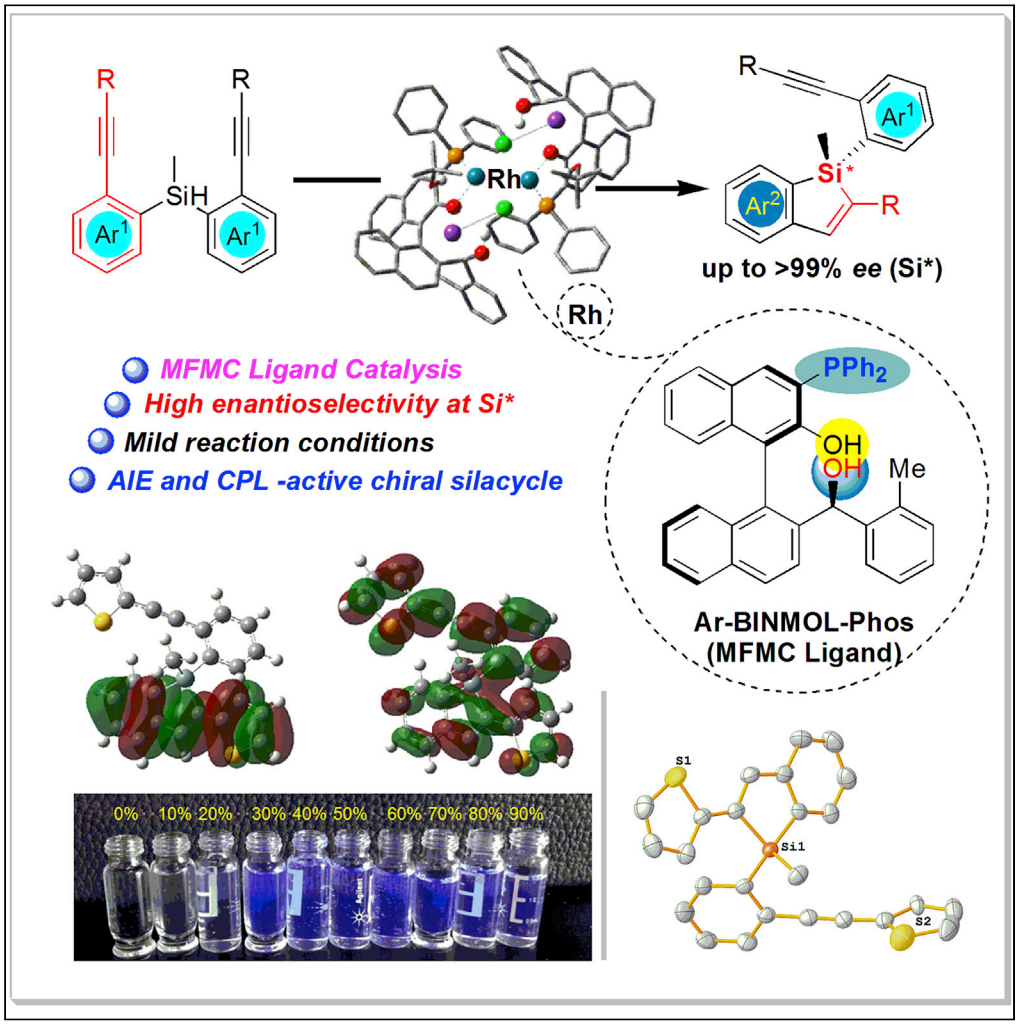

Ren-He Tang, Zheng Xu, Yi-Xue Nie, ..., Guan-Wu Yin, Xue-Min Yang, Li-Wen Xu

liwenxu@hznu.edu.cn

HIGHLIGHTS

Precise and facile construction of silicon-stereogenic center by desymmetrization

Highly enantioselective Rh-catalyzed hydrosilylation controlled by MFMC P,O,O-ligand

Catalytic asymmetric synthesis of AIE- and CPL-active chiral Si-center benzosiloles

The proposed mechanism is supported by NMR and kinetic studies

Tang et al., iScience *23*, 101268
July 24, 2020 © 2020 The Author(s).
https://doi.org/10.1016/j.isci.2020.101268

iScience

CellPress
OPEN ACCESS

Article

Catalytic Asymmetric *trans*-Selective Hydrosilylation of Bisalkynes to Access AIE and CPL-Active Silicon-Stereogenic Benzosiloles

Ren-He Tang,[1,3] Zheng Xu,[1,3] Yi-Xue Nie,[1] Xu-Qiong Xiao,[1] Ke-Fang Yang,[1] Jia-Le Xie,[1] Bin Guo,[1] Guan-Wu Yin,[1] Xue-Min Yang,[1] and Li-Wen Xu[1,2,4,*]

SUMMARY

Chirality widely exists in a diverse array of biologically active molecules and life forms, and the catalytic constructions of chiral molecules have triggered a heightened interest in the fields of chemistry and materials and pharmaceutical sciences. However, the synthesis of silicon-stereogenic organosilicon compounds is generally recognized as a much more difficult task than that of carbon-stereogenic centers because of no abundant organosilicon-based chiral sources in nature. Herein, we reported a highly enantioselective rhodium-catalyzed *trans*-selective hydrosilylation of silicon-tethered bisalkynes to access chiral benzosiloles bearing a silicon-stereogenic center. This protocol featured with chiral Ar-BINMOL-Phos bearing hydrogen-bond donors as a privileged P-ligand for catalytic asymmetric hydrosilylation that is operationally simple and has 100% atom-economy with good functional group tolerability as well as high enantioselectivity (up to >99:1 *er*). Benefiting from the *trans*-selective hydrosilylation with the aid of Rh/Ar-BINMOL-Phos-based asymmetric catalysis, the Si-stereogenic benzosiloles exhibited pronounced aggregation-induced emission (AIE) and circularly polarized luminescence (CPL) activity.

INTRODUCTION

Silacycles are considered as a new kind of σ*-π* conjugated organic material with low-lying lowest unoccupied molecular orbital (LUMO) energy levels (Chen and Cao, 2007; Fu and Cheng, 2012; Zhao et al., 2015; Pop et al., 2019; Dhbaibi et al., 2019), deriving from the interaction between the σ* orbital of two exocyclic silicon-carbon σ-bonds and the π* orbital of the butadiene moiety (Yamaguchi and Tamao, 1996). As one of the most important types of silacycles, siloles exhibit unique electronic structure with low-lying LUMO level with intriguing optical and electronic properties due to high electron affinity and fast electron mobility, enabling them to function as luminescent core and electron transporters in optoelectronic devices (Tamao et al., 1996a, 1996b; Uchida et al., 2001, Son et al., 2009), such as organic light-emitting diodes (Chen et al., 2002; Cai et al., 2017 Nie et al., 2018), fluorescent bioprobes (Wu et al., 2010; Zhuang et al., 2017), chemosensors (Toal et al., 2005; Li et al., 2009; Dedeoglu et al., 2014), and circular polarized luminescence (CPL) (Liu et al., 2012; Ng et al., 2014a and 2014b; Li et al., 2016). Therefore, the development of practical methods for the synthesis of silole scaffolds is highly important in both synthetic and materials chemistry, which has attracted increasing attention (Ohmura et al., 2008; Matsuda et al., 2007; Ureshino et al., 2010; Liang et al., 2011; Shimizu et al., 2008; Zhao et al., 2012; Liang et al., 2012; Zhang et al., 2014 and 2015; Ilies et al., 2008; Tobisu et al., 2009; Onoe et al., 2012; Minami et al., 2017; Gimferrer et al., 2018; Yang et al., 2018). Especially, the construction of a stereogenic Si-center of siloles in a catalytic enantioselective manner is an appealing yet challenging task, although there have been some efforts for the catalytic synthesis of chiral Si-centers (Oestreich, 2007; Weickgenannt et al., 2010; Xu et al., 2011; Xu, 2012; Shintani, 2015; Tamao et al., 1996a, 1996b; Igawa et al., 2012; Naganawa et al., 2015; Zhan et al., 2018; Wen et al., 2018; Guo et al., 2019). In this regard, the catalytic enantioselective synthesis of silicon-stereogenic heterocycles have been achieved via Pd-catalyzed C-H arylation (Shintani et al., 2012) or amination (Sato et al., 2017) of prochiral 2-(arylsilyl)aryl triflates or Rh-catalyzed aromatic C-H silylation (Scheme 1A) (Kuninobu et al., 2013; Zhang et al., 2016, 2017). Moreover, the rhodium-catalyzed [2 + 2 + 2] cycloaddition of silicon-containing prochiral triynes with internal alkynes was also a facile approach to the construction of

[1]Key Laboratory of Organosilicon Chemistry and Material Technology of Ministry of Education, and Key Laboratory of Organosilicon Material Technology of Zhejiang Province, Hangzhou Normal University, Hangzhou 311121, P. R. China

[2]State Key Laboratory for Oxo Synthesis and Selective Oxidation, Suzhou Research Institute (SRI), Lanzhou Institute of Chemical Physics (LICP), University of the Chinese Academy of Sciences (UCAS), Lanzhou 730000, P. R. China

[3]These authors contributed equally

[4]Lead Contact

*Correspondence: liwenxu@hznu.edu.cn

https://doi.org/10.1016/j.isci.2020.101268

This is an open access article under the CC BY license (http://creativecommons.org/licenses/by/4.0/).

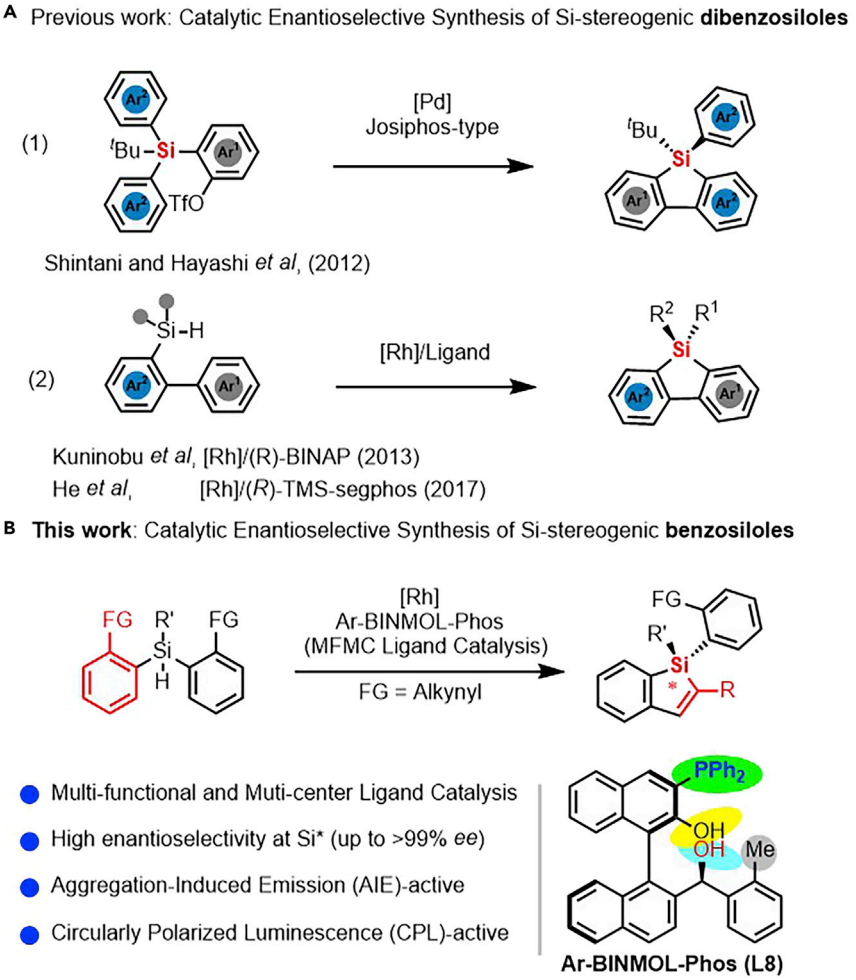

Scheme 1. Catalytic Enantioselective Synthesis of Silicon-Stereogenic Silole Analogues

(A) Previous reports on the catalytic asymmetric synthesis of silicon-stereogenic dibenzosiloles via C-H activation or silylations.

(B) Our strategy with MFMC ligand catalysis via Ar-BINMOL-Phos-controlled Rh-catalyzed intramolecular hydrosilylation to access silicon-stereogenic benzosiloles. MFMC is multi-functional and multi-center.

silicon-stereogenic DBS (Shintani et al., 2015). All these methods mentioned above provided complementary processes to the preparation of enantio-enriched chiral DBS bearing a silicon-stereogenic center. However, the construction of Si-chirality on unsymmetrical benzosiloles (BS) via catalytic hydrosilylation is still unknown to date.

Very recently, we reported the catalytic asymmetric synthesis of sila-bicyclo[4.1.0]heptanes via palladium-catalyzed [4 + 2] annulation of cyclopropenes with benzosilacyclobutanes (Wang et al., 2020), in which a variety of chiral bicyclic sila-heterocycle derivatives could be achieved with good enantioselectivity (up to 95.5:4.5 *er*). However, the construction of corresponding silacycles bearing a Si-stereogenic center is not successful in this reaction. Considering the powerful potential of rhodium catalysts for hydrosilylation of alkynes that can provide *E*- and *Z*-isomers depending on the precise nature of catalyst systems, substrates, and reaction conditions (Takeuchi and Tanouchi, 1993, 1994; Faller and D'Alliessi, 2002; Sato et al., 2004; Mori et al., 2004; Huckaba et al., 2013; Mancano et al., 2014; Diachenko et al., 2015), we envisioned that the Rh-catalyzed intramolecular and *trans*-type hydrosilylation might open the door to the enantioselective Si-C bond-forming construction of silicon-stereogenic benzosiloles. Although the desymmetrizative hydrosilylation of alkenes has been achieved to construct silicon-stereogenic center (Naganawa et al., 2015), this reaction suffered limited substrate scope and imperfect enantioselectivity.

CellPress
OPEN ACCESS

Comparably, the intramolecular hydrosilylation of Si-tethered bisalkynes is much challenging. This lack of available *trans*-selective methods with high enantioselectivity is presumably due to the difficulty in the chirality induction during desymmetrization of dihydrosilanes ($R^1R^2SiH_2$) or silicon-tethered bulky bisalkynes in catalytic asymmetric hydrosilylation. Herein, we reported such a *trans*-selective intramolecular hydrosilylation reaction with our strategy with Rh/Ar-BINMOL-Phos-based MFMC ligand catalysis (MFMC is multi-functional and multi-center) that can generate silicon-stereogenic siloles with good enantioselectivity (Scheme 1B). This P,O,O-ligand (Ar-BINMOL-Phos) -controlled approach affords a range of alkyne-substituted silicon-stereogenic siloles as potentially useful fluorescent probes from easily available alkynes and hydrosilanes. In addition, it should be noted that the extra alkynyl group on benzosiloles offered a potential functionalization with group transformations.

RESULTS

To construct the silicon-stereogenic BS via catalytic asymmetric hydrosilylation, we are confident that the Rh-catalyzed intramolecular and *trans*-type hydrosilylation would provide a robust and practical method to the synthesis of this type of alkynyl benzosiloles. Then we began our studies by examining the model hydrosilylation of Si-tethered bisalkyne **1a** using Rh catalysts. At 80°C in toluene, various phosphine ligands were evaluated in the $[Rh(cod)Cl]_2$-catalyzed intramolecular hydrosilylation (see Figure 1 and Table S1). Gratifyingly, most of our MFMC Ar-BINMOL-Phos (Song et al., 2014) gave silicon-stereogenic benzosilole **2a** in promising conversion (up to >99%) with moderate enantioselectivity (80:20 to 91:9 *er* in most cases) in the absence of any additives, demonstrating the good feasibility of this Rh-catalyzed hydrosilylation reaction with the aid of chiral P,O,O-ligand; especially, our Tao-Phos (**L3**) and methyl-substituted Ar-BINMOL-Phos (**L8**) (Song et al., 2015) gave the desired product **2a** with 89.5:10.5 *er* and 91:9 *er*, respectively. Notably, other phosphine ligands evaluated in this work, such as BINAP and Segphos, exhibited relatively low enantioselectivity (70:30 er as the best). Then with Tao-Phos in hand, we continued to optimize the reactions by changing rhodium precursors, additives, solvents, and temperature (for representative experimental data, see Tables S2–S4). And finally, the optimized reaction conditions were determined as follows (see Table 1, entry 1): $[Rh(cod)Cl]_2$ (5 mol%), Ar-BINMOL-Phos (*o*-Me) (12 mol%, simplified as **L8** in Supplemental Information), KO*t*Bu (5 mol%), at 70°C. The corresponding product **2a** could be obtained in 95.5:4.5 *er*, albeit the decrease of isolated yield because of low and almost same polarity in comparison with that of starting material **1a**. As shown in Table 1, representative reaction results were also important to understand the challenging Rh-catalyzed intramolecular hydrosilylation. The effect of temperature (70°C or 80°C) on enantioselectivity is not obvious as imagined (entry 2). Under the optimized reaction conditions, other rhodium sources did not give better results in term of conversion and enantioselectivity (entry 3). To support the importance of three functional groups (P atom, chiral secondary alcohol, and phenol moiety) on the MFMC P,O,O-ligand (Ar-BINMOL-Phos), we investigated the effect of four representative ligands (**CL1**-**CL4**) on the conversion and enantioselectivity (entries 5–9). In sharp contrast, these P-ligands without additional chirality at the carbon of secondary alcohol (**CL1** and **CL4**) gave inferior enantioselectivity (88:12 *er* for **CL1** and 67:33 *er* for **CL4**, respectively, entries 6, 9). And more importantly, ligands **CL2** and **CL4** without secondary alcohol or phenol were not effective in the Rh-catalyzed hydrosilylation because of only moderate conversion (entries 7 and 9). Replacing two OHs (both secondary alcohol and phenol) with MOM and OBn, respectively, deactivated the catalyst (entry 8), probably because of strong hydrogen-bonding interaction between Rh/ligand and substrate. It is easy to understand that Ar-BINMOL without phosphine center is not suitable ligand, which supports the importance of P-atom in the coordination with Rh catalyst. In addition, KO*t*Bu was proved to be an effective additive to promote the intramolecular hydrosilylation. As shown in Table 1 (entries 10–16), the use of other additives, including similar inorganic bases, resulted in inferior results in terms of conversion and enantioselectivity. In fact, we have also investigated the effect of the amount of KO*t*Bu on the Rh-catalyzed intramolecular hydrosilylation of **1a** (Table S5). The experimental results showed that the hydrogen-bonding activation from free chiral secondary alcohol is beneficial to the activation of Rh catalyst because large amount of KO*t*Bu could inhibit the hydrosilylation. To our delight, when cobalt and palladium catalysts instead of rhodium catalyst were used in this reaction under the same conditions, only a trace amount of product **2a** was detected, and poor enantioselectivity was observed in these experiments (entries 17–19).

With the optimized reaction conditions in hand, the substrate scope was next explored with respect to the variation of the silicon-tethered bisalkynes (Scheme 2). Si-linked bisalkynes with varied substitution patterns (Me, OMe, F, *i*-Pr, or *t*-Bu, etc.) could be smoothly converted to their corresponding hydrosilylation products in moderate to good yields (up to 87%) with high enantioselectivities (up to >99:1 *er*). Notably, this

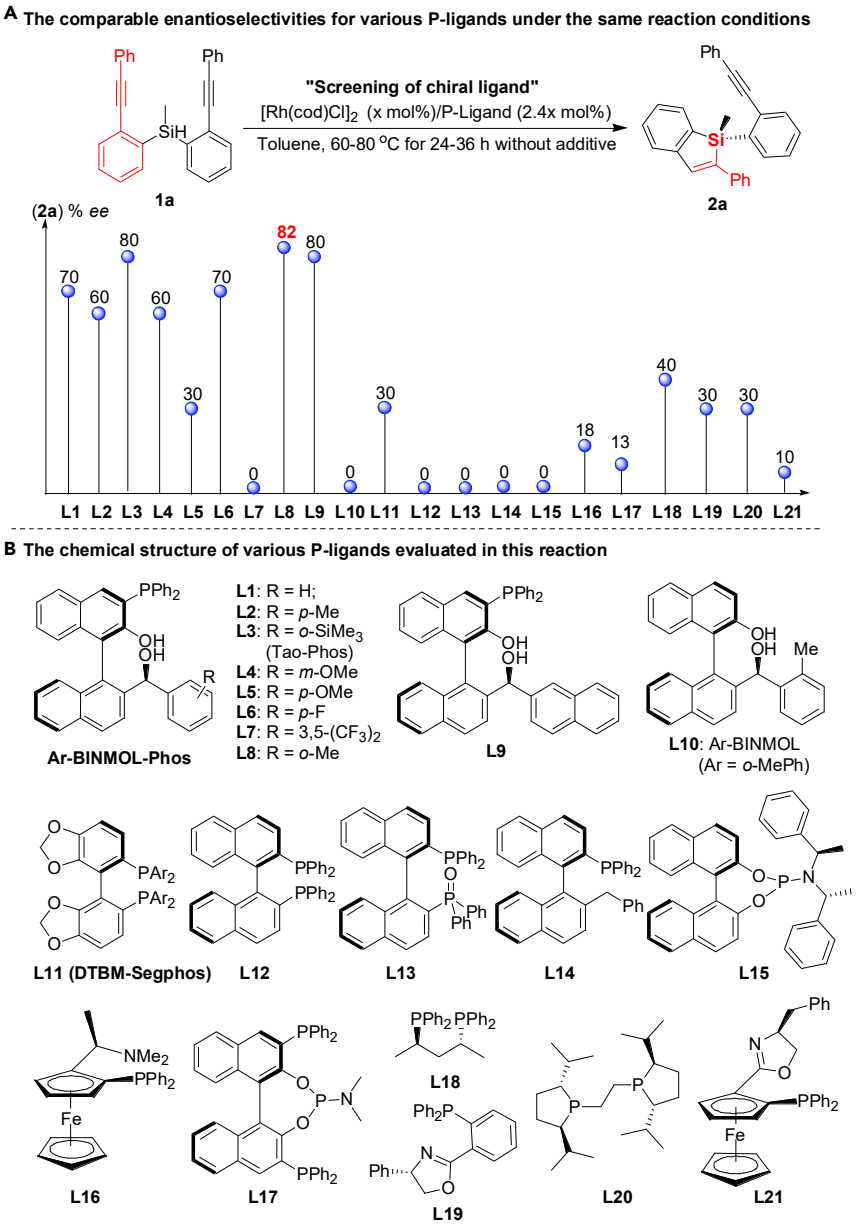

Figure 1. Representative Results on Enantioselectivity for Chiral Ligand-Controlled [Rh(cod)Cl]$_2$-Catalyzed Intramolecular Hydrosilylation

(A) The comparable enantioselectivities for various P-ligands (**L1-L21**) under the same reaction conditions (without any additive and no optimization of reaction conditions).

(B) The chemical structure of various P-ligands (**L1-L21**) evaluated in this reaction.

potassium-assisted Rh-catalyzed hydrosilylation reaction worked well with various types of substrates with electron-neutral, electron-withdrawing or electron-donating groups, having little influence on the Si-centered stereochemistry. When small ring or S-containing heterocycle-substituted bisalkynes were employed, the reaction also worked well under Rh/Ar-BINMOL-Phos catalyst system. For example, the hydrosilylation of **1r** proved to be highly enantioselective (93.5:6.5 *er*) with good yield (75%), and the cyclopropanyl group linked with the terminal position of alkyne on substrate **1q** or **1t** resulted in the corresponding alkynyl benzosilole **2q** or **2t** in good yield with high er value, respectively. In addition, the *ortho*-substituted group did not block the intramolecular hydrosilylation, as evidenced by the reaction of **1n** to

CellPress
OPEN ACCESS

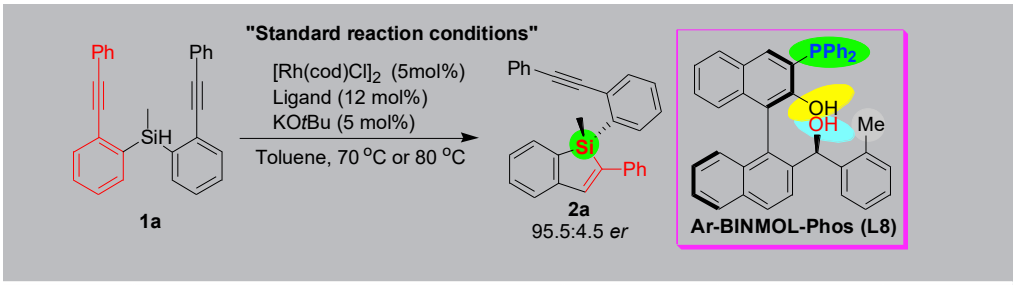

Entry	Variation from Standard Conditions[a]	T (°C/h)	2a/1a[b]	er[c]
1	None	70/72	>99:1 (50)	95.5:4.5
2	None	80/34	>99:1	94.5:5.5
3	$[Rh(cod)_2]BF_4$ instead of $[Rh(cod)Cl]_2$	80/34	n.r	–
4	$[Rh(OAc)_2]_2$ instead of $[Rh(cod)Cl]_2$	80/34	n.r	–
5	**Tao-Phos** instead of **L8**	80/22	80:20	92.5:7.5
6	**CL-1** instead of **L8**	70/72	>99:1	88:12
7	**CL-2** instead of **L8**	70/72	54:46	60:40
8	**CL-3** instead of **L8**	70/72	n.r	–
9	**CL-4** instead of **L8**	70/72	34:66	67:33
10	$NaHBEt_3$ instead of KO*t*Bu	80/34	98:2	92.5:7.5
11	NaO*t*Bu instead of KO*t*Bu	80/34	>99:1	90:10
12	$NaSbF_6$ instead of KO*t*Bu	80/34	n.r	–
13	CuI instead of KO*t*Bu	80/34	46:54	90:10
14	Ag_3PO_4 instead of KO*t*Bu	80/34	90:10	92.5:7.5
15	K_2CO_3 instead of KO*t*Bu	80/34	58:42	90.5:9.5
16	NaOEt instead of KO*t*Bu	80/34	98:2	53.5:46.5
17	OIP Co instead of [Rh][d]	80/14	10:90	50:50
18	$Pd_2(dba)_3$	80/14	10:90	62.5:37.5
19	$(\eta_3\text{-}C_3H_5)_2Pd_2Cl_2$	80/14	n.r	–

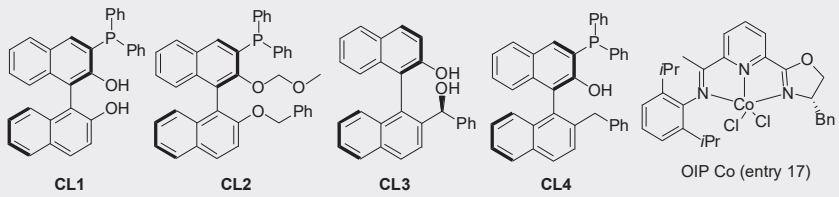

Table 1. Optimization of Reaction Conditions for Rh-catalyzed Desymmetric Hydrosilylation of Bisalkyne 1a

[a]Unless otherwise noted, the standard reaction conditions were as follows: **1a** (0.2 mmol), and solvent (2.0 mL). The structure of Tao-Phos with *o*-trimethylsilyl group is different from that of *o*-methyl substituent on phenyl ring (**L8**), the conversion is >99% for a family of Ar-BINMOL-Phos.

[b]It was difficult to isolate the product **2a** from the reaction mixture if the reaction was not completed because of the same polarity of **2a** and the starting material **1a**. The ratio of **2a/1a** was determined by HPLC. n.r = no reaction.

[c]The er value of **3a** was determined by chiral HPLC analysis.

[d]The catalyst OIP Co complex was used instead of $[Rh(cod)Cl]_2$/Ar-BINMOL-Phos catalyst system.

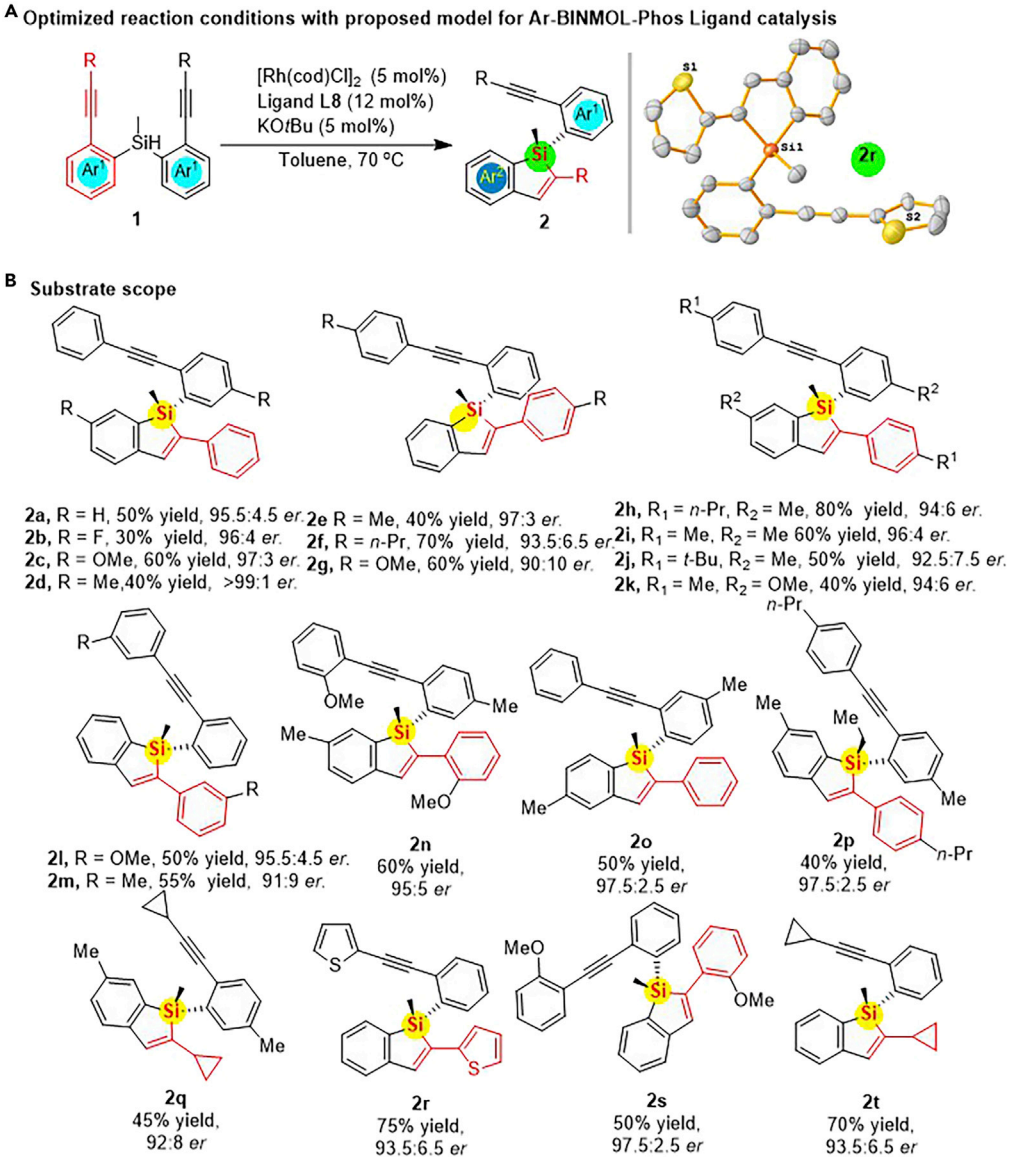

Scheme 2. Scope of MFMC Ar-BINMOL-Phos (L8)-controlled Rh-catalyzed Intramolecular Hydrosilylation of Si-Tethered Bisalkynes

(A) The optimized reaction conditions for the Ar-BINMOL-Phos-based MFMC ligand catalysis based on the experimental results.

(B) Substrate scope for the *trans*-selective hydrosilylation driven by the MFMC Ar-BINMOL-Phos ligand-controlled desymmetrization of bisalkynes.

2n with 60% yield and 95:5 *er*. The same level of experimental result was also provided by the intramolecular hydrosilylation reaction of Si-linked bisalkyne **1s**, giving the corresponding **2s** with 50% yield and 97.5:2.5 *er*. When the methyl group on silicon atom was replaced by ethyl group, the reaction was also proven to be enantioselective and gave the desired benzosilole **2p** in 97.5:2.5 *er*, albeit with some yield loss in comparison with that of methyl-substituted **2h** (80% yield, 94:6 *er*). Unfortunately, it was found that another bulky group on silicon center, such as *t*-Bu and phenyl, was not suitable for the construction of their corresponding benzosiloles because of the steric hindrance. Notably, the configuration of the silicon-stereogenic alkynyl benzosiloles (**2r**) was confirmed by X-ray diffraction pattern (Figure S1). Notably, these compounds were very stable for a long period of time (0.5 year), and its ee value was not changed after reflux in toluene for several days.

CellPress
OPEN ACCESS

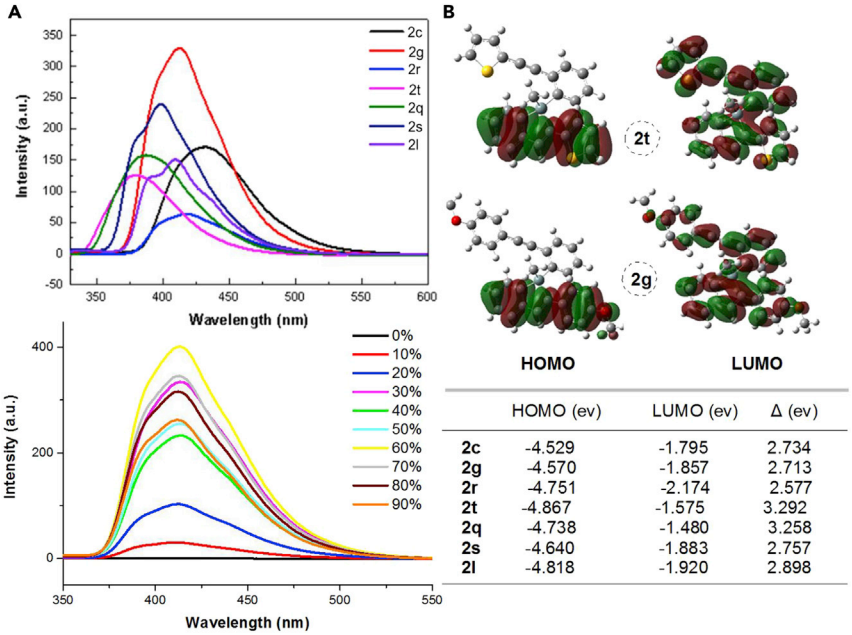

	HOMO (ev)	LUMO (ev)	Δ (ev)
2c	-4.529	-1.795	2.734
2g	-4.570	-1.857	2.713
2r	-4.751	-2.174	2.577
2t	-4.867	-1.575	3.292
2q	-4.738	-1.480	3.258
2s	-4.640	-1.883	2.757
2l	-4.818	-1.920	2.898

Figure 2. The Fluorescence Property of Silicon-Stereogenic Benzosiloles

(A) Left: Fluorescence spectra (top) of seven representative and enantioenriched benzosiloles and AIE phenomenon of benzosilole **2g**, the fluorescence emission spectra of 2g (5 μM) was achieved in THF/water mixtures (fw = 0% to 90%). λ_{ex} = 300 nm, λ_{es} = 550 nm.

(B) Right: Molecular orbital diagrams of HOMO and LUMO of **2t** and **2g**, and the energy levels of HOMO and LUMO with their difference (ΔE) of representative benzosiloles shown in this table.

Then, the further investigation of such alkynyl benzosiloles as optical material was highly attractive. The fluorescence property of benzosiloles (BS) was subsequently evaluated using **2c, 2g, 2r, 2t, 2q, 2s, and 2l** as candidates. As shown in Figure 2, the BS emission was enhanced by the introduction of electron-donating group (-OMe) on the aromatic ring, and *p*-OMe substituted BS **2g** exhibited a very distinctive behavior. The highest occupied molecular orbital (HOMO)-LUMO data might be useful information to distinguish the structural difference. Thus, we then checked the aggregation-induced emission (AIE) property of **2g** according to the standard method (Zhou et al., 2019). As expected, the benzosilole **2g** showed a blue fluorescence color when the water fraction was above 30% in the THF-water mixture (Figure S7 of Supporting Information). Notably, the relationship of AIE and chirality was also evaluated and it was found that there is no obvious effect for the fluorescence intense.

The phenomenon of circularly polarized luminescence (CPL) has attracted considerable attention owing to its wide applications in various research fields (Gao et al., 2019). Therefore, the circular dichroism (CD) and CPL analyses were next performed at 300 nm to evaluate the Si-centered chirality. To our delight, in the test of benzosilole **2g**, intensive CPL signs were observed in this case (Figure S8). We anticipated that CPL effect of benzosilole augments its great potential of enantioselective Rh-catalyzed intramolecular hydrosilylation of bisalkynes in the development of a CPL-active material linked with silole backbone.

DISCUSSION

In metal-catalyzed hydrosilylation (Zaranek and Pawluc, 2018; Wen et al., 2019), including the Rh catalysts (Sakaki et al., 2002; Wu et al., 2013 and 2014; Doyle et al., 1991; Sanada et al., 2006; Morales-Ceron et al., 2017) employed for alkyne hydrosilylation, cationic metal complexes usually give predominately (*E*)-isomer depending on the precise nature of substrates and reaction conditions (Ojima et al., 1990; Trost and Ball, 2005; Ding et al., 2013). In this work, we believed the Rh-catalyzed alkyne *trans*-hydrosilylation reactions are similar to that of previous reports (Ojima et al., 1990; Matsuda and Ichioka, 2012; Crabtree, 2003) on the isomerization of the M-vinyl complex intermediate to the less sterically congested isomer via an η^2-vinyl metal species. In addition, to understand what makes Rh/Ar-BINMOL-Phos (**L8**) a successful catalyst in

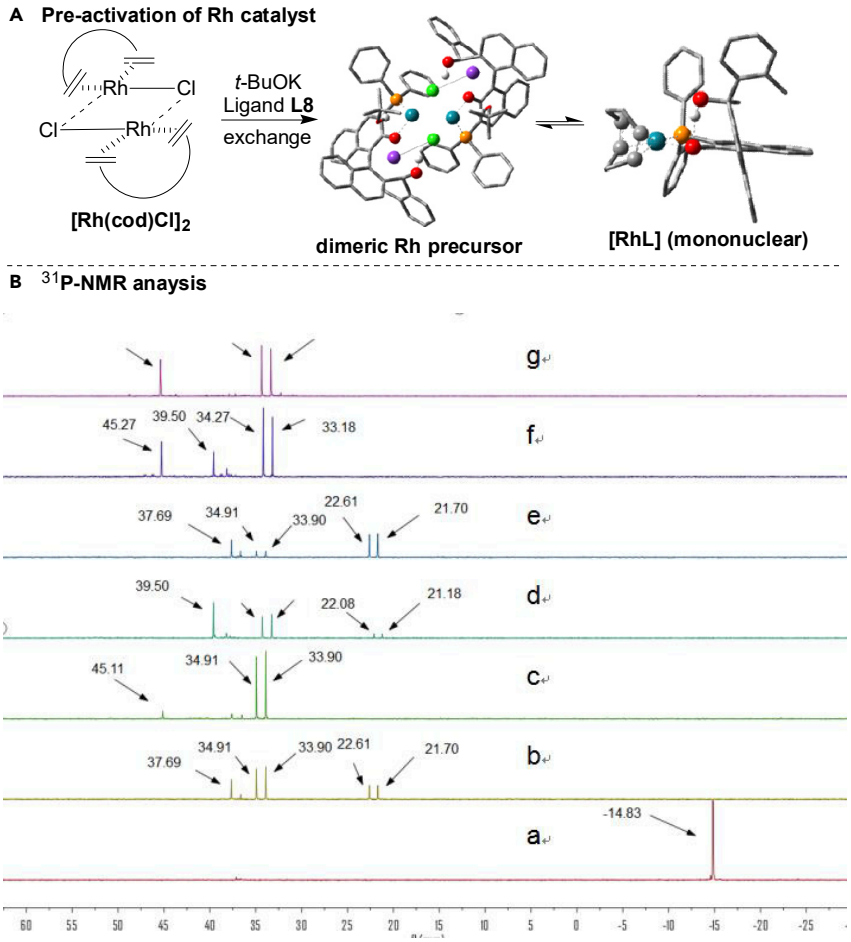

Figure 3. The Structural Analysis of the Active Rh Species by ^{31}P NMR

(A) The illustrative view of the *in situ* formed dimeric Rh complex and mononuclear Rh complex from $[Rh(cod)Cl]_2$ and Ar-BINMOL-Phos L8 in $CDCl_3$.

(B) Comparison of ^{31}P NMR of ligand and Rh complex. (a) only **L8**, a single peak at −14.83 ppm; (b) mixture of $[Rh(cod)Cl]_2$ and **L8** (5 min), two double peaks for the Rh/Ar-BINMOL-Phos complex appeared at 22.16 ppm with $^1J_{P\text{-}Rh}$ = 183 Hz and 34.40 ppm with $^1J_{P\text{-}Rh}$ = 204 Hz, and another single peak appeared at 37.69 ppm, respectively; (c) mixture of **L8** and $[Rh(cod)Cl]_2$ (20 min), the double peak at 22.16 ppm disappeared, and another single peak appeared at 45.11 ppm; (d) mixture of substrate **1a**, **L8** and $[Rh(cod)Cl]_2$ (20 min), a new and single peak appeared at 39.50 ppm; (e) mixture of **L8**, KO*t*Bu, and $[Rh(cod)Cl]_2$ (5 min); (f) mixture of **L8**, KO*t*Bu, and $[Rh(cod)Cl]_2$ (20 min); (g) mixture of **L8**, KO*t*Bu, $[Rh(cod)Cl]_2$, and substrate **1a** (20 min), a double peak appeared at 33.72 ppm with $^1J_{P\text{-}Rh}$ = 220 Hz and a single peak with 45.27 ppm.

the desymmetrization of Si-linked bisalkynes via hydrosilylation, its structure was examined by ^{31}P-NMR and ESI-MS (see Figure 3, and for ^{31}P-NMR analysis, see Figure 3B, and others see Figures S3–S5). And these experimental results indicate that the various types of Rh/**L8** complexes might be *in situ* formed in this reaction, and a dimeric Rh catalyst comprising a dirhodium core is a possible and active species in the pre-activation process (Meiβner et al., 2015a, 2015b; Mannu et al., 2018), which generated through dissociation of cod (1,5-cyclooctadiene) with two coordinating phosphorous centers from Ar-BINMOL-Phos ligands. It is generally accepted that treatment of $[Rh(cod)Cl]_2$ with diphosphine ligands smoothly affords neutral μ_2-bridged dimeric/dinuclear rhodium complexes (Meiβner et al., 2015a, 2015b); thus, accordingly, the μ_2-bridged dimeric Rh complex is formed probably in the reaction mixtures (the double peaks appeared probably at 33–34 ppm with $^1J_{P\text{-}Rh}$ = 204 or 220 Hz in Figure 3B). However, it is difficult to confirm the true structure of dimeric Rh/**L8** complex that formed in the pre-activation stage by NMR analysis. Furthermore, the *in situ* analysis of reaction mixtures with ESI-MS and NLE (Satyanarayana et al., 2009) and kinetic study (Figure 4) showed the mononuclear complex with single Rh(I) catalytic center with one ligand acted probably as majorly active species during the full reaction process. In addition, the stable

CellPress
OPEN ACCESS

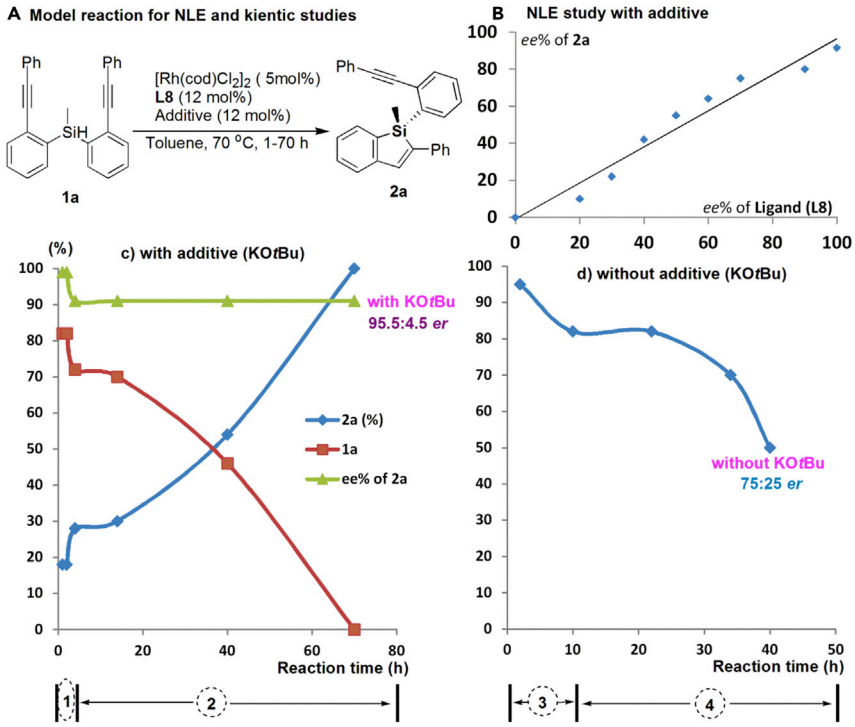

Figure 4. Experimental Results for Relationship of ee_{prod}/ee_{ligand} and the Reaction Rate and Enantioselectivity Data with or without KO*t*Bu

(A) The model reaction with intramolecular hydrosilylation of 1a under the optimized reaction conditions.

(B) The NLE result revealed that a mononuclear complex structure with single Rh(I) catalytic center with one ligand acted probably as the true active species.

(C) KO*t*Bu-activated Rh catalysis. There are two stages (before and after 5 h, respectively) for catalytic cycles in the Rh-catalyzed hydrosilylation that detected by *ee* values and reaction rate under the optimized reaction conditions.

(D) Without KO*t*Bu as additive. When no use of KO*t*Bu for this reaction, the corresponding ee value gradually decreases with reaction time.

P/O-coordination of Ar-BINMOL-Phos with $[Rh(cod)Cl]_2$ to give mononuclear Rh complex is supported by ^{31}P-NMR spectra data in which the related ^{31}P signal of such stable mononuclear Rh complex was observed at 41 ppm (Rani et al., 2008).

It should be noted that the potassium *tert*-butoxide (KO*t*Bu) played an important role in the *in situ* formation of the active Rh species to promote the catalytic asymmetric hydrosilylation. As shown in Figure 4, the absence of KO*t*Bu led to decreased enantioselectivity (only 75:25 er), in which the negative result revealed reaction between KO*t*Bu and chiral ligand **L8** could form a more stable mononuclear rhodium catalyst that is responsible for the high level of enantioselective induction shown in Figure 4C. When the reaction was performed without KO*t*Bu, enantioselectivity (ee value of **2a**) of the same intramolecular hydrosilylation was gradually decreased with time because of irreversible reactions of the active dimeric Rh catalyst with substrate in the catalytic cycle. And notably, excess amount of KO*t*Bu (>24 mol%) decreased the enantioselectivity and much more amount of KO*t*Bu (>36 mol%) inhibited the catalytic activities of all the Rh species reaction to result in almost no reaction. These results provided an indirect evidence for the importance of the chiral secondary alcohol of Ar-BINMOL-Phos (**L8**) in the enhancement of enantioselectivity and catalytic activity of Rh complex.

Therefore, based on the experimental results and related NMR and ESI-MS analysis, we proposed a reaction mechanism for the asymmetric Rh-catalyzed hydrosilylation (Figure 5). It is expected that the dirhodium core in the chlorine-bridged dimeric rhodium precursor is easily broken by a proton abstraction reaction with ligand **L8**, releasing HCl with the aid of KO*t*Bu and generating mononuclear precursor complex **M0**. The cod ligand in the four-coordinated neutral Rh(I) complex will further be replaced by the substrate and leads to an Rh intermediate, in which the alkenyl group and Si-H group of substrate is

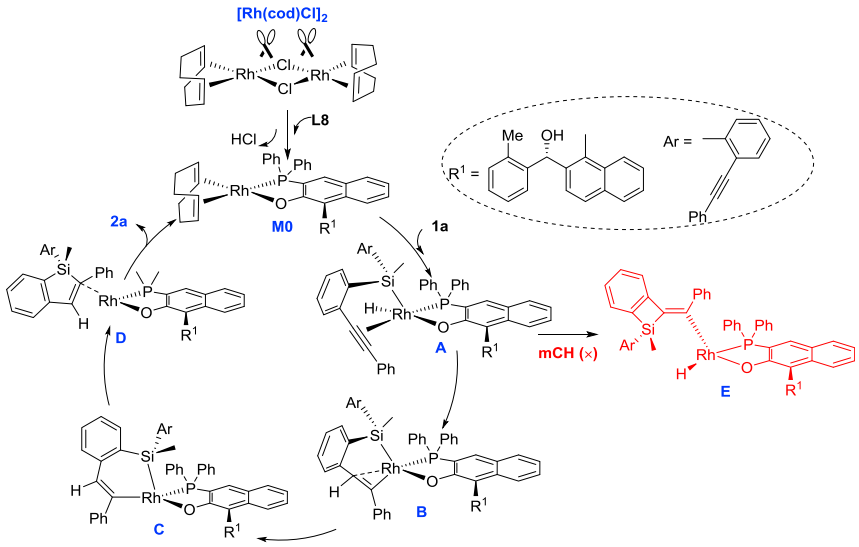

Figure 5. A Proposed Catalytic Cycle for Rh(I)/L8 Complex-Catalyzed Intramolecular Hydrosilylation with Monoalkyne as a Model Substrate

coordinated to the Rh center in η^2 and η^1 manner. Then the Rh intermediate underwent Si-H oxidative addition to form a five-coordinated Rh(III) intermediate **A**. The pre-coordinated alkynyl group is exactly the one to proceed migratory insertion, followed by the Si-H oxidative addition. That is, the two symmetric alkynyl groups in **1a** have already been discriminated during the formation of this precursor complex **B**, in which the reactive alkynyl group and Si-H group linked to the Rh center in enantioselective manner. And then the subsequent process is only related to the Z/E-selectivity but not the enantioselectivity. Similarly to previous Ru catalysis for the trans-selective hydrosilylation of alkynes (Ding et al., 2013), **B** can be further isomerized to the more stable **C** (metallacyclohexene intermediate). At this time, the H atom is completely inverted to the *trans* position, and the alkenyl group is at the *trans* position of the O-ligand. For the origin of stereoselective induction of such rhodium catalyst, more theoretic studies would be continuously undergoing in our laboratory to gain much more accurate understanding of the hydrosilylation reaction mechanism.

Conclusion

In summary, we accomplished a highly enantioselective Rh-catalyzed intramolecular and *trans*-type hydrosilylation of silicon-tethered bisalkynes, which provided a practical approach to the construction of AIE and CPL-active benzosiloles bearing silicon-stereogenic center. For this purpose, our chiral Ar-BINMOL-Phos bearing hydrogen-bond donors could be efficiently used as a privileged MFMC P,O,O-ligand in the desymmetrization process of silicon-tethered bisalkynes. The reaction is operationally robust and atom-economic with good functional group tolerability as well as high enantioselectivity (up to >99:1 *er*) with the aid of Rh/Ar-BINMOL-Phos-based MFMC ligand catalysis. More specially, the use of the basic additive KO*t*Bu is crucial to maintaining of high level of enantioselectivity in this reaction because the catalytic amount KO*t*Bu is responsible for the formation of active Rh/**L8** complex. Although the true reaction mechanism for the stereoselective induction of Rh catalyst system is still unclear, the highly enantioselective synthesis of chiral benzosiloles and corresponding construction of silicon-stereogenic center by desymmetric hydrosilylation opens a great opportunity to create the next generation of organosilicon material or possibly better targeted Si-containing biologically active molecules that bring silicon to material and life (Kan et al., 2016). At present, the DFT calculation studies are undergoing in our laboratory to gain a more accurate understanding of the mechanism of *trans*-selective hydrosilylation and will be reported elsewhere. In addition, the reactive alkyne groups as side chains in the silicon-stereogenic benzosiloles are expected to undergo further functionalization and hold promise for synthesis of conjugate polymers or cross-linked materials.

Limitations of the Study

Terminal alkynes were not applicable in the construction of silicon-stereogenic benzosiloles by the intramolecular hydrosilylation. And the reaction mechanism and the origin of enantioselectivity that is controlled by the Ar-BINMOL-Phos need to be clarified in more reliable manner.

CellPress
OPEN ACCESS

Resource Availability

Lead Contact

Li-Wen Xu, liwenxu@hznu.edu.cn.

Material Availability

No unique reagents or no restrictions to the availability of chemicals.

Data and Code Availability

The related figures and data in this article can be found at the Supplemental Information.

METHODS

All methods can be found in the accompanying Transparent Methods supplemental file.

SUPPLEMENTAL INFORMATION

Supplemental Information can be found online at https://doi.org/10.1016/j.isci.2020.101268.

ACKNOWLEDGMENTS

This work was supported by the grants of National Natural Science Foundation of China (21773051, 21801056 and 21901056), Zhejiang Provincial Natural Science Foundation of China (LZ18B020001 and LQ19B040001), and the Hangzhou Science and Technology Bureau of China (20170533B08 and 20180432B05). The authors thank Dr. L. Li and Dr. K.Z. Jiang for their assistance on the NMR and MS analysis. L.-W.X. also thanks Prof. Y.X. Zheng (Nanjing University) for his assistance on the CPL analysis, and thanks to Prof. C. Liu (LICP, CAS) and Prof. X.Q. Hu (ZUT) for their help and discussion in this work.

AUTHOR CONTRIBUTIONS

R.-H.T., Z.X., and Y.-X.N. are co-first authors. L.-W.X. conceived the concept. R.-H.T. carried out experiments, including the preparation of chiral ligands and the rhodium-catalyzed hydrosilylation. Y.-X.N. and Z.X. carried out the experiments for the proposed reaction mechanism. X.-Q.X. carried the X-ray analysis. K.-F.Y. and J.-L.X. carried out partial reactions and the NMR analysis for the products and reaction intermediates. G.-W.Y., B.G., and X.-M.Y. synthesized the substrates and conducted the structural analysis of unknown compounds. L.-W.X wrote the manuscript, and all authors discussed the results and participated in revising the manuscript. L.-W.X. supervised the project.

DECLARATION OF INTERESTS

The authors declare no competing financial interests.

Received: April 3, 2020
Revised: May 27, 2020
Accepted: June 8, 2020
Published: July 24, 2020

REFERENCES

Cai, Y., Qin, A., and Tang, B.Z. (2017). Siloles in optoelectronic devices. J. Mater. Chem. C *5*, 7375–7389.

Chen, J., and Cao, Y. (2007). Silole-containing polymers: chemistry and optoelectronic properties. Macromol. Rapid Commun. *28*, 1714–1742.

Chen, H.Y., Lam, W.Y., Luo, J.D., Ho, Y.L., Tang, B.Z., Zhu, D.B., Wong, M., and Kwok, H.S. (2002). Highly efficient organic light-emitting diodes with a silole-based compound. Appl. Phys. Lett. *81*, 574–576.

Crabtree, R.H. (2003). An η 2-vinyl pathway may explain net trans hydrosilylation via transition metal catalysis even in cyclic cases. New J. Chem. *27*, 771–772.

Dedeoglu, B., Monari, A., Etienne, T., Aviyente, V., and Özen, A.S. (2014). Detection of nitroaromatic explosives based on fluorescence quenching of silafluorene-and silole-containing polymers: a time-dependent density functional theory study. J. Phys. Chem. C *118*, 23946–23953.

Dhbaibi, K., Favereau, L., and Crassous, J. (2019). Enantioenriched helicenes and helicenoids containing main-group elements (B, Si, N, P). Chem. Rev. *119*, 8846–8953.

Diachenko, V., Page, M.J., Gatus, M.R., Bhadbhade, M., and Messerle, B.A. (2015). Bimetallic N-heterocyclic carbene Rh (I) complexes: probing the cooperative effect for the catalyzed hydroelementation of alkynes. Organometallics *34*, 4543–4552.

Ding, S., Song, L.J., Chung, L.W., Zhang, X., Sun, J., and Wu, Y.D. (2013). Ligand-controlled remarkable regio-and stereodivergence in intermolecular hydrosilylation of internal alkynes: experimental and theoretical studies. J. Am. Chem. Soc. *135*, 13835–13842.

Doyle, M.P., High, K.G., Nesloney, C.L., Clayton, T.W., and Lin, J. (1991). Rhodium (II)

perfluorobutyrate catalyzed hydrosilylation of 1-alkynes. Trans addition and rearrangement to allylsilanes. Organometallics *10*, 1225–1226.

Faller, J.W., and D'Alliessi, D.G. (2002). Tunable stereoselective hydrosilylation of PhC: CH catalyzed by Cp* Rh complexes. Organometallics *21*, 1743–1746.

Fu, H., and Cheng, Y. (2012). Electroluminescent and photovoltaic properties of silole-based materials. Curr. Org. Chem. *16*, 1423–1446.

Gao, R., Xu, L., Hao, C., Xu, C., and Kuang, H. (2019). Circular polarized light activated chiral satellite nanoprobes for the imaging and analysis of multiple metal ions in living cells. Angew. Chem. Int. Ed. *131*, 3953–3957.

Gimferrer, M., Minami, Y., Noguchi, Y., Hiyama, T., and Poater, A. (2018). Monitoring of the phosphine role in the mechanism of palladium-catalyzed benzosilole formation from aryloxyethynyl silanes. Organometallics *37*, 1456–1461.

Guo, J., Wang, H., Xing, S., Hong, X., and Lu, Z. (2019). Cobalt-catalyzed asymmetric synthesis of gem-bis (silyl) alkanes by double hydrosilylation of aliphatic terminal alkynes. Chem *5*, 881–895.

Huckaba, A.J., Hollis, T.K., Howell, T.O., Valle, H.U., and Wu, Y. (2013). Synthesis and characterization of a 1, 3-phenylene-bridged N-alkyl bis (benzimidazole) CCC-NHC pincer ligand precursor: homobimetallic silver and rhodium complexes and the catalytic hydrosilylation of phenylacetylene. Organometallics *32*, 63–69.

Igawa, K., Yoshihiro, D., Ichikawa, N., Kokan, N., and Tomooka, K. (2012). Catalytic enantioselective synthesis of alkenylhydrosilanes. Angew. Chem. Int. Ed. *51*, 12745–12748.

Ilies, L., Tsuji, H., Sato, Y., and Nakamura, E. (2008). Modular synthesis of functionalized benzosiloles by tin-mediated cyclization of (o-alkynylphenyl) silane. J. Am. Chem. Soc. *130*, 4240–4241.

Kan, S.B.J., Lewis, R.D., Chen, K., and Arnold, F.H. (2016). Directed evolution of cytochrome c for carbon–silicon bond formation: bringing silicon to life. Science *354*, 1048–1051.

Kuninobu, Y., Yamauchi, K., Tamura, N., Seiki, T., and Takai, K. (2013). Rhodium-catalyzed asymmetric synthesis of spirosilabifluorene derivatives. Angew. Chem. Int. Ed. *52*, 1520–1522.

Li, Z., Dong, Y.Q., Lam, J.W.Y., Sun, J., Qin, A., Häußler, M., Dong, Y.P., Sung, H.H.Y., Williams, L.D., Tang, B.Z., et al. (2009). Functionalized siloles: versatile synthesis, aggregation-induced emission, and sensory and device applications. Adv. Funct. Mater. *19*, 905–917.

Li, H., Xue, S., Su, H., Shen, B., Cheng, Z., Lam, J.W., Wong, K.S., Wu, H., Li, B.S., and Tang, B.Z. (2016). Click synthesis, aggregation-induced emission and chirality, circularly polarized luminescence, and helical self-assembly of a leucine-containing silole. Small *12*, 6593–6601.

Liang, Y., Zhang, S., and Xi, Z. (2011). Palladium-catalyzed synthesis of benzosilolo [2, 3-b] indoles via cleavage of a C (sp3)–Si bond and consequent intramolecular C (sp2)–Si coupling. J. Am. Chem. Soc. *133*, 9204–9207.

Liang, Y., Geng, W., Wei, J., and Xi, Z. (2012). Palladium-catalyzed intermolecular coupling of 2-silylaryl bromides with alkynes: synthesis of benzosiloles and heteroarene-fused siloles by catalytic cleavage of the C (sp3)-Si bond. Angew. Chem. Int. Ed. *51*, 1934–1937.

Liu, J., Su, H., Meng, L., Zhao, Y., Deng, C., Ng, J.C.Y., Lu, P., Faisat, M., and Lam, J.W.Y. (2012). What makes efficient circularly polarised luminescence in the condensed phase: aggregation-induced circular dichroism and light emission. Chem. Sci. *3*, 2737–2747.

Mancano, G., Page, M.J., Bhadbhade, M., and Messerle, B.A. (2014). Hemilabile and bimetallic coordination in Rh and Ir complexes of NCN pincer ligands. Inorg. Chem. *53*, 10159–10170.

Mannu, A., Drexler, H.J., Thede, R., Ferro, M., Baumann, W., Rüger, J., and Heller, D. (2018). Oxidative addition of CH2Cl2 to neutral dimeric rhodium diphosphine complexes. J. Organomet. Chem. *871*, 178–184.

Matsuda et al. reported an intramolecular trans-bis-silylation (addition of a Si-Si bond) of alkynes to the preparation of 3-silyl-1-benzosiloles, and they proposed a mechanistic process with η2-vinyl transition metal intermediates featured with with 1,2-silyl shift: Matsuda, T., and Ichioka, Y. (2012). Rhodium-catalysed intramolecular trans-bis-silylation of alkynes to synthesise 3-silyl-1-benzosiloles Org. Biomol. Chem. *10*, 3175–3177.

Matsuda, T., Kadowaki, S., Goya, T., and Murakami, M. (2007). Synthesis of silafluorenes by iridium-catalyzed [2 + 2 + 2] cycloaddition of silicon-bridged diynes with alkynes. Org. Lett. *9*, 133–136.

Meißner, A., Alberico, E., Drexler, H.J., Baumann, W., and Heller, D. (2015a). Rhodium diphosphine complexes: a case study for catalyst activation and deactivation. Cat. Sci. Technol. *4*, 3409–3425.

Meißner, A., Preetz, A., Drexler, H.J., Baumann, W., Spannenberg, A., König, A., and Heller, D. (2015b). In situ synthesis of neutral dinuclear rhodium diphosphine complexes [{Rh(diphosphine)(m2-X)}2]: systematic investigations. ChemPlusChem *80*, 169–180.

Minami, Y., Noguchi, Y., and Hiyama, T. (2017). Synthesis of benzosiloles by intramolecular anti-hydroarylation via ortho-C–H activation of aryloxyethynyl silanes. J. Am. Chem. Soc. *139*, 14013–14016.

Morales-Ceron, J.P., Lara, P., López-Serrano, J., Santos, L.L., Salazar, V., Alvarez, E., and Suárez, A. (2017). Rhodium (I) complexes with ligands based on N-heterocyclic carbene and hemilabile pyridine donors as highly E stereoselective alkyne hydrosilylation catalysts. Organometallics *36*, 2460–2469.

Mori, A., Takahisa, E., Yamamura, Y., Kato, T., Mudalige, A.P., Kajiro, H., Hirabayashi, K., Nishihara, Y., and Hiyama, T. (2004). Stereodivergent syntheses of (Z)-and (E)-alkenylsilanes via hydrosilylation of terminal alkynes catalyzed by rhodium (I) iodide complexes and application to silicon-containing polymer syntheses. Organometallics *23*, 1755–1765.

Naganawa, Y., Namba, T., Kawagishi, M., and Nishiyama, H. (2015). Construction of a chiral silicon center by rhodium-catalyzed enantioselective intramolecular hydrosilylation. Chem. Eur. J. *21*, 9319–9322.

Ng, J.C.Y., Li, H., Yuan, Q., Liu, J., Liu, C., Fan, X., Li, B.S., and Tang, B.Z. (2014a). Valine-containing silole: synthesis, aggregation-induced chirality, luminescence enhancement, chiral-polarized luminescence and self-assembled structures. J. Mater. Chem. C *2*, 4615–4621.

Ng, J.C.Y., Liu, J., Su, H., Hong, Y., Li, H., Lam, J.W., Wong, K.S., and Tang, B.Z. (2014b). Complexation-induced circular dichroism and circularly polarised luminescence of an aggregation-induced emission luminogen. J. Mater. Chem. C *2*, 78–83.

Nie, H., Chen, B., Zeng, J., Xiong, Y., Zhao, Z., and Tang, B.Z. (2018). Excellent n-type light emitters based on AIE-active silole derivatives for efficient simplified organic light-emitting diodes. J. Mater. Chem. *6*, 3690–3698.

Oestreich, M. (2007). Silicon-stereogenic silanes in asymmetric catalysis. Synlett *2007*, 1629–1643.

Ohmura, T., Masuda, K., and Suginome, M. (2008). Silylboranes bearing dialkylamino groups on silicon as silylene equivalents: palladium-catalyzed regioselective synthesis of 2, 4-disubstituted siloles. J. Am. Chem. Soc. *130*, 1526–1527.

Ojima, I., Clos, N., Donovan, R.J., and Ingallina, P. (1990). Hydrosilylation of 1-hexyne catalyzed by rhodium and cobalt-rhodium mixed-metal complexes. Mechanism of apparent trans addition. Organometallics *9*, 3127–3133.

Onoe, M., Baba, K., Kim, Y., Kita, Y., Tobisu, M., and Chatani, N. (2012). Rhodium-catalyzed carbon–silicon bond activation for synthesis of benzosilole derivatives. J. Am. Chem. Soc. *134*, 19477–19488.

Pop, F., Zigon, N., and Avarvari, N. (2019). Main-group-based electro-and photoactive chiral materials. Chem. Rev. *119*, 8435–8478.

Rani, P.U., Reddy, P.M., Shanker, K., and Ravinder, V. (2008). Synthesis, characterization and catalytic applications of rhodium(I) organometallics with substituted tertiary phosphines. Transit. Met. Chem. *33*, 153–160.

Sakaki, S., Sumimoto, M., Fukuhara, M., Sugimoto, M., Fujimoto, H., and Matsuzaki, S. (2002). Why does the rhodium-catalyzed hydrosilylation of alkenes take place through a modified Chalk— harrod mechanism: a theoretical study. Organometallics *21*, 3788–3802.

Sanada, T., Kato, T., Mitani, M., and Mori, A. (2006). Rhodium-catalyzed hydrosilylation of internal alkynes with silane reagents bearing heteroatom substituents. Studies on the regio-/stereochemistry and transformation of the produced alkenylsilanes by rhodium-catalyzed conjugate addition. Adv. Synth. Catal. *348*, 51–54.

Sato, A., Kinoshita, H., Shinokubo, H., and Oshima, K. (2004). Hydrosilylation of alkynes with a cationic rhodium species formed in an anionic micellar system. Org. Lett. *6*, 2217–2220.

Sato, Y., Takagi, C., Shintani, R., and Nozaki, K. (2017). Palladium-catalyzed asymmetric synthesis

of silicon-stereogenic 5, 10-dihydrophenazasilines via enantioselective 1, 5-palladium migration. Angew. Chem. Int. Ed. *56*, 9211–9216.

For the importance of nonlinear effect (NLE) in asymmetric catalysis, see: Satyanarayana, T., Abraham, S., and Kagan, H.B. (2009). Nonlinear effects in asymmetric catalysis Angew. Chem. Int. Ed. *48*, 456–494.

Shimizu, M., Mochida, K., and Hiyama, T. (2008). Modular approach to silicon-bridged biaryls: palladium-catalyzed intramolecular coupling of 2-(arylsilyl)aryl triflates. Angew. Chem. Int. Ed. *47*, 9760–9764.

Shintani, R. (2015). Recent advances in the transition-metal-catalyzed enantioselective synthesis of silicon-stereogenic organosilanes. Asian J. Org. Chem. *4*, 510–514.

Shintani, R., Otomo, H., Ota, K., and Hayashi, T. (2012). Palladium-catalyzed asymmetric synthesis of silicon-stereogenic dibenzosiloles via enantioselective C–H bond functionalization. J. Am. Chem. Soc. *134*, 7305–7308.

Shintani, R., Takagi, C., Ito, T., Naito, M., and Nozaki, K. (2015). Rhodium-catalyzed asymmetric synthesis of silicon-stereogenic dibenzosiloles by enantioselective [2+ 2+ 2] cycloaddition. Angew. Chem. Int. Ed. *54*, 1616–1620.

Son, H.J., Han, W.S., Wee, K.R., Lee, S.H., Hwang, A.R., Kwon, S., Cho, D.W., Suh, I.H., and Kang, S.O. (2009). Intermolecular peripheral 2, 5-bipyridyl interactions by cyclization of 1, 1′-silanylene unit of 2, 3, 4, 5-aryl substituted siloles: enhanced thermal stability, high charge carrier mobility, and their application to electron transporting layers for OLEDs. J. Mater. Chem. *19*, 8964–8973.

Song, T., Zheng, L.S., Ye, F., Deng, W.H., Wei, Y.L., Jiang, K.Z., and Xu, L.W. (2014). Modular synthesis of Ar-BINMOL-Phos for catalytic asymmetric alkynylation of aromatic aldehydes with unexpected reversal of enantioselectivity. Adv. Synth. Catal. *356*, 1708–1718.

Song, T., Li, L., Zhou, W., Zheng, Z.J., Deng, Y., Xu, Z., and Xu, L.W. (2015). Enantioselective copper-catalyzed azide–alkyne click cycloaddition to desymmetrization of maleimide-based bis (alkynes). Chem. Eur. J. *21*, 554–558.

Takeuchi, R., and Tanouchi, N. (1993). Complete reversal of stereoselectivity in rhodium complex-catalysed hydrosilylation of alk-1-yne. J. Chem. Soc. Chem. Commun. 1319–1320.

Takeuchi, R., and Tanouchi, N. (1994). Solvent-controlled stereoselectivity in the hydrosilylation of alk-1-ynes catalysed by rhodium complexes. J. Chem. Soc. Perkin Trans. *1*, 2909–2913.

Tamao, K., Uchida, M., Izumizawa, T., Furukawa, K., and Yamaguchi, S. (1996a). Silole derivatives as efficient electron transporting materials. J. Am. Chem. Soc. *118*, 11974–11975.

Tamao, K., Nakamura, K., Ishii, H., Yamaguchi, S., and Shiro, M. (1996b). Axially chiral Spirosilanes via catalytic asymmetric intramolecular hydrosilation. J. Am. Chem. Soc. *118*, 12469–12470.

Toal, S.J., Jones, K.A., Magde, D., and Trogler, W.C. (2005). Luminescent silole nanoparticles as chemoselective sensors for Cr (VI). J. Am. Chem. Soc. *127*, 11661–11665.

Tobisu, M., Onoe, M., Kita, Y., and Chatani, N. (2009). Rhodium-catalyzed coupling of 2-Silylphenylboronic acids with alkynes leading to benzosiloles: catalytic cleavage of the Carbon— silicon bond in trialkylsilyl groups. J. Am. Chem. Soc. *131*, 7506–7507.

Trost, B.M., and Ball, Z.T. (2005). Alkyne hydrosilylation catalyzed by a cationic ruthenium complex: efficient and general trans addition. J. Am. Chem. Soc. *127*, 17644–17655.

Uchida, M., Izumizawa, T., Nakano, T., Yamaguchi, S., Tamao, K., and Furukawa, K. (2001). Structural optimization of 2, 5-diarylsiloles as excellent electron-transporting materials for organic electroluminescent devices. Chem. Mater. *13*, 2680–2683.

Ureshino, T., Yoshida, T., Kuninobu, Y., and Takai, K. (2010). Rhodium-catalyzed synthesis of silafluorene derivatives via cleavage of silicon— hydrogen and carbon— hydrogen bonds. J. Am. Chem. Soc. *132*, 14324–14326.

Wang, X.B., Zheng, Z.J., Xie, J.L., Gu, X.W., Mu, Q.C., Yin, G.W., Ye, F., Xu, Z., and Xu, L.W. (2020). Silicon-mediated catalytic synthesis of chiral acylsilane-substituted pyrrolidines as a Springboard to access structurally diverse amino acid derivatives. Angew. Chem. Int. Ed. *59*, 790–797.

Weickgenannt, A., Mewald, M., and Oestreich, M. (2010). Asymmetric Si–O coupling of alcohols. Org. Biomol. Chem. *8*, 1497–1504.

Wen, H., Wan, X., and Huang, Z. (2018). Asymmetric synthesis of silicon-stereogenic vinylhydrosilanes by cobalt-catalyzed regio-and enantioselective alkyne hydrosilylation with dihydrosilanes. Angew. Chem. Int. Ed. *57*, 6319–6323.

Wen, H., Liu, G., and Huang, Z. (2019). Recent advances in tridentate iron and cobalt complexes for alkene and alkyne hydrofunctionalizations. Chem. Rev. *386*, 138–153.

Wu, W.C., Chen, C.Y., Tian, Y., Jang, S.H., Hong, Y., Liu, Y., Hu, R., Tang, B.Z., Lee, Y.T., Chen, C.T., et al. (2010). Enhancement of aggregation-induced emission in dye-encapsulating polymeric micelles for bioimaging. Adv. Funct. Mater. *20*, 1413–1423.

Wu, Y., Karttunen, V.A., Parker, S., Genest, A., and Rösch, N. (2013). Olefin hydrosilylation catalyzed by a bis-N-heterocyclic carbene rhodium complex. A density functional theory study. Organometallics *32*, 2363–2372.

Wu, Y., Genest, A., and Rösch, N. (2014). Does the preferred mechanism of a catalytic transformation depend on the density functional Ethylene hydrosilylation by a metal complex as a case study. J. Phys. Chem. A *118*, 3004–3013.

Xu, L.W. (2012). Desymmetrization catalyzed by transition-metal complexes: enantioselective formation of silicon-stereogenic silanes. Angew. Chem. Int. Ed. *51*, 12932–12934.

Xu, L.W., Li, L., Lai, G.Q., and Jiang, J.X. (2011). The recent synthesis and application of silicon-stereogenic silanes: a renewed and significant challenge in asymmetric synthesis. Chem. Soc. Rev. *40*, 1777–1790.

Yamaguchi, S., and Tamao, K. (1996). Theoretical study of the electronic structure of 2, 2′-Bisilole in comparison with 1, 1′-Bi-1, 3-cyclopentadiene: σ^*–π^* conjugation and a low-lying LUMO as the origin of the unusual optical properties of 3, 3′, 4, 4′-tetraphenyl-2, 2′-bisilole. Bull. Chem. Soc. Jpn. *69*, 2327–2334.

Yang, Q., Liu, L., Chi, Y., Hao, W., Zhang, W.X., and Xi, Z. (2018). Rhodium-catalyzed intramolecular carbosilylation of alkynes via C (sp 3)–Si bond cleavage. Org. Chem. Front. *5*, 860–863.

Zaranek, M., and Pawluc, P. (2018). Markovnikov hydrosilylation of alkenes: how an oddity becomes the goal. ACS Catal. *8*, 9865–9876.

Zhan, G., Teng, H.L., Luo, Y., Lou, S.J., Nishiura, M., and Hou, Z. (2018). Enantioselective construction of silicon-stereogenic silanes by Scandium-catalyzed intermolecular alkene hydrosilylation. Angew. Chem. *130*, 12522–12526.

Zhang, Q.W., An, K., and He, W. (2014). Rhodium-catalyzed tandem cyclization/Si-C activation reaction for the synthesis of siloles. Angew. Chem. Int. Ed. *53*, 5667–5671.

Zhang, Q.W., An, K., Liu, L.C., Yue, Y., and He, W. (2015). Rhodium-catalyzed enantioselective intramolecular C-H silylation for the syntheses of planar-chiral metallocene siloles. Angew. Chem. Int. Ed. *54*, 6918–6921.

Zhang, Q.W., An, K., Liu, L.C., Guo, S., Jiang, C., Guo, H., and He, W. (2016). Rhodium-catalyzed intramolecular C— H silylation by silacyclobutanes. Angew. Chem. Int. Ed. *55*, 6319–6323.

Zhang, Q.W., An, K., Liu, L.C., Zhang, Q., Guo, H., and He, W. (2017). Construction of chiral tetraorganosilicons by tandem desymmetrization of silacyclobutanes/intermolecular dehydrogenative silylation. Angew. Chem. Int. Ed. *56*, 1125–1129.

Zhao, Z., Guo, Y., Jiang, T., Chang, Z., Lam, J.W.Y., Xu, L., Qiu, H., and Tang, B. (2012). A fully substituted 3-silolene functions as promising building block for hyperbranched poly(silylenevinylene). Macromol. Rapid Commun. *33*, 1074–1079.

Zhao, Z., He, B., and Tang, B.Z. (2015). Aggregation-induced emission of siloles. Chem. Sci. *6*, 5347–5365.

Zhou, Z., Xie, S., Chen, X., Tu, Y., Xiang, J., Wang, J., He, Z., Zeng, Z., and Tang, B.Z. (2019). Spiro-functionalized diphenylethenes: suppression of a reversible photocyclization contributes to the aggregation-induced emission effect. J. Am. Chem. Soc. *141*, 9803–9807.

Zhuang, Y., Shang, C., Lou, X., and Xia, F. (2017). Construction of AIEgens-based bioprobe with two fluorescent signals for enhanced monitor of extracellular and intracellular telomerase activity. Anal. Chem. *89*, 2073–2079.

iScience, Volume *23*

Supplemental Information

Catalytic Asymmetric *trans*-Selective Hydrosilylation of Bisalkynes to Access AIE and CPL-Active Silicon-Stereogenic Benzosiloles

Ren-He Tang, Zheng Xu, Yi-Xue Nie, Xu-Qiong Xiao, Ke-Fang Yang, Jia-Le Xie, Bin Guo, Guan-Wu Yin, Xue-Min Yang, and Li-Wen Xu

More details for reaction condition optimization:

Table S1. Optimization of reaction conditions by screening of chiral ligands. [a] Related to Figure 1.

Entry	Rh (X mol%)	Ligand	Temp (^{o}C)	Time (h)	**2a**/**1a**[b]	er (%)[c]
1	2.5	**L1**	80	36	>99:1	85:15
2	2.5	**L2**	80	34	60:40	80:20
3	10	**L3**	60	24	80:20	90:10
4	2.5	**L4**	80	34	62:38	80:20
5	2.5	**L5**	80	34	94:6	70:40
6	2.5	**L6**	80	36	54:46	85:15
7	2.5	**L7**	80	36	60:40	50:50
8	2.5	**L8**	80	34	60:40	85:15
9	2.5	**L9**	80	34	70:30	87.5:12.5
10	2.5	**L10**	80	36	60:40	50:50
11	10	**L11**	60	24	-	65:35
12	10	**L12**	60	24	-	50:50
13	2.5	**L13**	80	36	20:80	50:50
14	10	**L14**	60	24	-	50:50
15	10	**L15**	60	24	-	50:50
16	10	**L16**	60	24	-	59:41
17	10	**L17**	60	24	-	56:44
18	10	**L18**	60	24	-	70:30
19	10	**L19**	60	24	-	65:35
20	10	**L20**	60	24	-	65:35
21	2.5	**L21**	80	24	10:90	55:45
22	5	**L9**	80	24	76:24	90:10
23	5	**L8**	80	24	82:18	91:9

[a] Reaction conditions: **1a** (0.2 mmol), $[Rh(cod)Cl]_2$ (10 mol%), and solvent (1 mL) at 60-80 ^{o}C. [b] The ratio of **2a**/**1a** was determined by HPLC. [c] The er value was determined by chiral HPLC.

Table S2. Optimization of reaction conditions by screening of solvents.[a] Related to Figure 1.

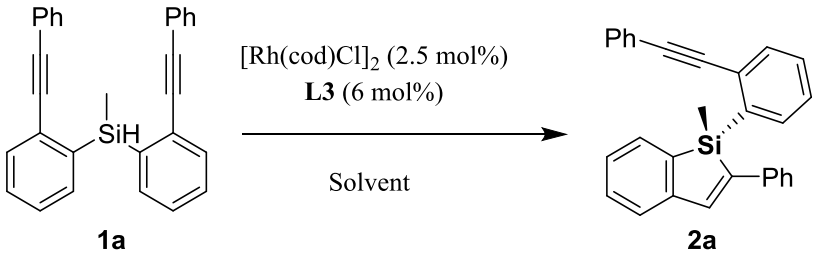

Entry	Solvent	Temp (°C)	Time (h)	**2a/1a**[b]	er (%)[c]
1	Dioxane	70	36	NR	-
2	CH_3CN	70	36	-	50:50
3	Ethanol	70	36	NR	-
4	THF	70	36	-	77.5:25.5
5	DCE	70	36	NR	50:50
6	Benzene	80	22	>99:1	91:9
7	*m*-Xylene	80	22	>99:1	90:10
8	*p*-Xylene	80	22	80:20	85:15
9	*o*-Xylene	80	22	94:6	82.5:17.5
10	Toluene	70	24	80:20	90:10
11	1,2,4-Trimethylbenzene	80	22	88:12	90:10

[a] Reaction conditions: **1a** (0.2 mmol), $[Rh(cod)Cl]_2$ (10 mol%), and solvent (1 mL) at 70-80 °C. [b] Determined by HPLC. [c] The er value was determined by chiral HPLC with a chiral stationary phase.

Table S3. Evaluation of catalytic activity of transition-metal catalysts. [a] Related to Table 1.

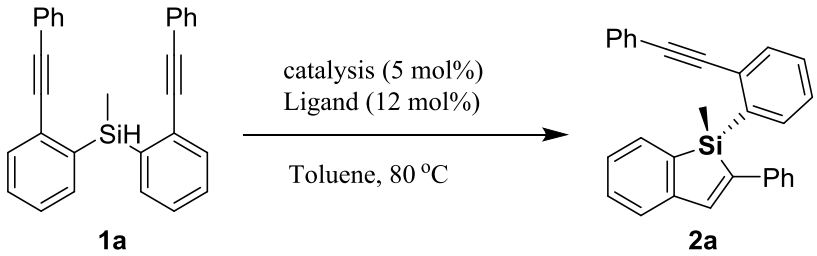

Entry	Catalyst	Ligand	Time (h)	**2a/1a**[b]	er (%)[c]
1	$[RhCl(C_2H_2)]_2$	**L3**	34	NR	-
2	$[(C_6H_5)_3P]_3RhCl$	**L3**	34	NR	-
3	$Rh_2(OOCCH_3)_4$	**L3**	34	NR	-
4	$[Rh(cod)_2]BF_4$	**L3**	34	NR	-
5	$[Rh(OAc)_2]_2$	**L3**	34	NR	-
6	$[Rh(nbd)_2]Cl_2$	**L3**	34	NR	-
7	$Rh(CO)_2(C_5H_7O_2)$	**L3**	34	NR	-
8	$RhCl_2(CO)_4$	**L3**	34	NR	-
9	$(\eta_3\text{-}C_3H_5)_2Pd_2Cl_2$	**L8**	14	NR	-
10	$PdCl_2$	**L8**	14	NR	-
11	$Pd_2(dba)_3$	**L8**	14	10:90	62.5:37.5
12	$PdCl_2(dppb)$	**L8**	14	14:86	50:50
13	$Pd(PPh_3)Cl_2$	**L8**	14	22:78	65:35
14	OIP Co	-	14	10:90	50:50
15[d]	$[Rh(cod)Cl]_2$.	**L8**	14	20:80	90:10
16[e]	$[Rh(cod)Cl]_2$.	**L8**	14	8:92	95.5:4.5

[a] Reaction conditions: **1a** (0.2 mmol), $[Rh(cod)Cl]_2$ (10 mol%), and solvent (1 mL) at 80 °C. [b] Determined by HPLC. [c] The er value was determined by chiral HPLC with a chiral stationary phase. [d] At 80 °C. [e] At 60 °C.

Table S4. Optimization of reaction conditions by screening of additives. [a] Related to Table 1.

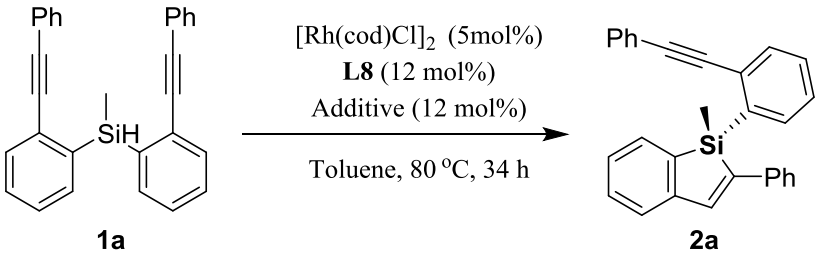

Entry	Additive	**2a/1a**[b]	er (%)[c]
1	$AlCl_3$	NR	
2	$NaHBEt_3$	>99:1	92.5:7.5
3	$NaSbF_6$	NR	
4	K_2CO_3	60:40	90.5:9.5
5	$AlCl_3$	30:70	85:15
6	CuI	60:40	90:10
7	KO*t*Bu	>99:1	95:5
8	Ag_3PO_4	90:10	92:8
9	NEt_3	90:10	92:8
10	NaO^tBu	>99:1	90:10
11	NaOEt	>99:1	85:15

[a] Reaction conditions: **1a** (0.2 mmol), $[Rh(cod)Cl]_2$ (5 mol%), and solvent (1 mL) at 70 °C. [b] Determined by HPLC. NR is no reaction. [c] The er value was determined by chiral HPLC with a chiral stationary phase.

Table S5. The effect of KO*t*Bu on the Rh-catalyzed intramolecular hydrosilylati on.[a] Related to Table 1.

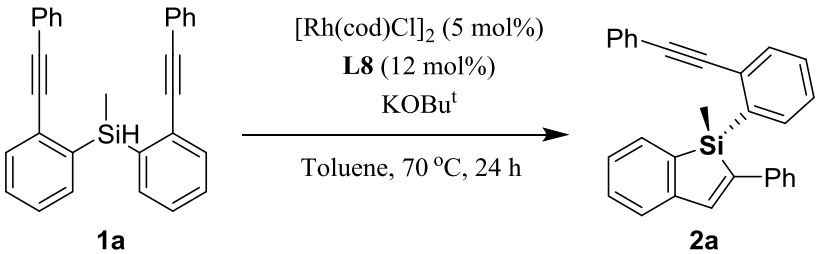

Entry	KO*t*Bu (X mol%)	**2a/1a**[b]	er (%)[c]
1	6	>99:1	95.5:4.5
2	12	>99:1	95.5:4.5
3	24	>99:1	95.5:4.5
4	36	>99:1	75:25
5	48	NR	-
6	60	NR	-

[a] Reaction conditions: **1a** (0.2 mmol), $[Rh(cod)Cl]_2$ (5 mol%), and solvent (1 mL) at 70 °C. [b] Determined by HPLC. [c] The er value was determined by chiral HPLC with a chiral stationary phase.

Table S6a. Kinetic studies on the Rh-catalyzed intramolecular hydrosilylation: a) with KO*t*Bu. [a] Related to Figure 4.

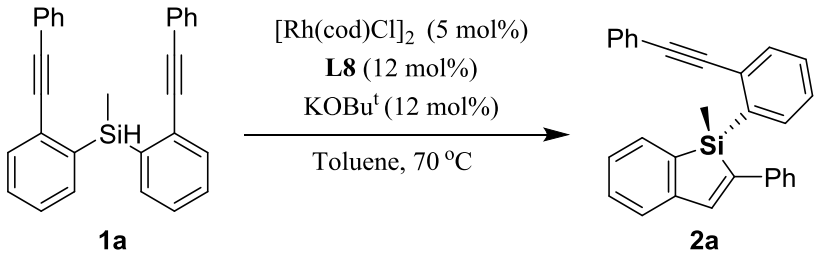

Entry	Catalyst	Temp (°C)	Time (h)	**2a/1a**[b]	*er* (%)[c]
1	$[Rh(cod)Cl]_2$	70	1	18:82	>99:1
2	$[Rh(cod)Cl]_2$	70	2	18:82	>99:1
3	$[Rh(cod)Cl]_2$	70	4	28:72	95.5:4.5
4	$[Rh(cod)Cl]_2$	70	14	30:70	95.5:4.5
5	$[Rh(cod)Cl]_2$	70	40	54:46	95.5:4.5
6	$[Rh(cod)Cl]_2$	70	70	>99:1	95.5:4.5

[a] Reaction conditions: **1a** (0.2 mmol), $[Rh(cod)Cl]_2$ (5 mol%), and solvent (1 mL) at 70 °C. [b] Determined by HPLC. [c] The er value was determined by chiral HPLC with a chiral stationary phase.

Table S6b. Kinetic studies on the Rh-catalyzed intramolecular hydrosilylation: b) without KO*t*Bu. [a] Related to Figure 4.

Entry	Catalyst	Temp (°C)	Time (h)	*er* (%)[b]
1	$[Rh(cod)Cl]_2$	70	2	97.5:2.5
2	$[Rh(cod)Cl]_2$	70	10	91:9
3	$[Rh(cod)Cl]_2$	70	22	91:9
4	$[Rh(cod)Cl]_2$	70	34	85:15
5	$[Rh(cod)Cl]_2$	70	50	75:25

[a] Reaction conditions: **1a** (0.2 mmol), $[Rh(cod)Cl]_2$ (5 mol%), and solvent (1 mL) at 70 °C. [b] The er value was determined by chiral HPLC with a chiral stationary phase.

Figure S1. X-ray structures of **2r** (CCDC 1954490). Related to Scheme 2.

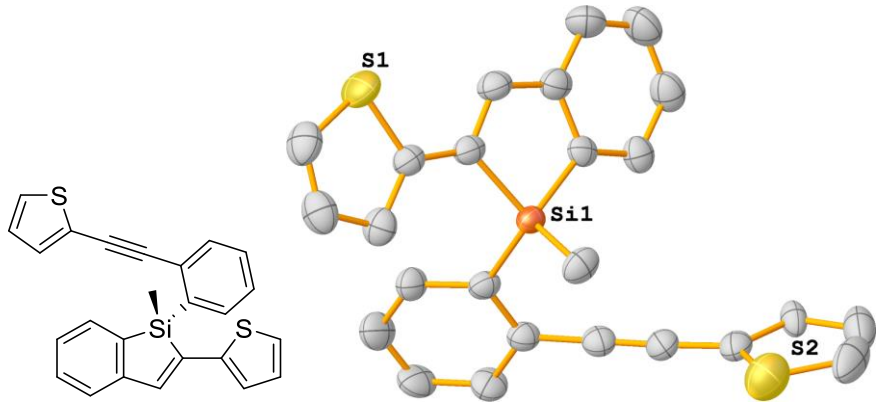

2r

Crystallographic data and data collection for the product **2r**

Formula	$C_{25}H_{18}S_2Si$	*Z*	2
Dcalc./ g cm^{-3}	1.298	*Z'*	2
μ/mm^{-1}	2.887	Wavelength/Å	1.54178
Formula Weight	410.60	Radiation type	CuK
Colour	colourless	θ_{min}/ °	4.076
Shape	prism	θ_{max}/ °	71.022
Size/mm^3	0.15×0.12×0.10	Measured Refl's.	33860
T/K	296.15	Ind't Refl's	7453
Crystal System	triclinic	Refl's with I > 2(I)	7409
Flack Parameter	0.101(7)	R_{int}	0.0342
Hooft Parameter	0.103(5)	Parameters	696
Space Group	*P1*	Restraints	195
a/Å	8.6621(2)	Largest Peak	0.180
b/Å	11.3298(3)	Deepest Hole	-0.221
c/Å	11.8647(3)	GooF	1.050
α/ °	73.2290(10)	wR_2 *(all data)*	0.0871
β/ °	70.5240(10)	wR_2	0.0870
γ/ °	83.5540(10)	R_1 *(all data)*	0.0315
V/Å^3	1050.92(5)	R_1	0.0314

Supplemental Figures for NMR spectrums:

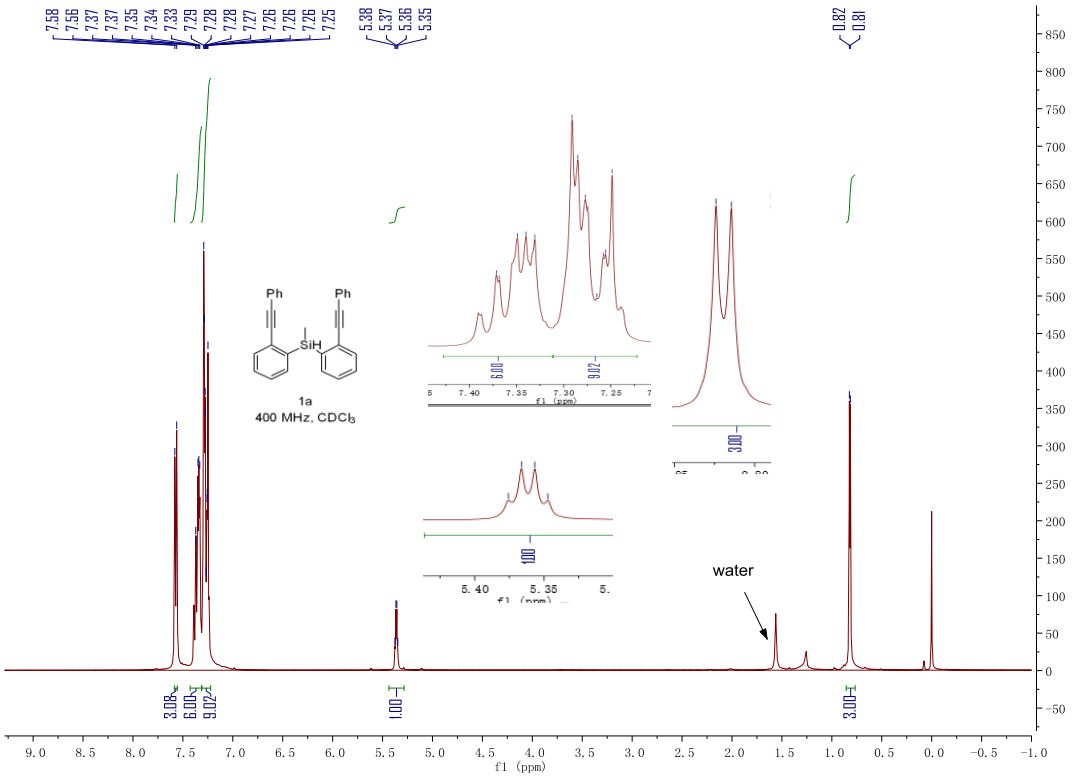

Figure S2. ^{1}H NMR (400 MHz, $CDCl_3$) spectrum of compound **1a**, related to **Scheme 2**

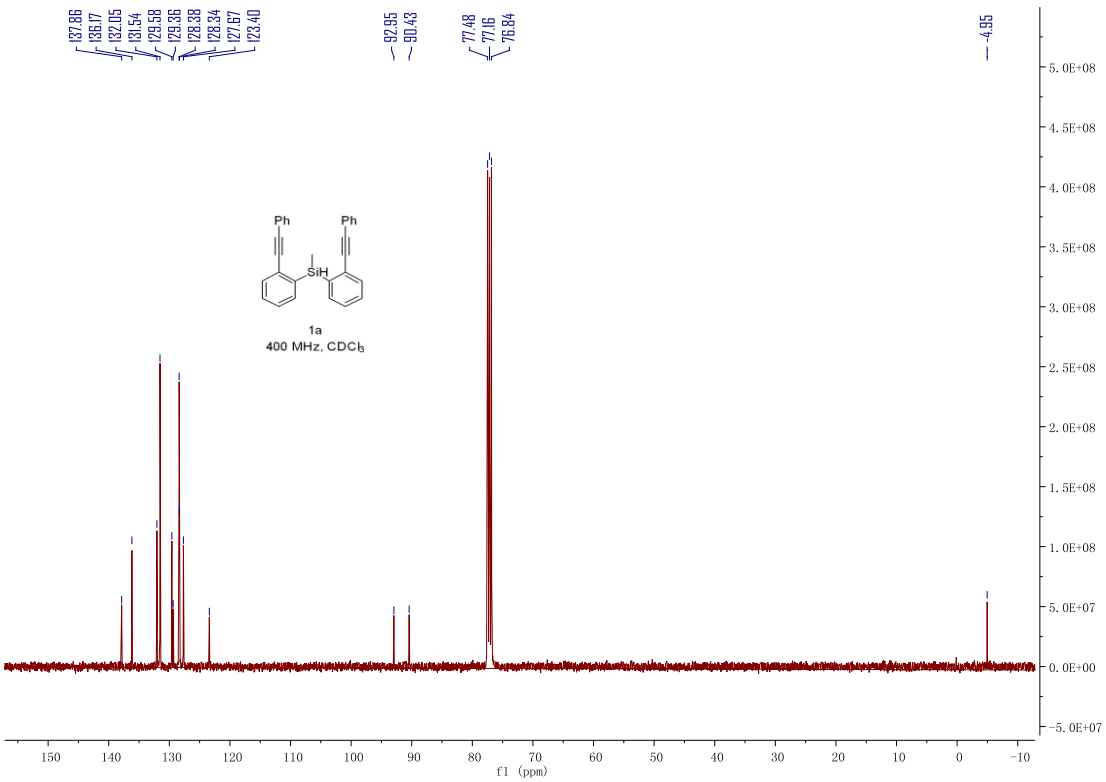

Figure S3. ^{13}C NMR (100 MHz, $CDCl_3$) spectrum of compound **1a**, related to **Scheme 2**

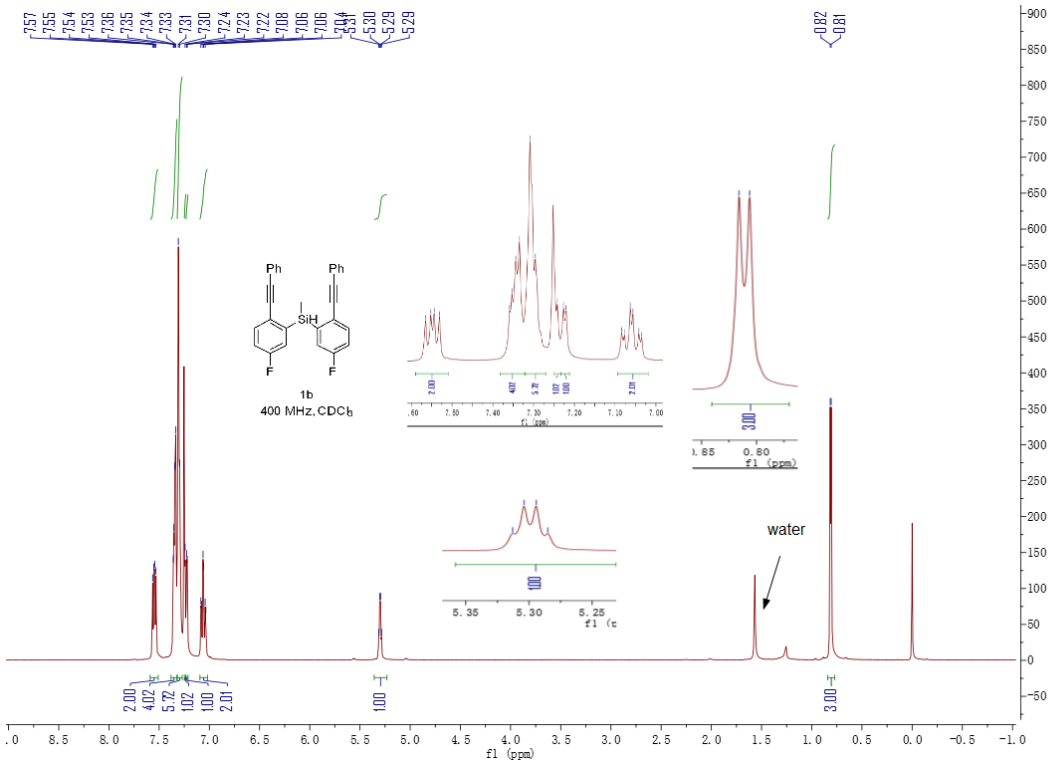

Figure S4. ^{1}H NMR (400 MHz, $CDCl_3$) spectrum of compound **1b** , related to **Scheme 2**

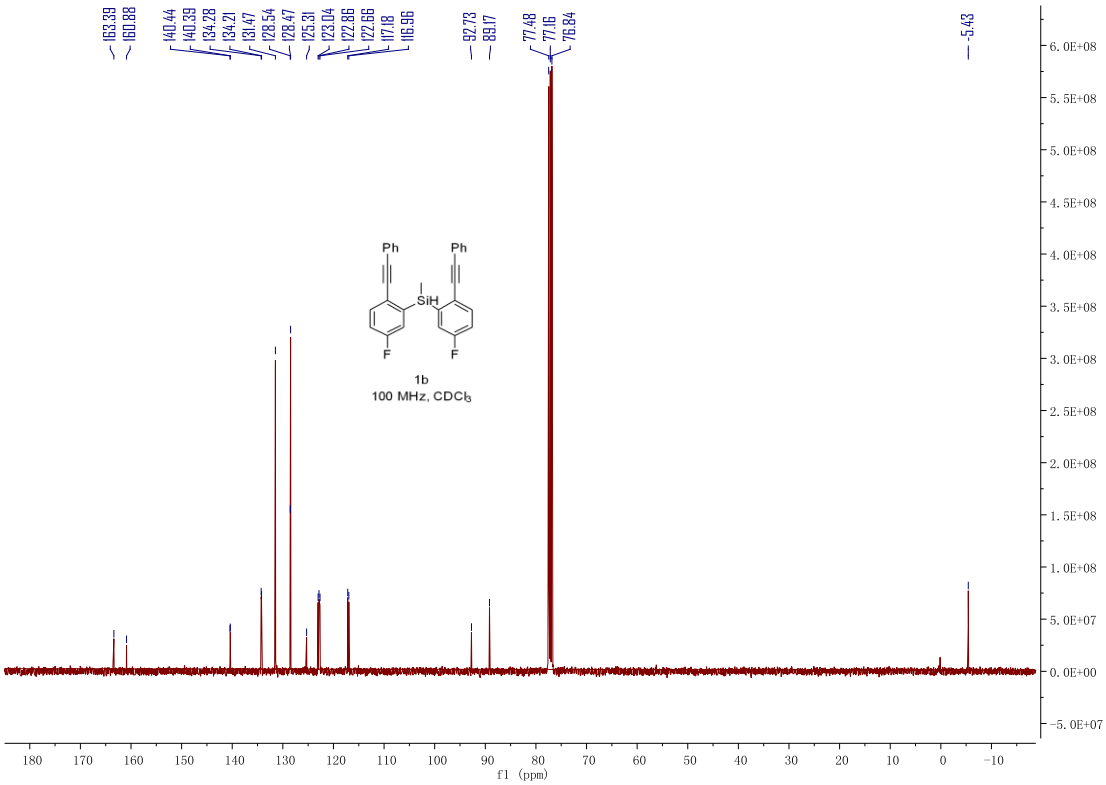

Figure S5. ^{13}C NMR (100 MHz, $CDCl_3$) spectrum of compound **1b**, related to **Scheme 2**

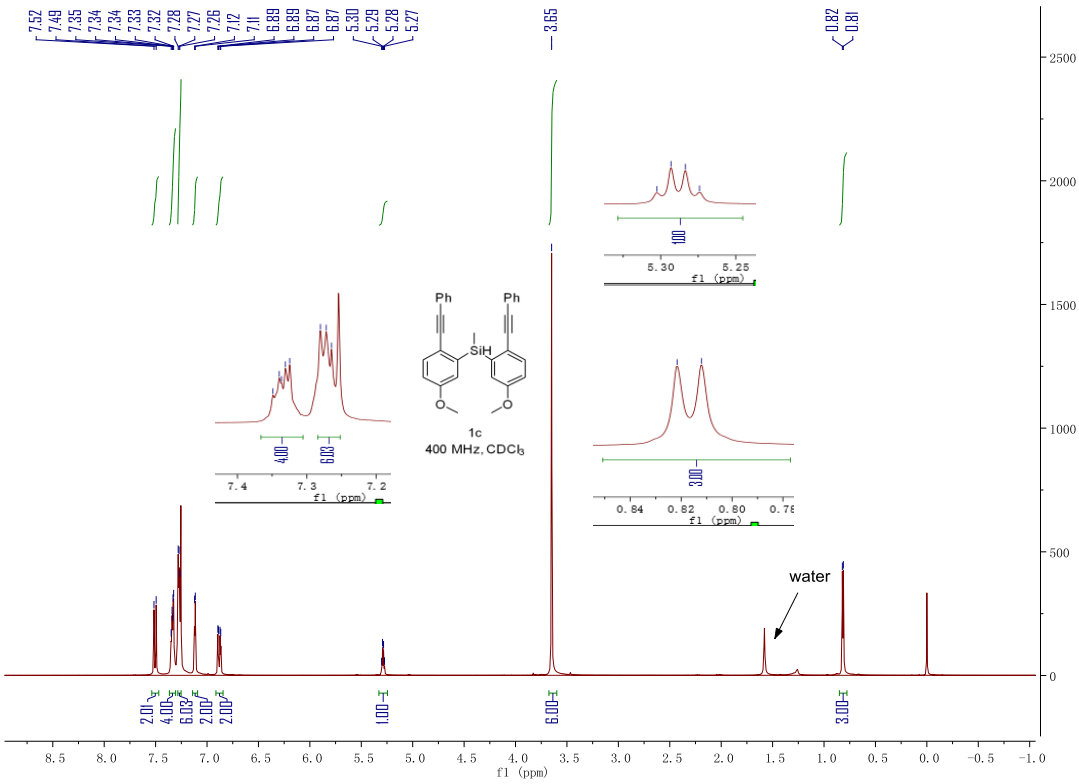

Figure S6. ^{1}H NMR (400 MHz, $CDCl_3$) spectrum of compound **1c**, related to **Scheme 2**

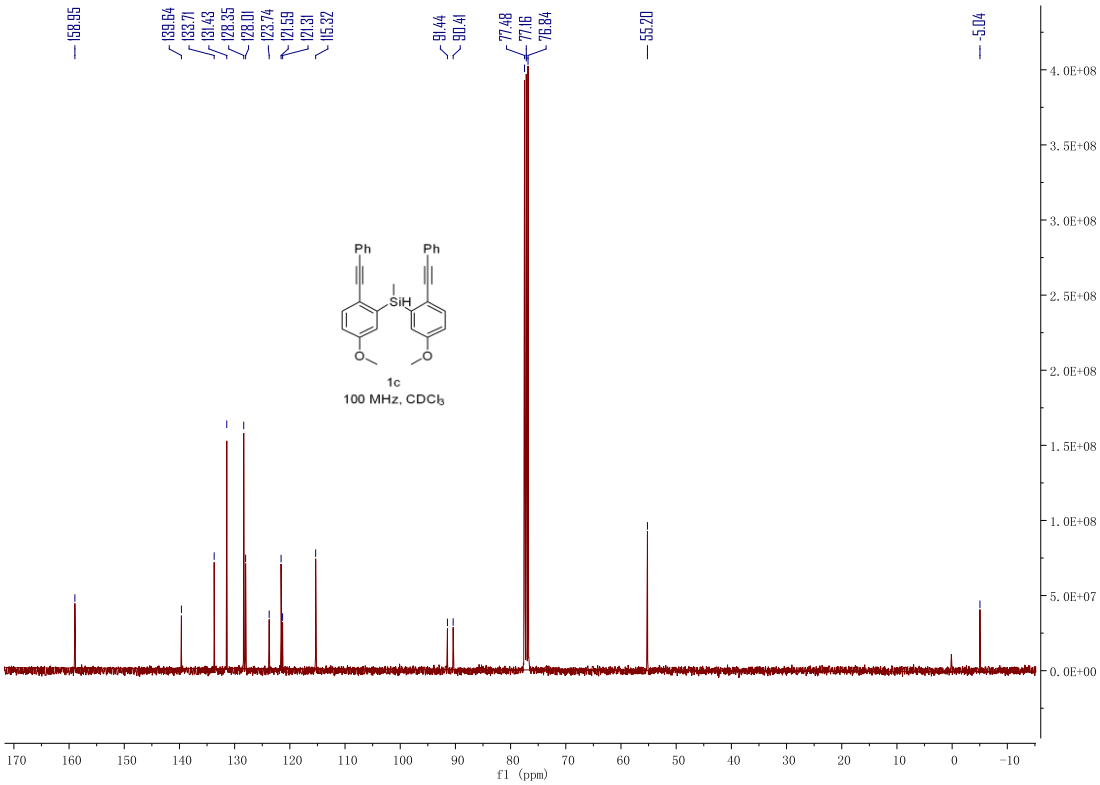

Figure S7. ^{13}C NMR (100 MHz, $CDCl_3$) spectrum of compound **1c**, related to **Scheme 2**

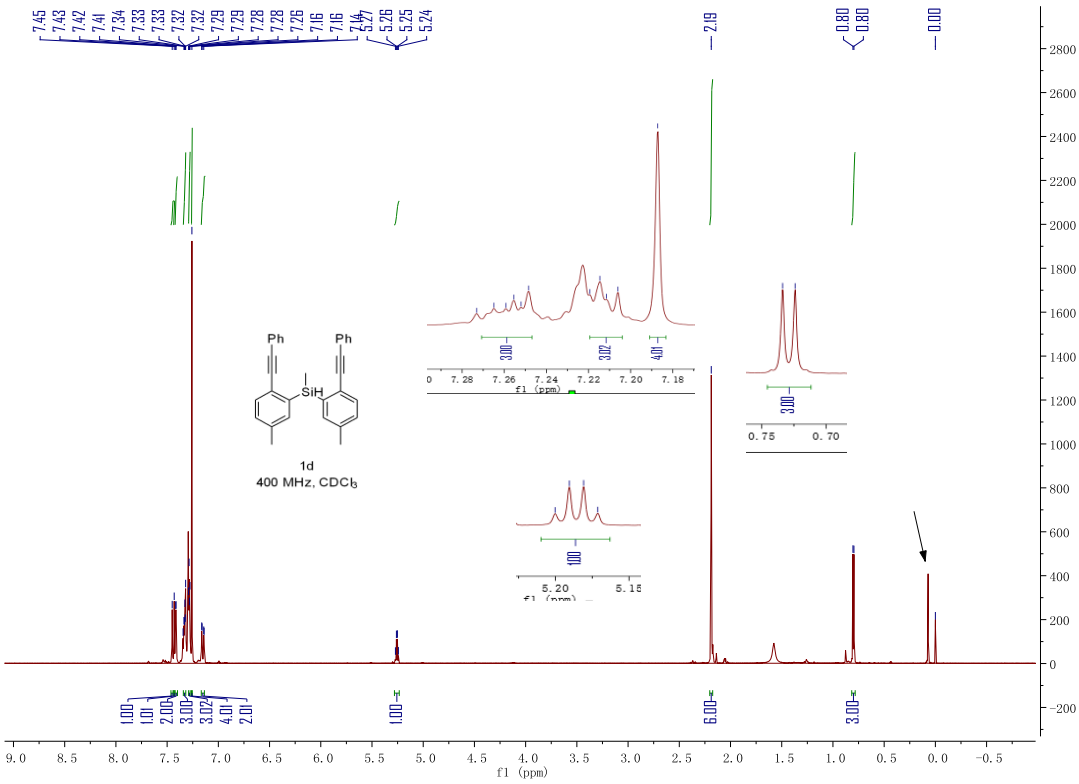

Figure S8. ^{1}H NMR (400 MHz, $CDCl_3$) spectrum of compound **1d**, related to **Scheme 2**

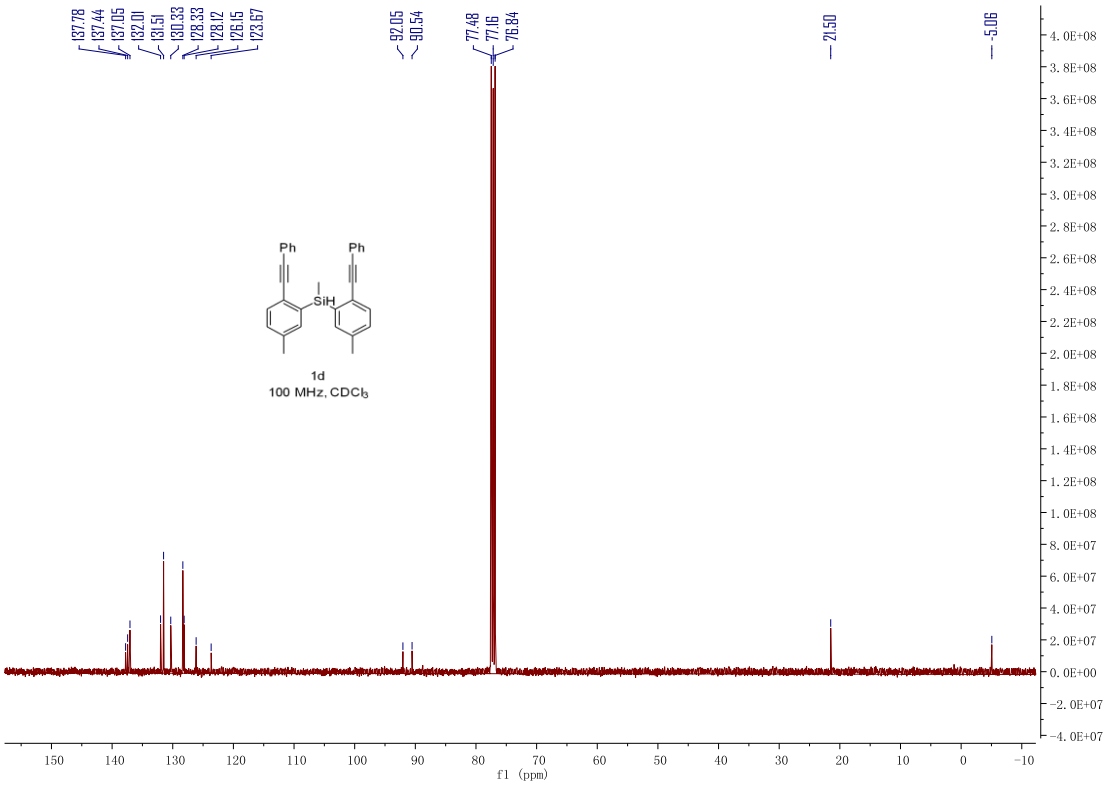

Figure S9. ^{13}C NMR (100 MHz, $CDCl_3$) spectrum of compound **1d**, related to **Scheme 2**

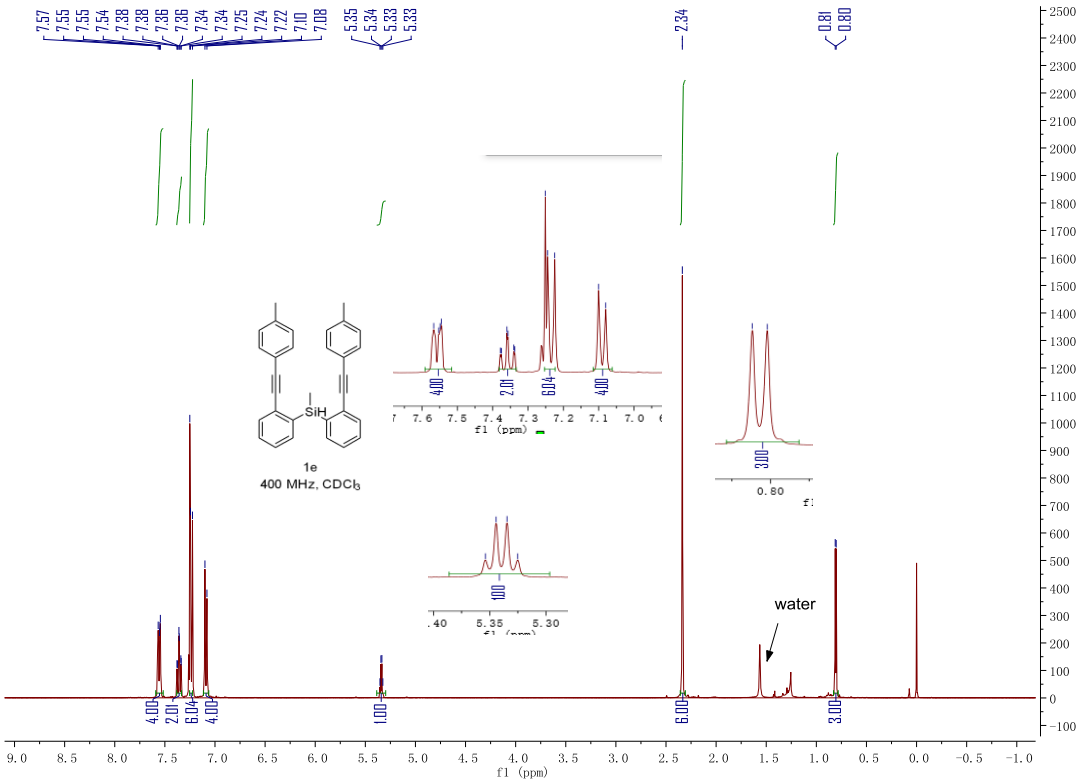

Figure S10. ^{1}H NMR (400 MHz, $CDCl_3$) spectrum of compound **1e**, related to **Scheme 2**

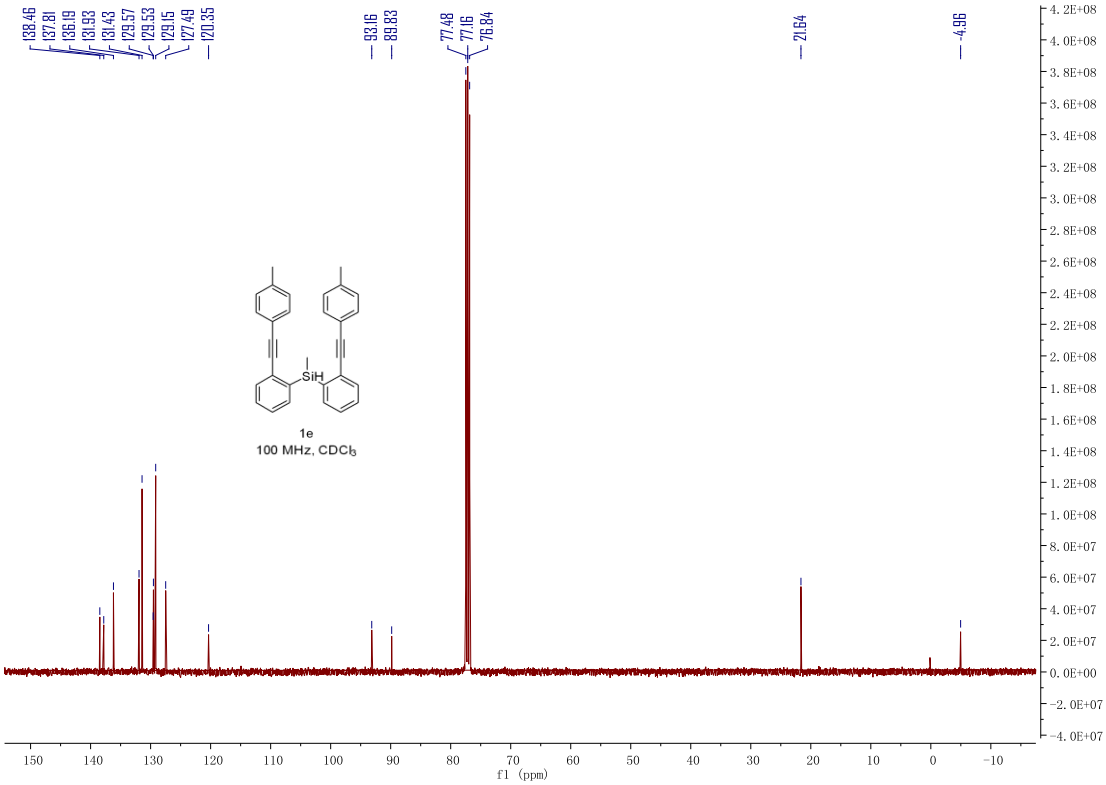

Figure S11. ^{13}C NMR (100 MHz, $CDCl_3$) spectrum of compound **1e**, related to **Scheme 2**

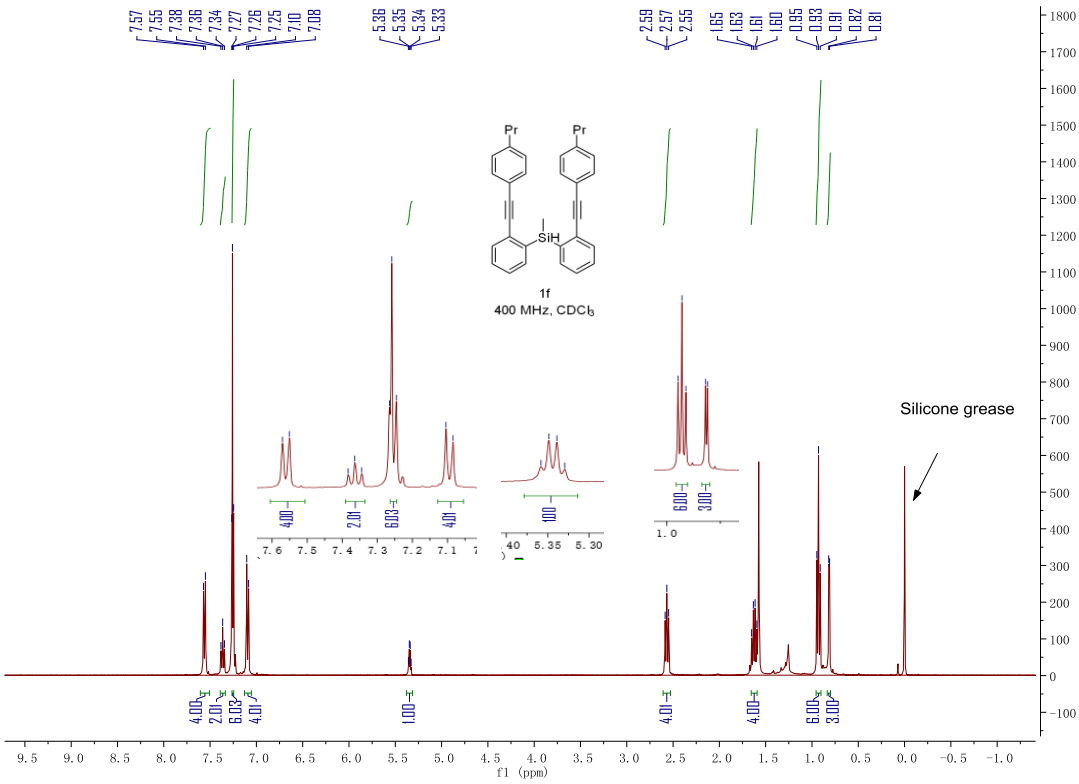

Figure S12. ^{1}H NMR (400 MHz, $CDCl_3$) spectrum of compound **1f**, related to **Scheme 2**

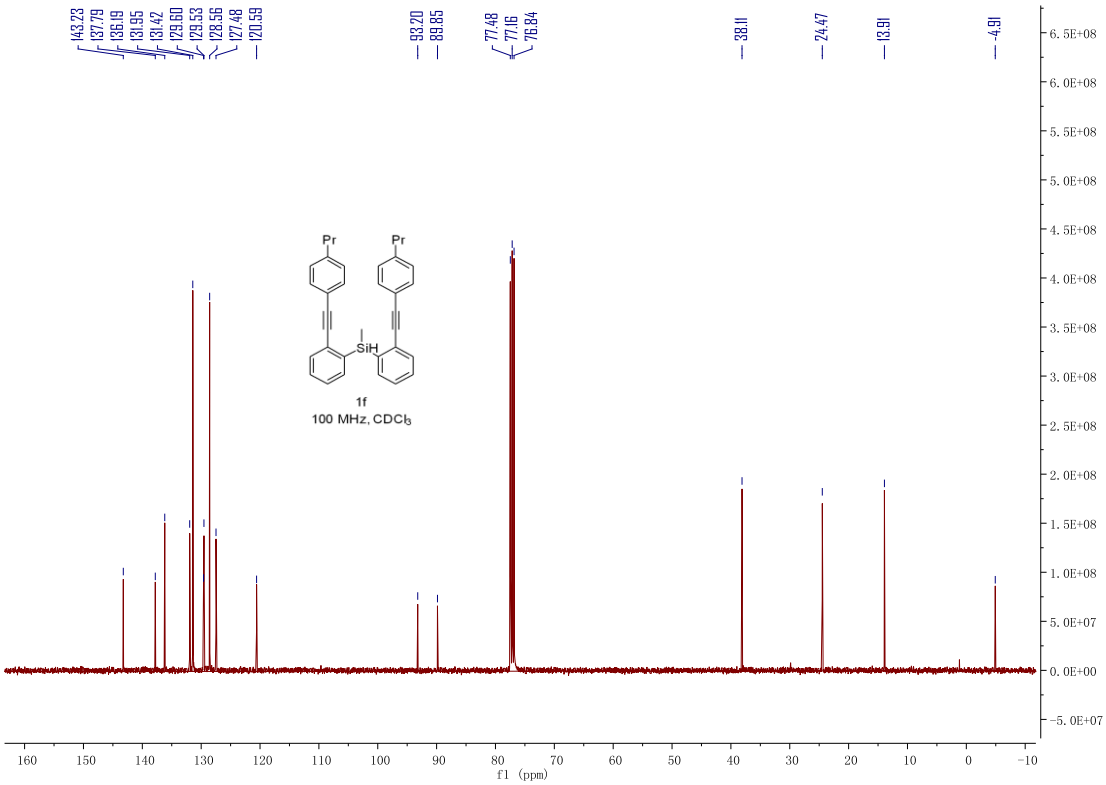

Figure S13. ^{13}C NMR (100 MHz, $CDCl_3$) spectrum of compound **1f**, related to **Scheme 2**

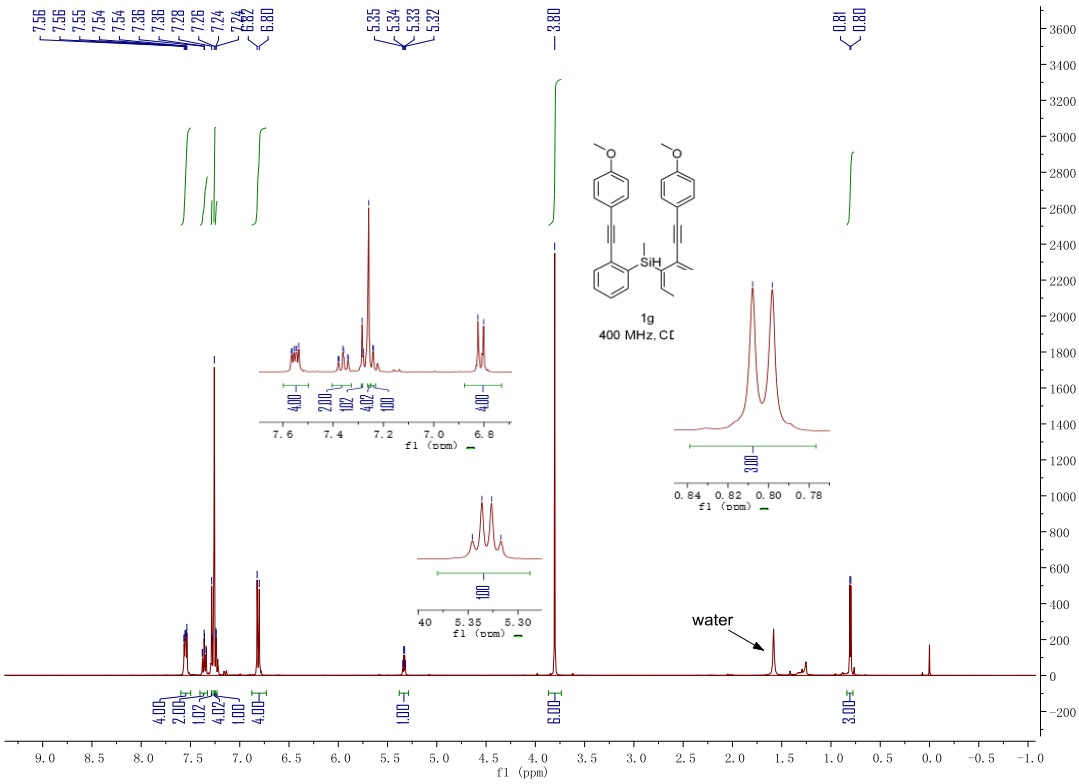

Figure S14. ^{1}H NMR (400 MHz, $CDCl_3$) spectrum of compound **1g**, related to **Scheme 2**

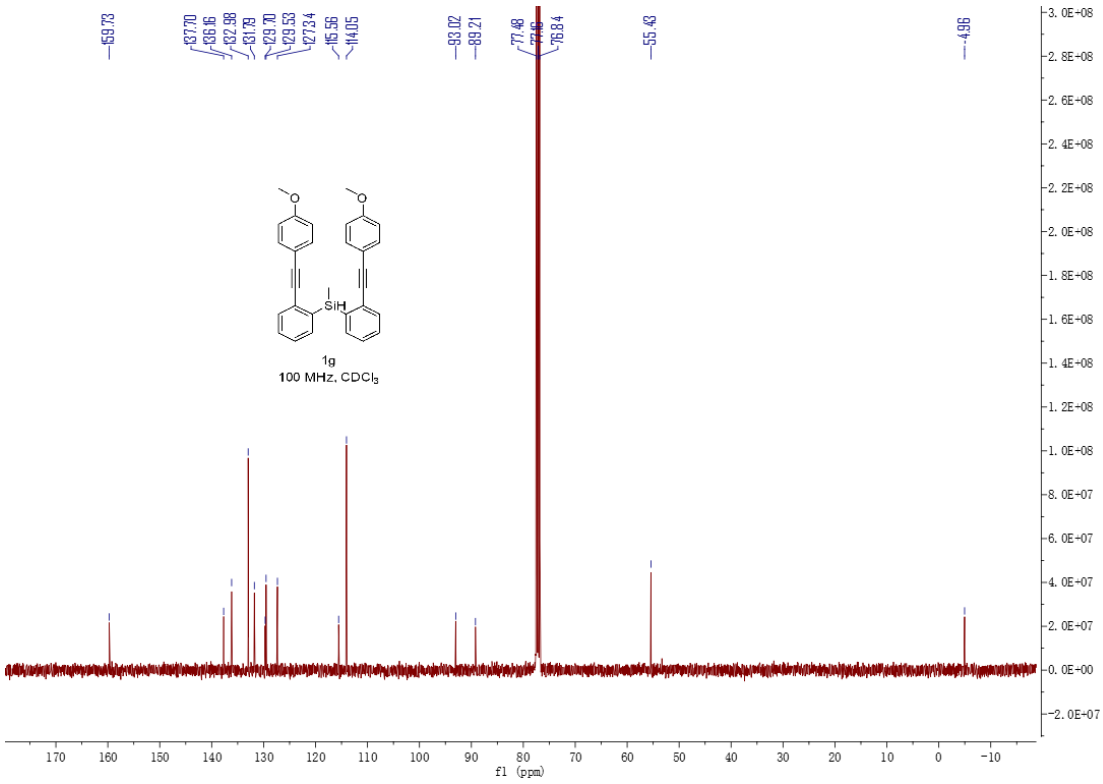

Figure S15. ^{13}C NMR (100 MHz, $CDCl_3$) spectrum of compound **1g**, related to **Scheme 2**

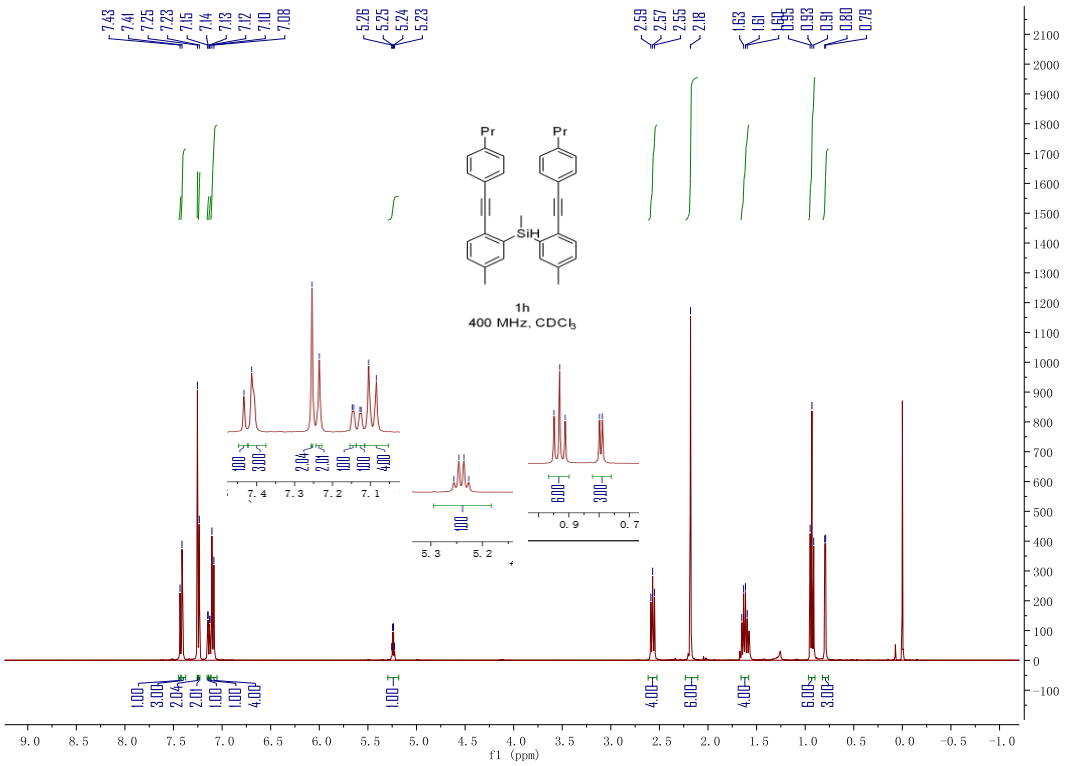

Figure S16. ^{1}H NMR (400 MHz, $CDCl_3$) spectrum of compound **1h**, related to **Scheme 2**

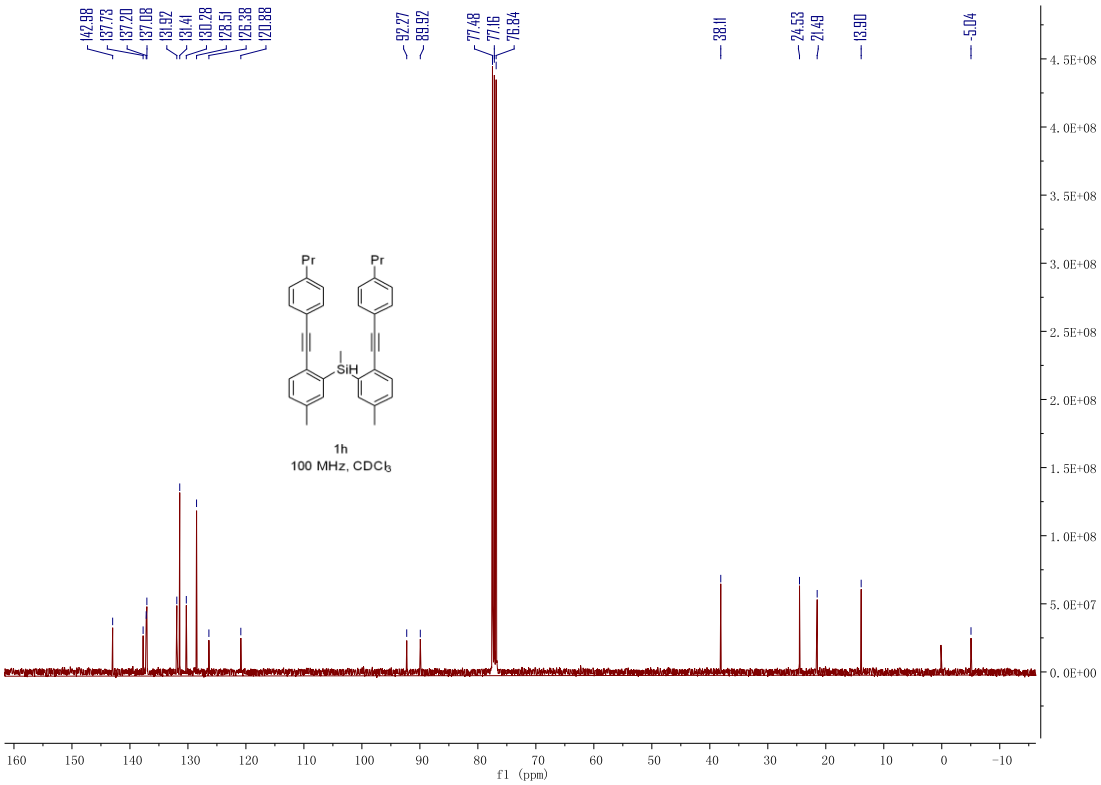

Figure S17. ^{13}C NMR (100 MHz, $CDCl_3$) spectrum of compound **1h**, related to **Scheme 2**

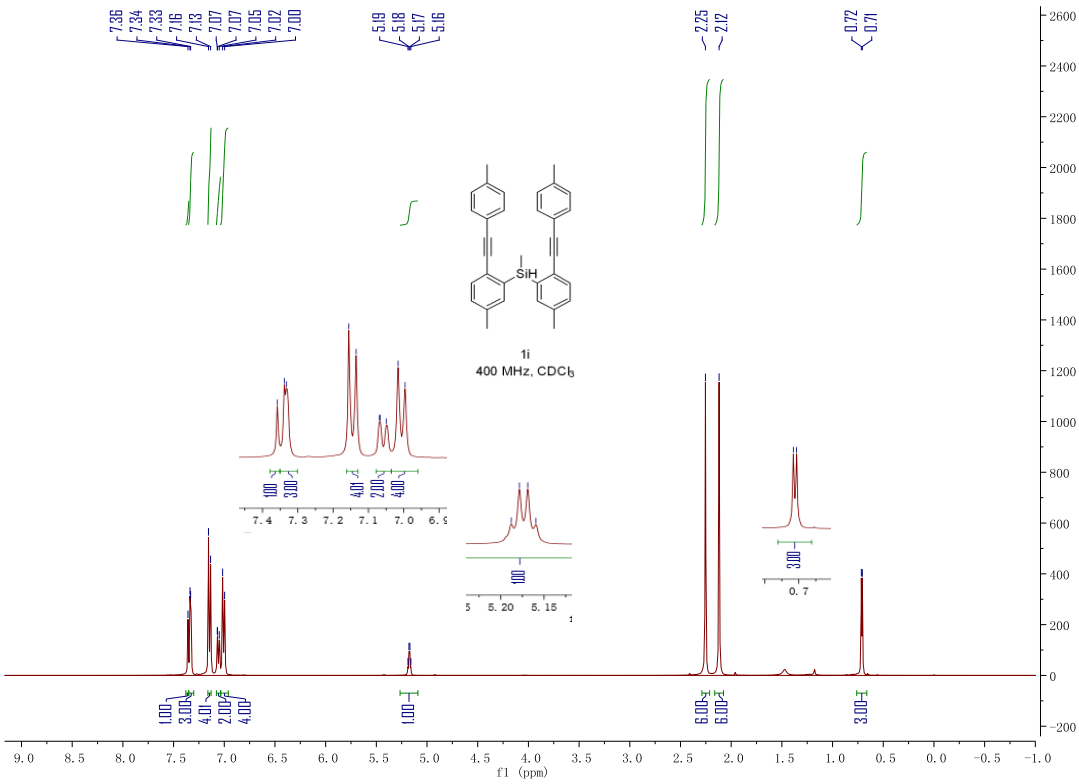

Figure S18. ^{1}H NMR (400 MHz, $CDCl_3$) spectrum of compound **1i**, related to **Scheme 2**

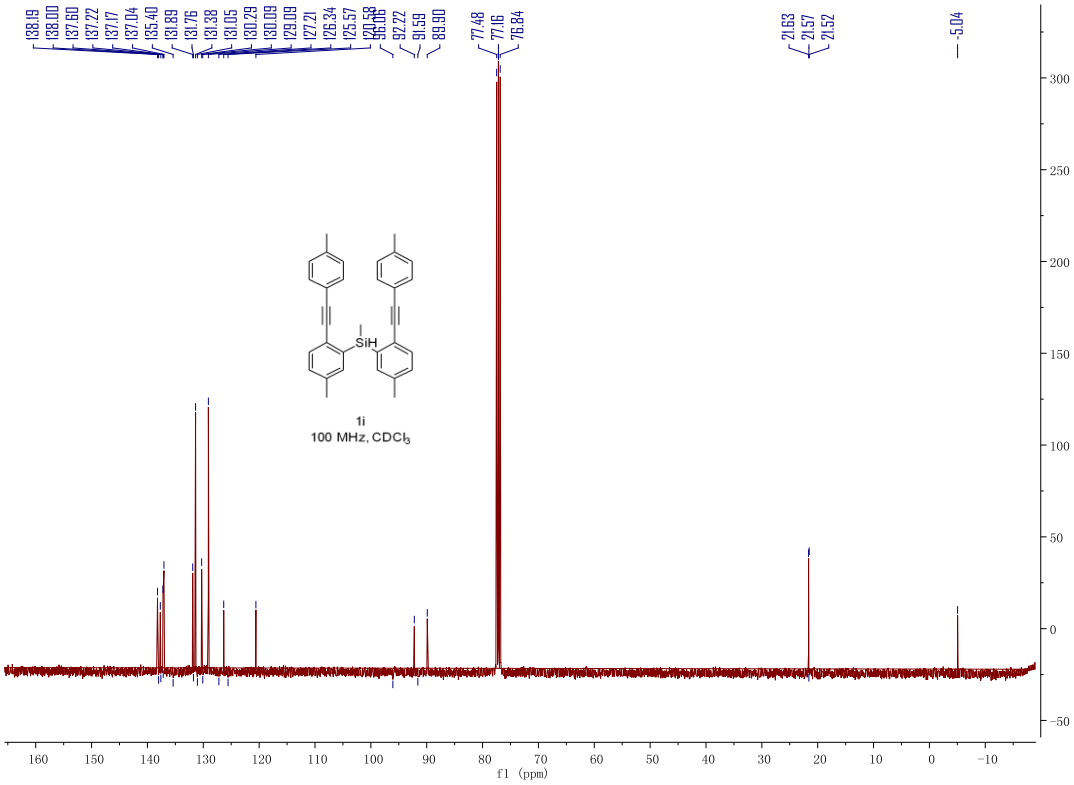

Figure S19. ^{13}C NMR (100 MHz, $CDCl_3$) spectrum of compound **1i**, related to **Scheme 2**

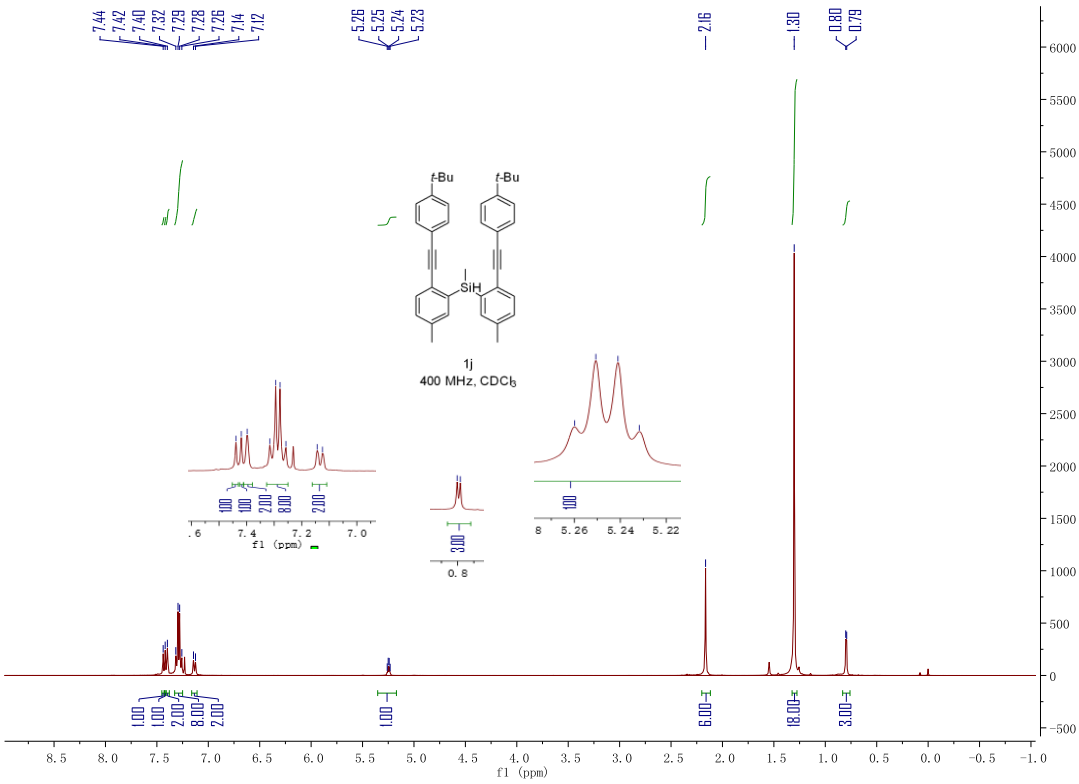

Figure S20. ^{1}H NMR (400 MHz, $CDCl_3$) spectrum of compound **1j**, related to **Scheme 2**

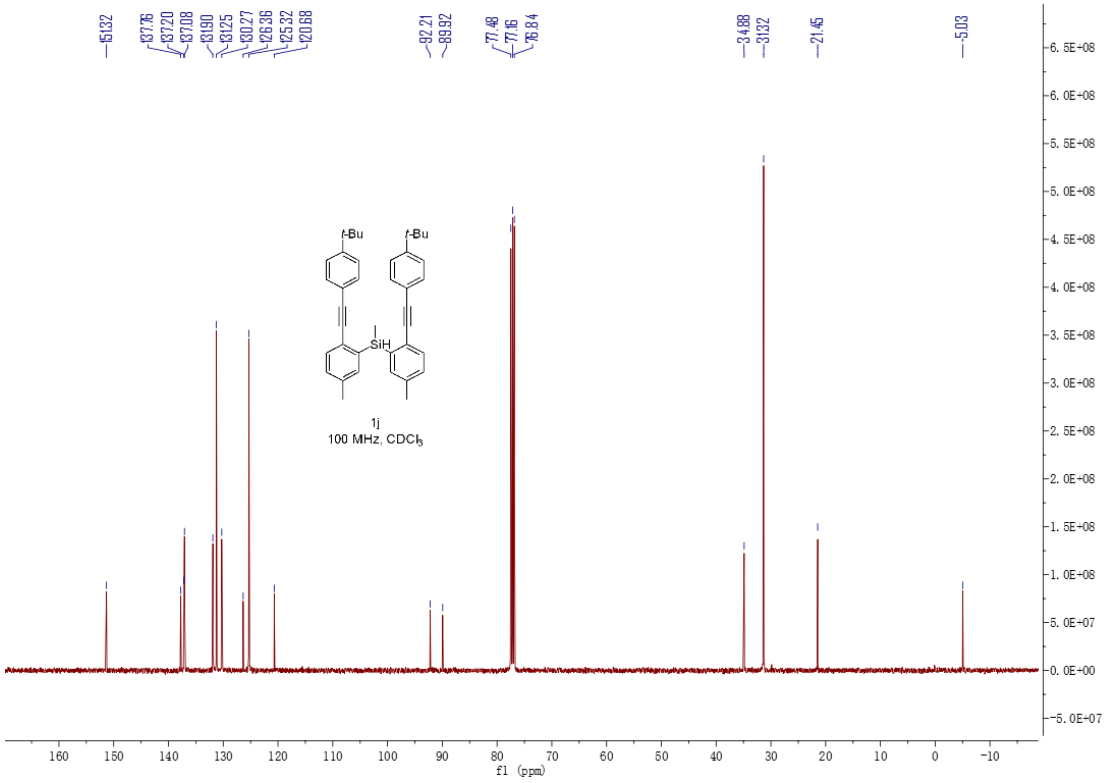

Figure S21. ^{13}C NMR (100 MHz, $CDCl_3$) spectrum of compound **1j**, related to **Scheme 2**

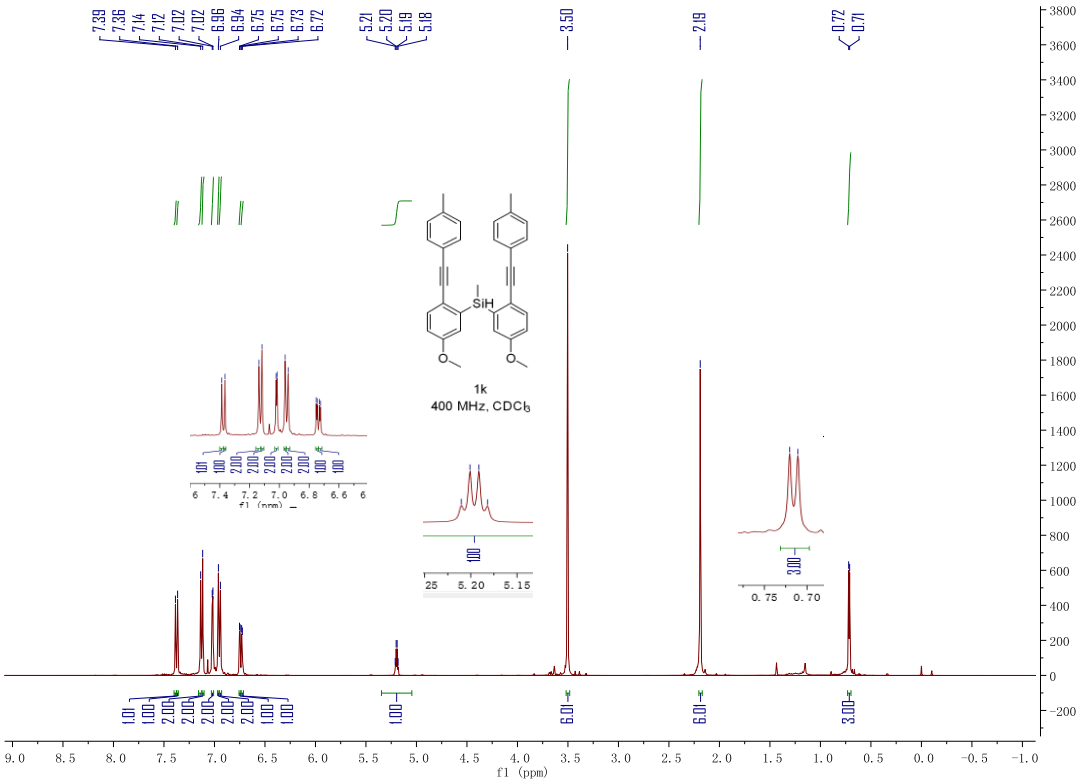

Figure S22. ^{1}H NMR (400 MHz, $CDCl_3$) spectrum of compound **1k**, related to **Scheme 2**

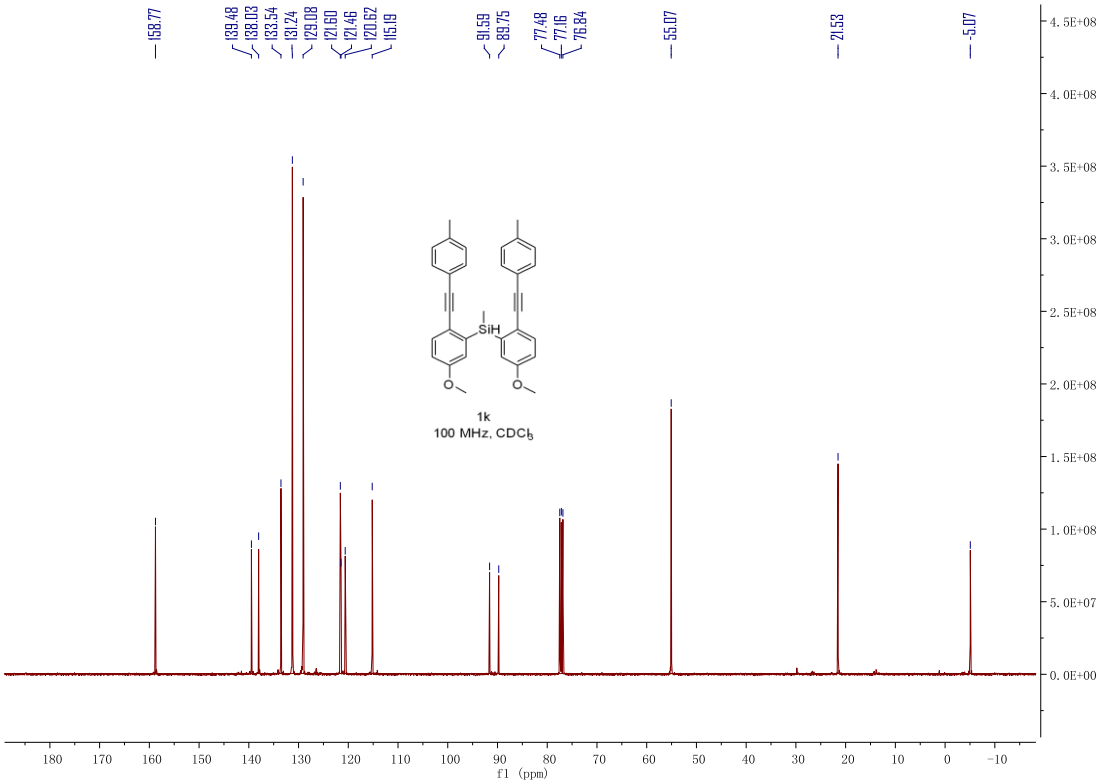

Figure S23. ^{13}C NMR (100 MHz, $CDCl_3$) spectrum of compound **1k**, related to **Scheme 2**

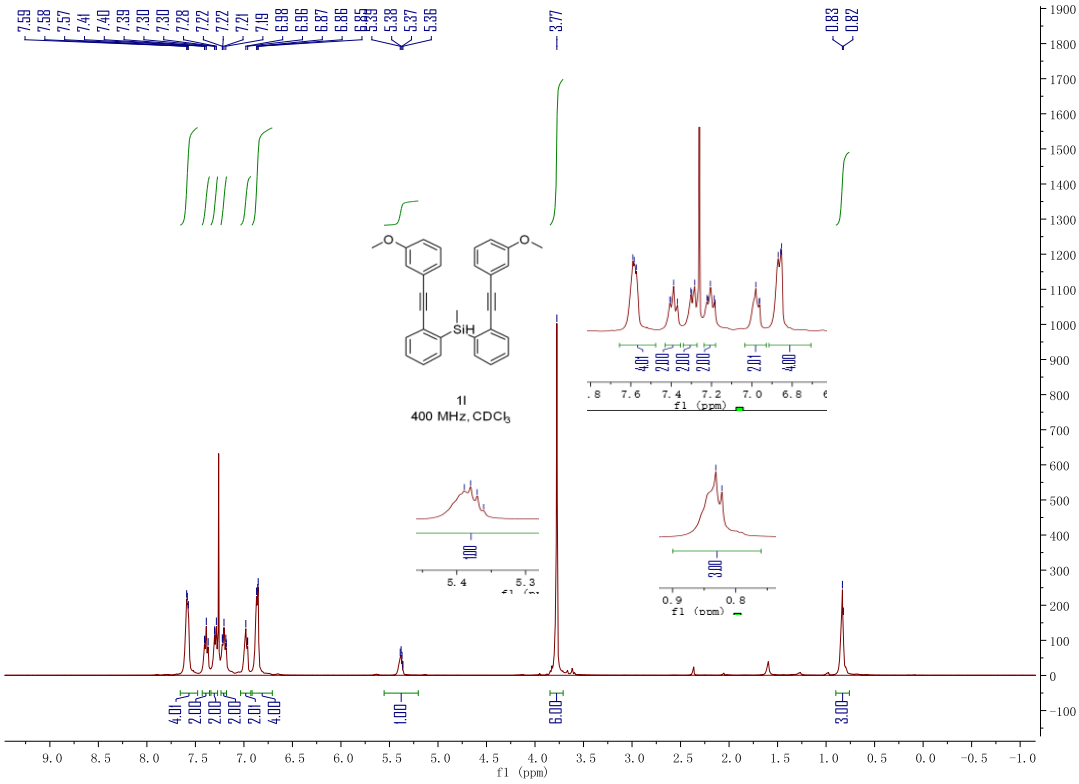

Figure S24. ^{1}H NMR (400 MHz, $CDCl_3$) spectrum of compound **1l**, related to **Scheme 2**

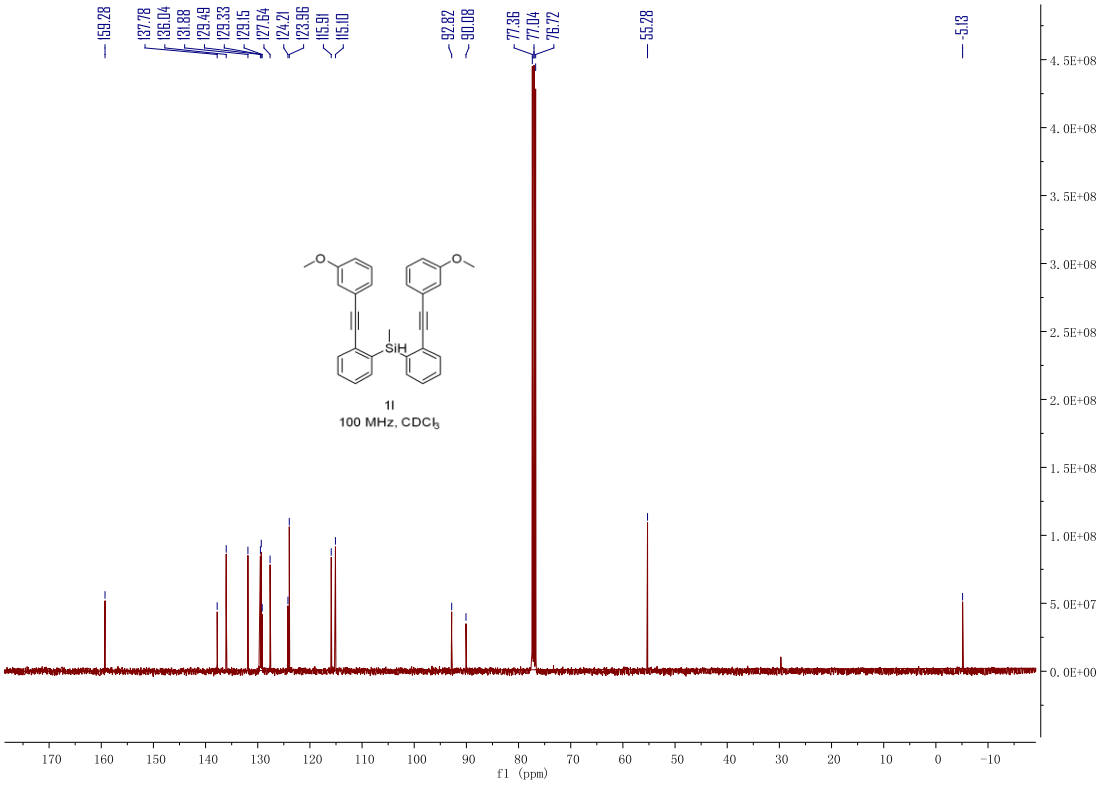

Figure S25. ^{13}C NMR (100 MHz, $CDCl_3$) spectrum of compound **1l**, related to **Scheme 2**

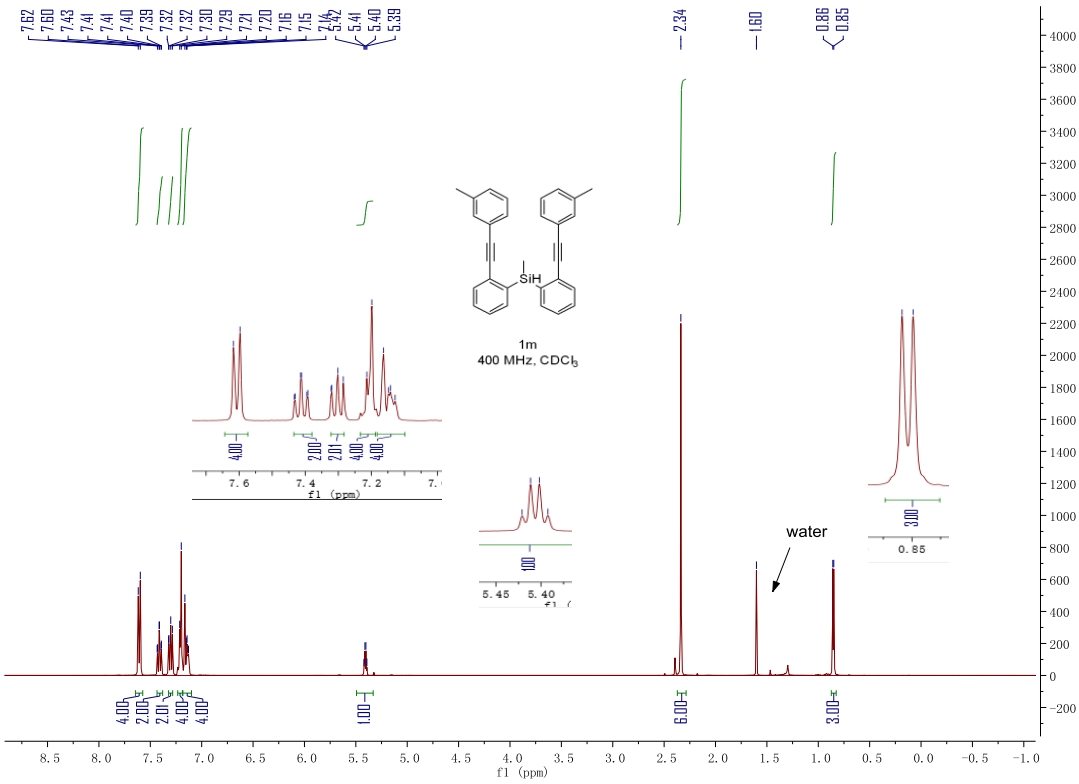

Figure S26. ^{1}H NMR (400 MHz, $CDCl_3$) spectrum of compound **1m**, related to **Scheme 2**

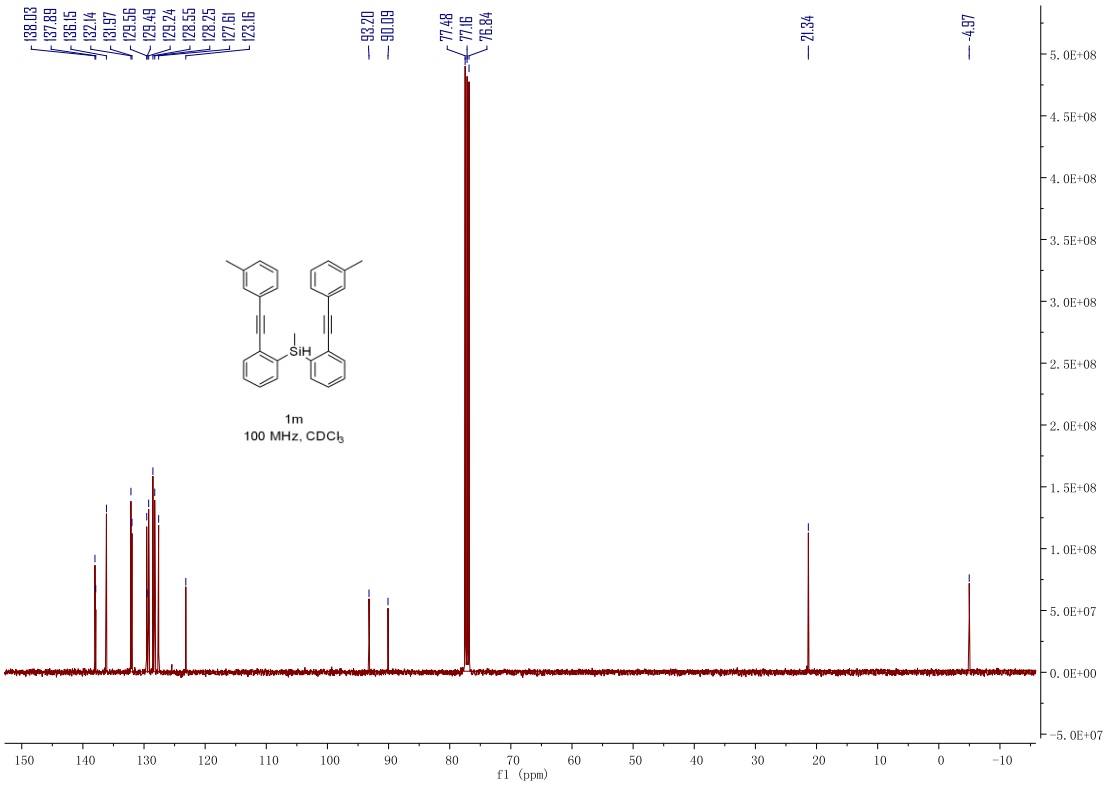

Figure S27. ^{13}C NMR (100 MHz, $CDCl_3$) spectrum of compound **1m**, related to **Scheme 2**

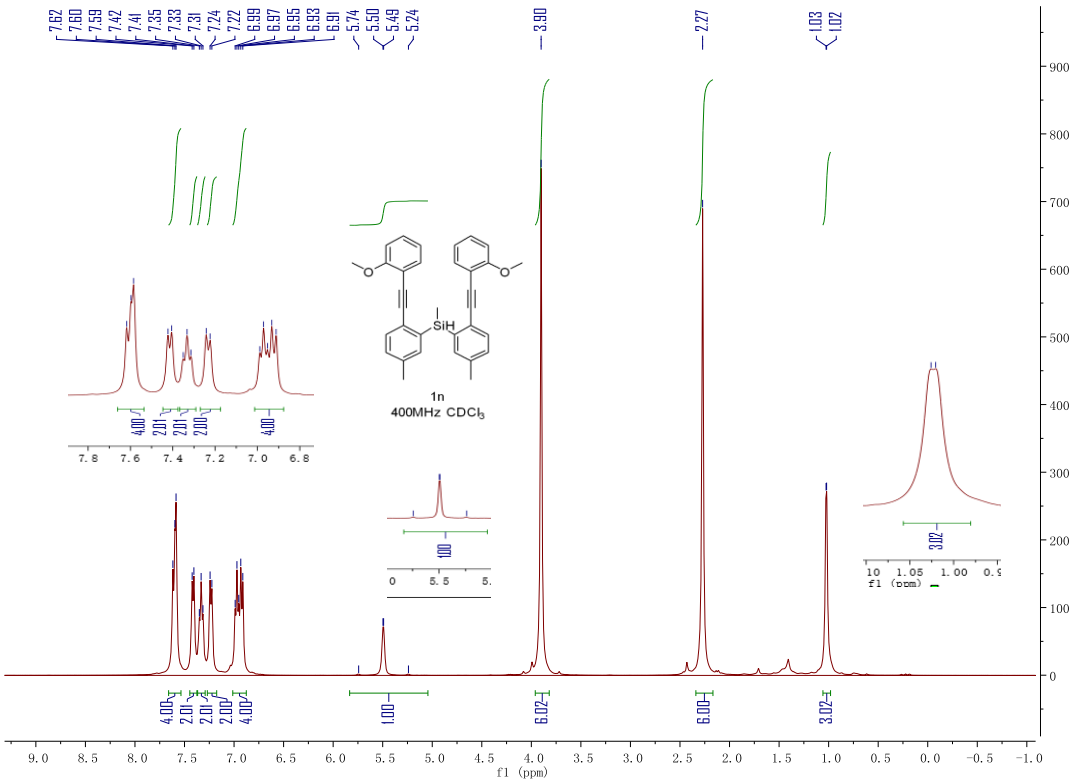

Figure S28. ^{1}H NMR (400 MHz, $CDCl_3$) spectrum of compound **1n**, related to **Scheme 2**

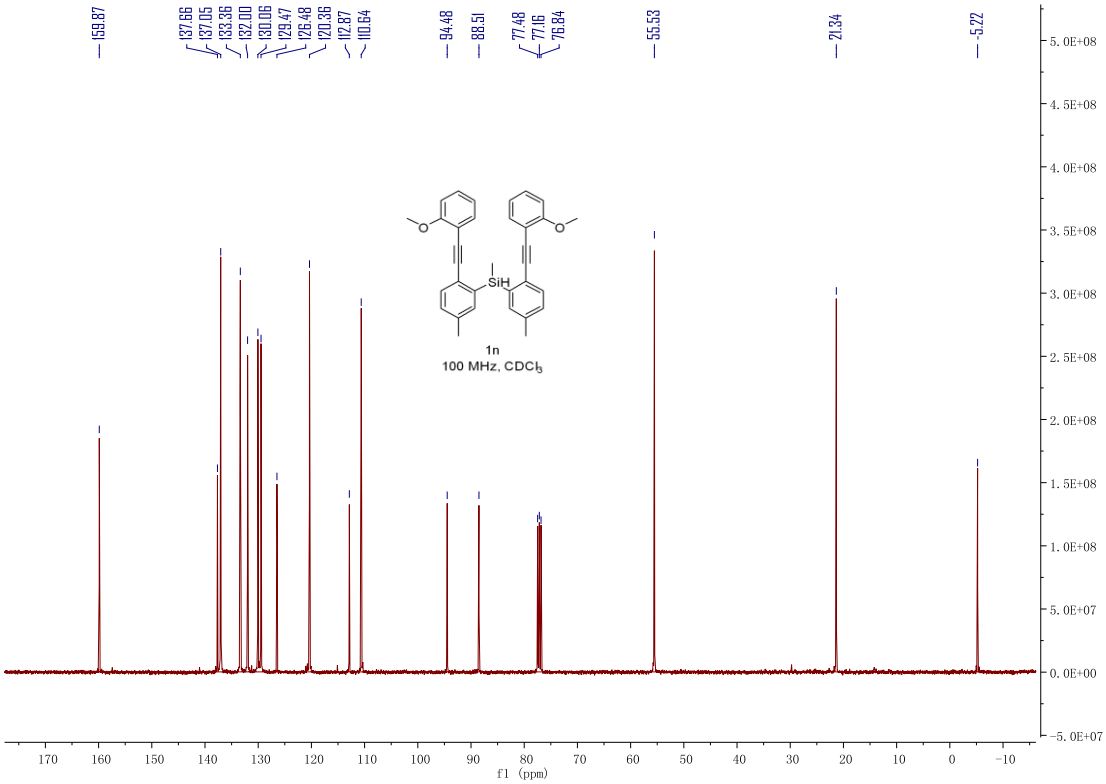

Figure S29. ^{13}C NMR (100 MHz, $CDCl_3$) spectrum of compound **1n**, related to **Scheme 2**

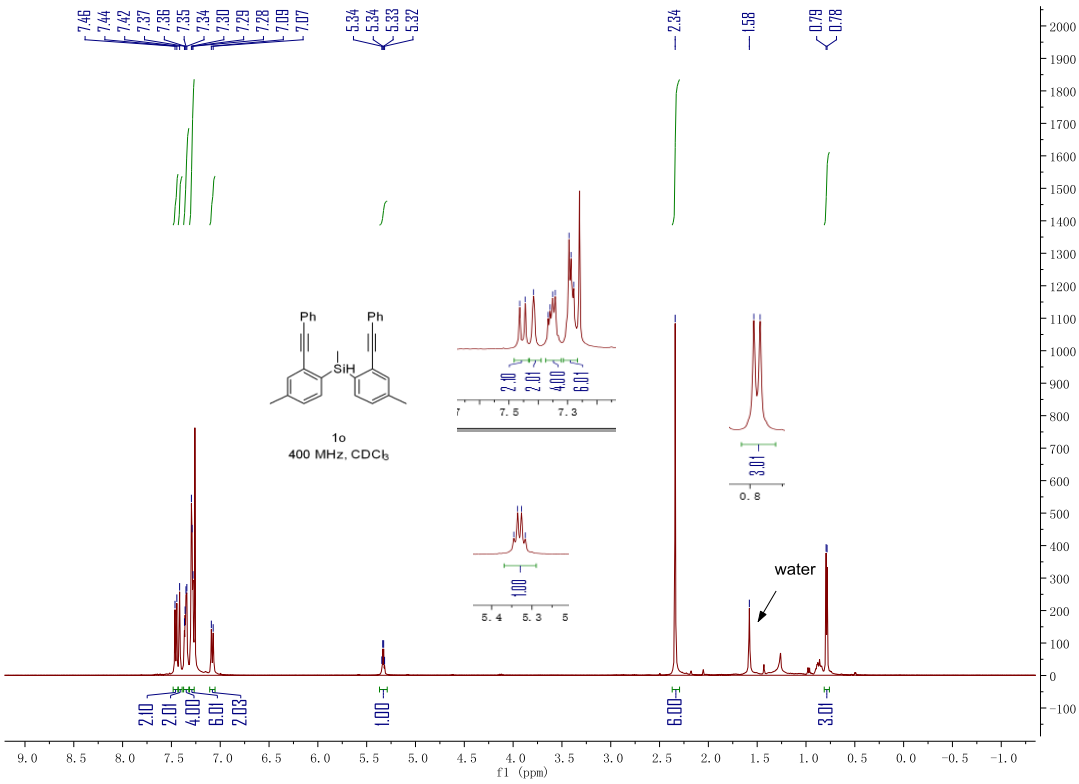

Figure S30. ^{1}H NMR (400 MHz, $CDCl_3$) spectrum of compound **1o**, related to **Scheme 2**

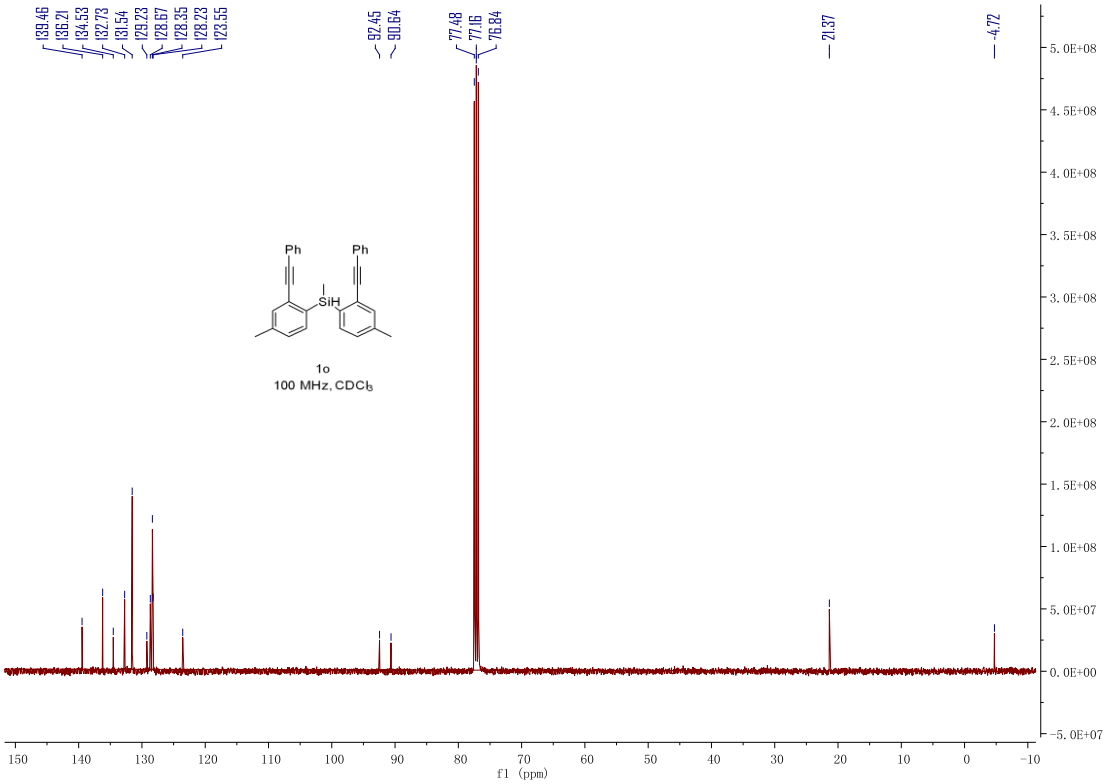

Figure S31. ^{13}C NMR (100 MHz, $CDCl_3$) spectrum of compound **1o**, related to **Scheme 2**

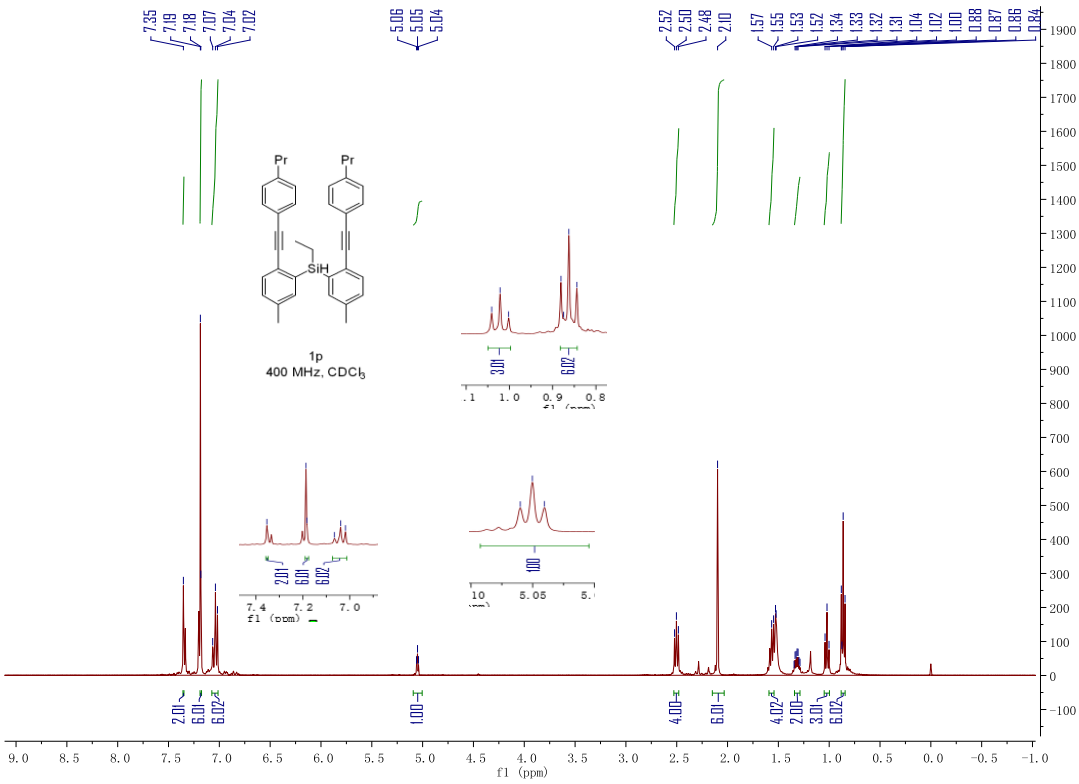

Figure S32. ^{1}H NMR (400 MHz, $CDCl_3$) spectrum of compound **1p**, related to **Scheme 2**

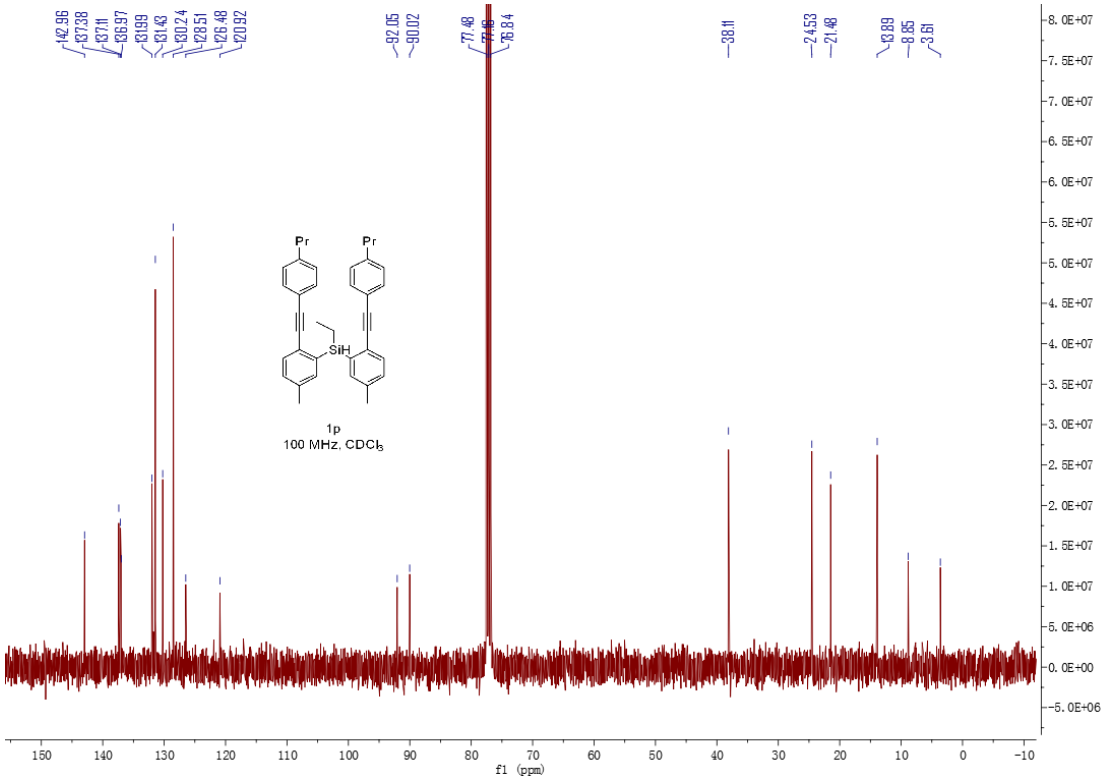

Figure S33. ^{13}C NMR (100 MHz, $CDCl_3$) spectrum of compound **1p**, related to **Scheme 2**

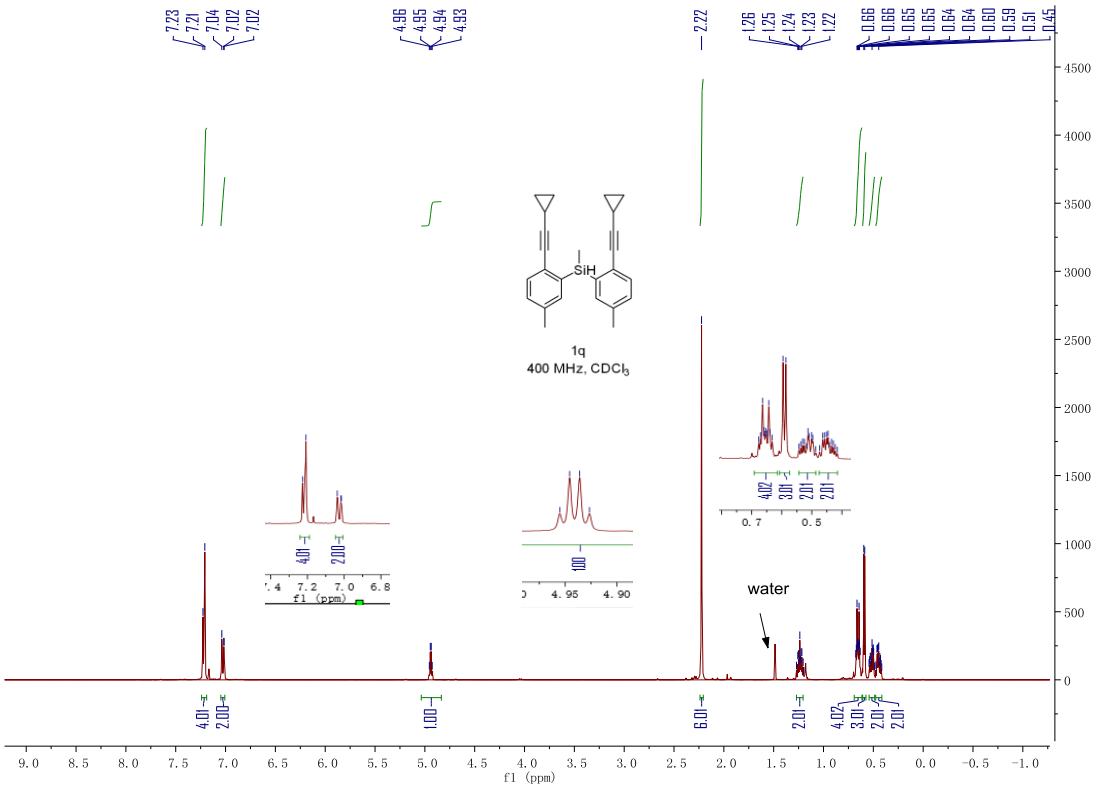

Figure S34. ^{1}H NMR (400 MHz, $CDCl_3$) spectrum of compound **1q**, related to **Scheme 2**

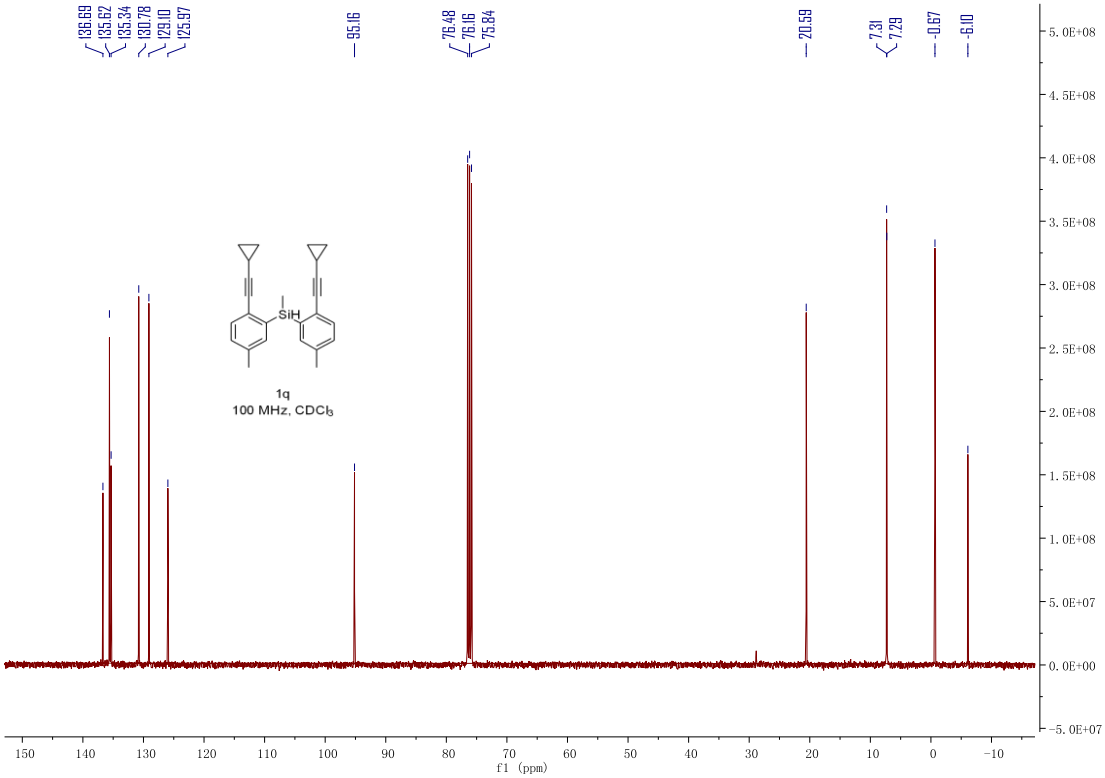

Figure S35. ^{13}C NMR (100 MHz, $CDCl_3$) spectrum of compound **1q**, related to **Scheme 2**

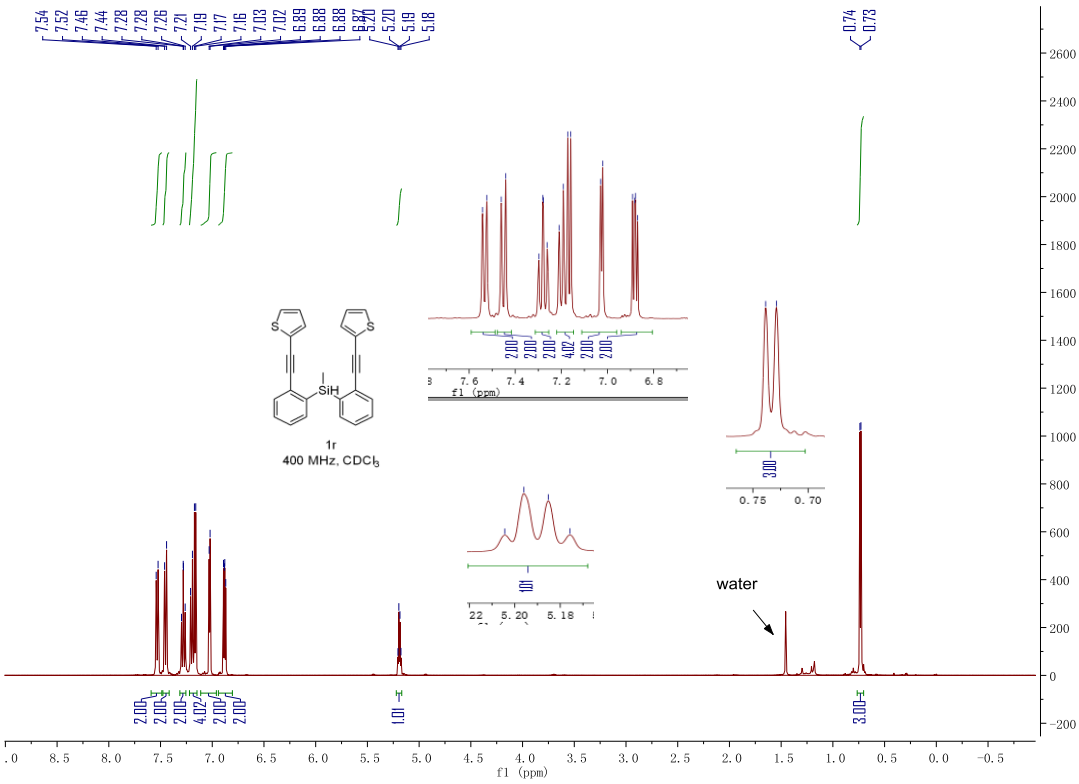

Figure S36. ^{1}H NMR (400 MHz, $CDCl_3$) spectrum of compound **1r**, related to **Scheme 2**

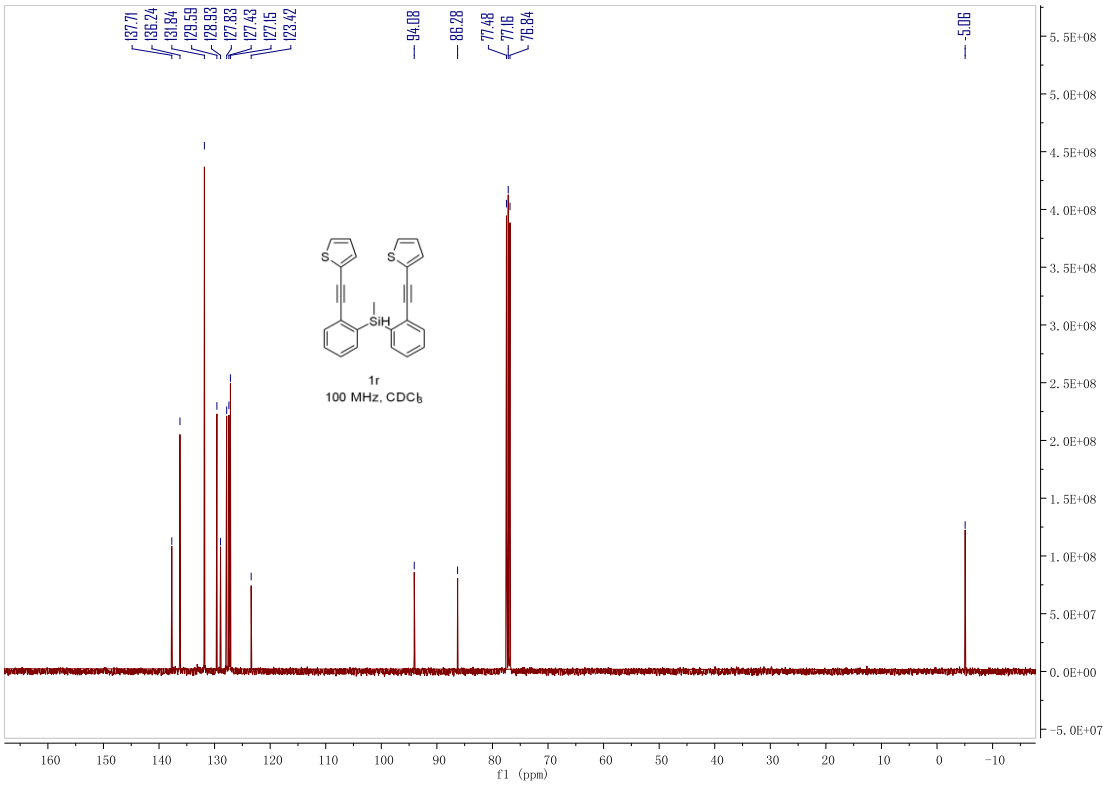

Figure S37. ^{13}C NMR (100 MHz, $CDCl_3$) spectrum of compound **1r**, related to **Scheme 2**

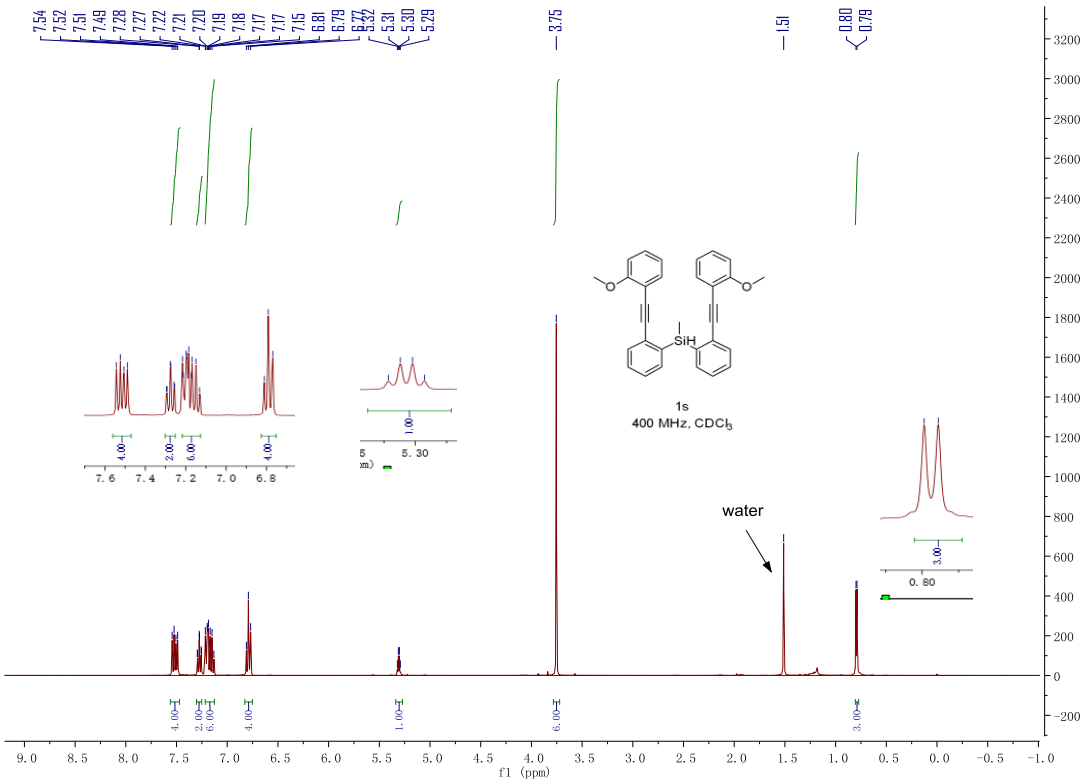

Figure S38. ^{1}H NMR (400 MHz, $CDCl_3$) spectrum of compound **1s**, related to **Scheme 2**

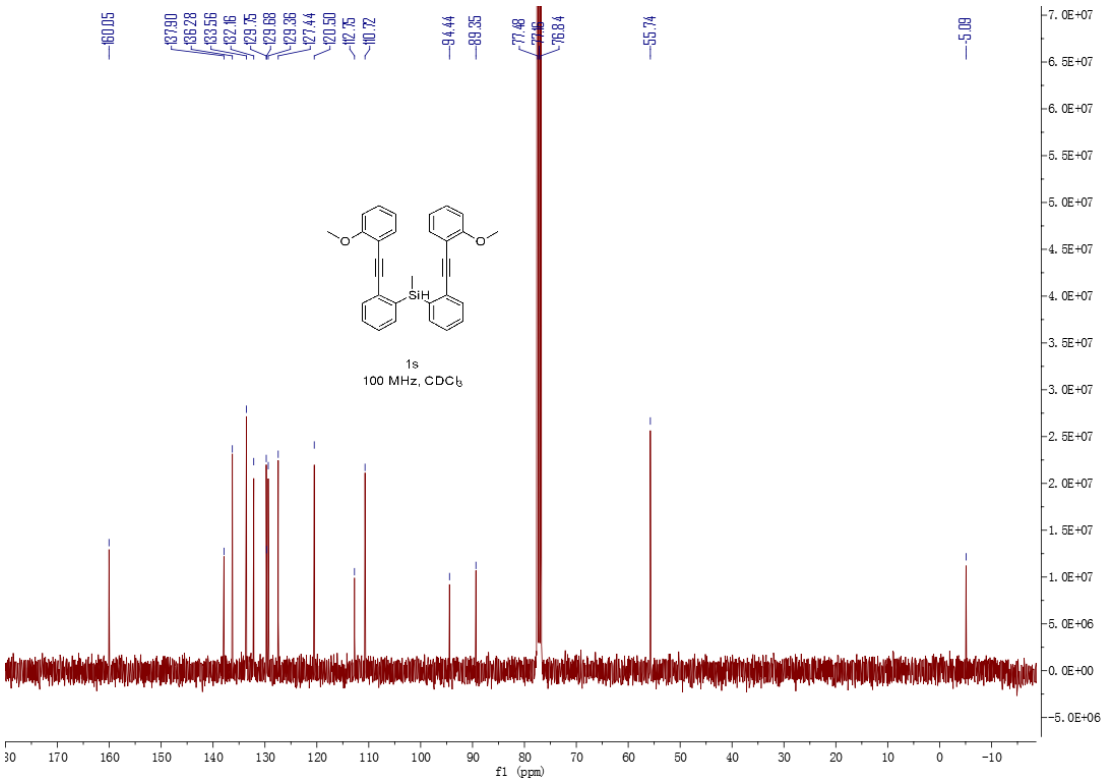

Figure S39. ^{13}C NMR (100 MHz, $CDCl_3$) spectrum of compound **1s**, related to **Scheme 2**

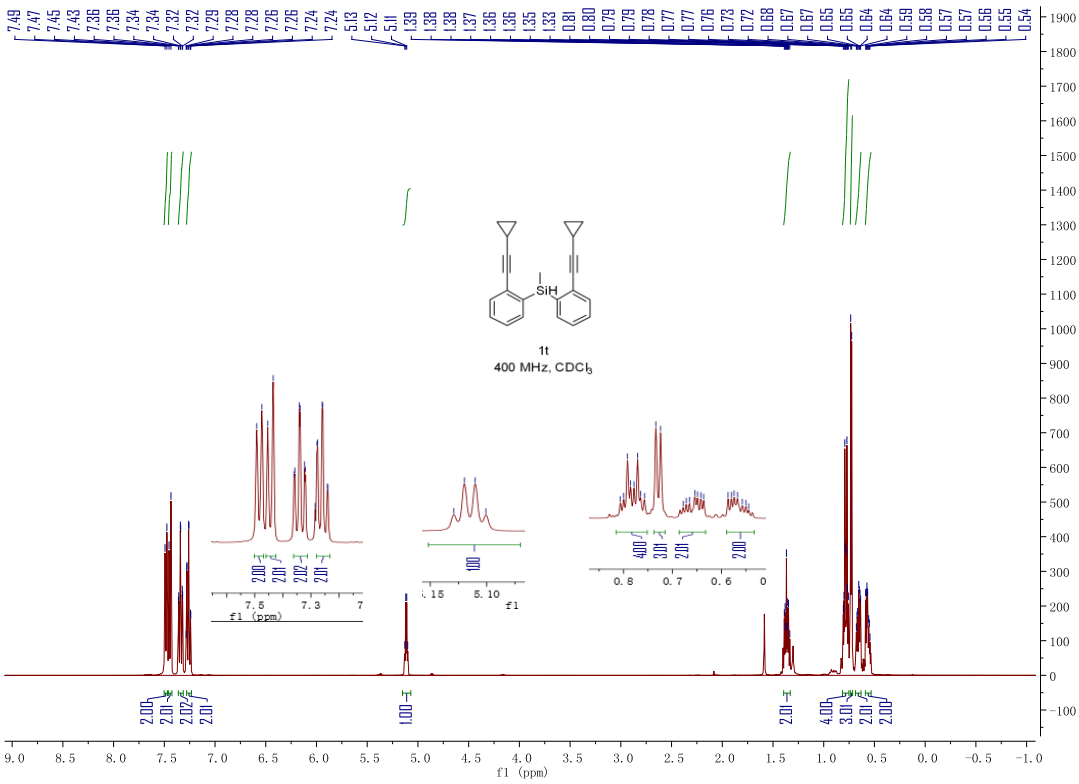

Figure S40. ^{1}H NMR (400 MHz, $CDCl_3$) spectrum of compound **1t**, related to **Scheme 2**

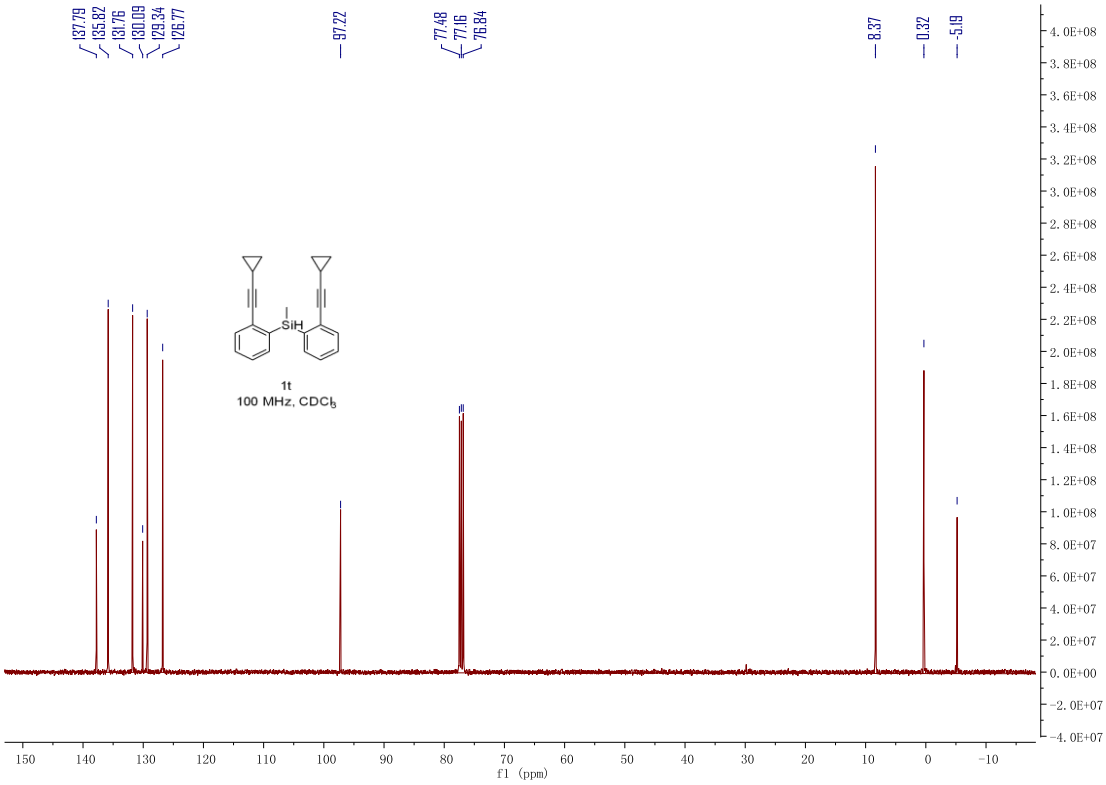

Figure S41. ^{13}C NMR (100 MHz, $CDCl_3$) spectrum of compound **1t**, related to **Scheme 2**

5.2 NMR spectra of products 2 (benzosiloles)

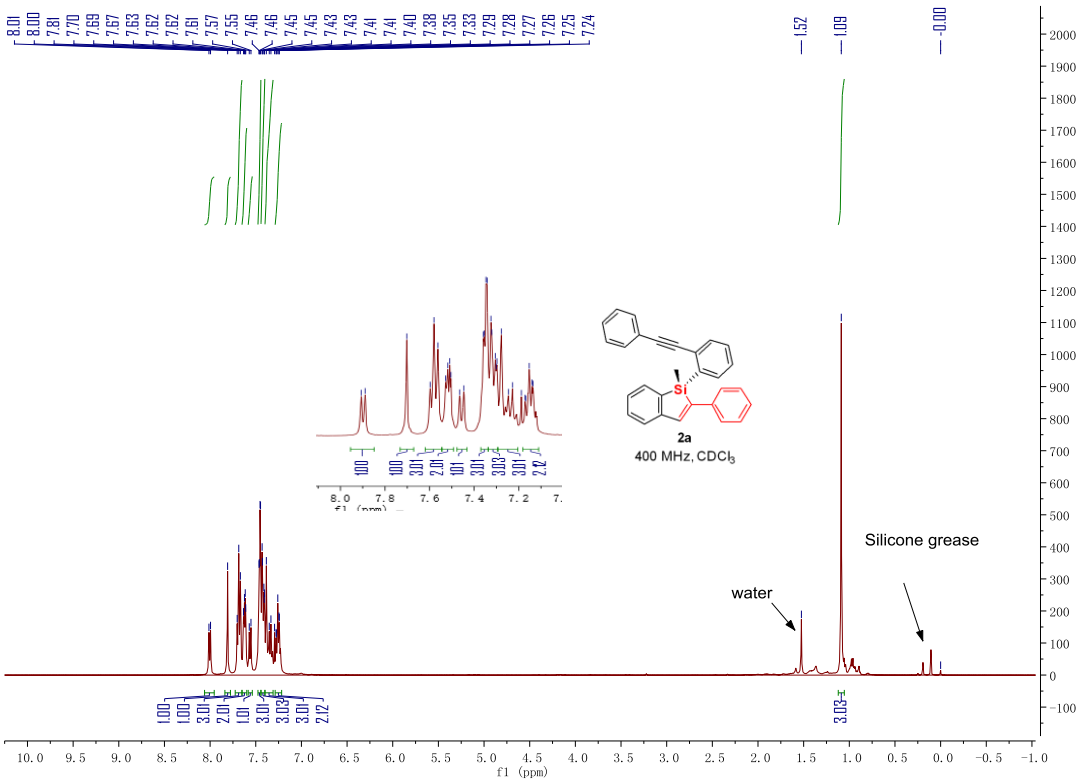

Figure S42. ^{1}H NMR (400 MHz, $CDCl_3$) spectrum of compound **2a** , related to **Scheme 2**

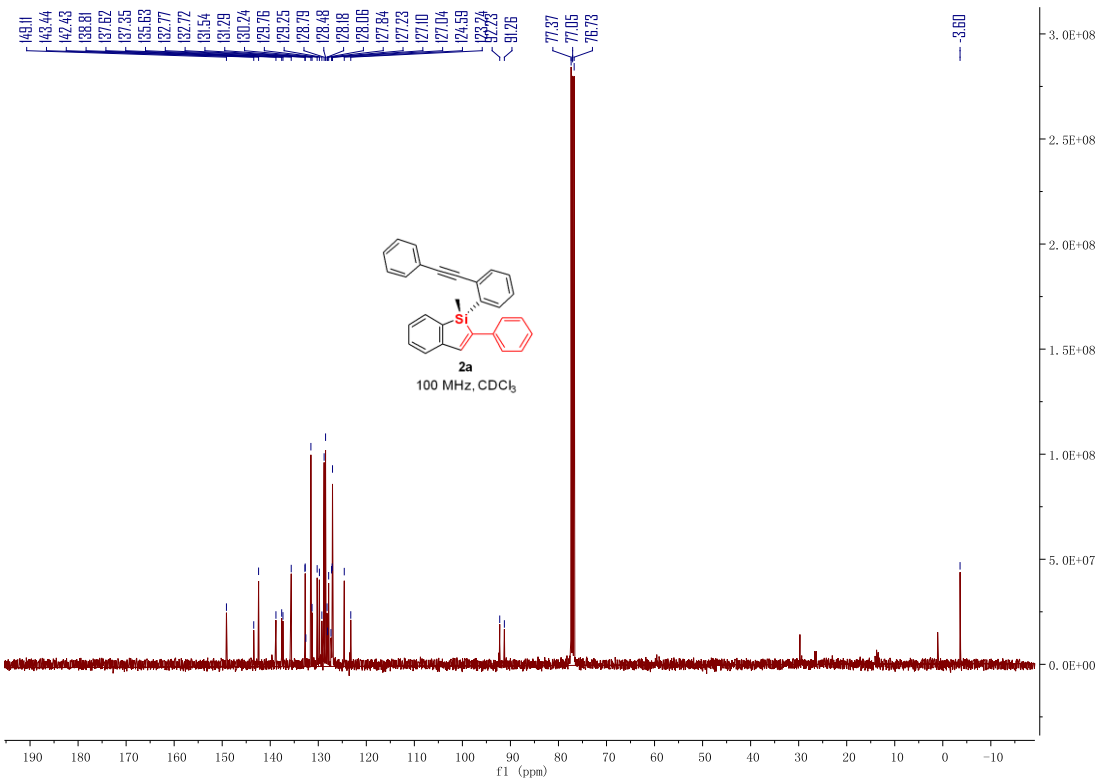

Figure S43. ^{13}C NMR (100 MHz, $CDCl_3$) spectrum of compound **2a,** related to **Scheme 2**

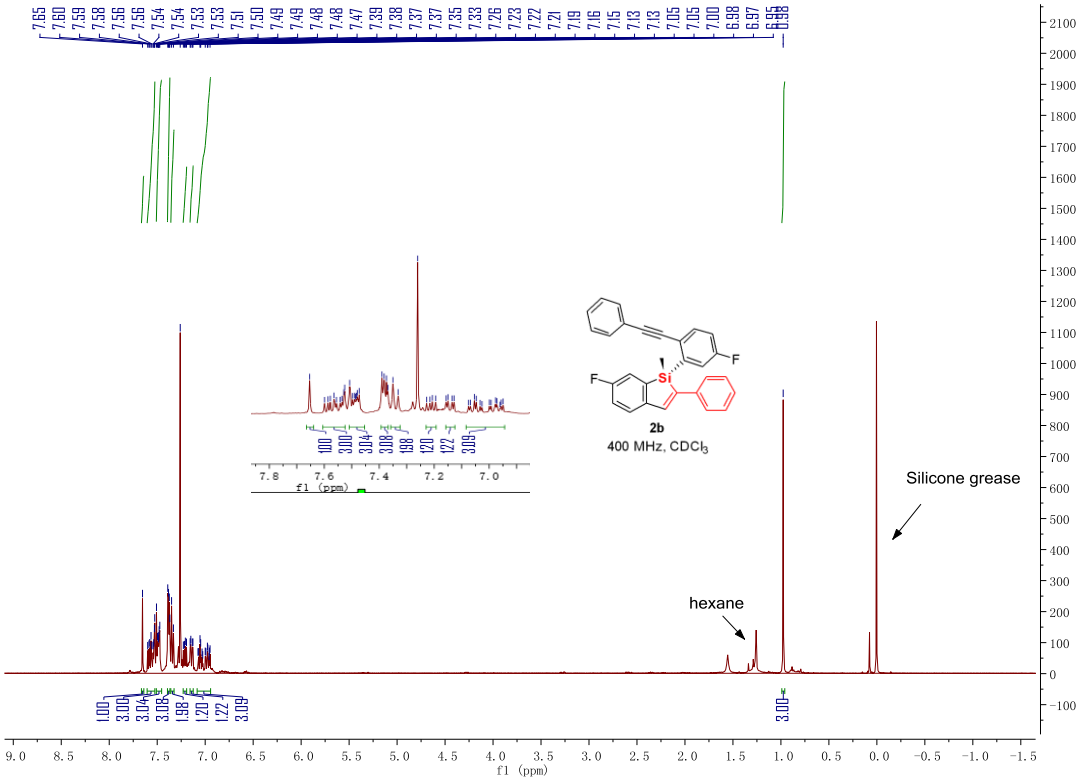

Figure S44. ^{1}H NMR (400 MHz, $CDCl_3$) spectrum of compound **2b** , related to **Scheme 2**

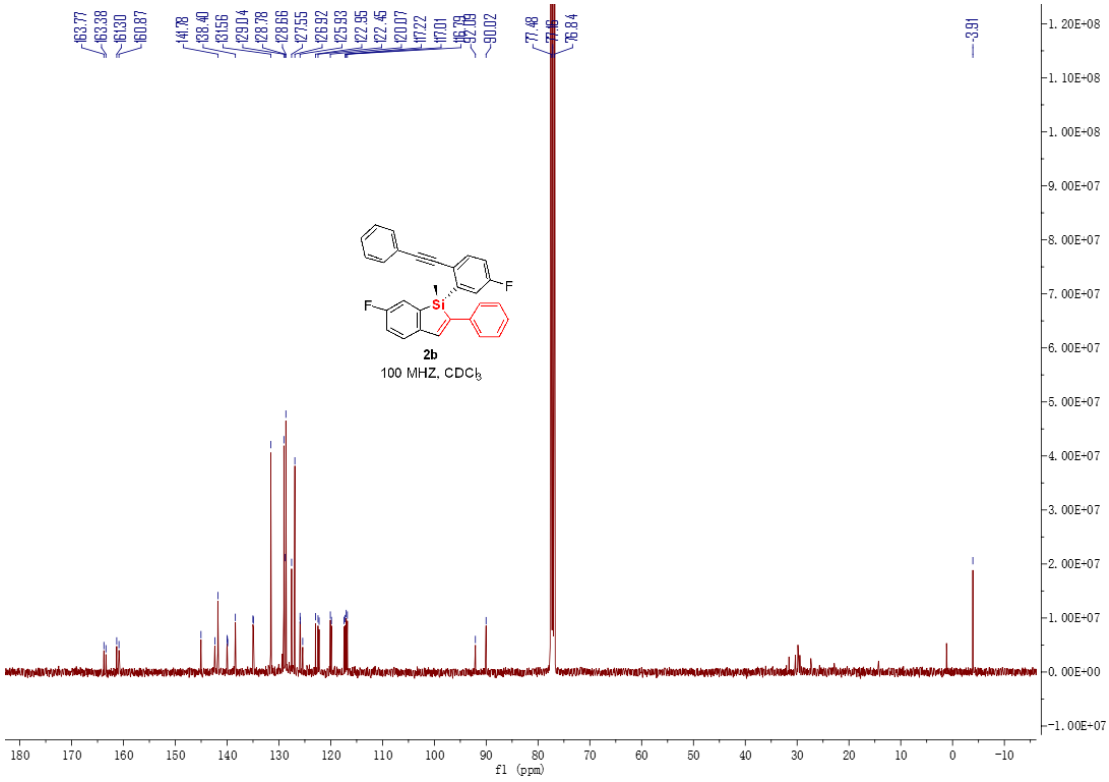

Figure S45. ^{13}C NMR (100 MHz, $CDCl_3$) spectrum of compound **2b,** related to **Scheme 2**

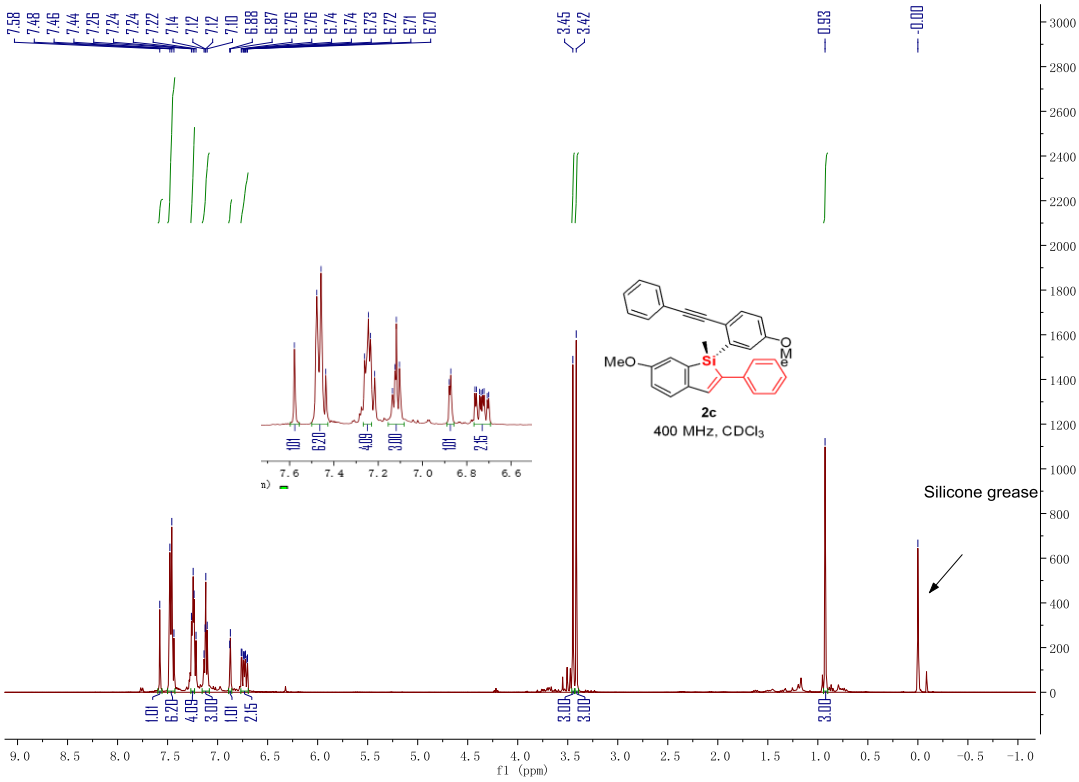

Figure S46. ^{1}H NMR (400 MHz, $CDCl_3$) spectrum of compound **2c** , related to **Scheme 2**

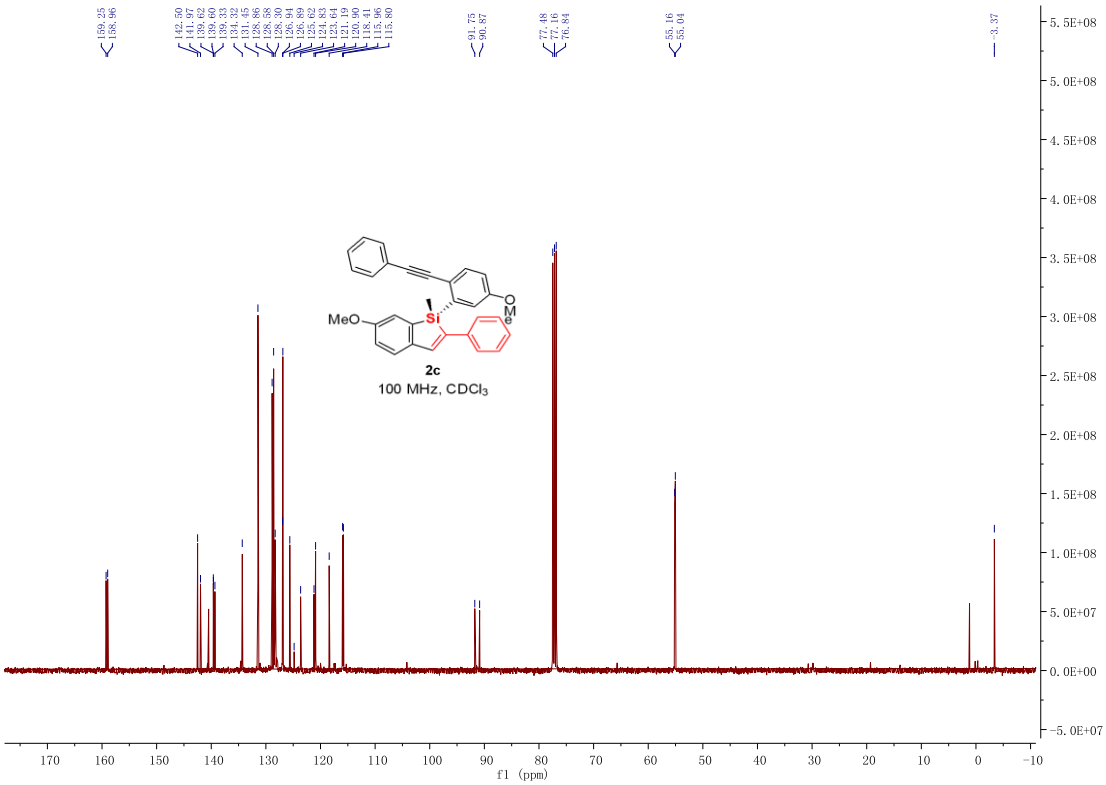

Figure S47. ^{13}C NMR (100 MHz, $CDCl_3$) spectrum of compound **2c,** related to **Scheme 2**

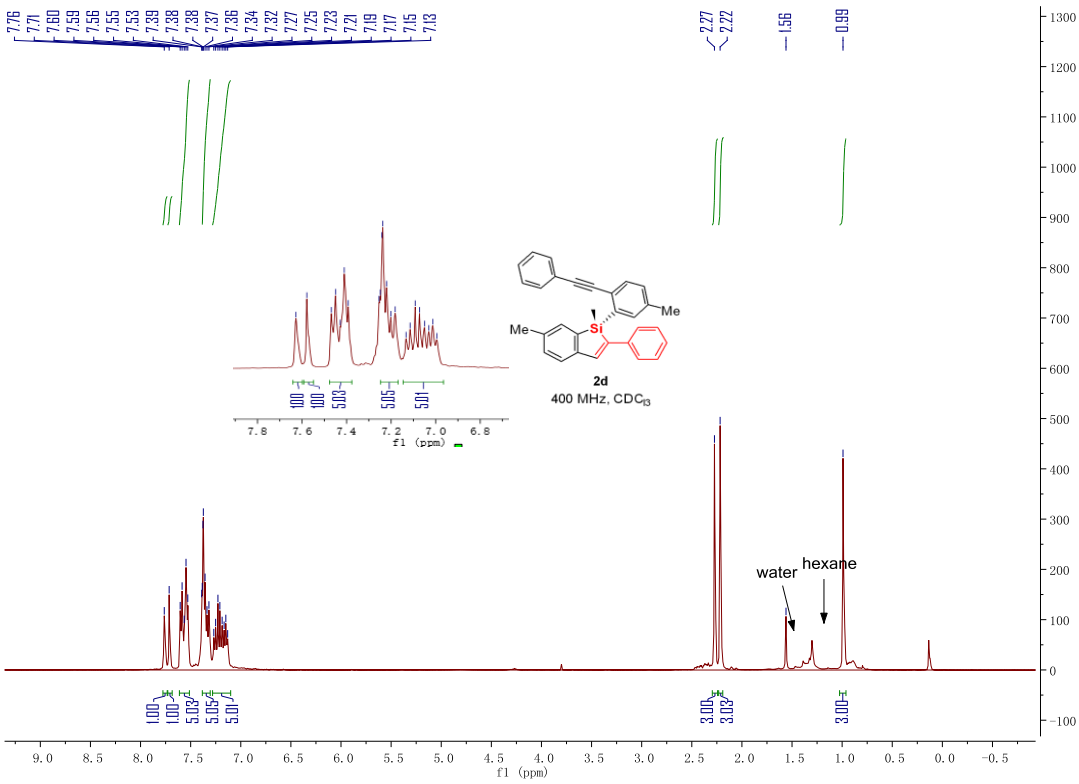

Figure S48. ^{1}H NMR (400 MHz, $CDCl_3$) spectrum of compound **2d** , related to **Scheme 2**

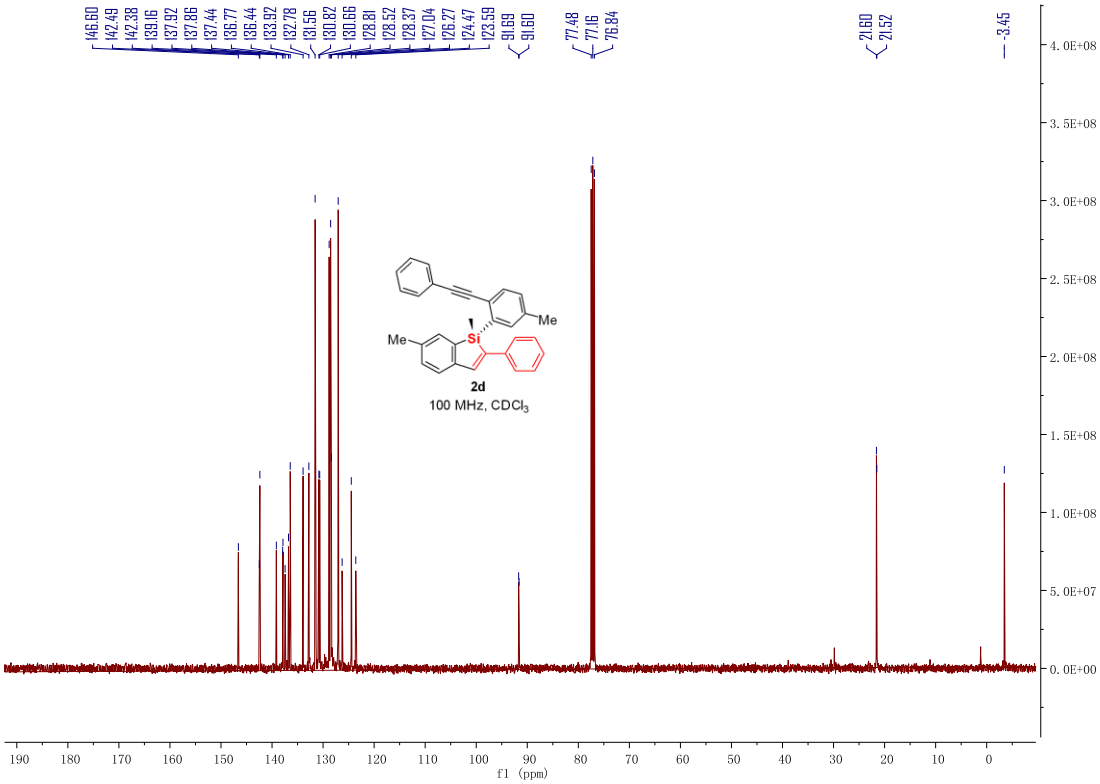

Figure S49 ^{13}C NMR (100 MHz, $CDCl_3$) spectrum of compound **2d,** related to **Scheme 2**

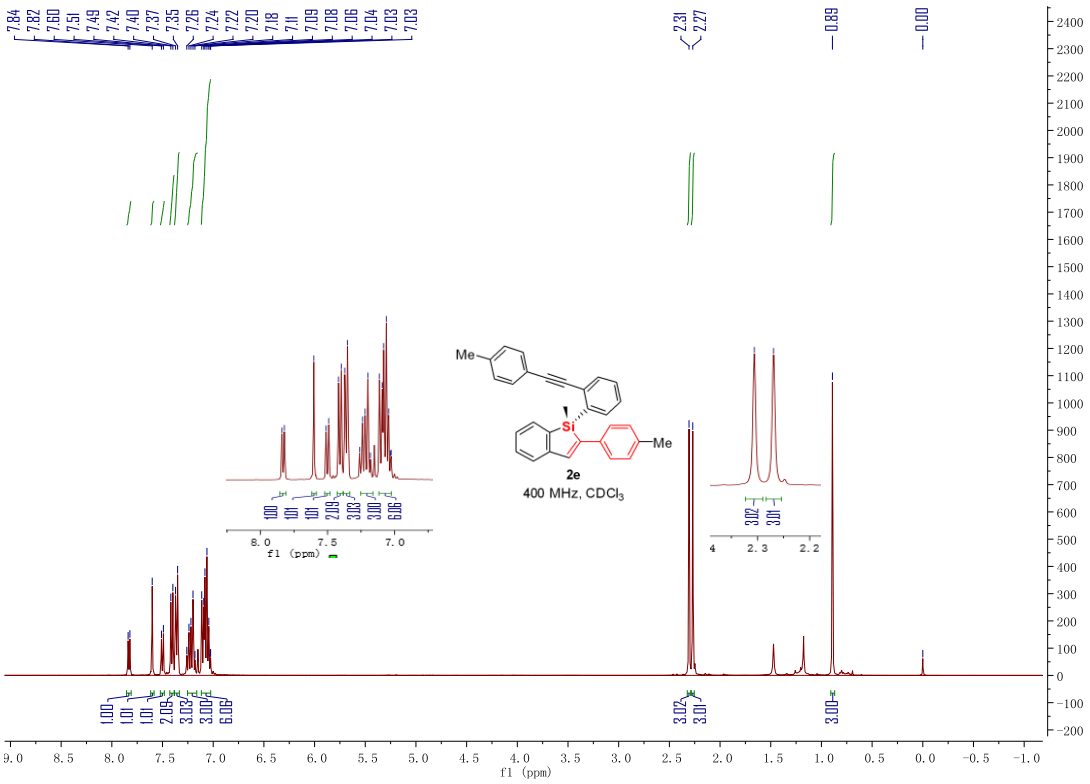

Figure S50. ^{1}H NMR (400 MHz, $CDCl_3$) spectrum of compound **2e** , related to **Scheme 2**

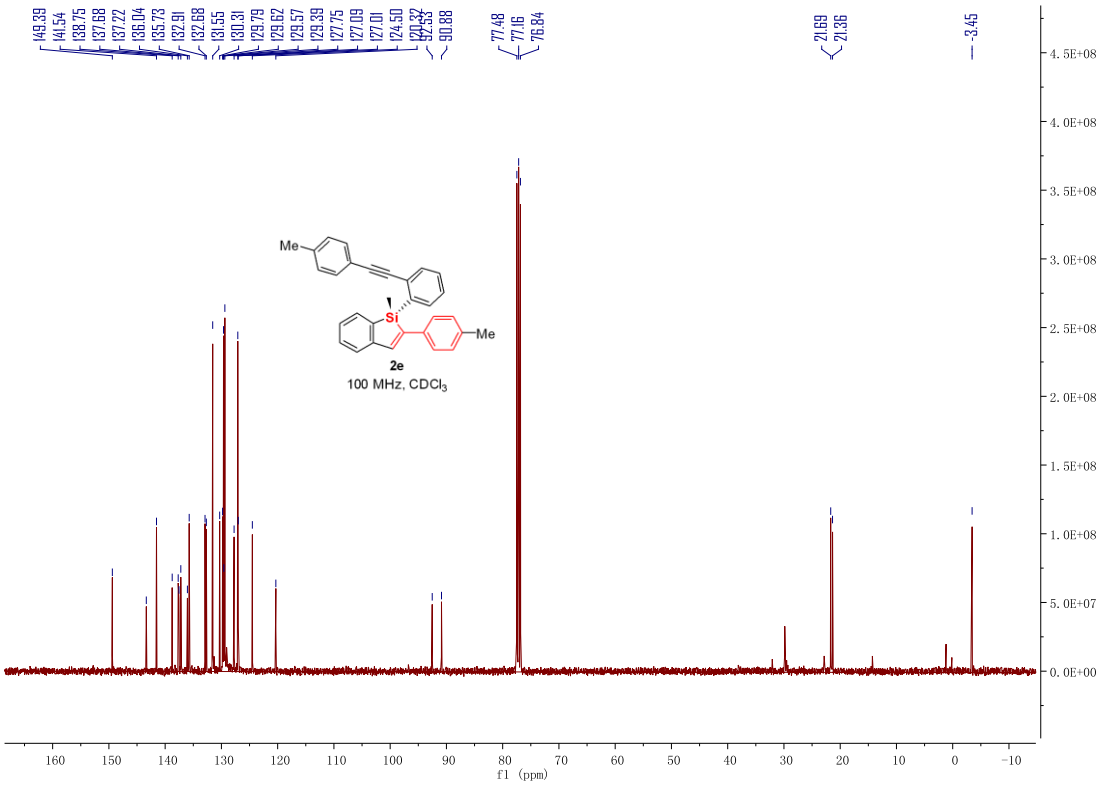

Figure S51. ^{13}C NMR (100 MHz, $CDCl_3$) spectrum of compound **2e,** related to **Scheme 2**

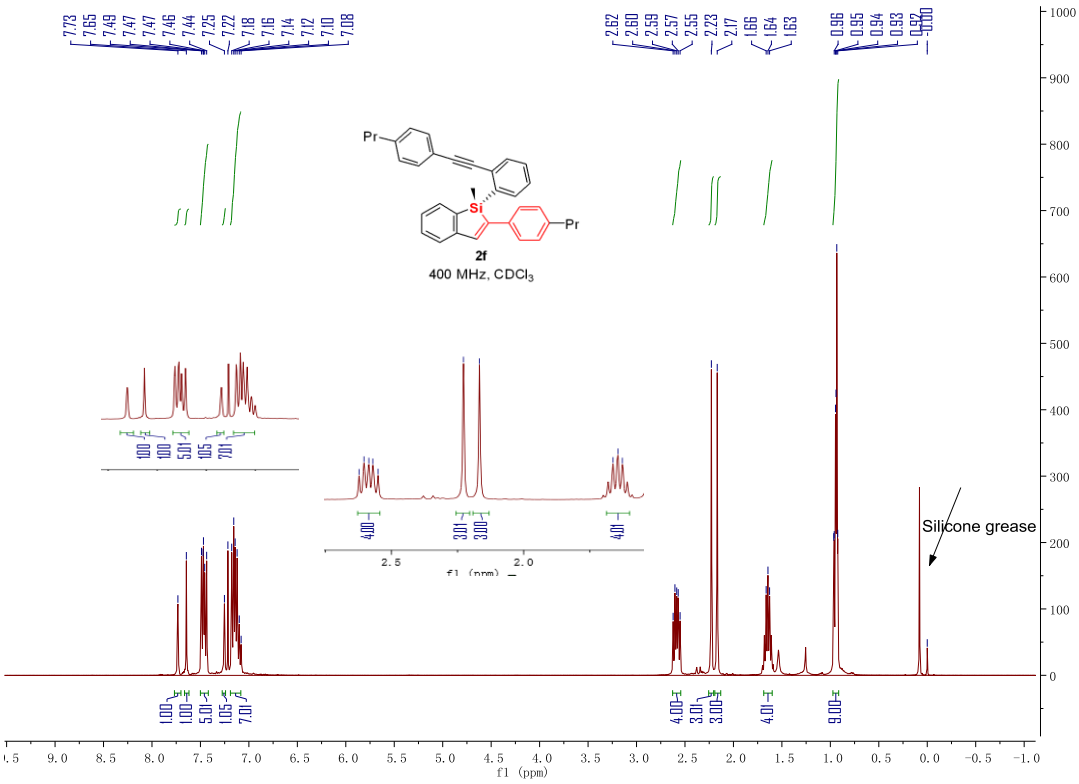

Figure S52. ^{1}H NMR (400 MHz, $CDCl_3$) spectrum of compound **2f** , related to **Scheme 2**

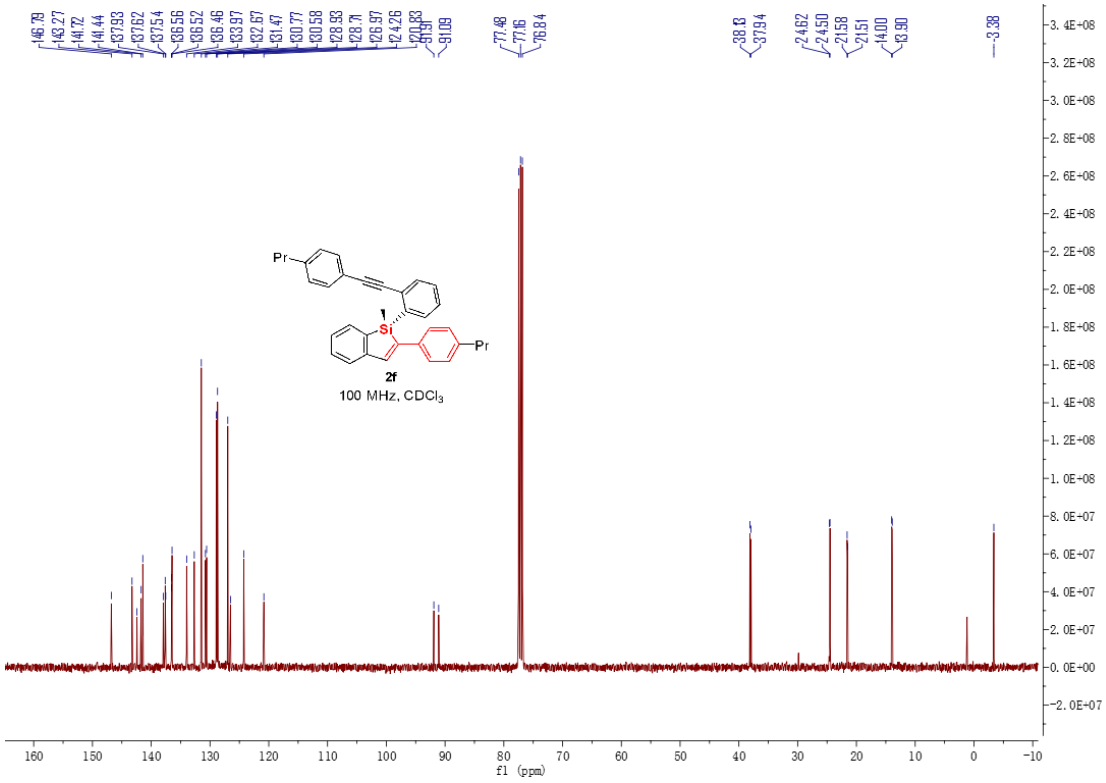

Figure S53. ^{13}C NMR (100 MHz, $CDCl_3$) spectrum of compound **2f,** related to **Scheme 2**

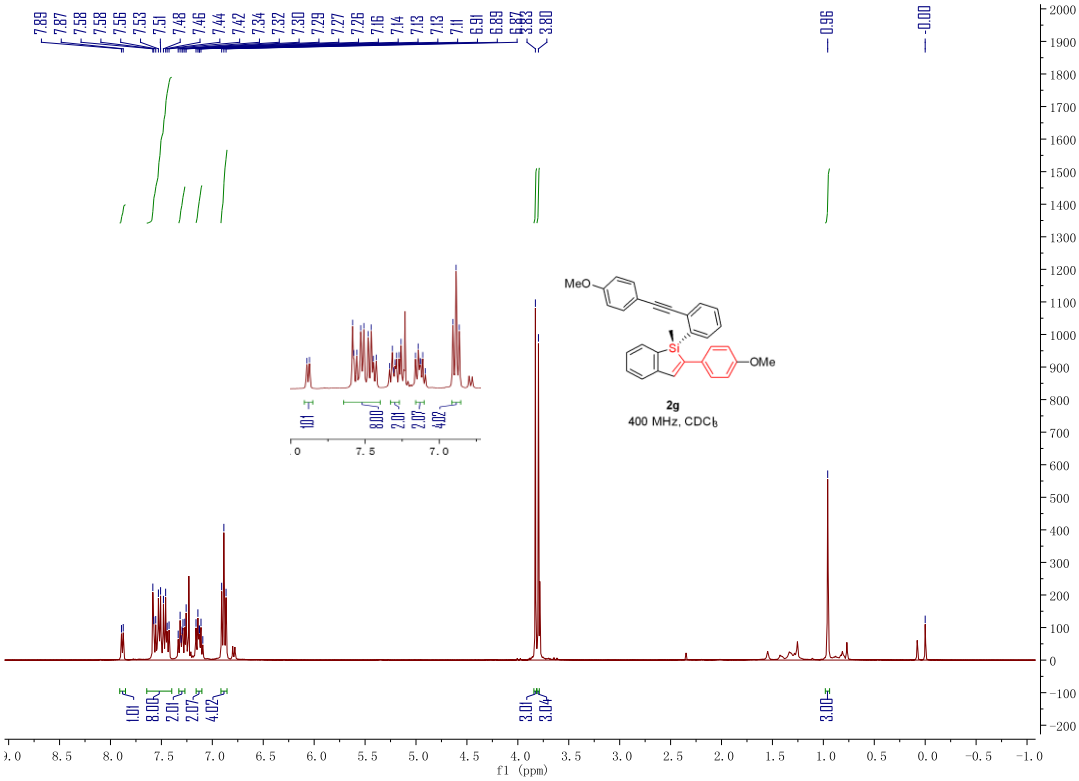

Figure S54. ^{1}H NMR (400 MHz, $CDCl_3$) spectrum of compound **2g** , related to **Scheme 2**

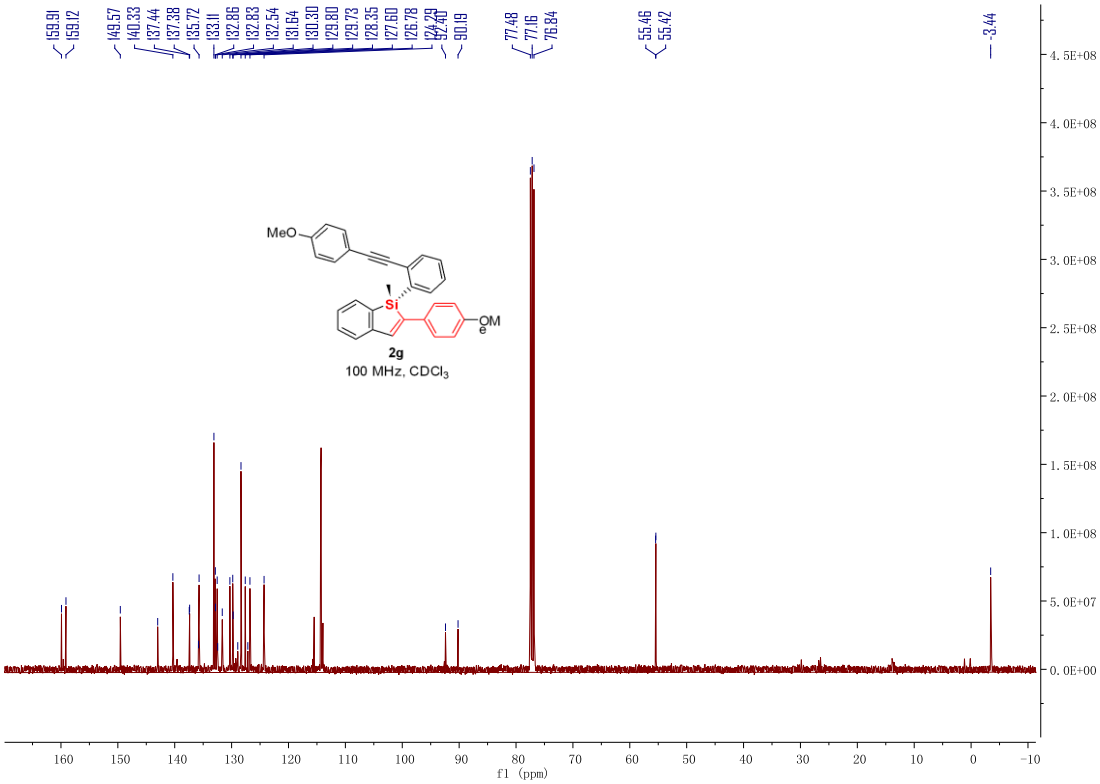

Figure S55. ^{13}C NMR (100 MHz, $CDCl_3$) spectrum of compound **2g,** related to **Scheme 2**

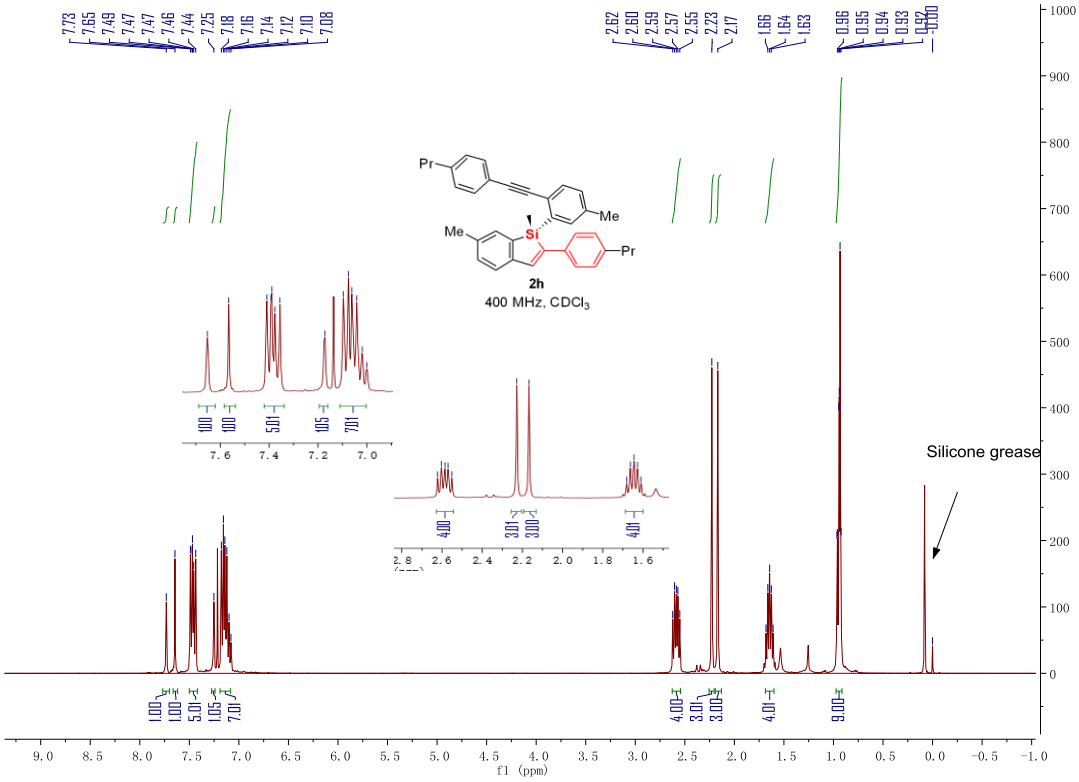

Figure S56. ^{1}H NMR (400 MHz, $CDCl_3$) spectrum of compound **2h** , related to **Scheme 2**

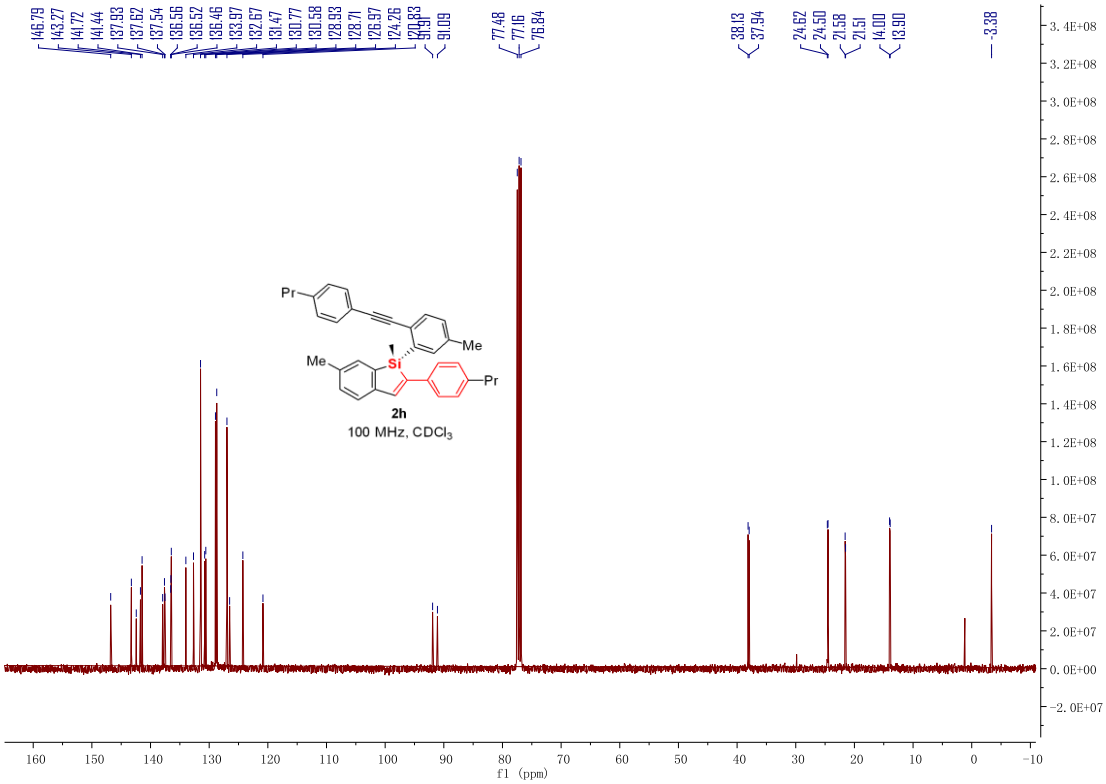

Figure S57. ^{13}C NMR (100 MHz, $CDCl_3$) spectrum of compound **2h,** related to **Scheme 2**

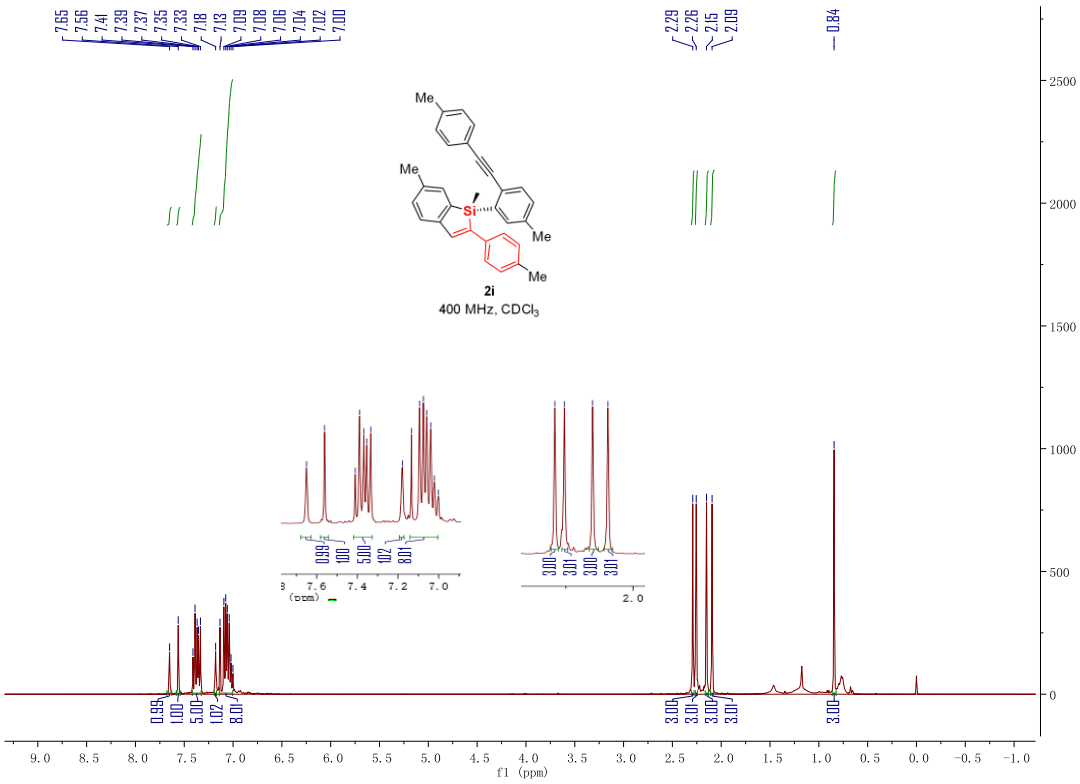

Figure S58. ^{1}H NMR (400 MHz, $CDCl_3$) spectrum of compound **2i** , related to **Scheme 2**

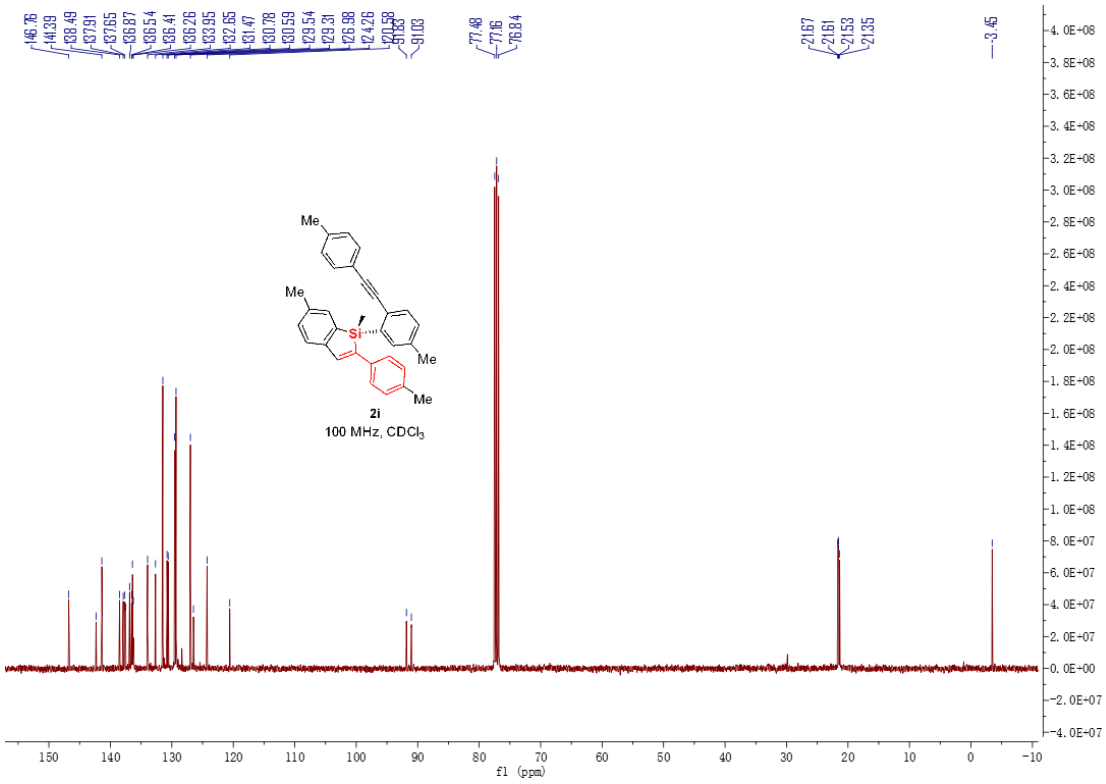

Figure S59. ^{13}C NMR (100 MHz, $CDCl_3$) spectrum of compound **2i,** related to **Scheme 2**

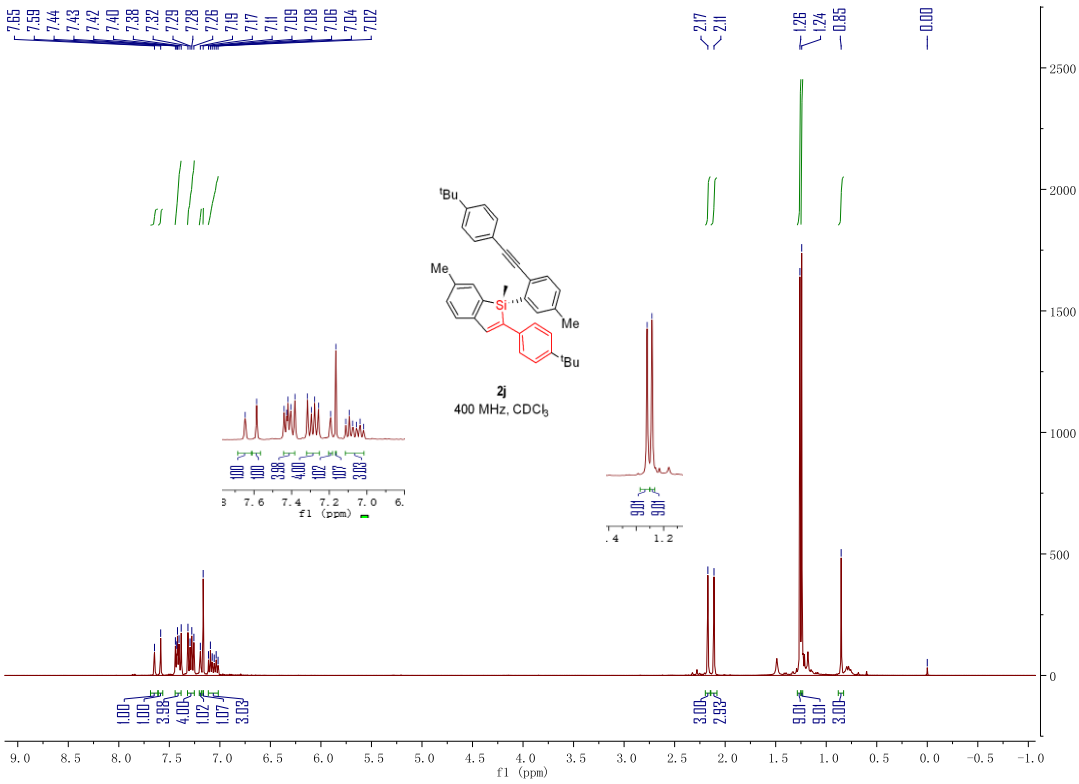

Figure S60. ^{1}H NMR (400 MHz, $CDCl_3$) spectrum of compound **2j**, related to **Scheme 2**

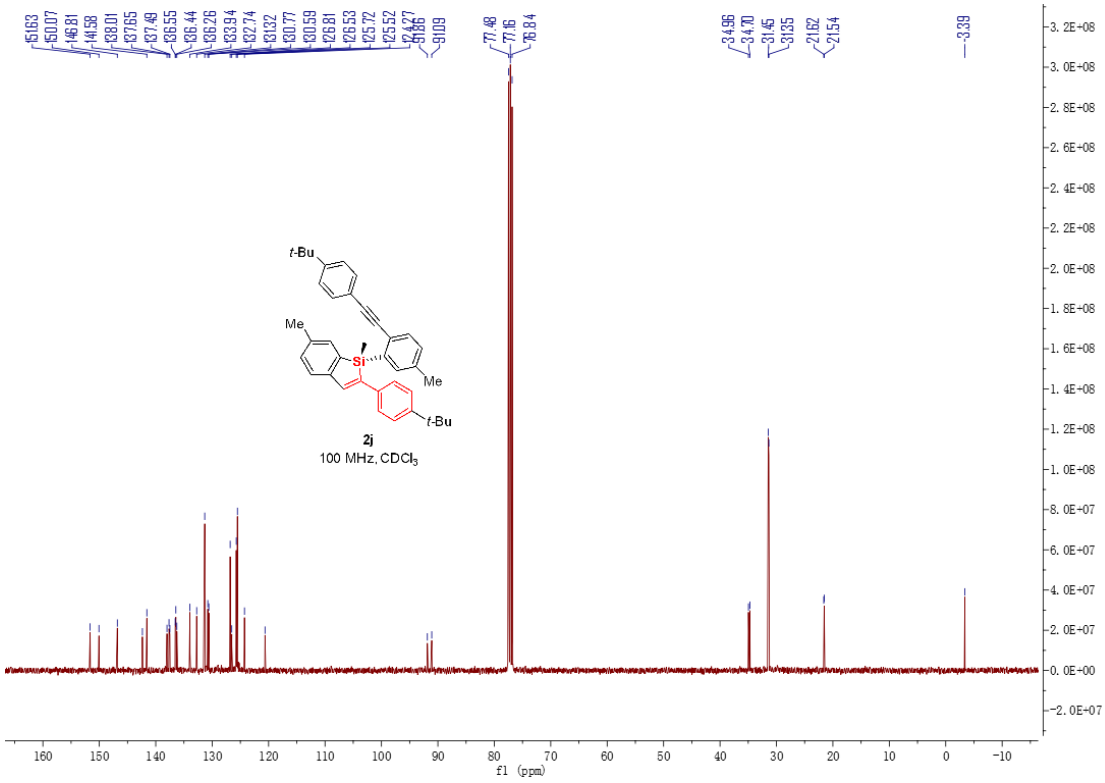

Figure S61. ^{13}C NMR (100 MHz, $CDCl_3$) spectrum of compound **2j,** related to **Scheme 2**

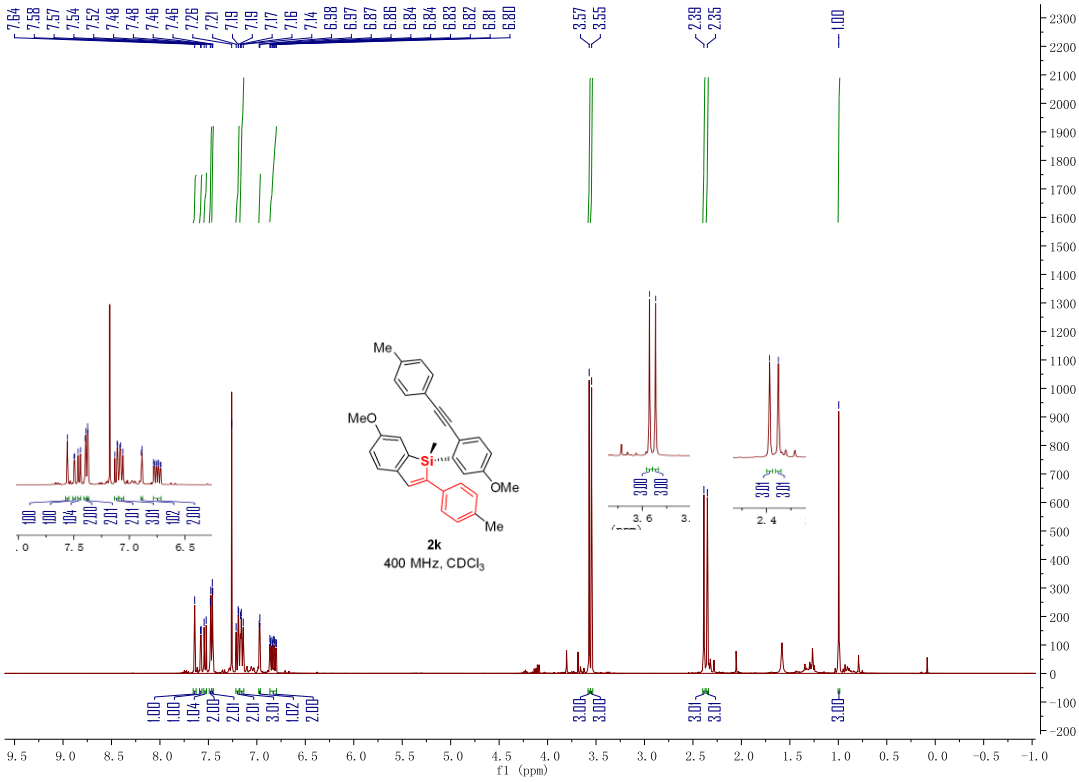

Figure S62. ^{1}H NMR (400 MHz, $CDCl_3$) spectrum of compound **2k** , related to **Scheme 2**

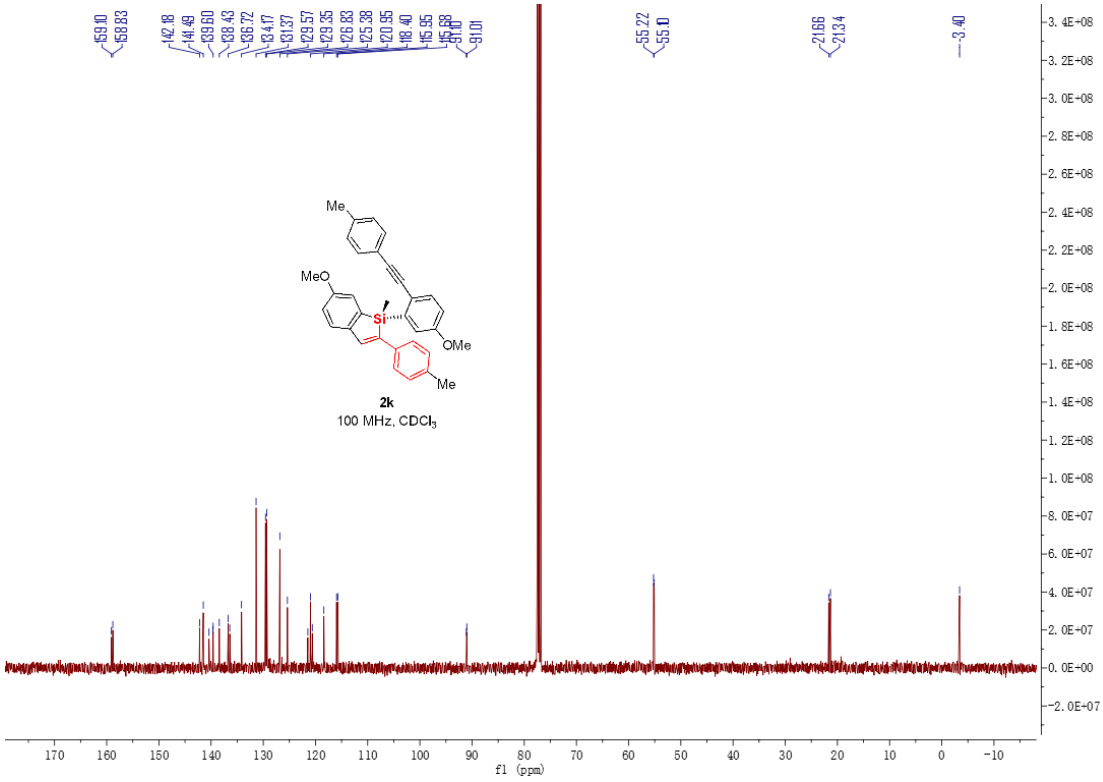

Figure S63. ^{13}C NMR (100 MHz, $CDCl_3$) spectrum of compound **2k,** related to **Scheme 2**

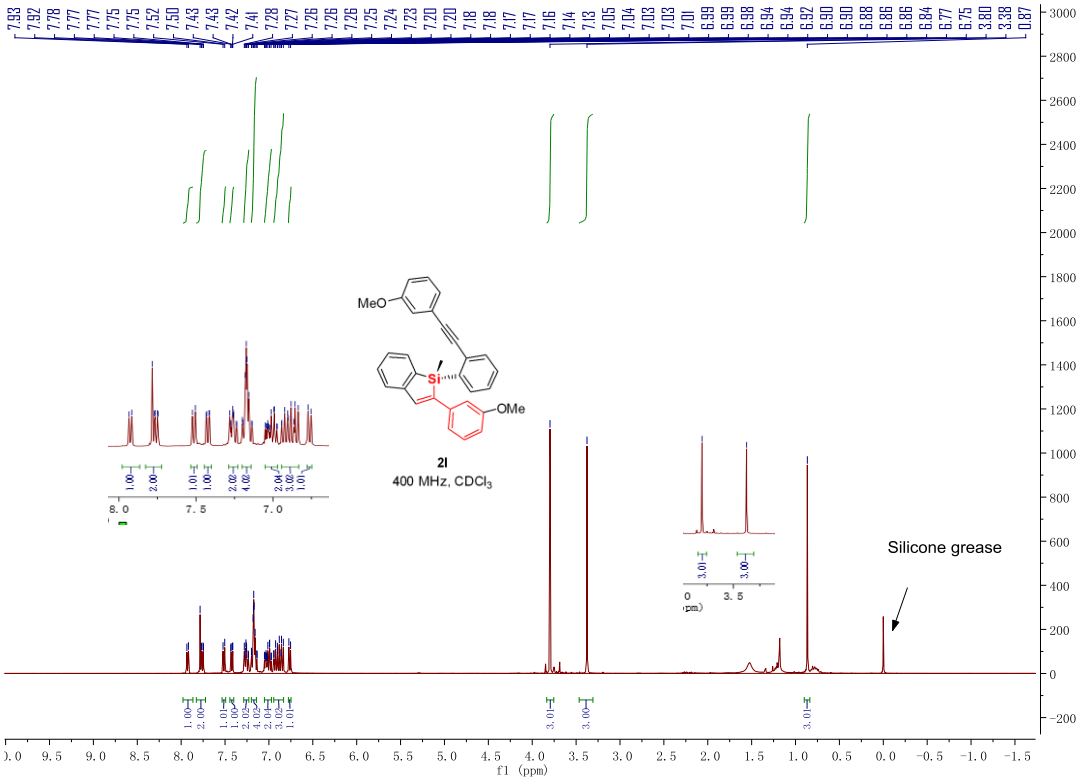

Figure S64. ^{1}H NMR (400 MHz, $CDCl_3$) spectrum of compound **2l** , related to **Scheme 2**

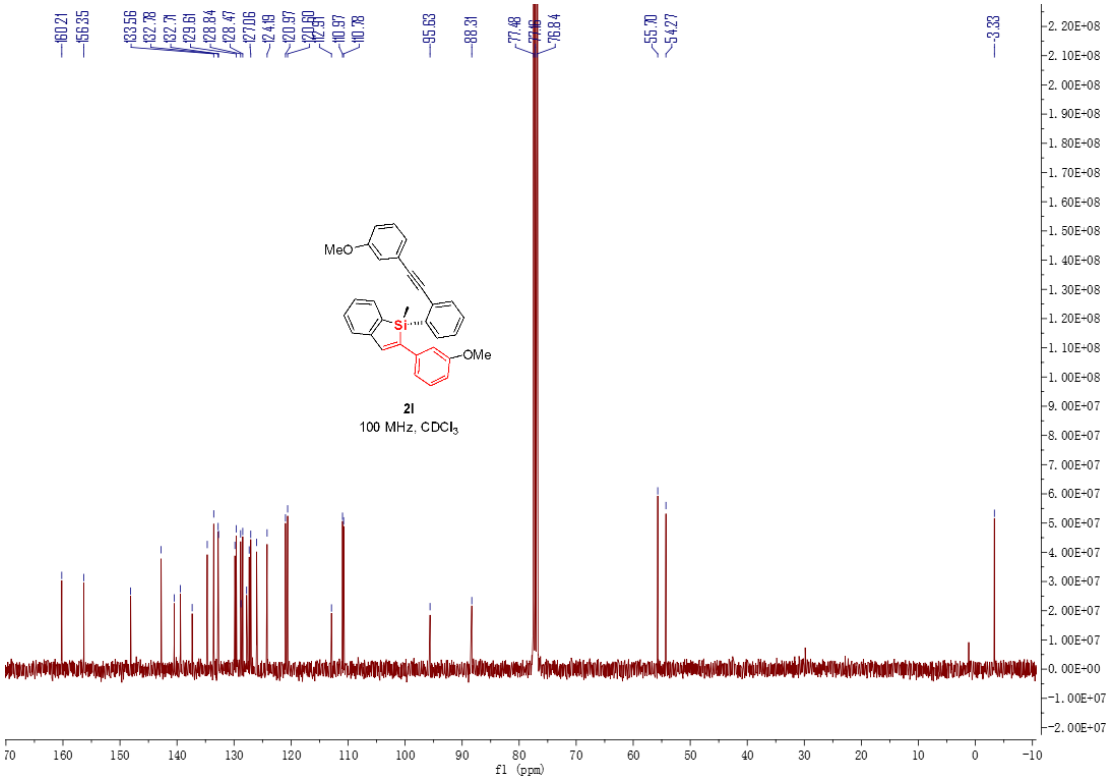

Figure S65. ^{13}C NMR (100 MHz, $CDCl_3$) spectrum of compound **2l,** related to **Scheme 2**

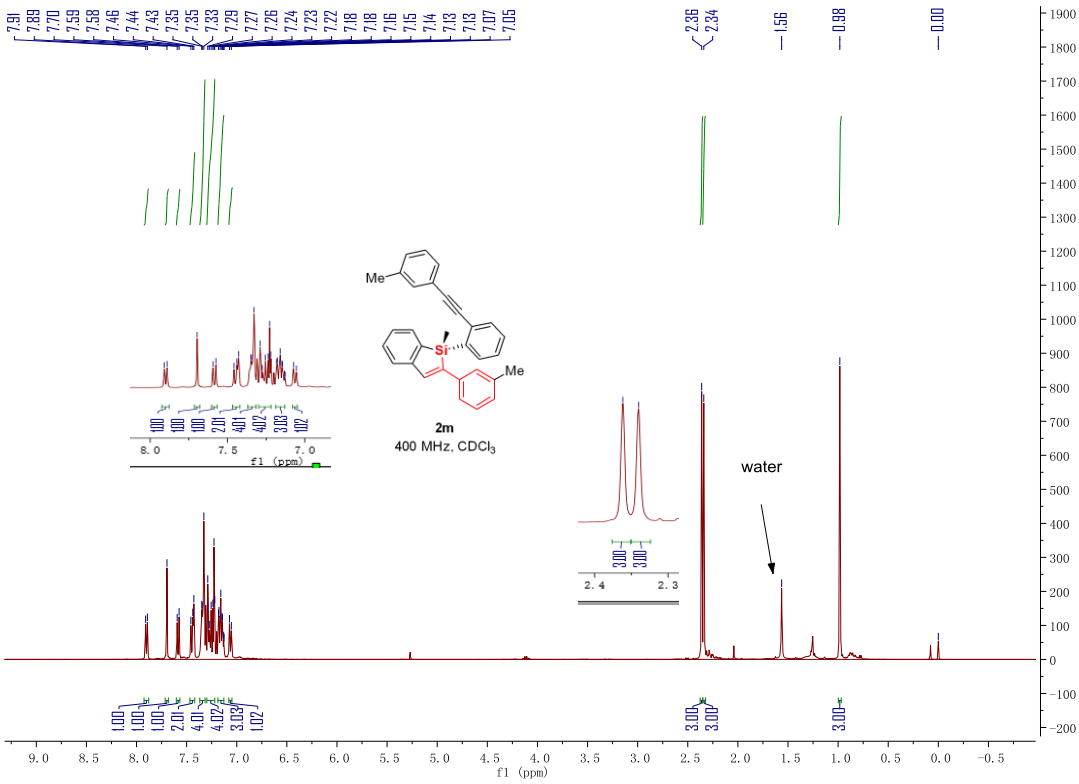

Figure S66. ^{1}H NMR (400 MHz, $CDCl_3$) spectrum of compound **2m** , related to Scheme 2

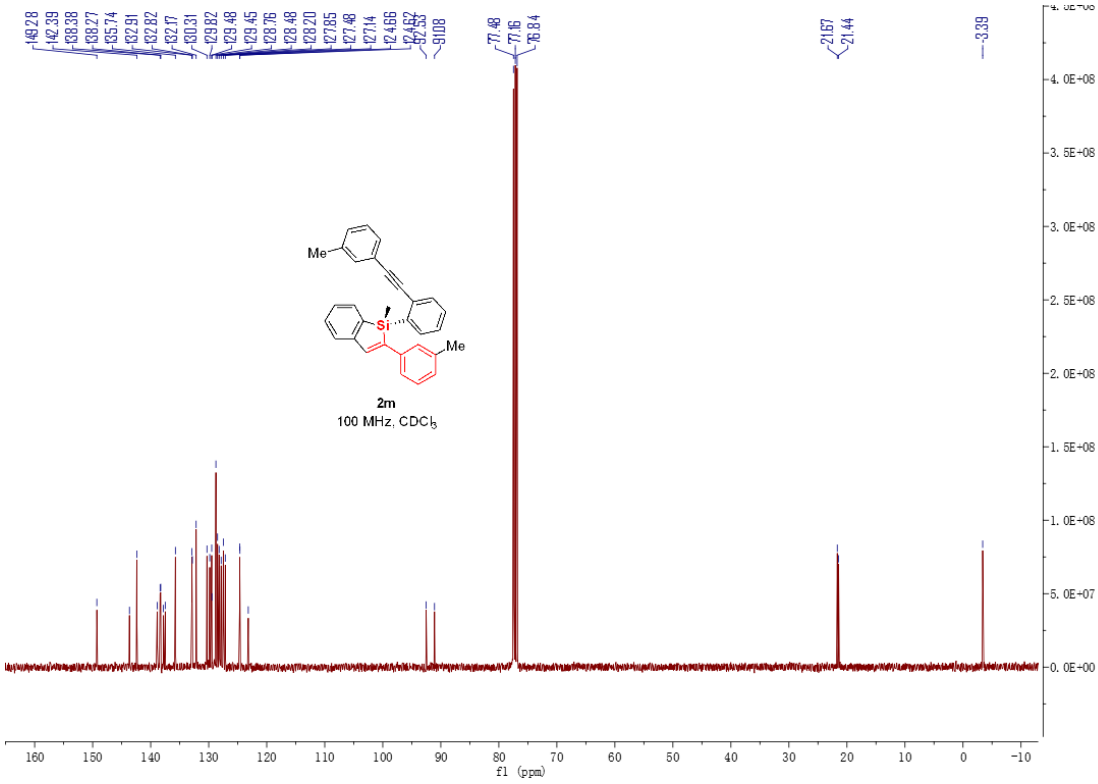

Figure S67. ^{13}C NMR (100 MHz, $CDCl_3$) spectrum of compound **2m,** related to **Scheme 2**

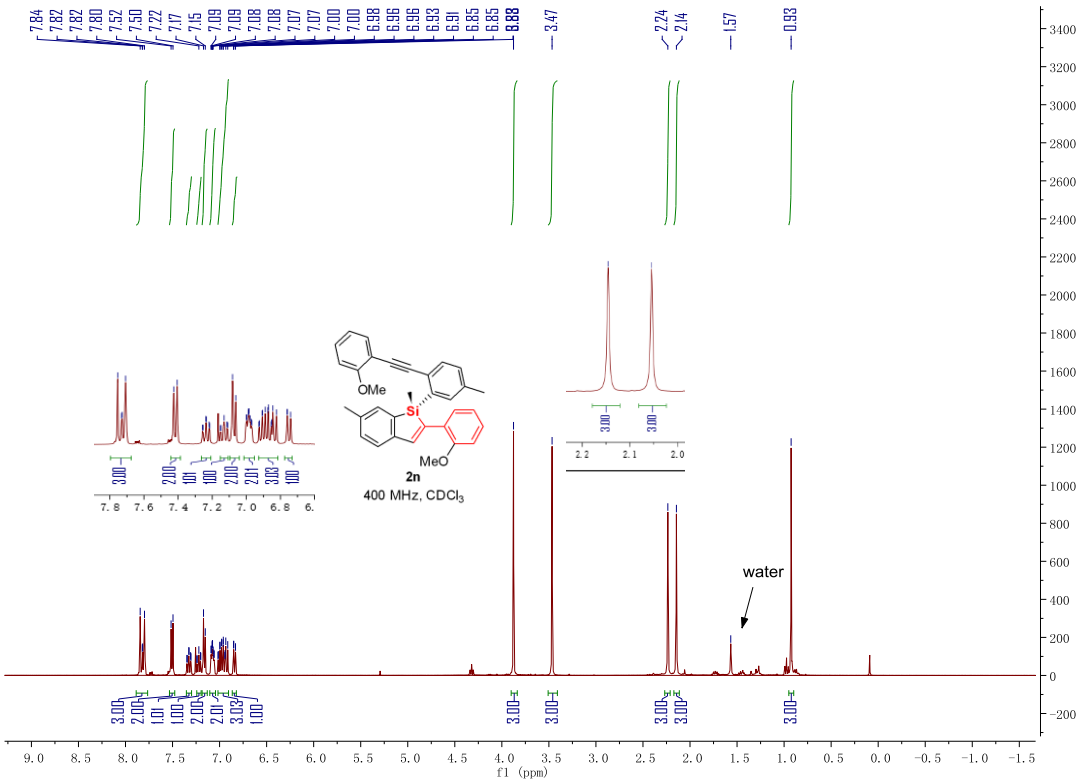

Figure S68. ^{1}H NMR (400 MHz, $CDCl_3$) spectrum of compound **2n** , related to **Scheme 2**

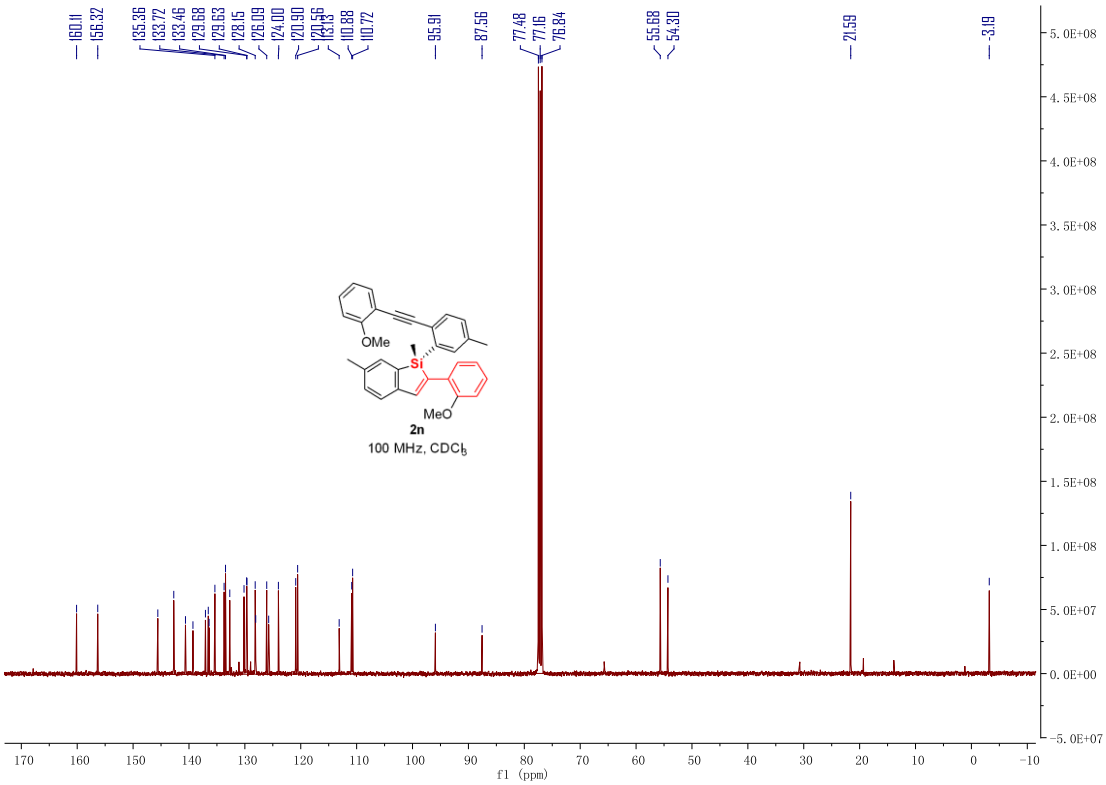

Figure S69. ^{13}C NMR (100 MHz, $CDCl_3$) spectrum of compound **2n,** related to **Scheme 2**

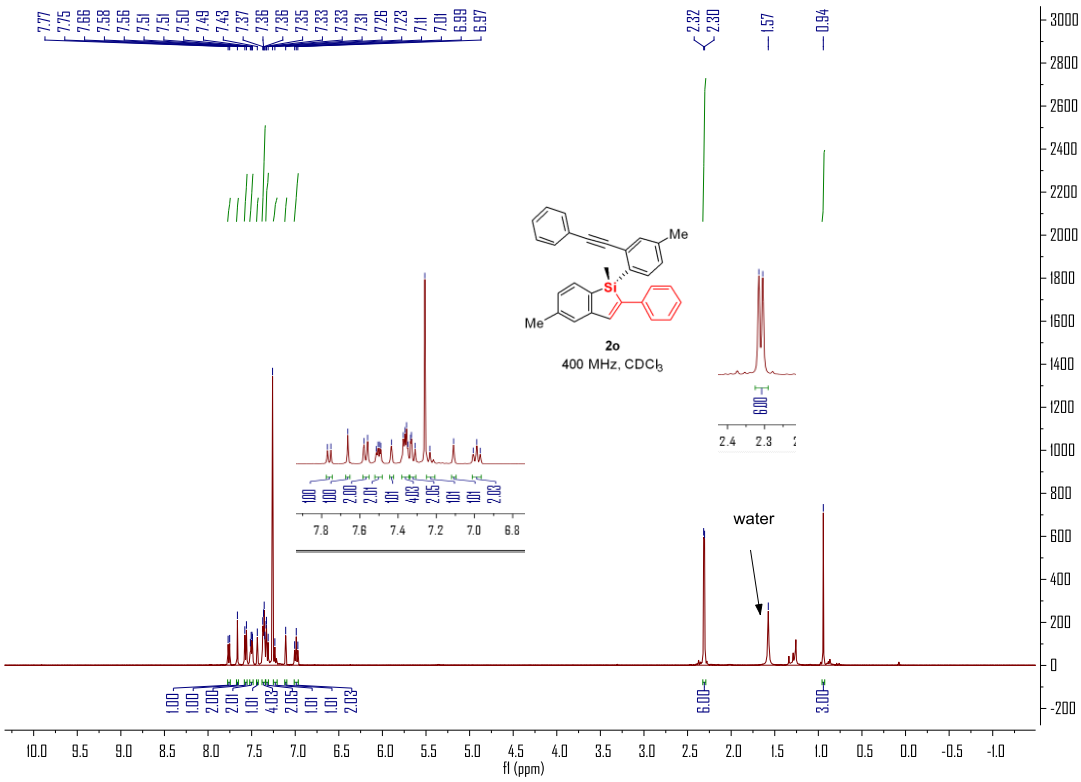

Figure S70. ^{1}H NMR (400 MHz, $CDCl_3$) spectrum of compound **2o** , related to **Scheme 2**

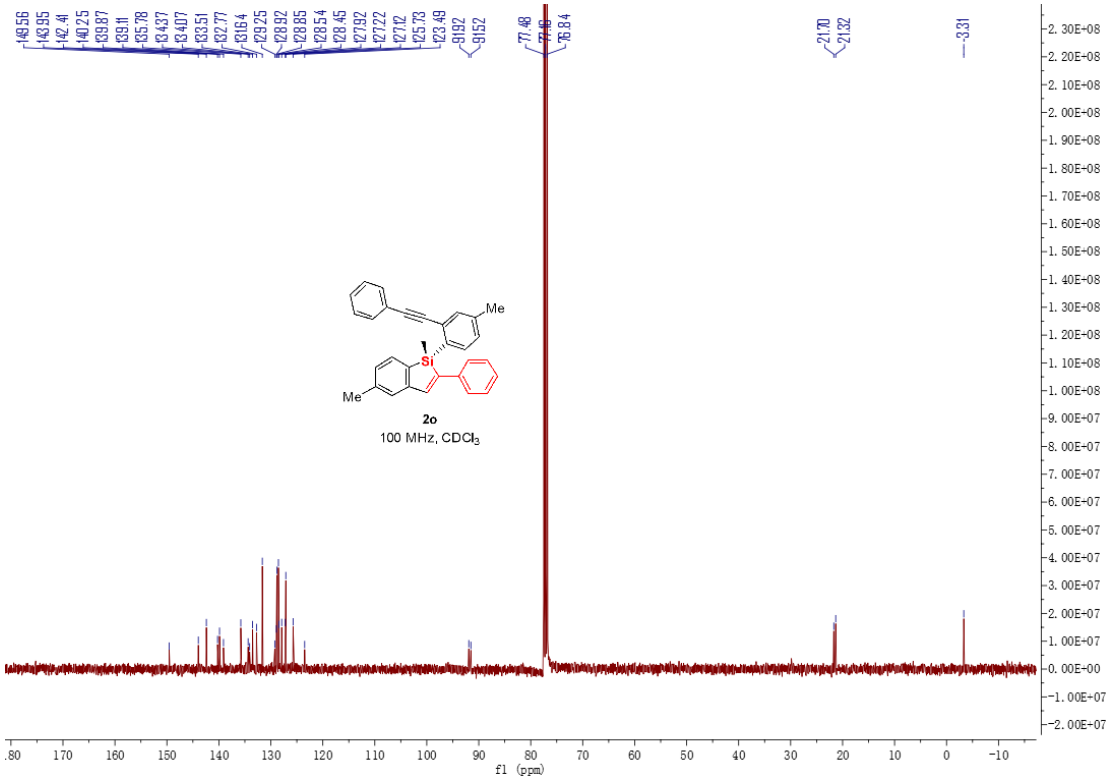

Figure S71. ^{13}C NMR (100 MHz, $CDCl_3$) spectrum of compound **2o,** related to **Scheme 2**

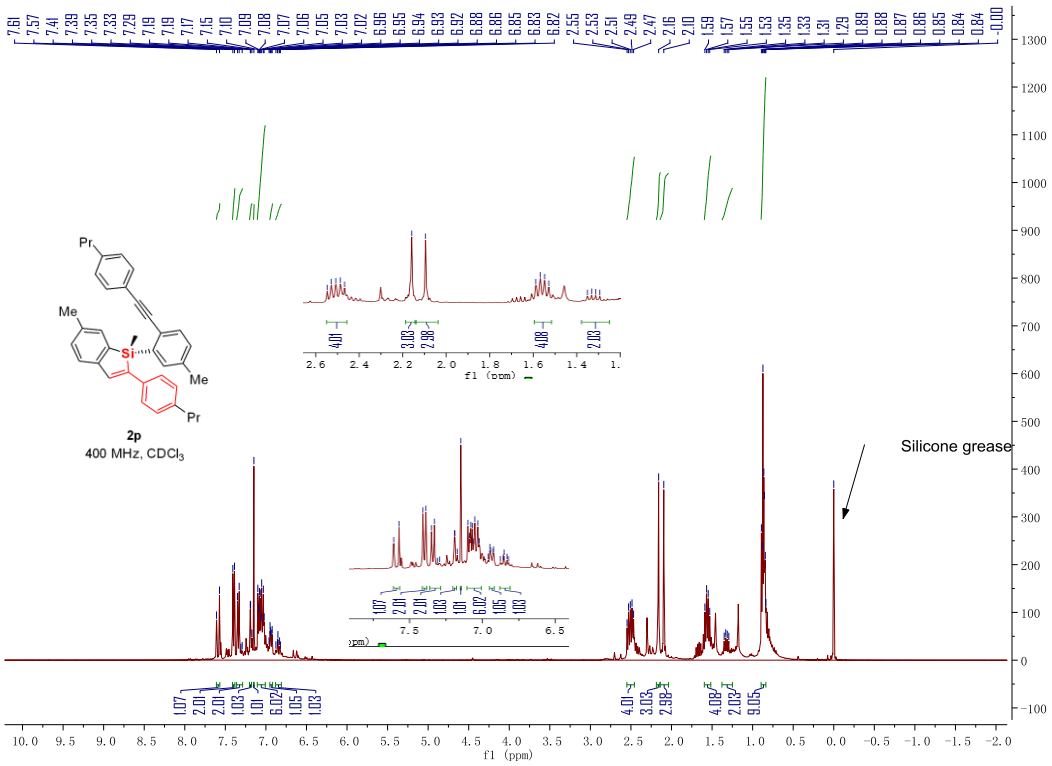

Figure S72. ^{1}H NMR (400 MHz, $CDCl_3$) spectrum of compound **2p** , related to **Scheme 2**

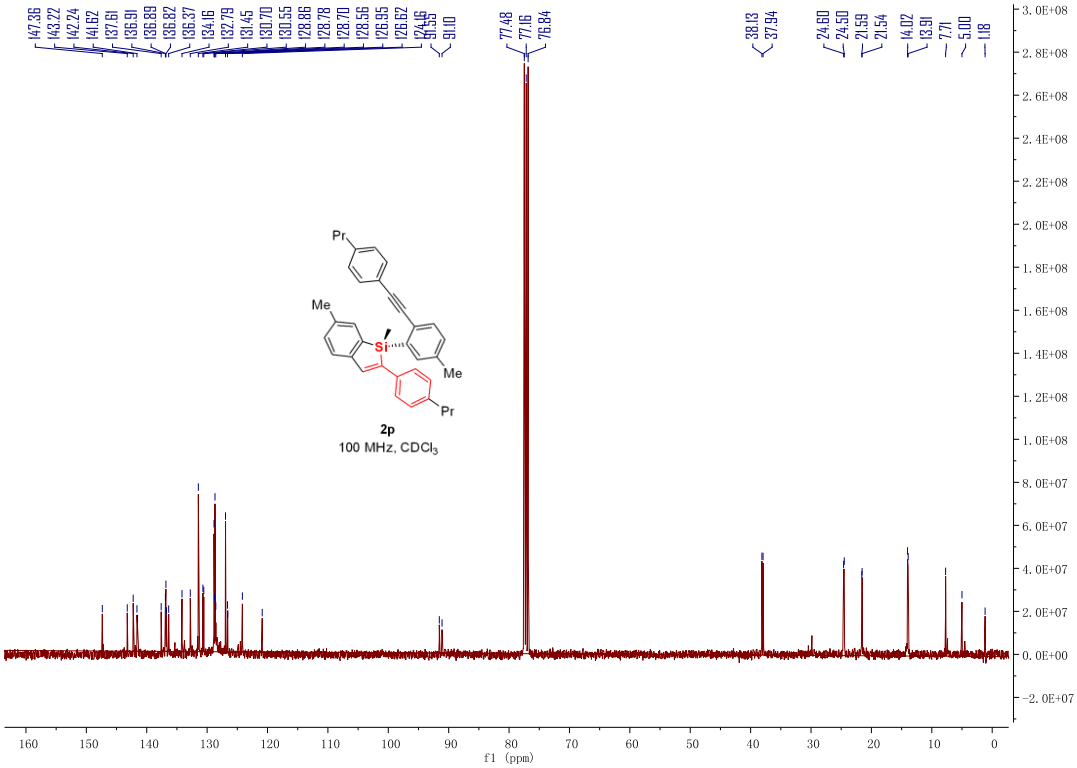

Figure S73. ^{13}C NMR (100 MHz, $CDCl_3$) spectrum of compound **2p,** related to **Scheme 2**

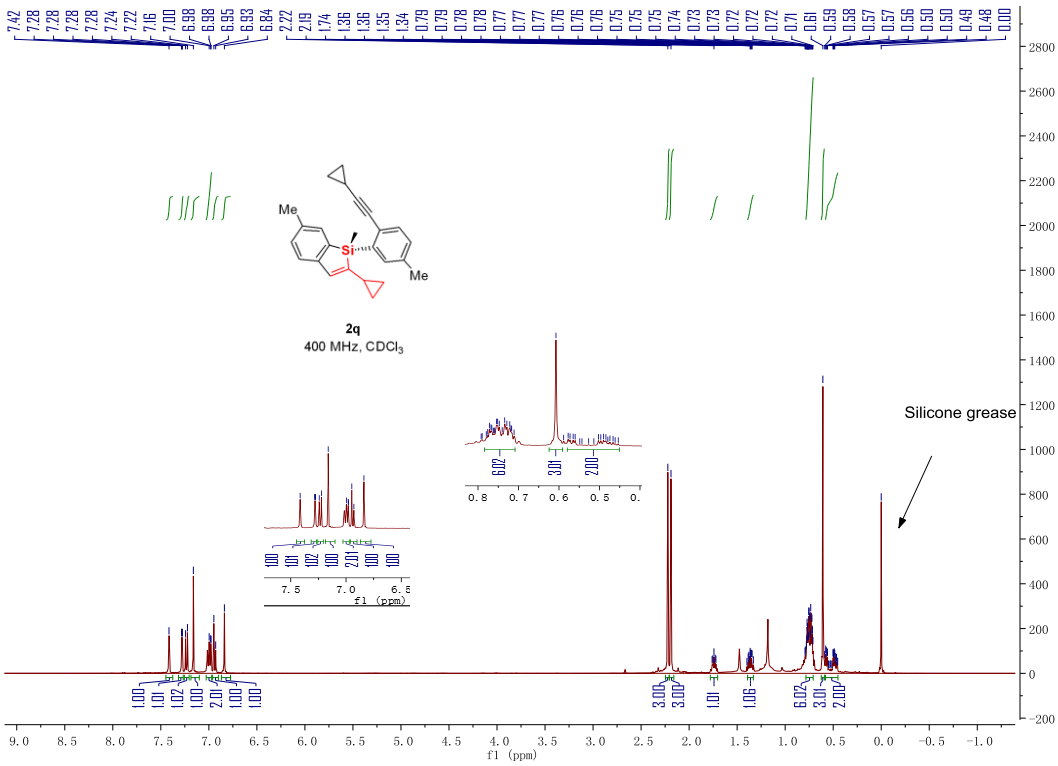

Figure S74. ^{1}H NMR (400 MHz, $CDCl_3$) spectrum of compound **2q** , related to **Scheme 2**

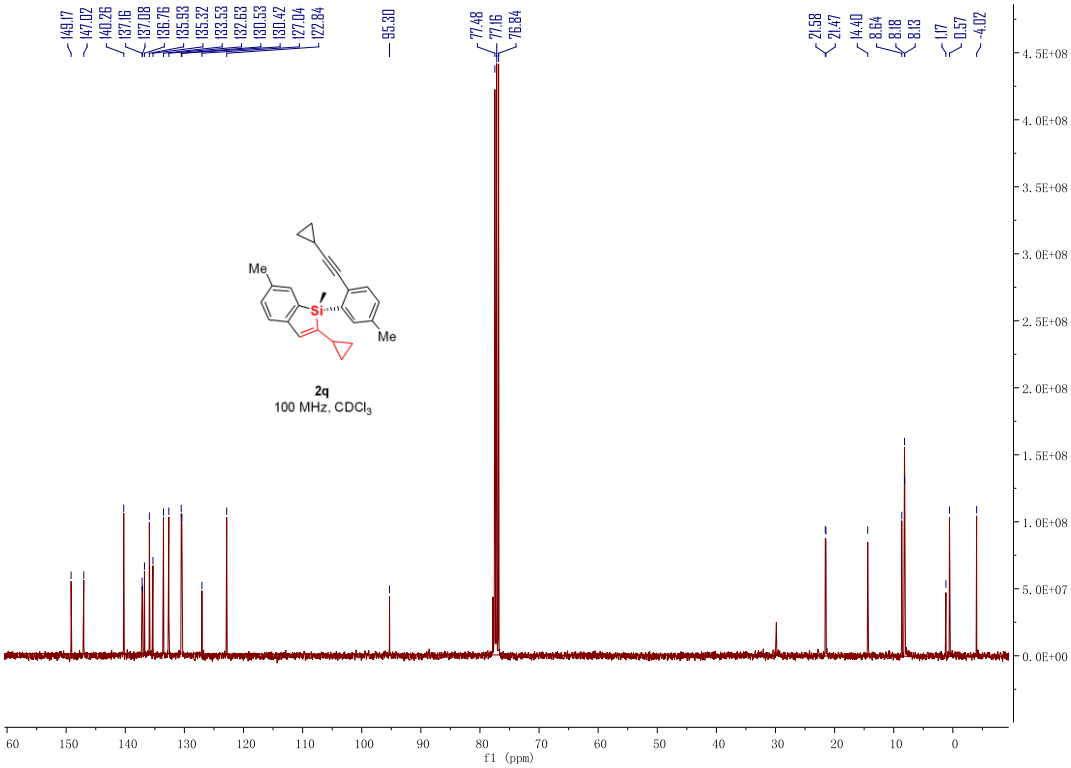

Figure S75. ^{13}C NMR (100 MHz, $CDCl_3$) spectrum of compound **2q,** related to **Scheme 2**

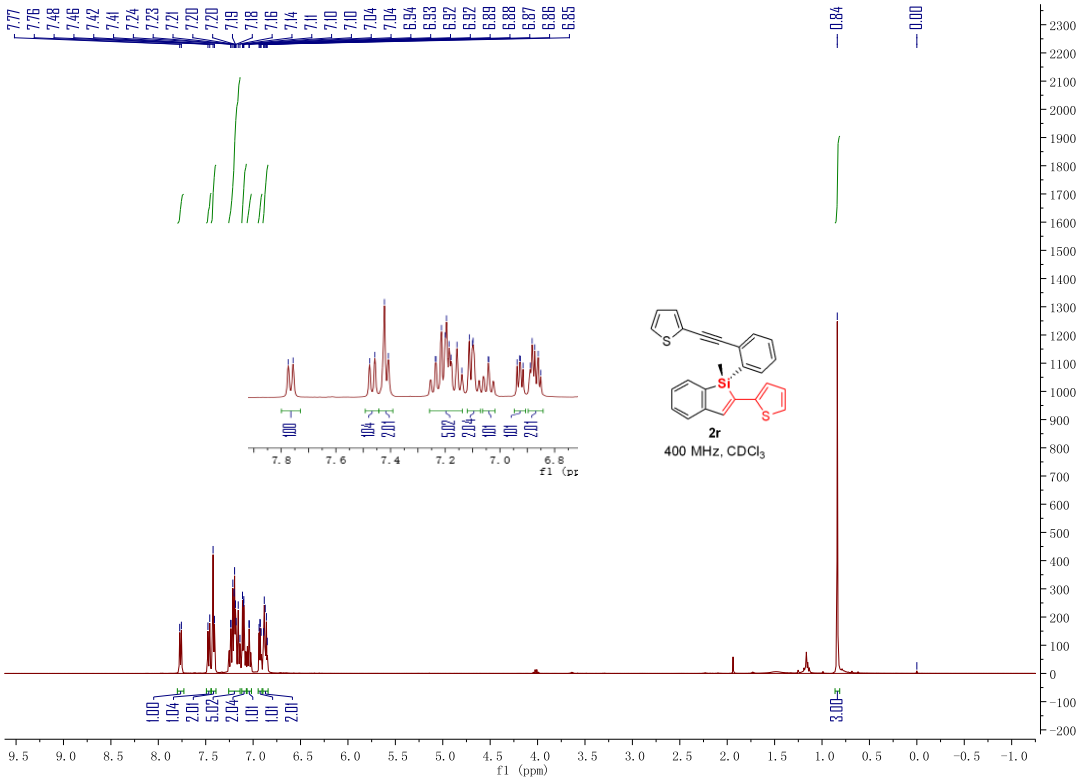

Figure S76. ^{1}H NMR (400 MHz, $CDCl_3$) spectrum of compound **2r** , related to **Scheme 2**

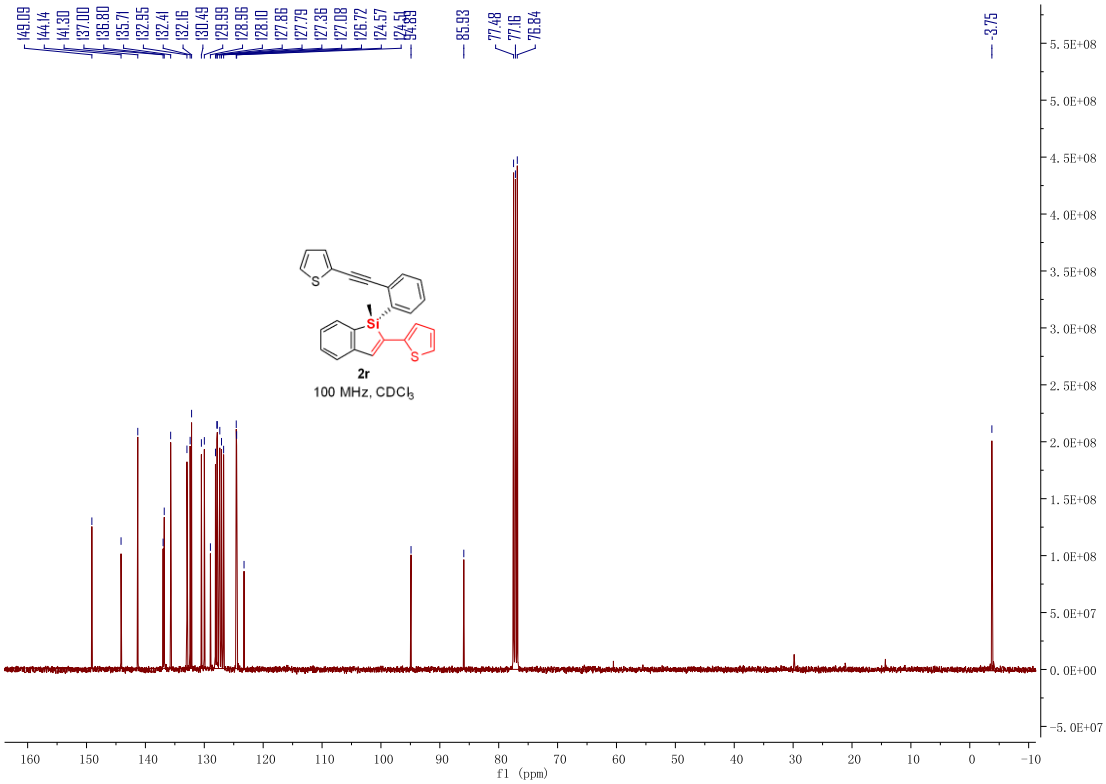

Figure S77. ^{13}C NMR (100 MHz, $CDCl_3$) spectrum of compound **2r,** related to **Scheme 2**

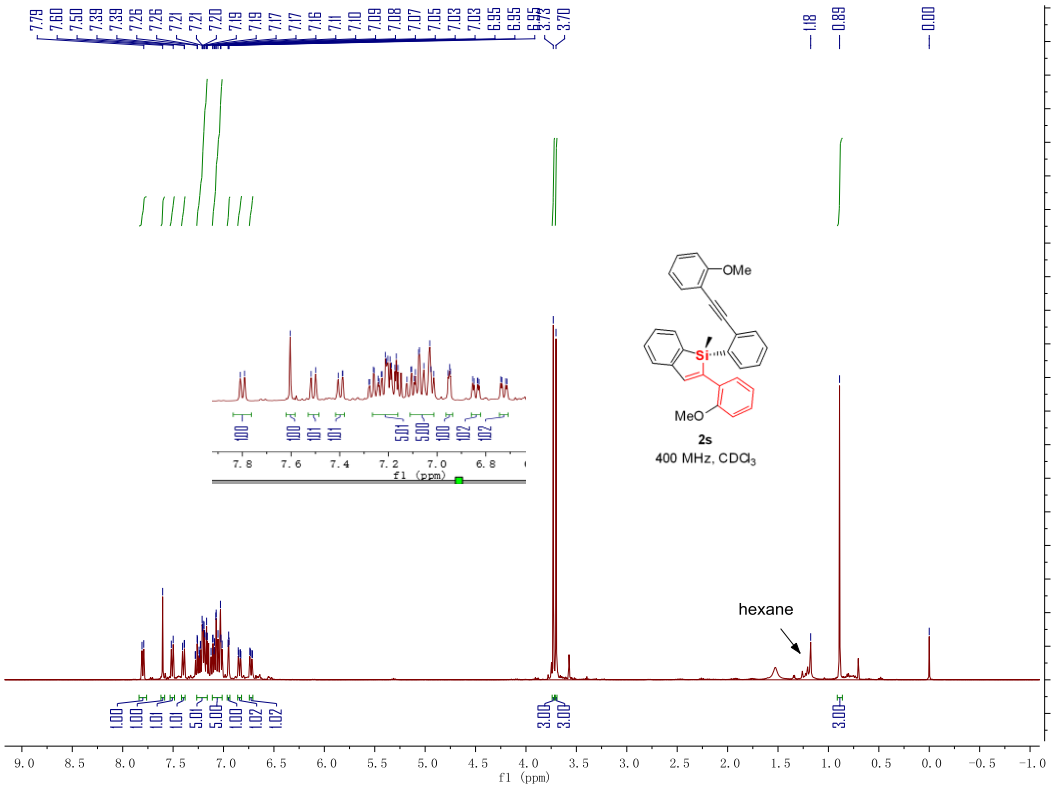

Figure S78. ^{1}H NMR (400 MHz, $CDCl_3$) spectrum of compound **2s** , related to **Scheme 2**

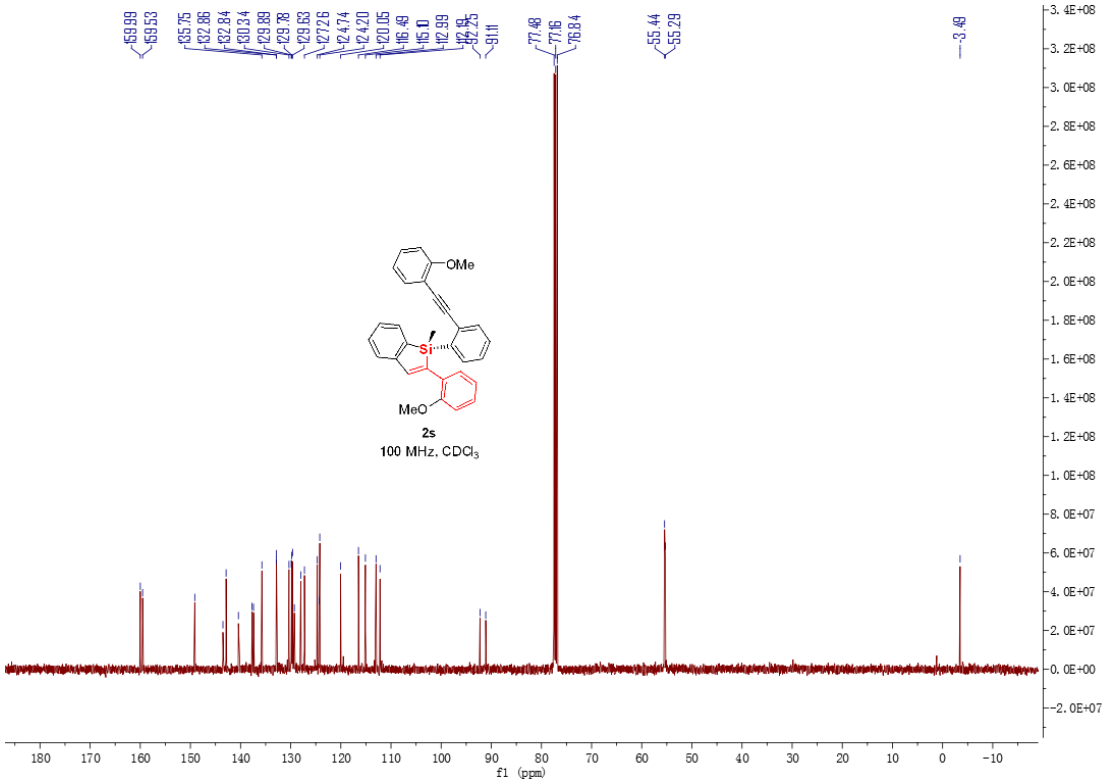

Figure S79. ^{13}C NMR (100 MHz, $CDCl_3$) spectrum of compound **1s,** related to **Scheme 2**

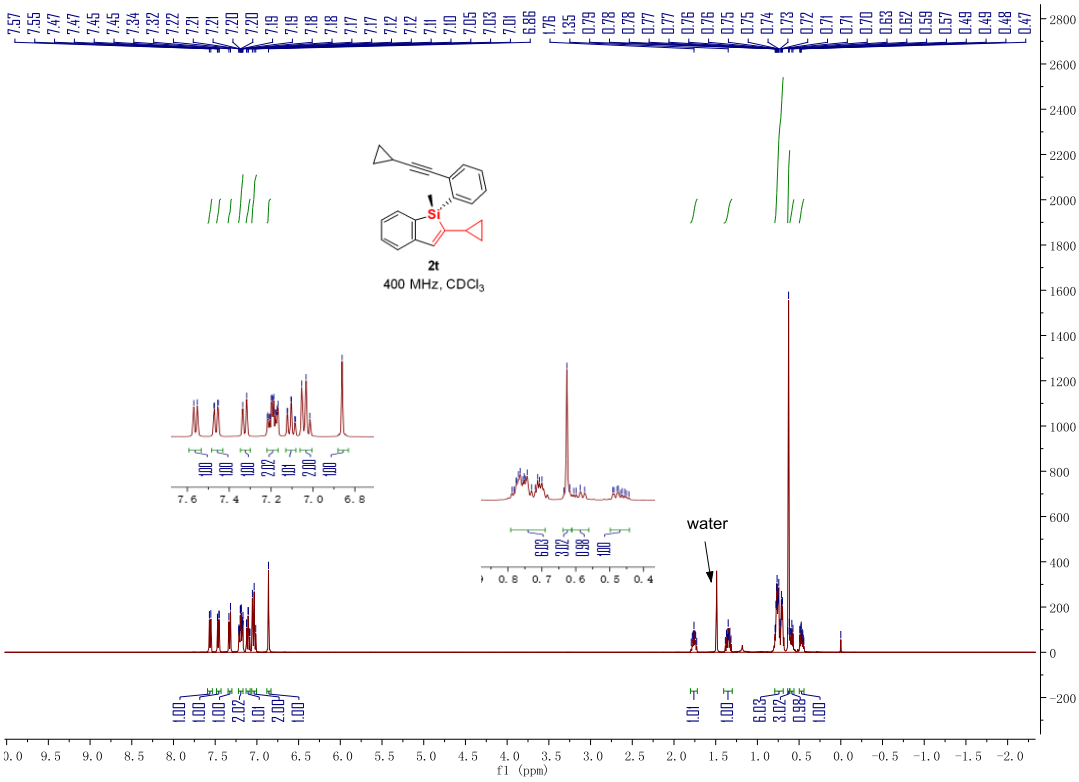

Figure S80. ^{1}H NMR (400 MHz, $CDCl_3$) spectrum of compound **2t** , related to **Scheme 2**

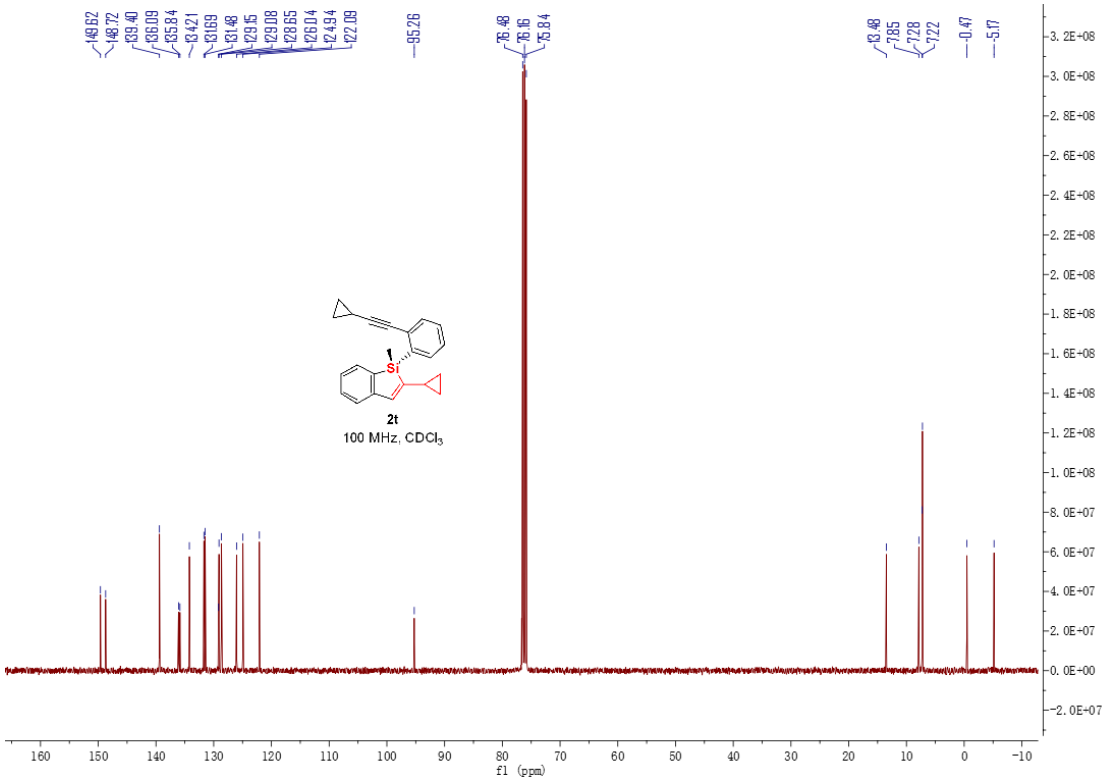

Figure S81. ^{13}C NMR (100 MHz, $CDCl_3$) spectrum of compound **1t,** related to **Scheme 2**

React IR experiment for the detection of benzosilole backbone

IR analysis was carried out under the reaction conditions: Under N_2 atmosphere, $[Rh(cod)Cl]_2$ (4.9 mg, 5 mol%), **L8** (13.8 mg, 12 mol%), KOtBu (2.7 mg, 12 mol%) and evacuated under high vacuum and backfilled with N_2. Toluene (1 mL) was next added and stirred at room temperature for about 0.5 h. Then methylbis(2-(phenylethynyl)phenyl)silane **1a** (79.6 mg, 0.2 mmol) were added sequentially, The mixture was stirred at 70 ^{o}C in a preheated oil. Then the IR probe was inserted and the IR data collection was started. The mixture was stirred at 70 ^{o}C for about 72 h.

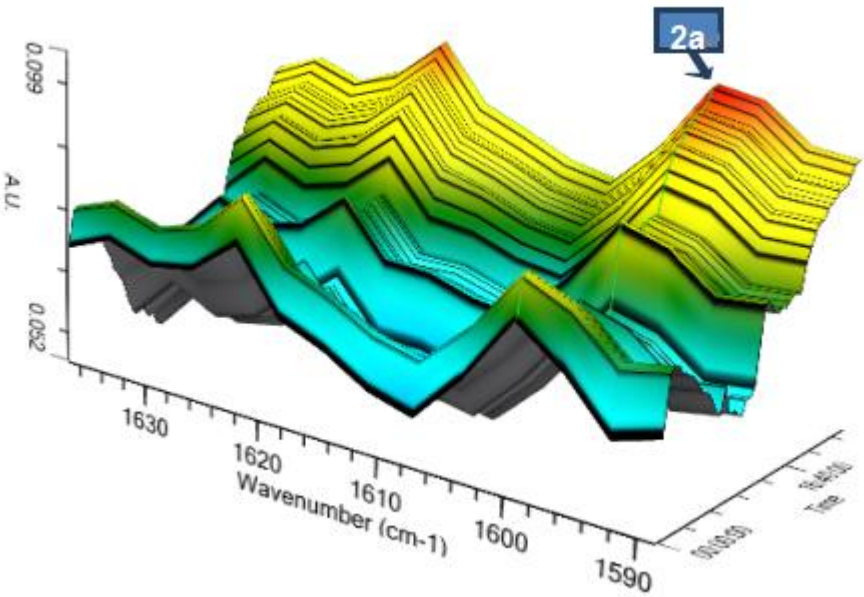

Figure S82. IR spectra for detection of the formation of benzosilole **2a** from the hydrosilylation of alkynyl C(sp)-C(sp) bond. Related to Figure 5

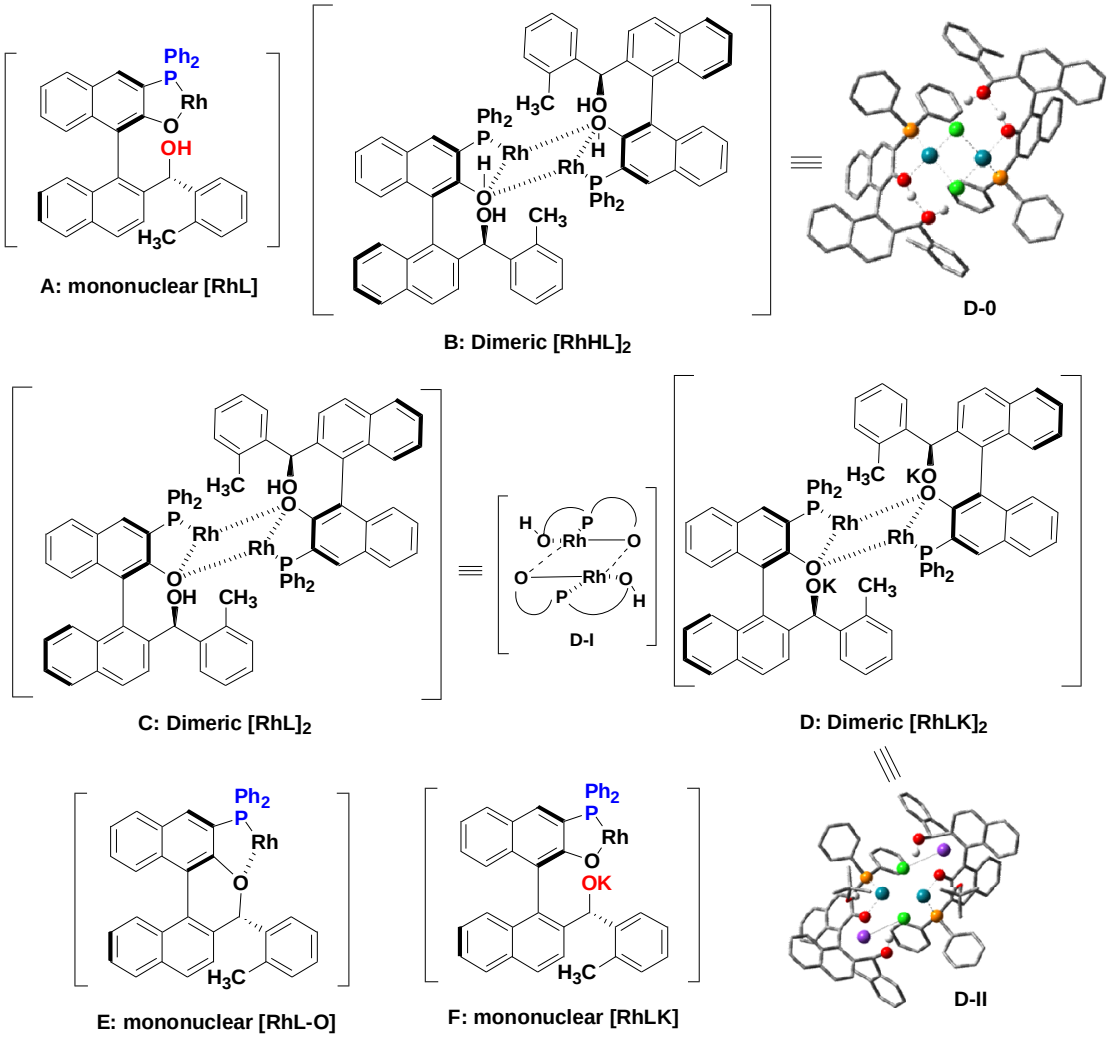

Figure S83 (continued). Possible Rh complex or intermediates in this reaction could be confirmed on the basis of the ^{31}P-NMR and ESI-MS analysis. For the Rh complexes, B-D, the existence of couplings between Rh and P in the ^{31}P NMR spectra. Related to Figure 5

Supplemental Figures for ESI-MS spectrums:

Figure S84. ESI(+)-MS analysis for the mixture of only $[Rh(cod)Cl]_2$ and Ar-BINMOL-Phos (*o*-Me) in toluene. Related to Figure 5

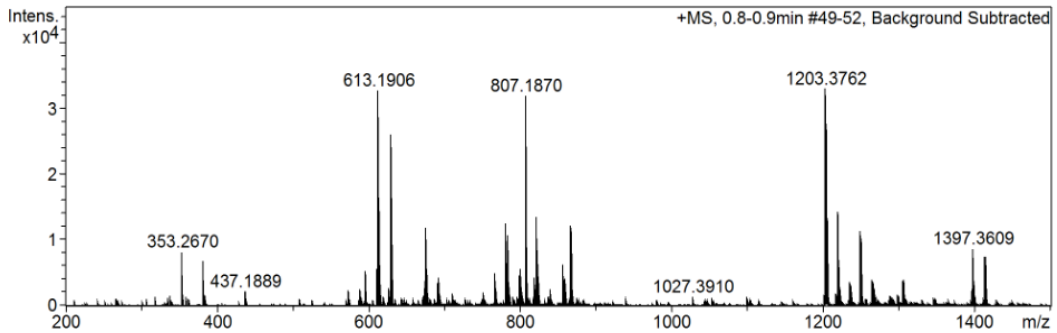

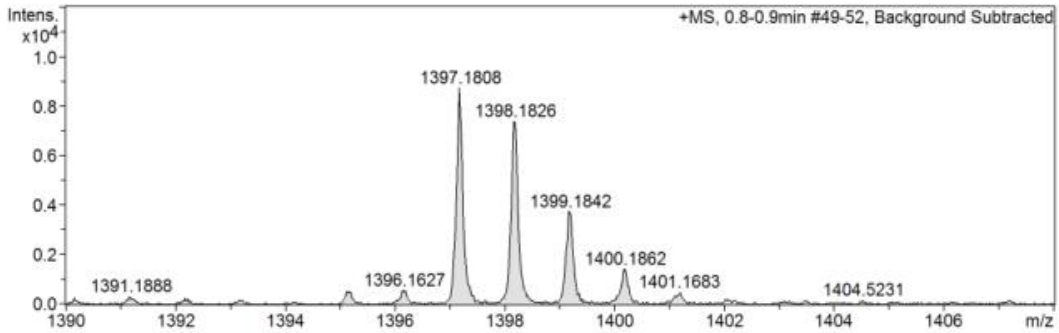

Meas. m/z	#	Ion Formula	m/z	err [ppm]	mSigma	# Sigma	Score	rdb	e⁻ Conf	N-Rule
1397.1808	1	C80H59Na2O4P2Rh2	1397.1789	-1.4	32.8	1	-1.#J	52.5	even	ok

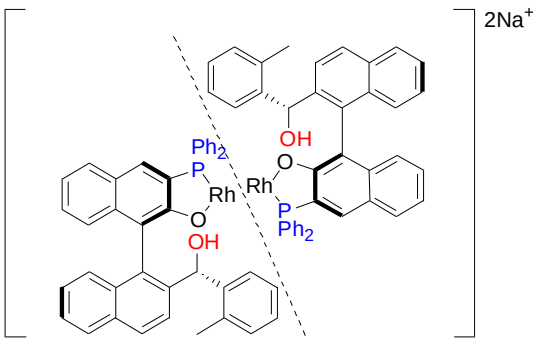

Chemical Formula: $C_{80}H_{60}O_4P_2Rh_2$
Exact Mass: 1352.2077
Molecular Weight: 1353.1145

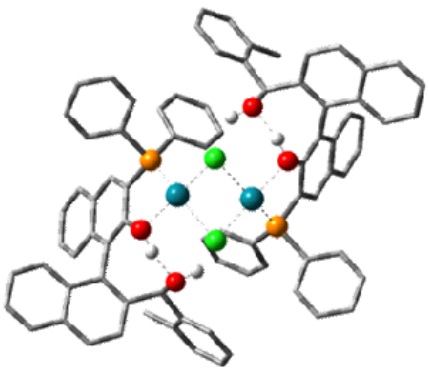

D-0

Figure S85. ESI(+)-MS analysis for the mixture of $[Rh(cod)Cl]_2$, alkyne, Ar-BINMOL-Phos (*o*-Me) in toluenen. Related to Figure 5

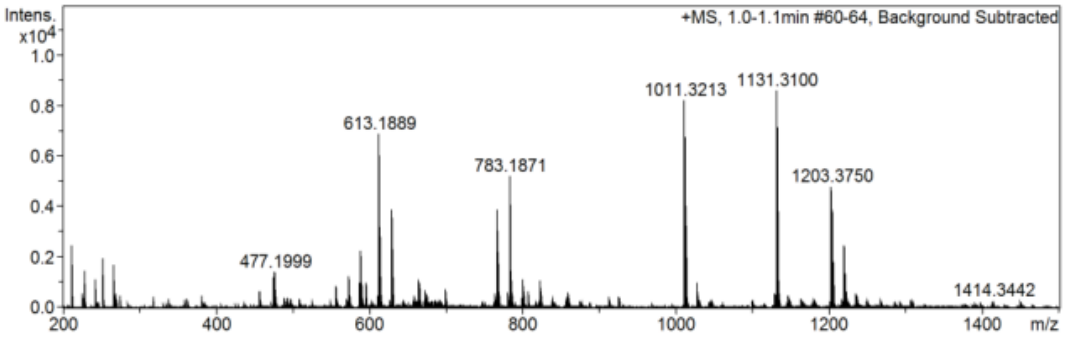

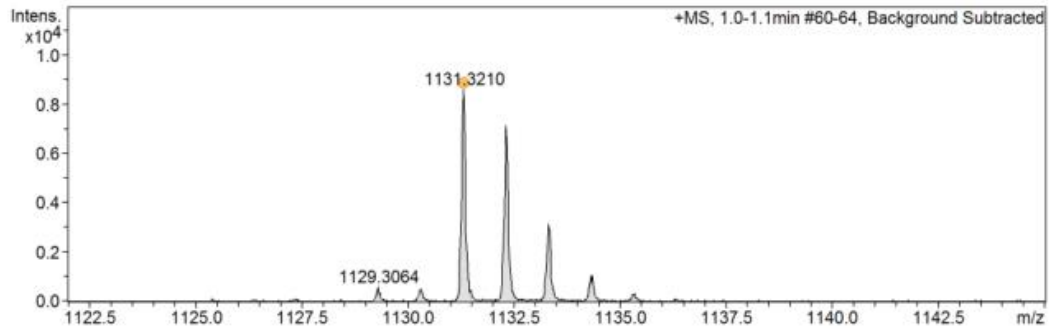

Meas. m/z	#	Ion Formula	m/z	err [ppm]	mSigma	# Sigma	Score	rdb	e⁻ Conf	N-Rule
1131.3210	1	C73H61O2PRhSi	1131.3228	1.5	15.1	1	100.00	45.5	even	ok

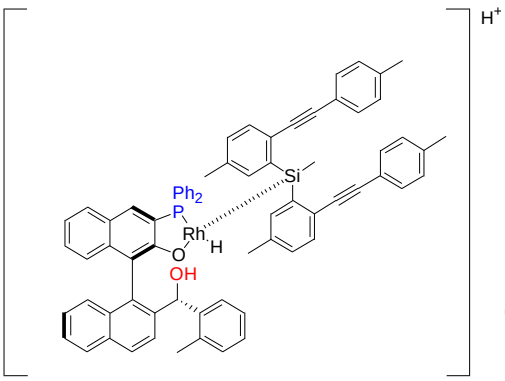

Chemical Formula: $C_{73}H_{61}O_2PRhSi$
Exact Mass: 1131.3233
Molecular Weight: 1132.2533

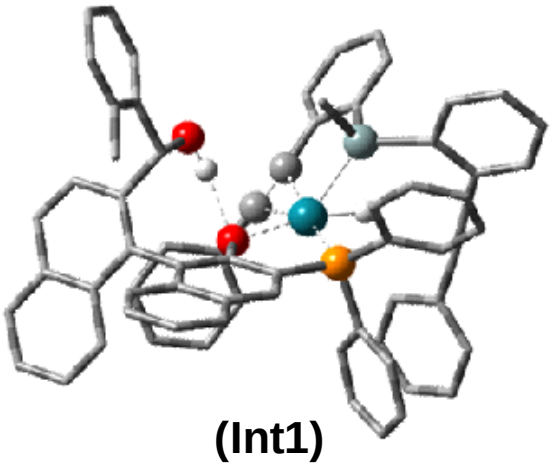

Supplemental Figures for fluorescence spectra of product:

Figure S86. UV-vis absorption (down) and fluorescence emission (up) properties of seven compounds in DCM solvents.(10^{-5} M). related to Figure 2

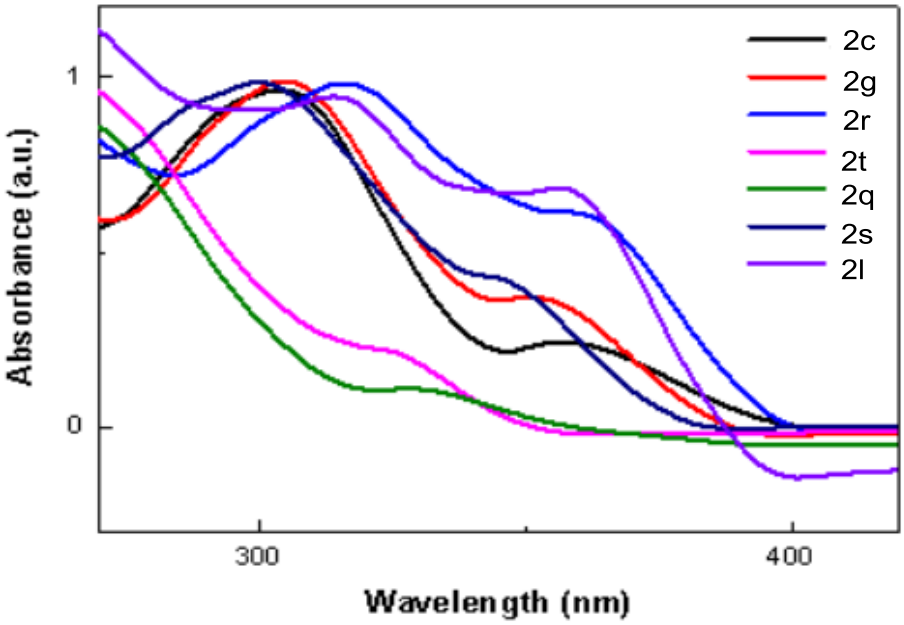

Figure S87. Fluorescence emission spectra of **2g** (5 μM) in THF/water mixtures (fw = 0 to 90%). λ_{ex}=300 nm, λ_{es}=550 nm. related to Figure 2

.

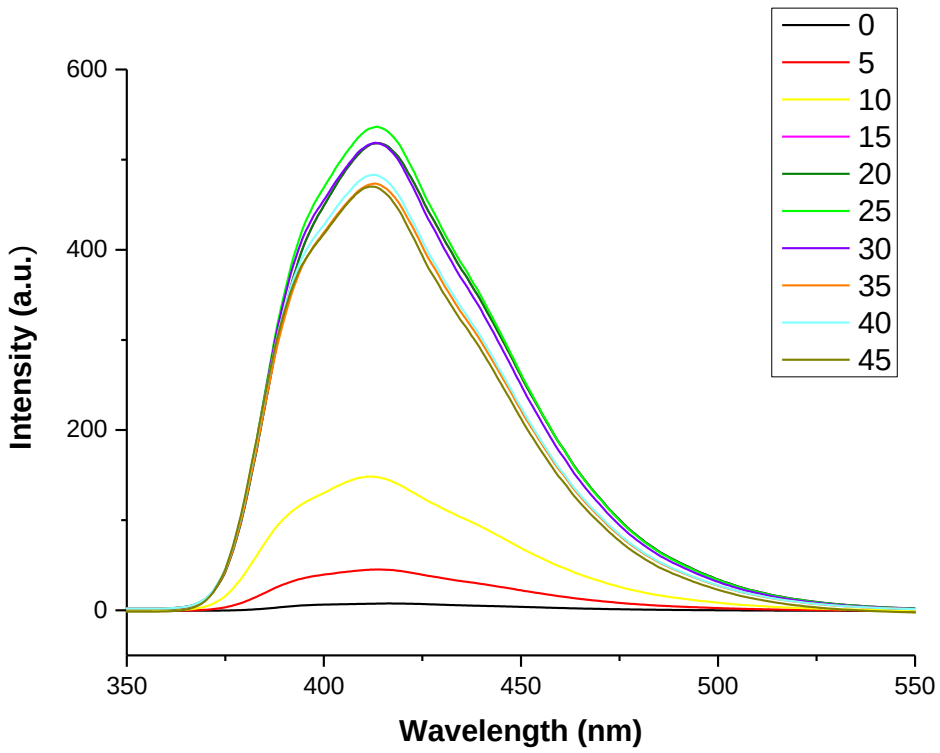

Figure S88. For racemic **2g** (AIE) related to Figure 2

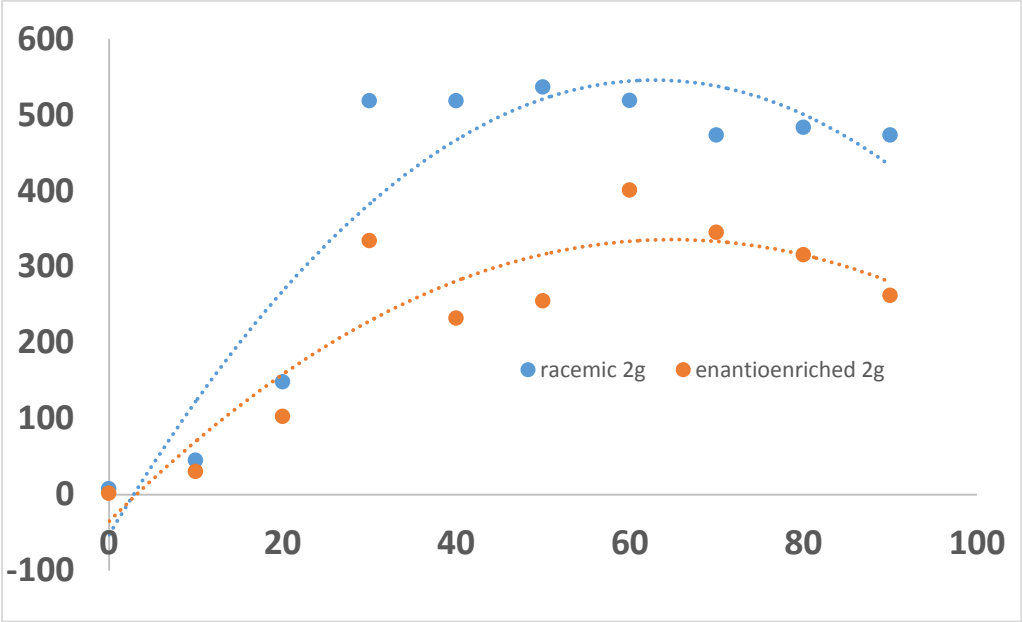

Figure S89. The photography for the AIE phenomena of **2g.** Related to Figure 2

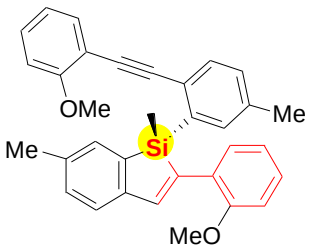

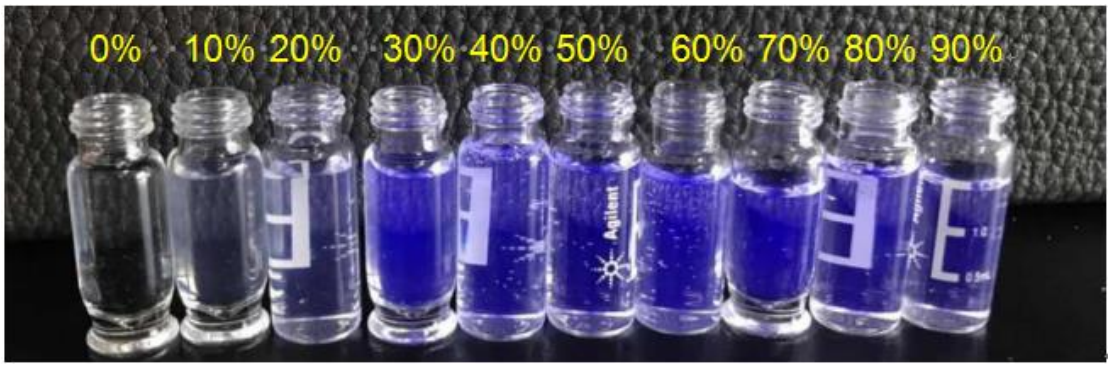

Figure S90. The industrial method for preparation of silicon rubber with blue blue-fluorescence because of the additive of alkyne-substituted benzosilole **2g** (10^{-4} w/w). Related to Figure 2

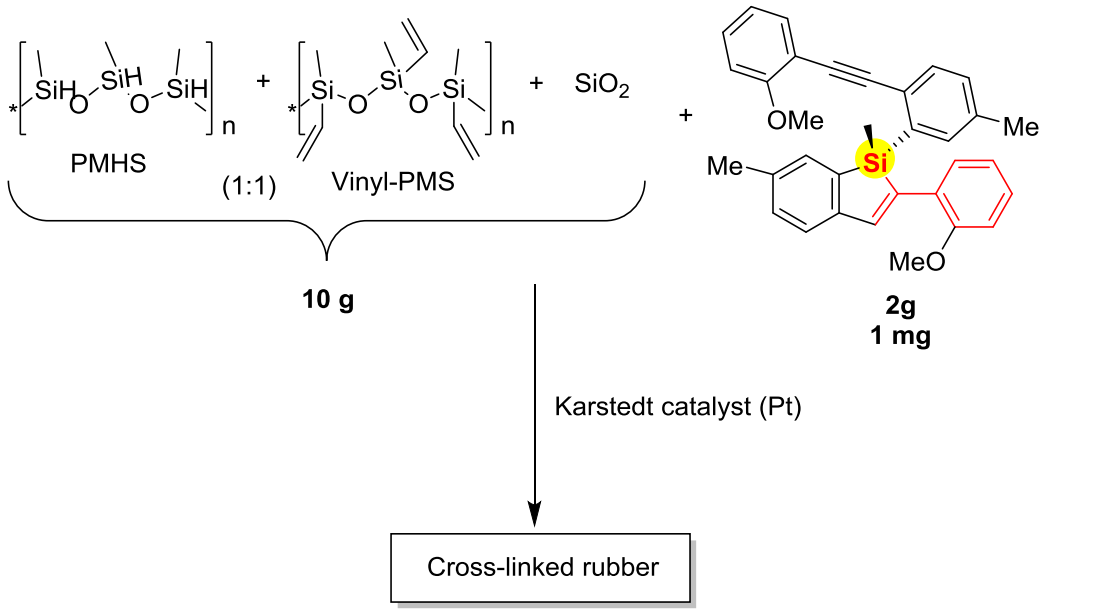

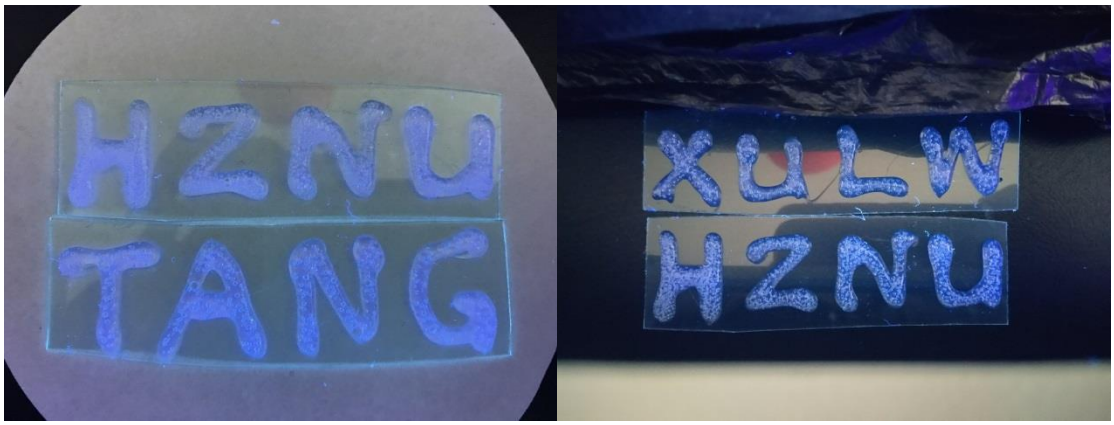

CPL spectra of product 2g:

Figure S91. CPL (upper panel) and DC (nether panel) spectra of (*S*) (black lines) and (*R*) (red lines) in $CHCl_3$ (1.0×10^{-3} M). Related to Figure 2

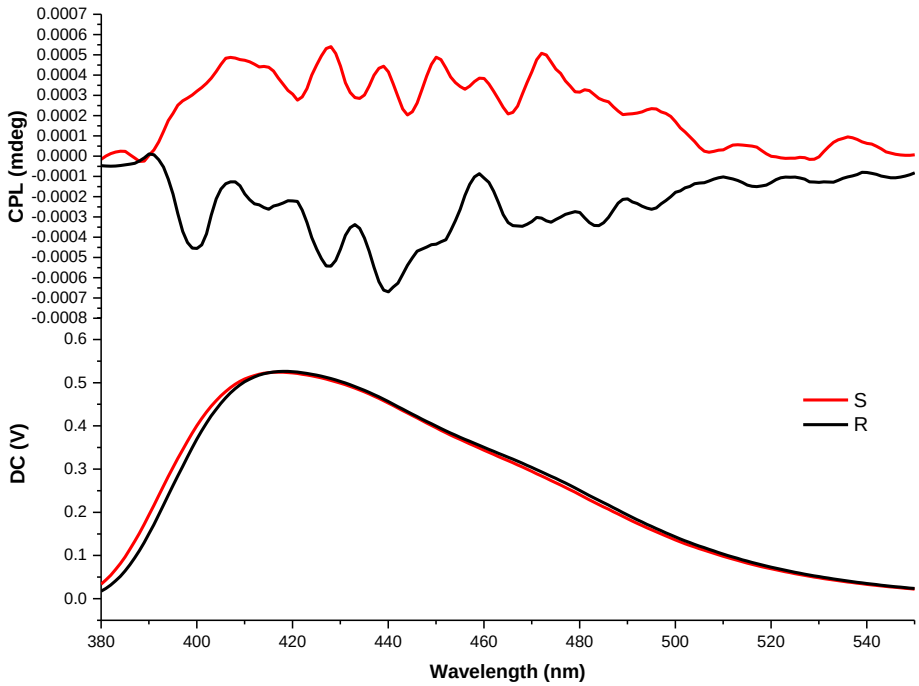

Table S92. HOMO and LUMO energy computed for product. Related to Figure 2

product	HOMO	LUMO	Δ (ev)
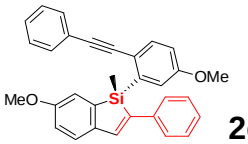 **2c**	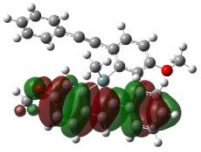 -4.529ev	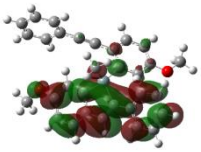 -1.795ev	2.734
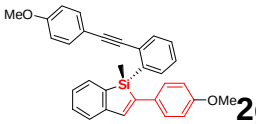 **2g**	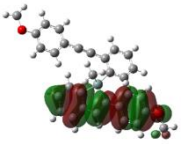 -4.570ev	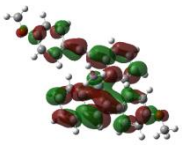 -1.857ev	2.713
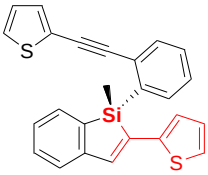 **2r**	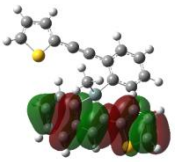 -4.751ev	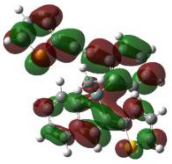 -2.174ev	2.577
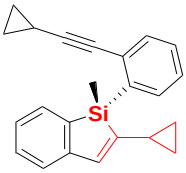 **2t**	 -4.867ev	 -1.575ev	3.292
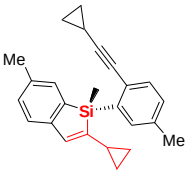 **2q**	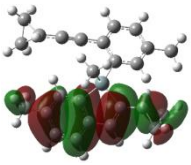 -4.738ev	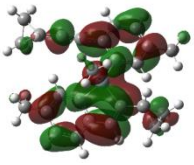 -1.480ev	3.258
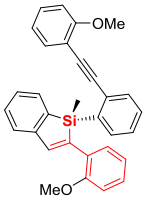 **2S**	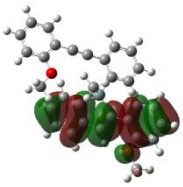 -4.640ev	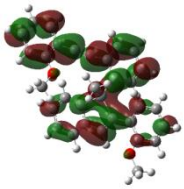 -1.883ev	2.757
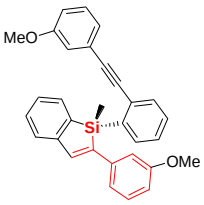 **2l**	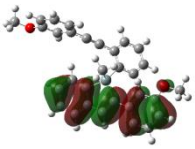 -4.818ev	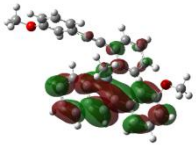 -1.920ev	2.898

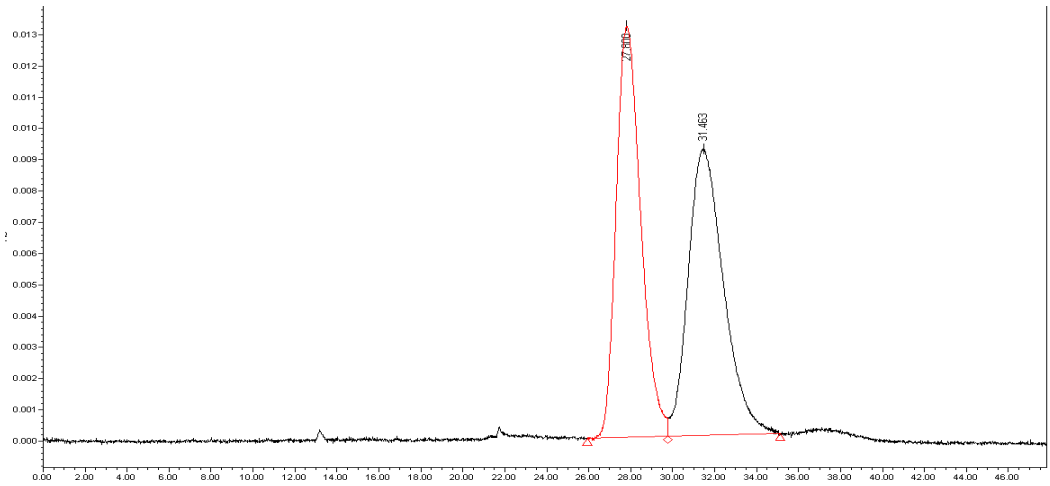

	Time/min	Area	Height	Area%
1	27.800	1075240	13152	50
2	31.463	1075240	9160	50

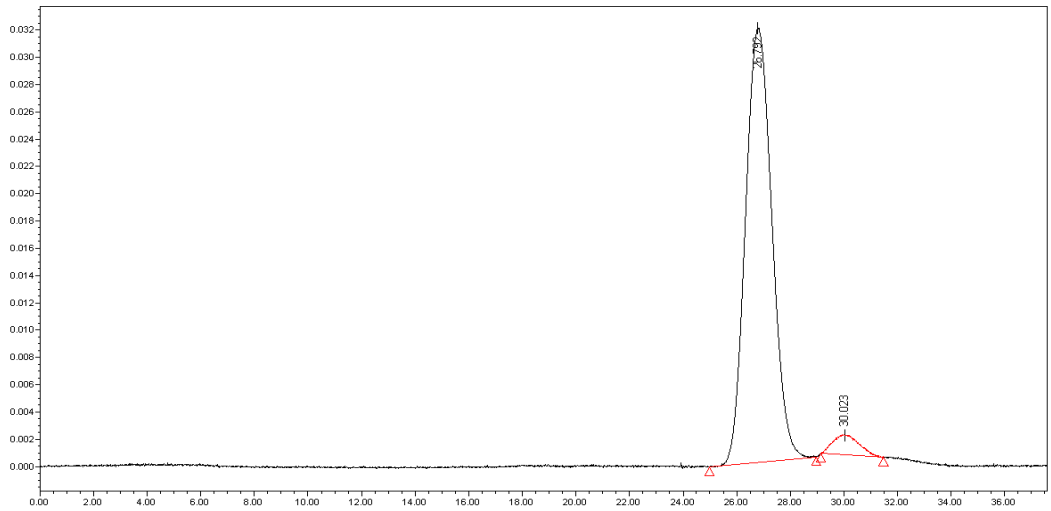

	Time/min	Area	Height	Area%
1	26.792	2193457	31842	95.51
2	30.023	103043	1485	4.49

Figure S93, the HPLC spectrum of compound **2a**, related to **Scheme 2**

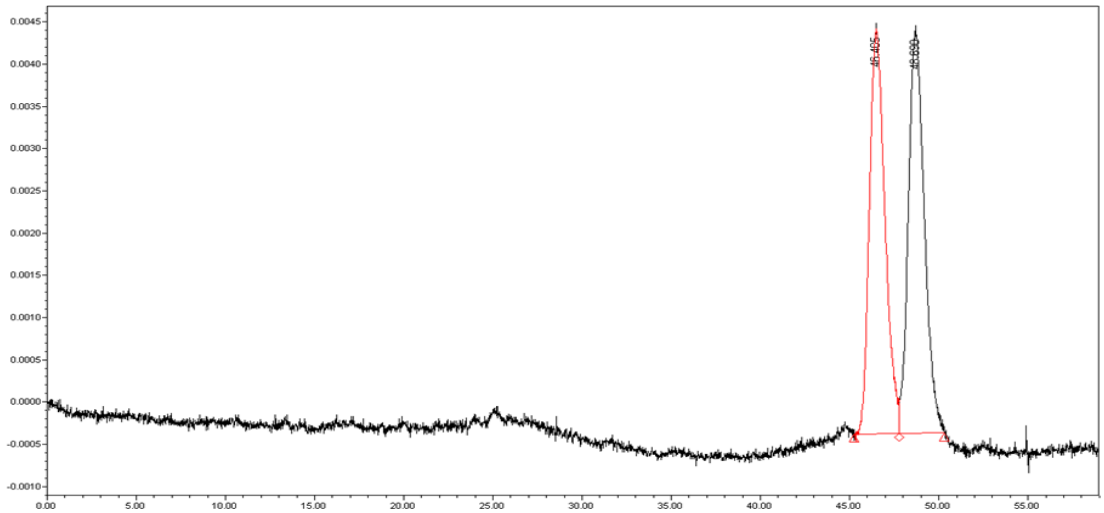

	Time/min	Area	Height	Area%
1	46.485	291019	4784	49.38
2	48.690	298330	4768	50.62

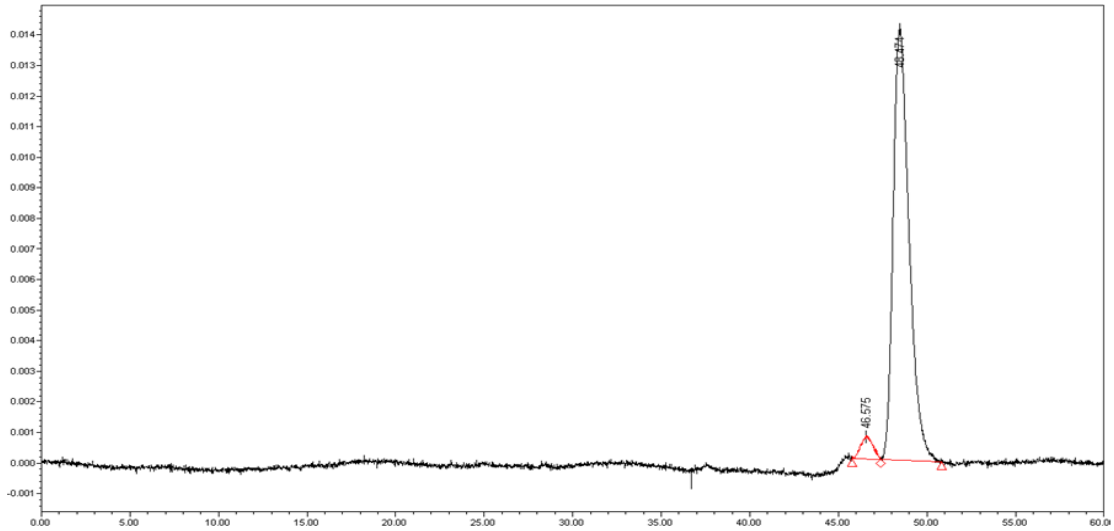

	Time/min	Area	Height	Area%
1	46.575	35478	739	3.86
2	48.474	883685	14102	96.14

Figure S94, the HPLC spectrum of compound **2b**, related to **Scheme 2**

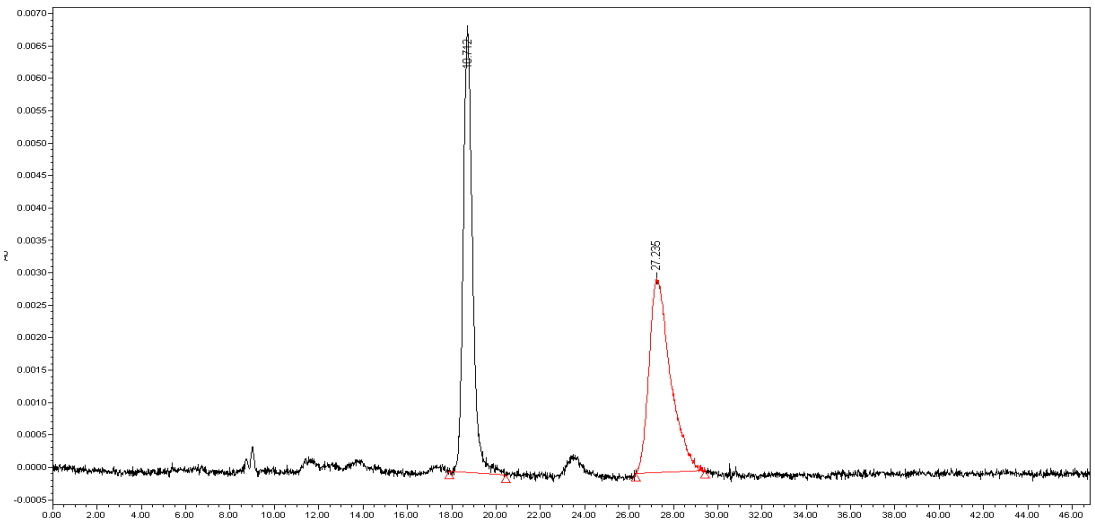

	Time/min	Area	Height	Area%
1	18.712	199777	6793	50.03
2	27.235	199505	2981	49.97

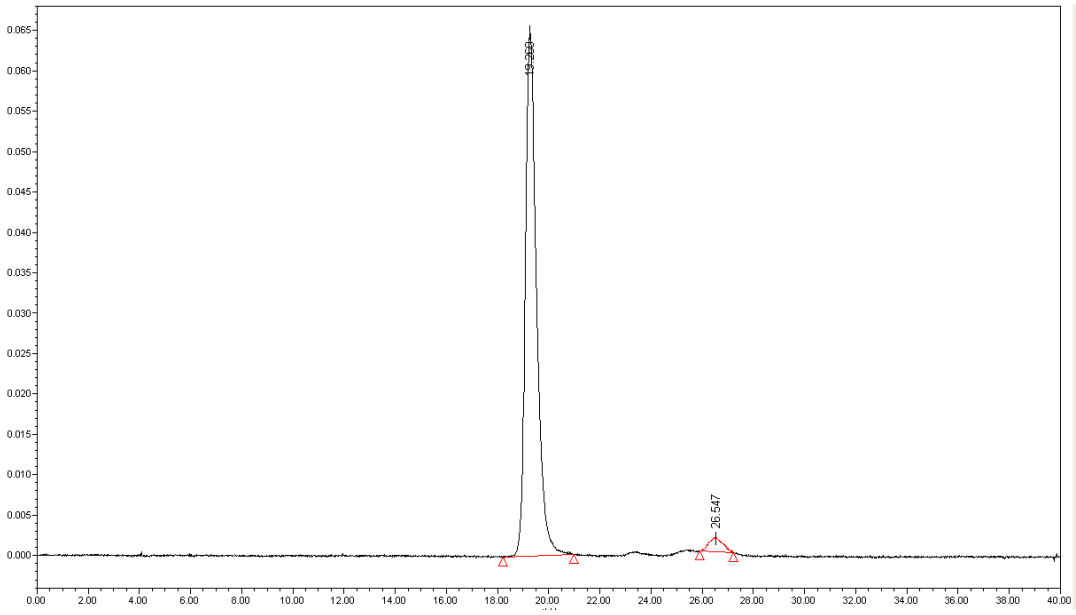

	Time/min	Area	Height	Area%
1	19.268	1979257	64815	96.69
2	26.547	68054	1716	3.32

Figure S95, the HPLC spectrum of compound **2c**, related to **Scheme 2**

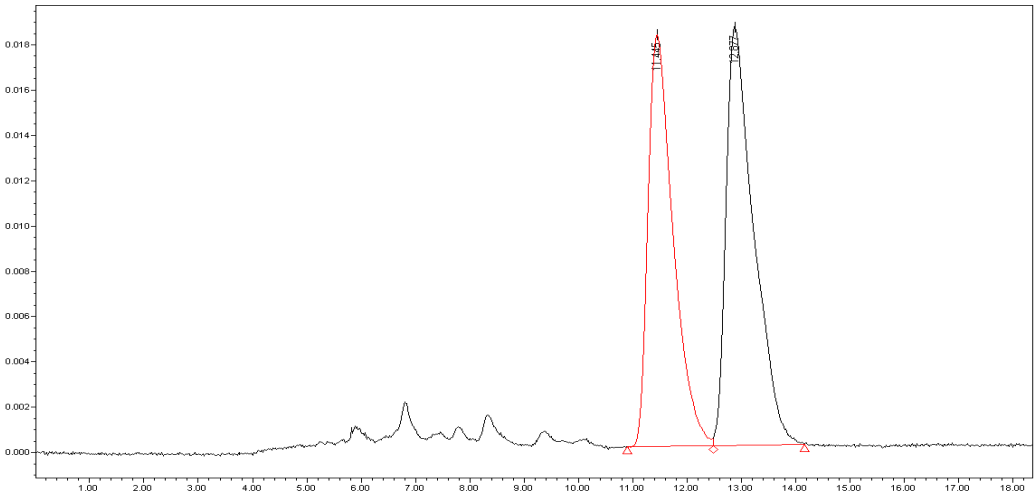

	Time/min	Area	Height	Area%
1	11.445	585900	18153	47.25
2	12.877	654006	18480	52.75

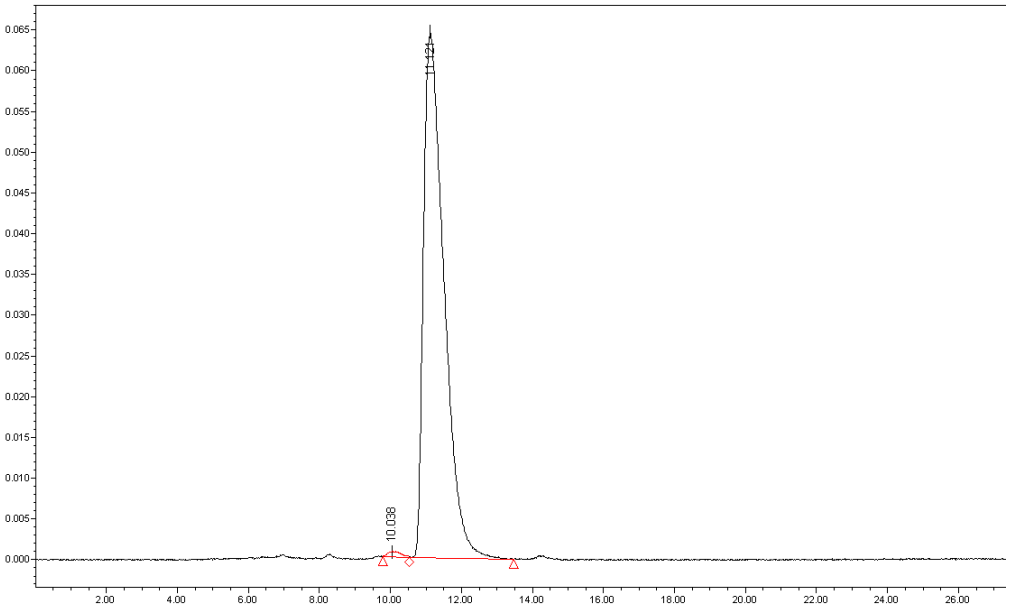

	Time/min	Area	Height	Area%
1	10.038	17535	673	0.68
2	11.121	2578652	64490	99.32

Figure S96, the HPLC spectrum of compound **2d**, related to **Scheme 2**

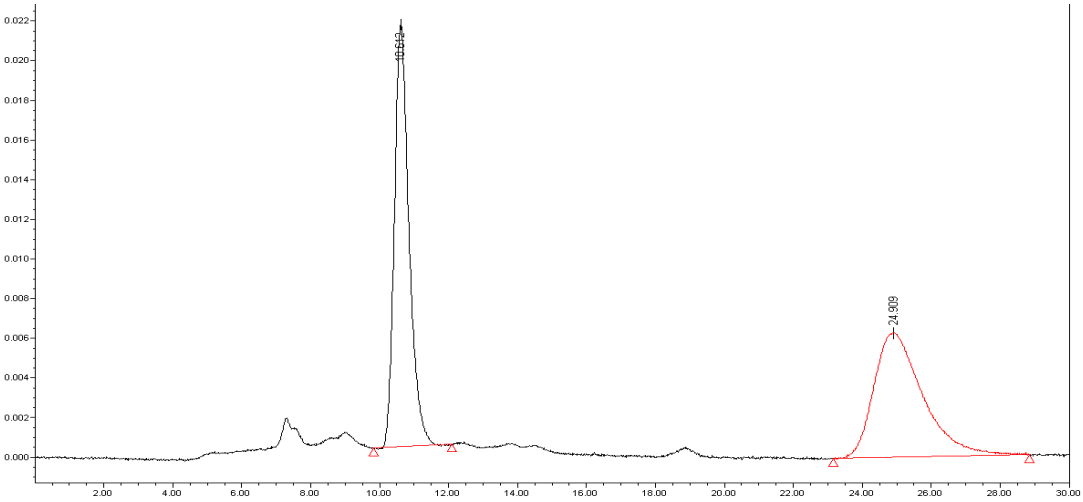

	Time/min	Area	Height	Area%
1	10.612	628213	21274	50.39
2	24.909	618583	6286	49.61

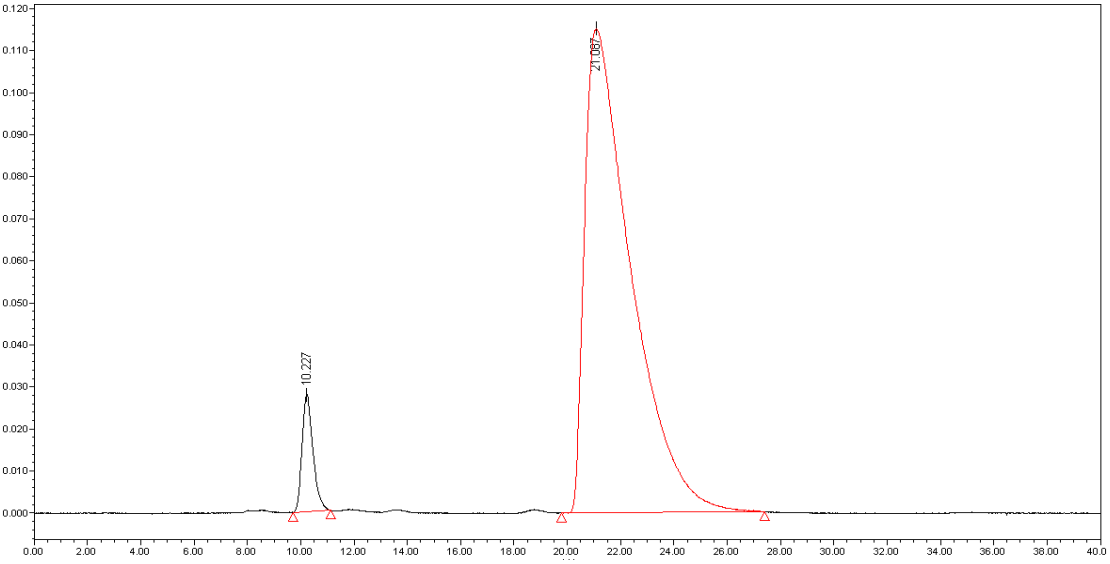

	Time/min	Area	Height	Area%
1	10.227	793482	27894	5.4
2	21.087	13896236	115139	94.6

Figure S97, the HPLC spectrum of compound **2e**, related to **Scheme 2**

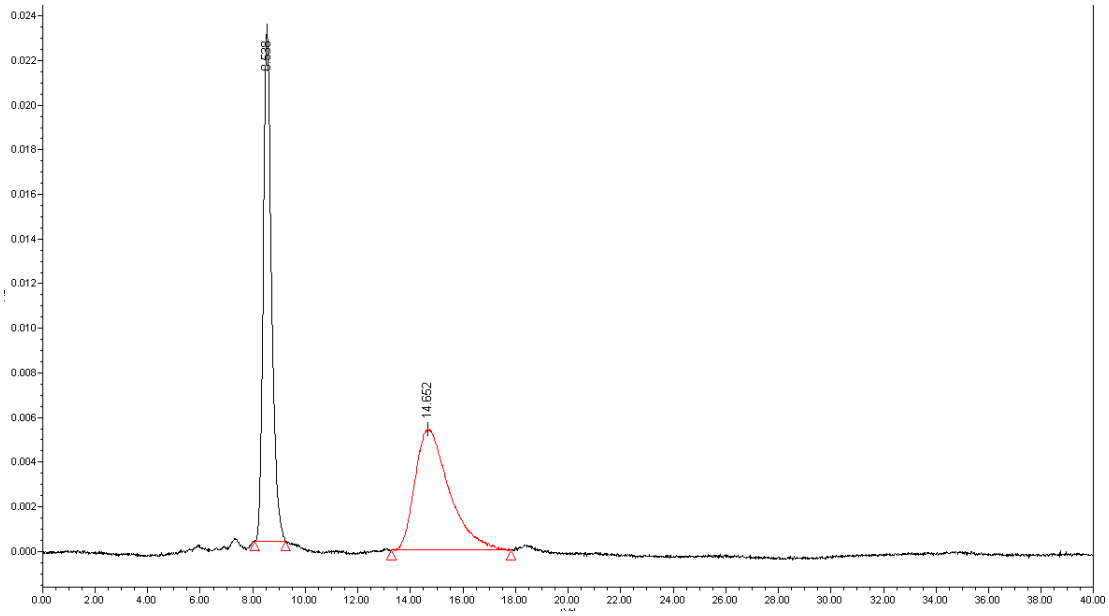

	Time/min	Area	Height	Area%
1	8.538	504871	22886	50.72
2	14.625	490480	5420	49.28

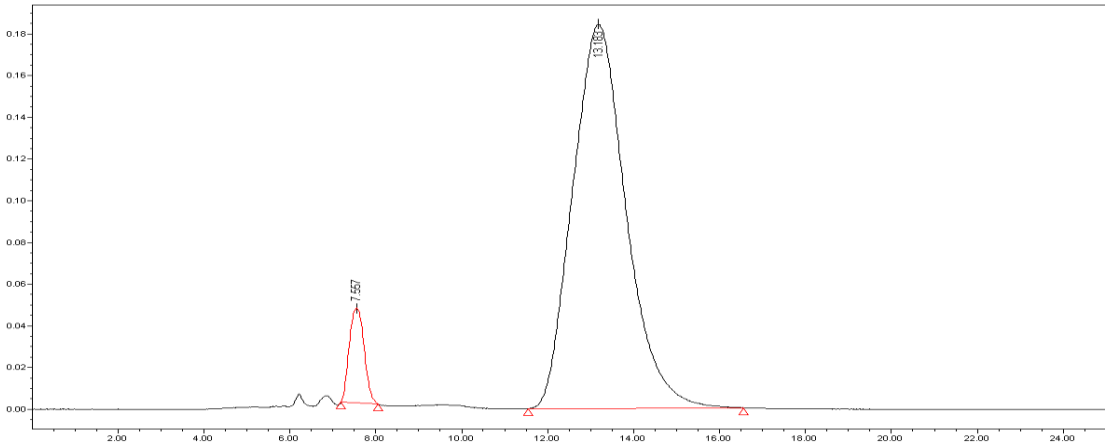

	Time/min	Area	Height	Area%
1	7.557	1098019	45399	6.47
2	13.183	15874214	184180	93.53

Figure S98, the HPLC spectrum of compound **2f**, related to **Scheme 2**

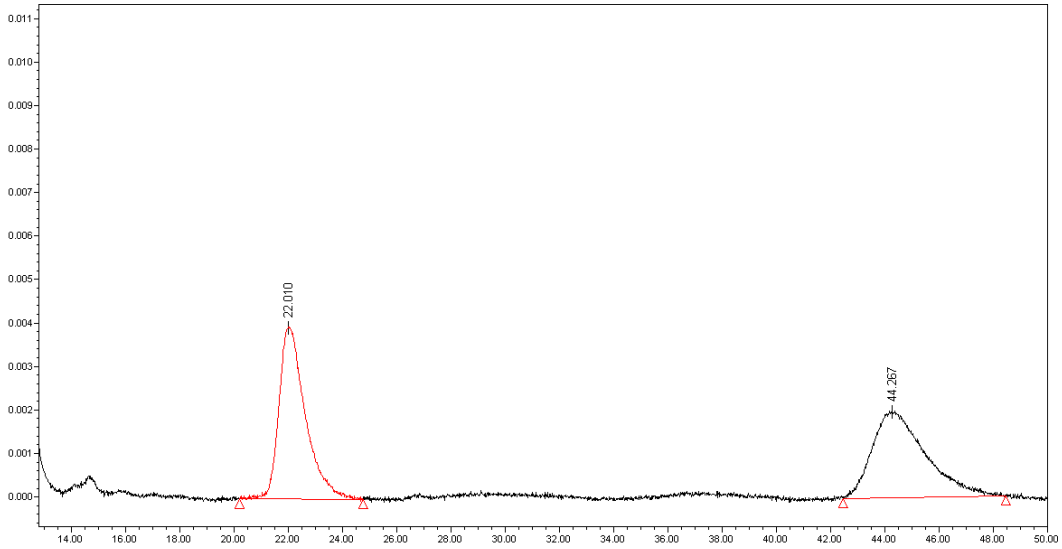

	Time/min	Area	Height	Area%
1	22.010	269297	3960	49.89
2	44.267	270455	1965	50.11

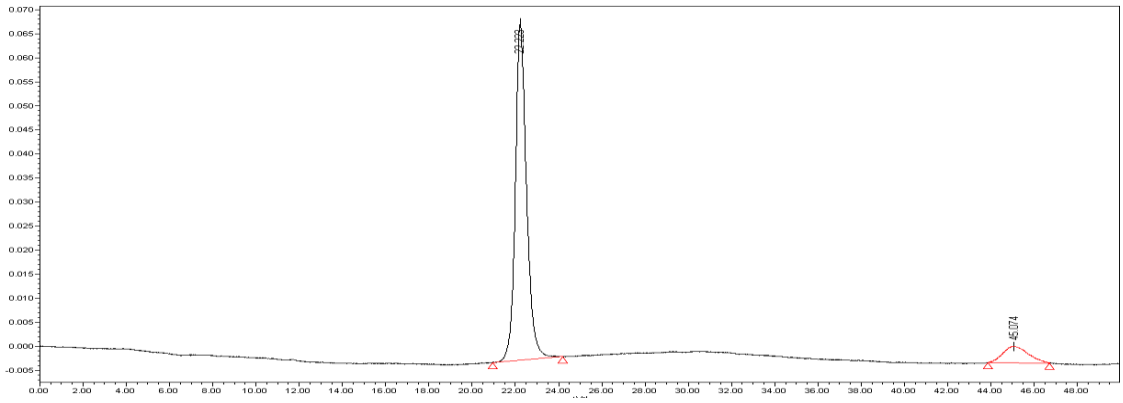

	Time/min	Area	Height	Area%
1	22.223	2515042	70131	90.16
2	45.074	273306	3394	9.84

Figure S99, the HPLC spectrum of compound **2g**, related to **Scheme 2**

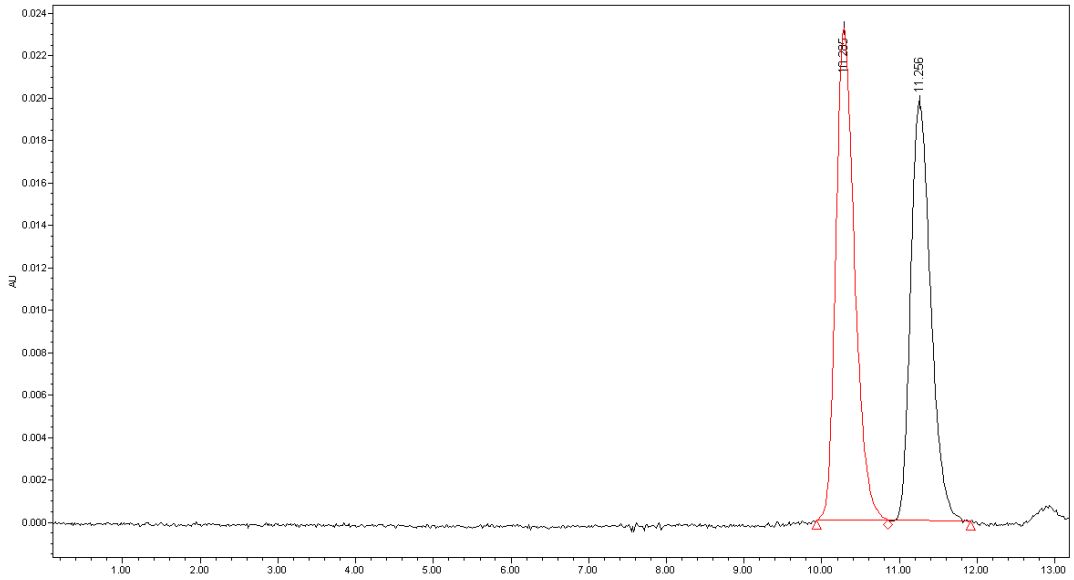

	Time/min	Area	Height	Area%
1	11.286	353752	20995	52.68
2	11.258	317785	17791	47.32

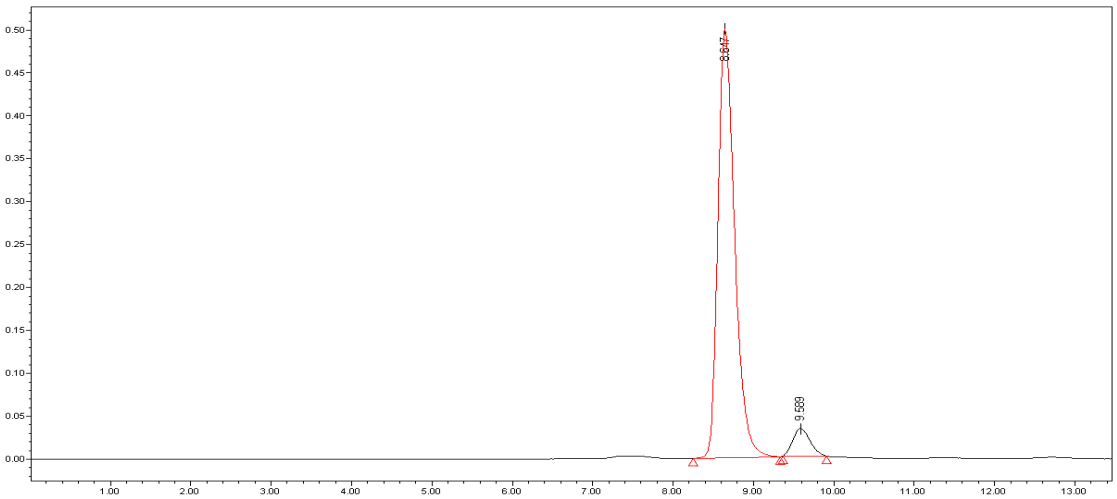

	Time/min	Area	Height	Area%
1	8.647	7203931	499663	93.88
2	9.589	469848	31878	6.12

Figure S100, the HPLC spectrum of compound **2h**, related to **Scheme 2**

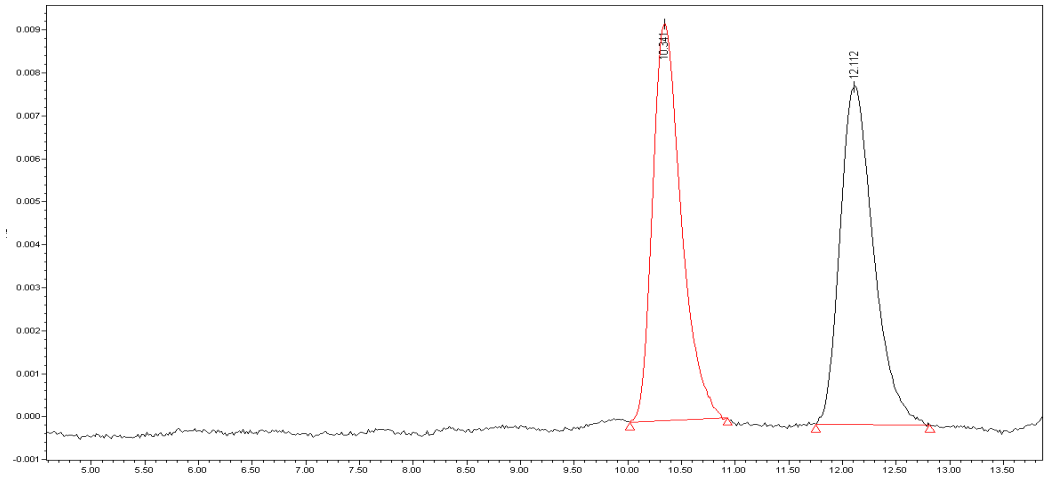

	Time/min	Area	Height	Area%
1	10.341	174103	9238	50.16
2	12.112	173006	7895	49.84

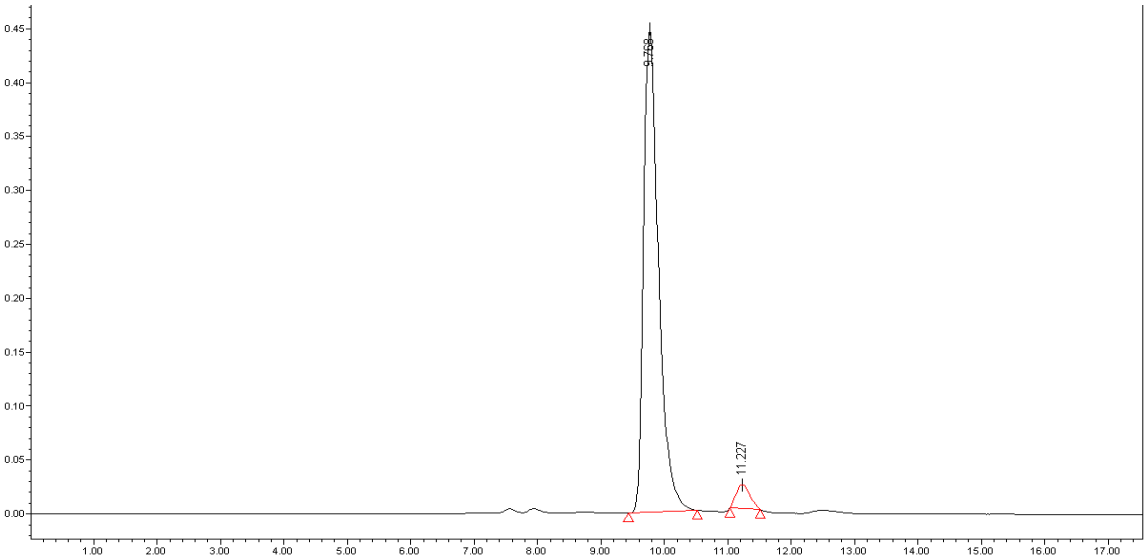

	Time/min	Area	Height	Area%
1	9.768	7356783	447901	95.66
2	11.227	333700	22215	4.34

Figure S101, the HPLC spectrum of compound **2i**, related to **Scheme 2**

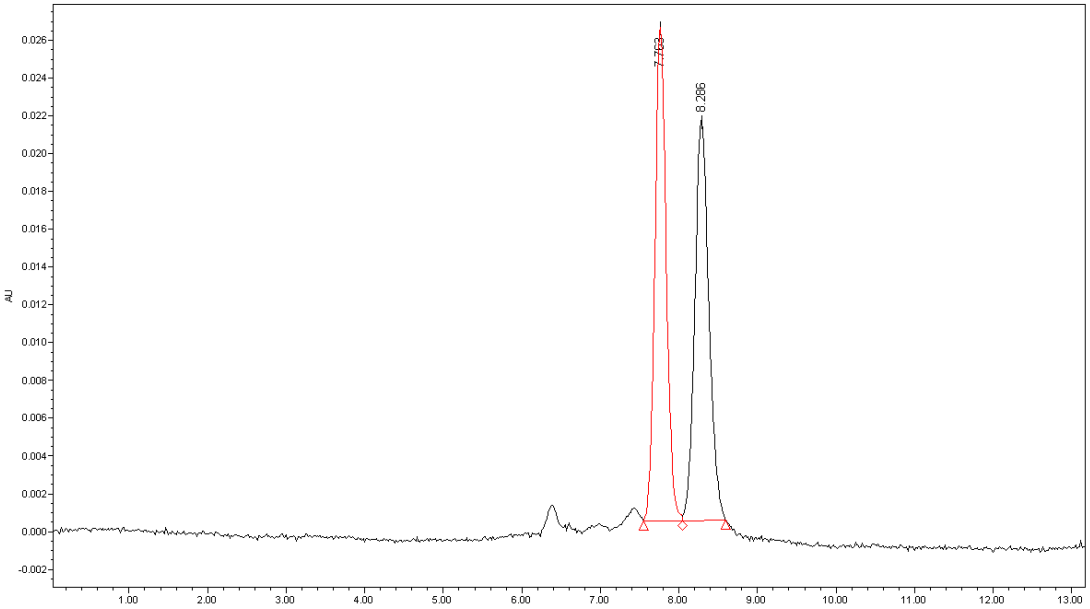

	Time/min	Area	Height	Area%
1	7.762	376725	35806	49.28
2	8.286	387792	29118	50.72

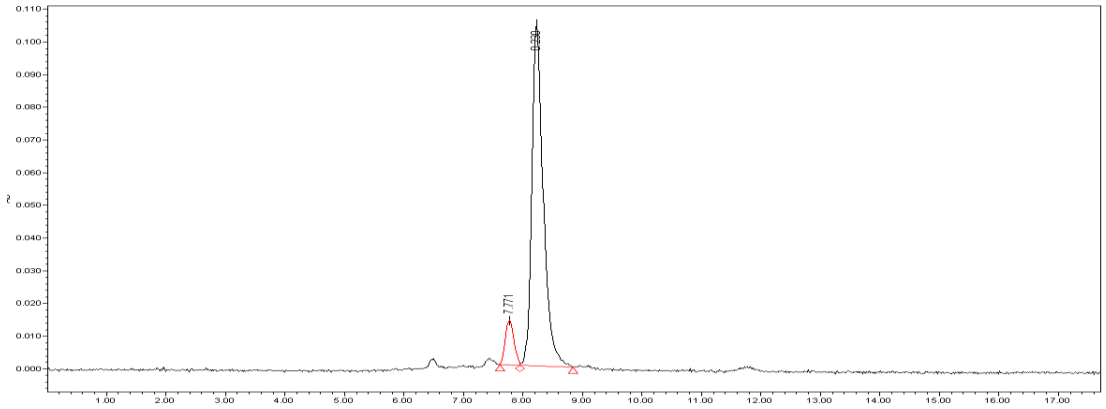

	Time/min	Area	Height	Area%
1	7.775	22408	2239	7.57
2	8.232	273573	20073	92.43

Figure S102, the HPLC spectrum of compound **2j**, related to **Scheme 2**

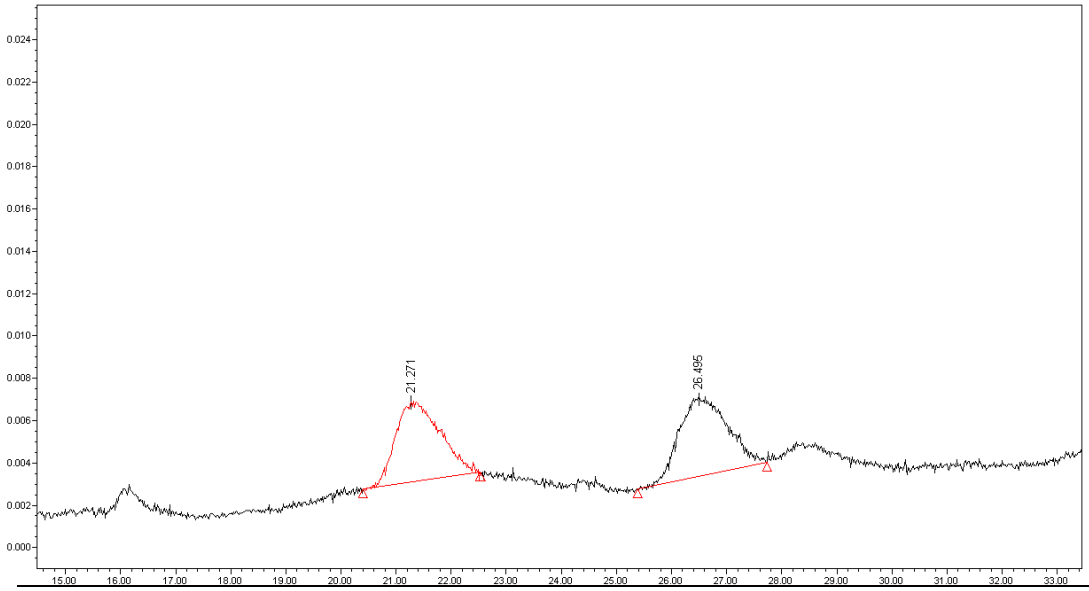

	Time/min	Area	Height	Area%
1	21.271	212218	3772	48.36
2	26.495	226588	3669	51.64

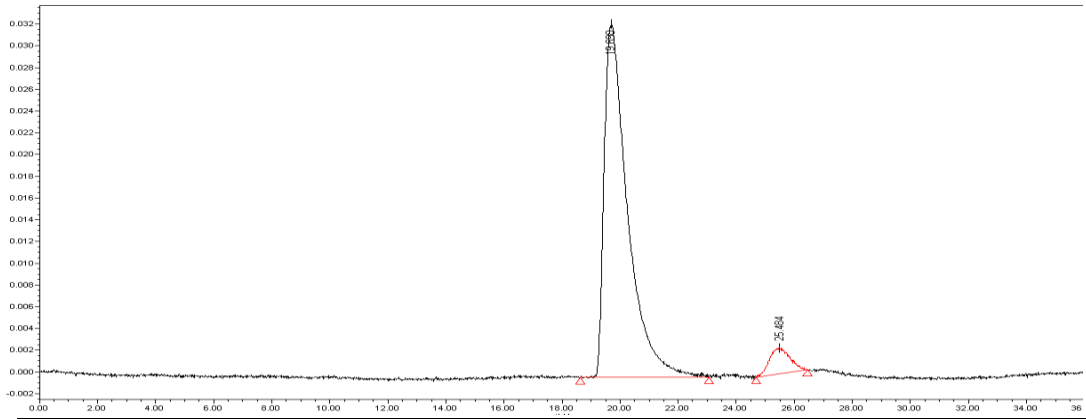

	Time/min	Area	Height	Area%
1	19.698	1824895	32485	93.99
2	25.383	116669	2388	6.01

Figure S103, the HPLC spectrum of compound **2k**, related to **Scheme 2**

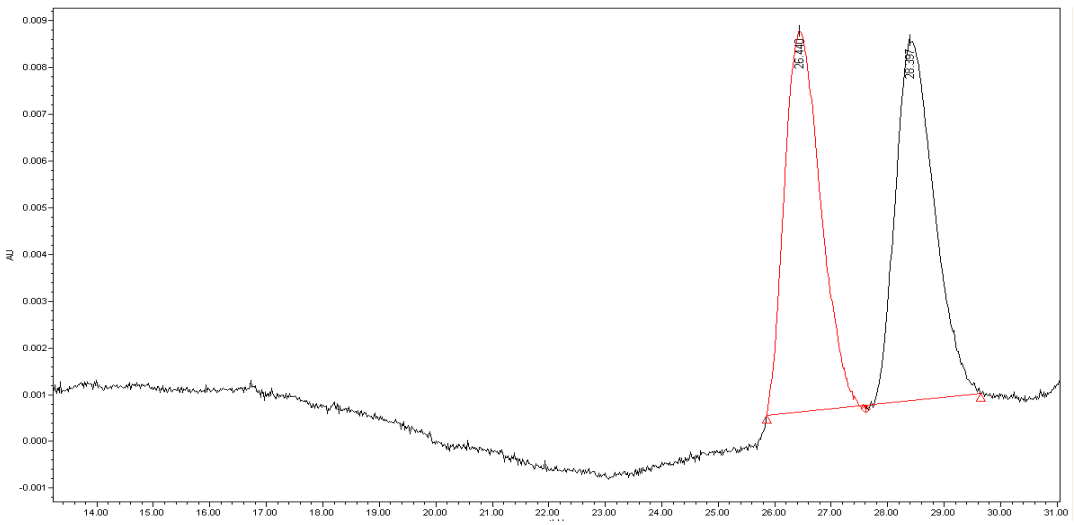

	Time/min	Area	Height	Area%
1	26.429	558438	12010	50.01
2	28.422	558275	11269	49.99

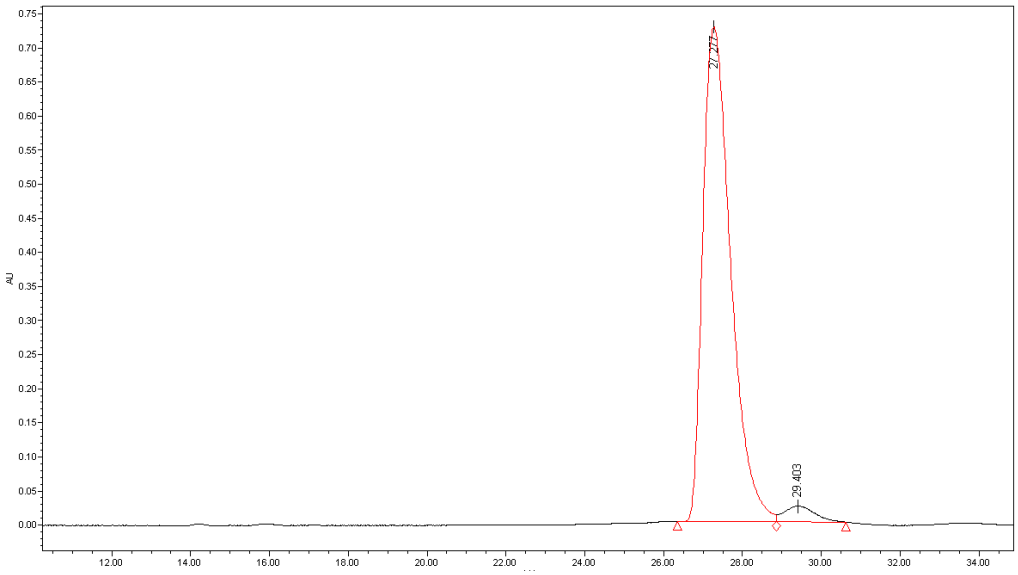

	Time/min	Area	Height	Area%
1	26.164	22488323	466399	95.46
2	28.709	1070176	19025	4.54

Figure S104, the HPLC spectrum of compound **2l**, related to **Scheme 2**

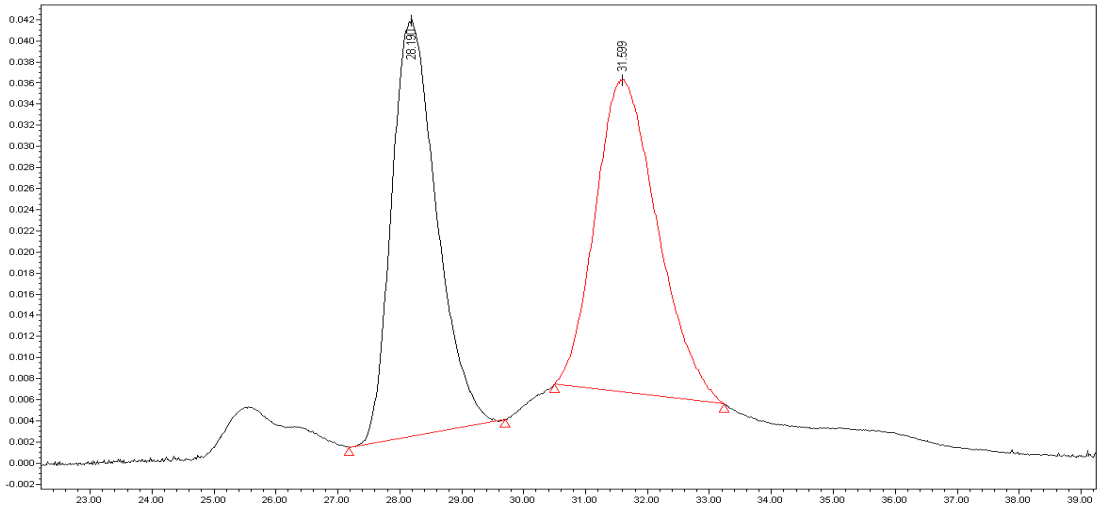

	Time/min	Area	Height	Area%
1	28.190	1993930	39346	49.06
2	31.599	2070135	29805	50.94

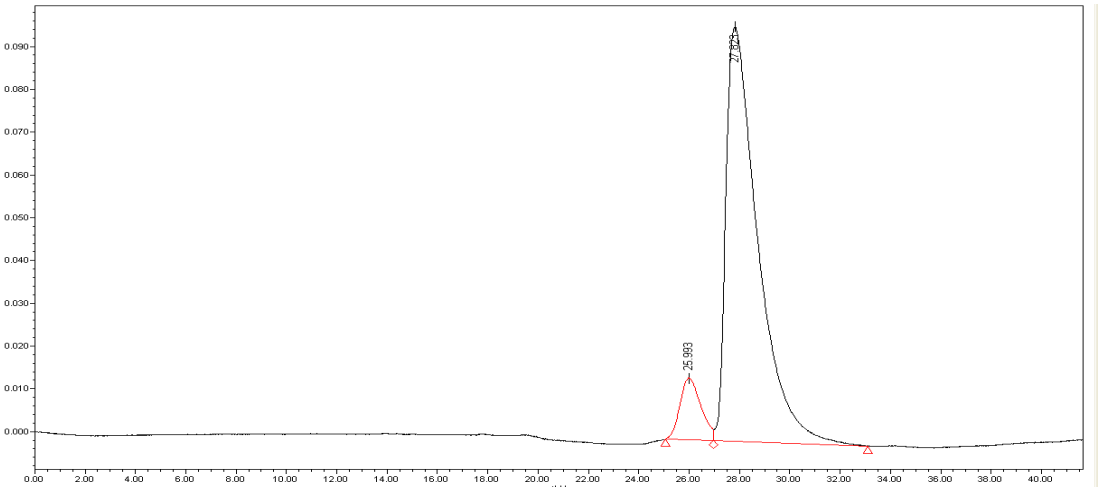

	Time/min	Area	Height	Area%
1	25.993	835540	14483	8.92
2	27.823	8531993	96905	91.08

Figure S105, the HPLC spectrum of compound **2m**, related to **Scheme 2**

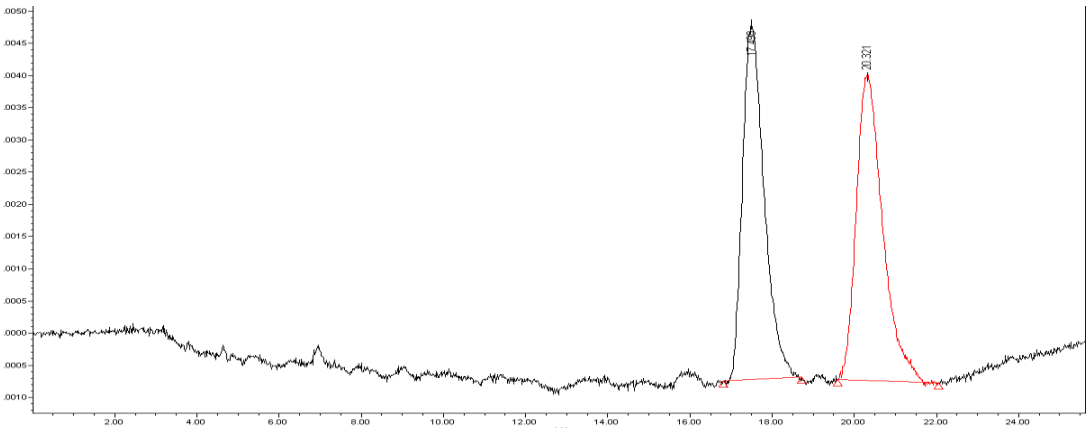

	Time/min	Area	Height	Area%
1	**17.498**	**202433**	**5487**	**48.76**
2	**20.321**	**212717**	**4739**	**51.24**

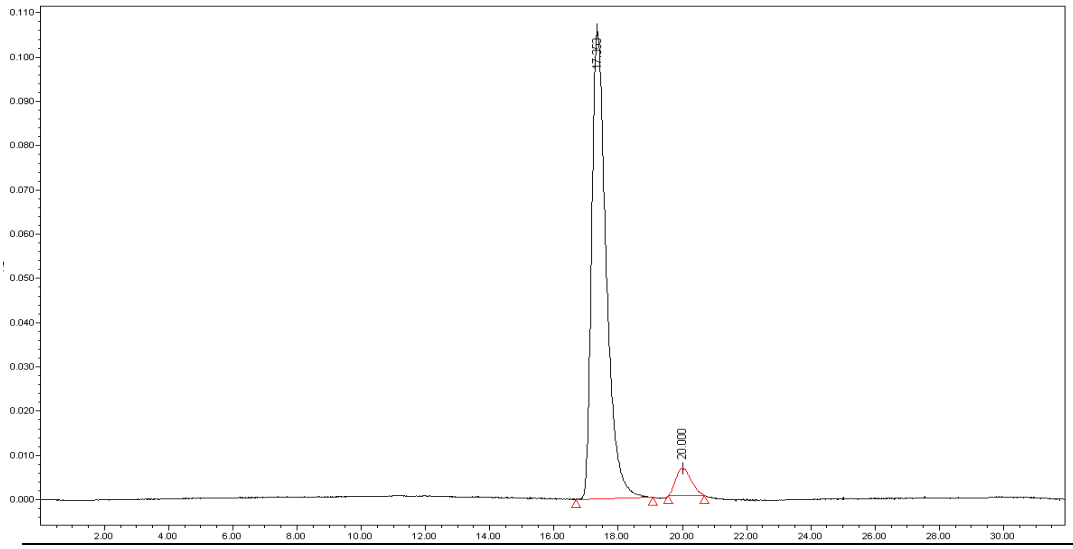

	Time/min	Area	Height	Area%
1	**17.353**	**3337311**	**105949**	**92.24**
2	**20.000**	**204123**	**6238**	**5.76**

Figure S106, the HPLC spectrum of compound **2n**, related to **Scheme 2**

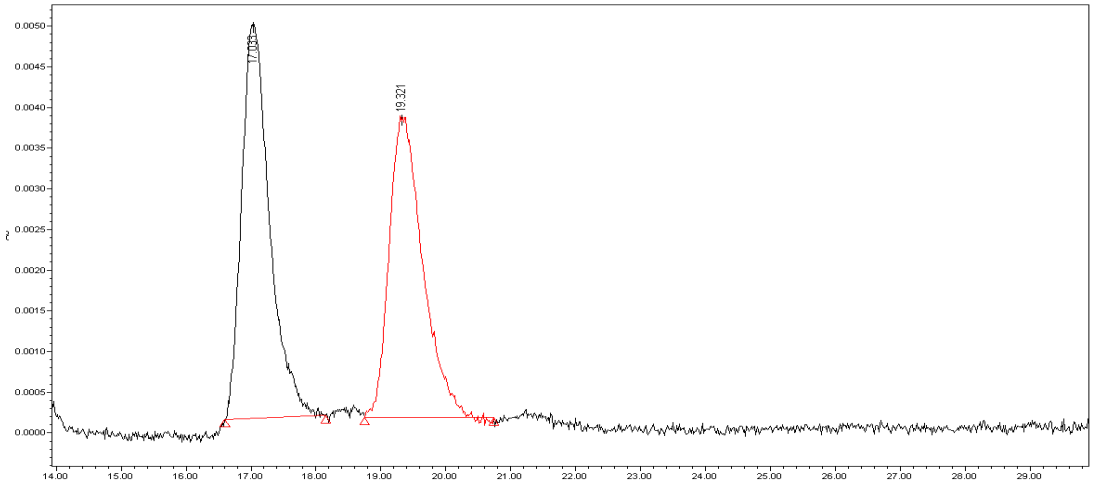

	Time/min	Area	Height	Area%
1	17.027	164795	5122	50.30
2	19.334	162811	3939	49.70

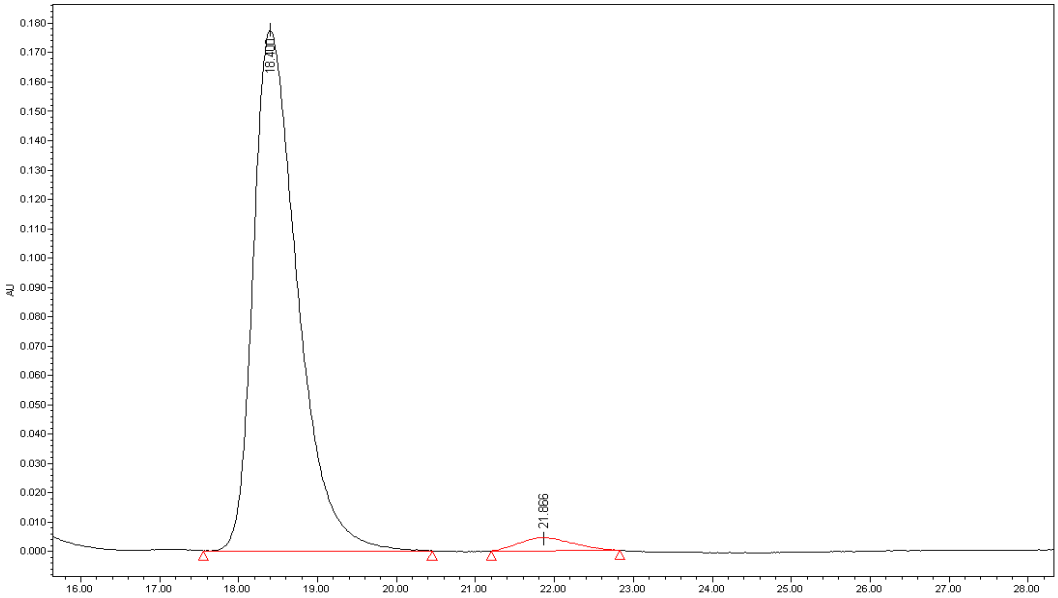

	Time/min	Area	Height	Area%
1	18.401	7131377	184341	97.26
2	21.860	200971	4212	2.74

Figure S107, the HPLC spectrum of compound **2o**, related to **Scheme 2**

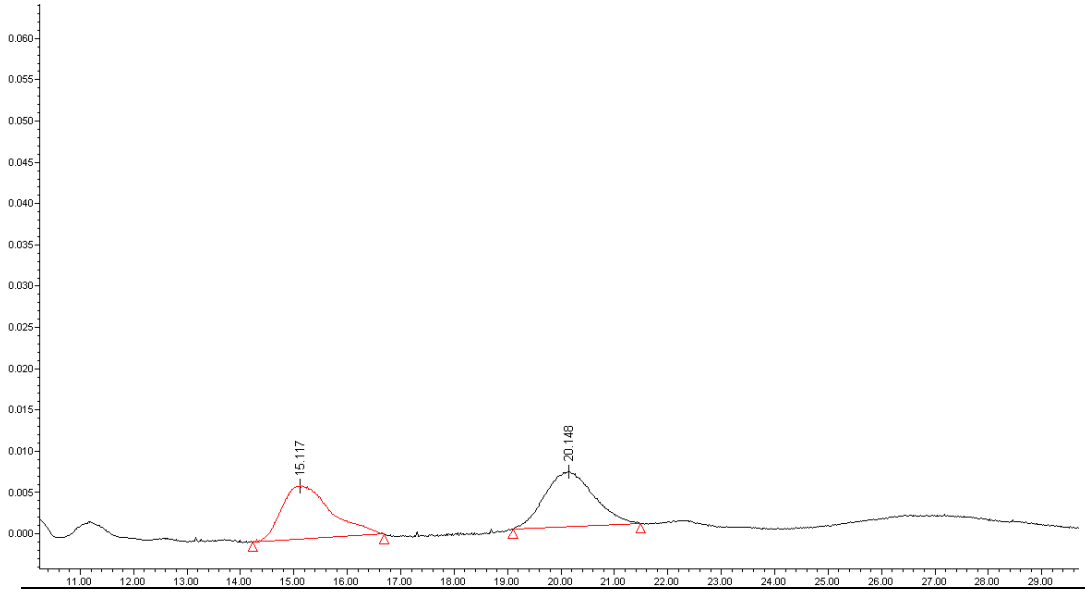

	Time/min	Area	Height	Area%
1	15.1117	410167	49.22	49.22
2	20.148	423245	6676	50.78

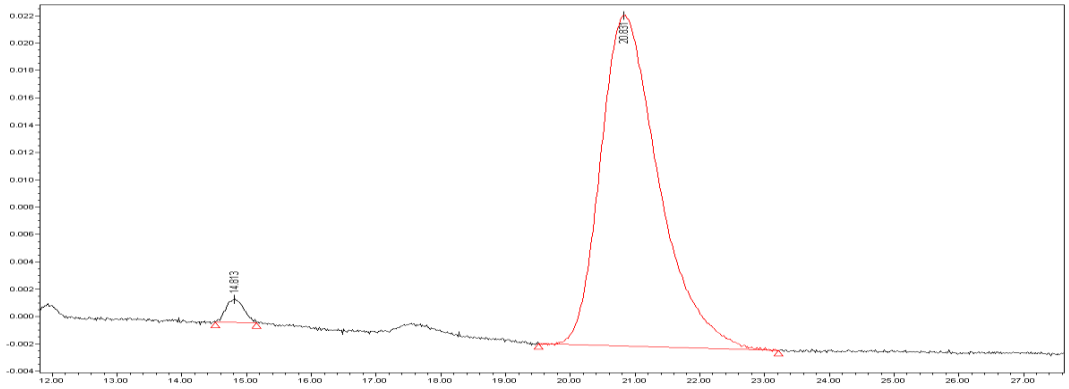

	Time/min	Area	Height	Area%
1	14.813	32464	1678	2.11
2	20.831	1506048	24186	97.89

Figure S108, the HPLC spectrum of compound **2p**, related to **Scheme 2**

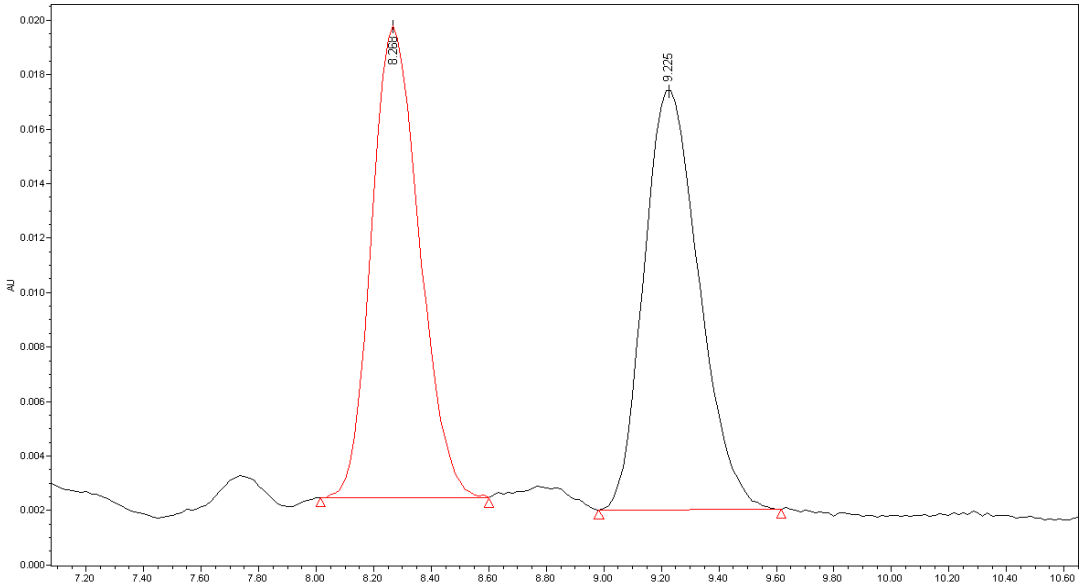

	Time/min	Area	Height	Area%
1	8.268	200472	17266	49.74
2	9.225	202602	15387	50.26

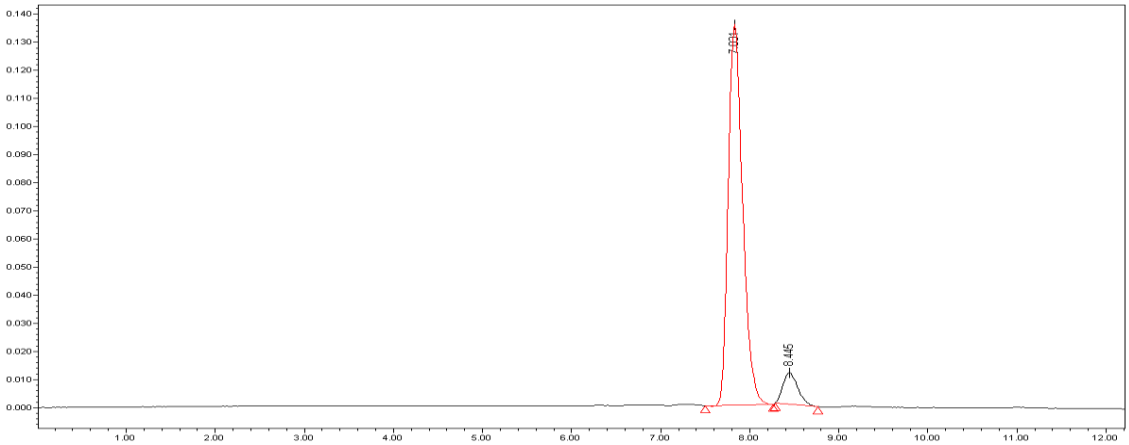

	Time/min	Area	Height	Area%
1	7.831	1527382	135633	92.00
2	8.445	132880	11364	8.00

Figure S109, the HPLC spectrum of compound **2q**, related to **Scheme 2**

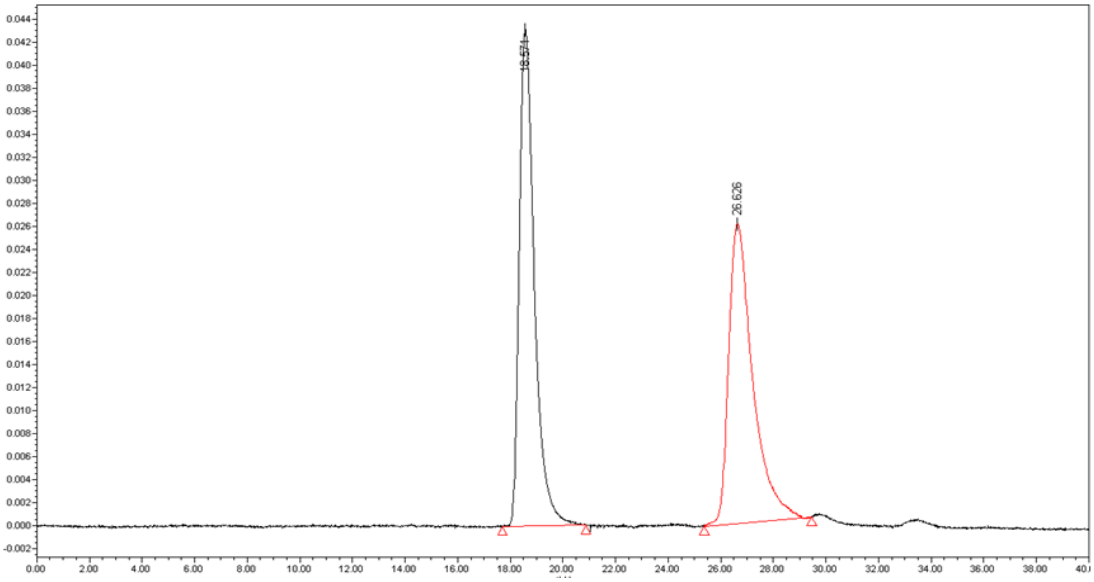

	Time/min	Area	Height	Area%
1	18.571	1716021	43100	50.95
2	26.626	1652184	26019	49.05

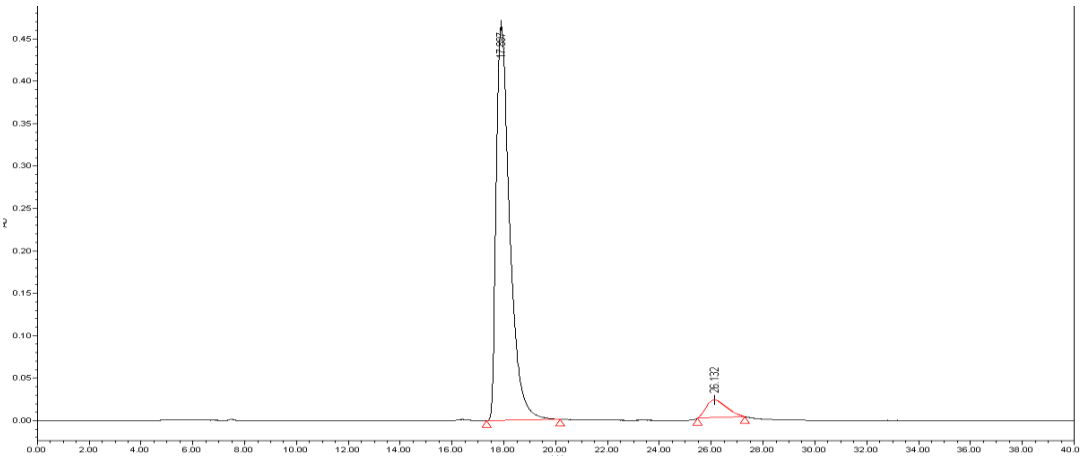

	Time/min	Area	Height	Area%
1	17.897	16892981	465377	93.60
2	26.132	1154284	21004	6.40

Figure S110, the HPLC spectrum of compound **2r**, related to **Scheme 2**

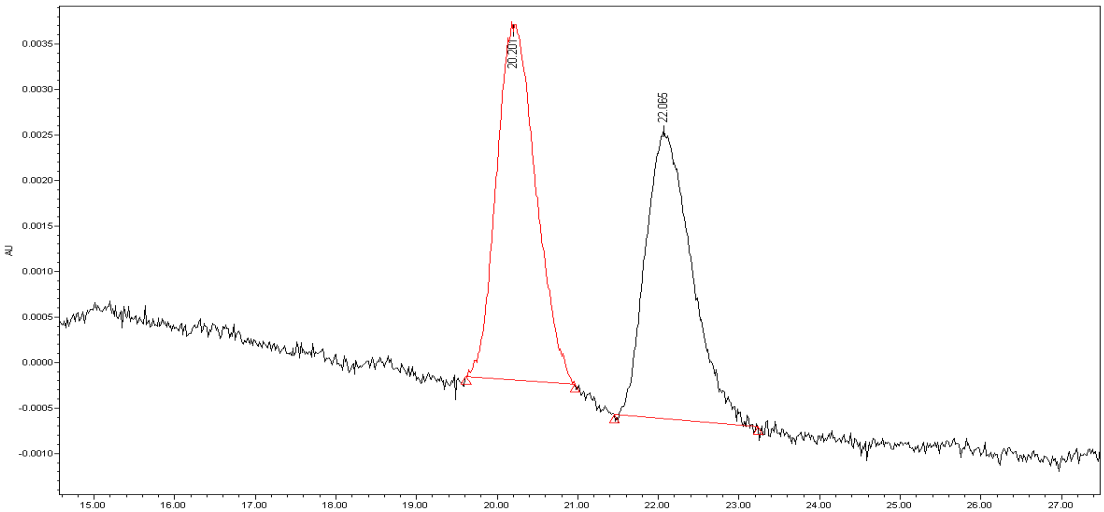

	Time/min	Area	Height	Area%
1	20.208	202251	5635	51.22
2	22.060	192607	4481	48.78

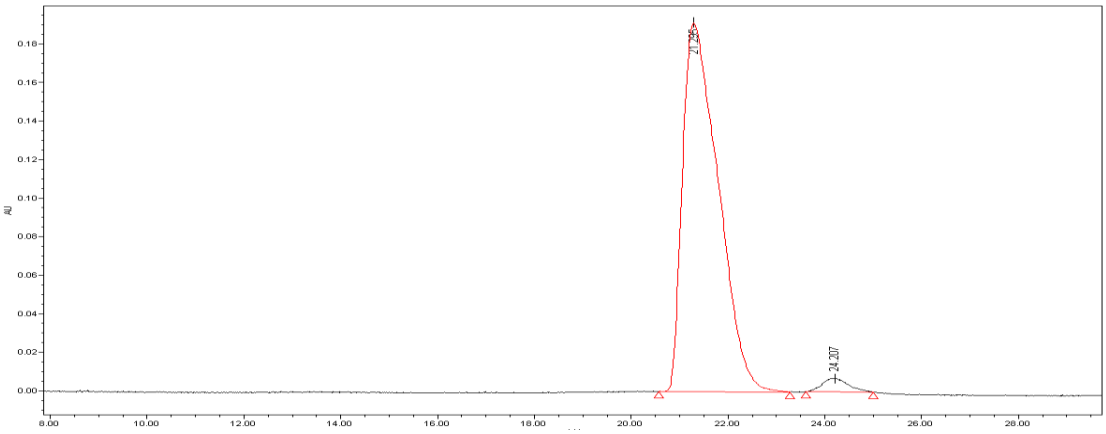

	Time/min	Area	Height	Area%
1	21.295	9808883	191494	97.19
2	24.207	283094	7215	2.81

Figure S111, the HPLC spectrum of compound **2s**, related to **Scheme 2**

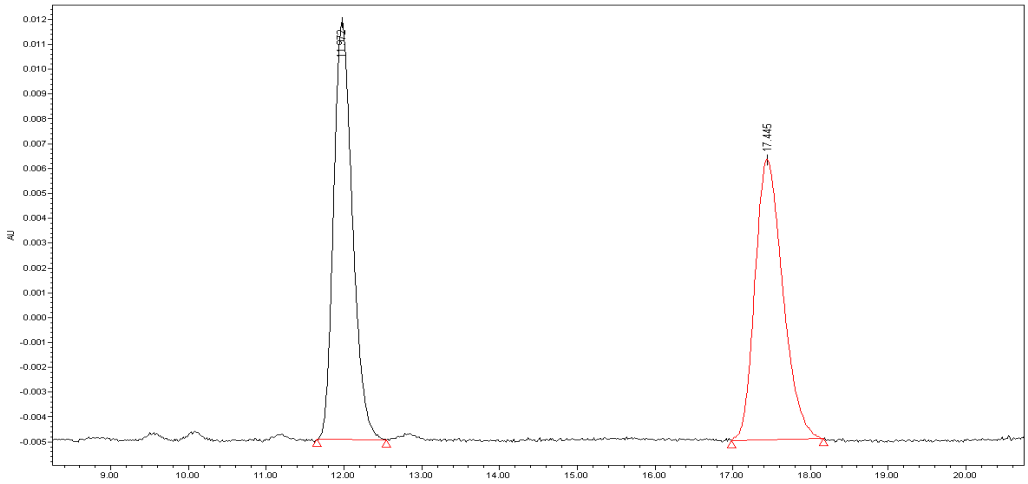

	Time/min	Area	Height	Area%
1	11.972	284419	16853	49.77
2	17.445	287023	11358	50.23

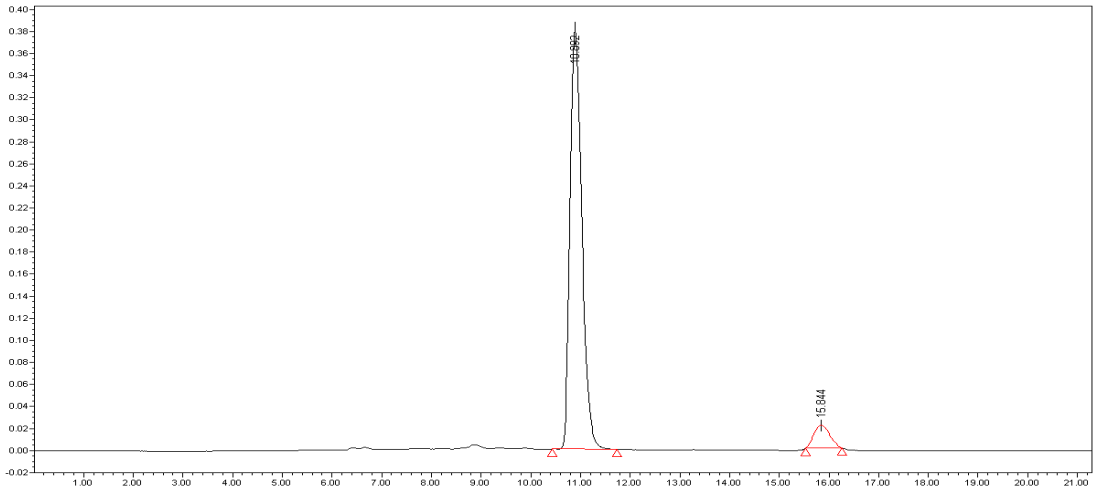

	Time/min	Area	Height	Area%
1	10.892	383689	383689	93.22
2	15.844	462586	20793	6.78

Figure S112, the HPLC spectrum of compound **2t**, related to **Scheme 2**

Transparent Methods

1. General information:

Unless specifically stated, all reagents were commercially obtained and where appropriate, purified prior to use. For example, all the aldehydes recrystallized or distilled prior to use. Dichloromethane, toluene, were freshly distilled from CaH_2, Ether (Et_2O), tetrahydrofuran (THF) and 1, 4-dioxane were dried and distilled from metal sodium and benzophenone. Alcohol solvents were dried and distilled from metal magnesium. Other commercially available reagents and solvents were used directly without purification. Reactions were monitored by thin layer chromatography (TLC) using silica gel plates. Flash column chromatography was performed over silica (300 - 400 mesh). ^{1}H, ^{13}C, ^{31}P, ^{19}F and ^{29}Si NMR spectra were recorded on a *Bruker* 400 MHz or 500 MHz spectrometer in $CDCl_3$. Multiplicities were given as: s (singlet); d (doublet); dd (doublets of doublet); t (triplet); q (quartet); td (triplet of doublets); tt (triplet of triplets) ddd (doublet of doublet of doublets) or m (multiplets). or m (multiplets). High resolution mass spectra (HRMS) of the products were obtained on a *Bruker* Daltonics micro TOF-spectrometer. HPLC was carried out with a *Agilent* 1260 infinity or Waters AcQuity UPLC using a chiralcel IA column, a chiral INA column (from *Phenomenex*) and a Chiralcel OD-H column.

2. General procedure for the synthesis of Si-tethered bisalkynes (Substrate 1)

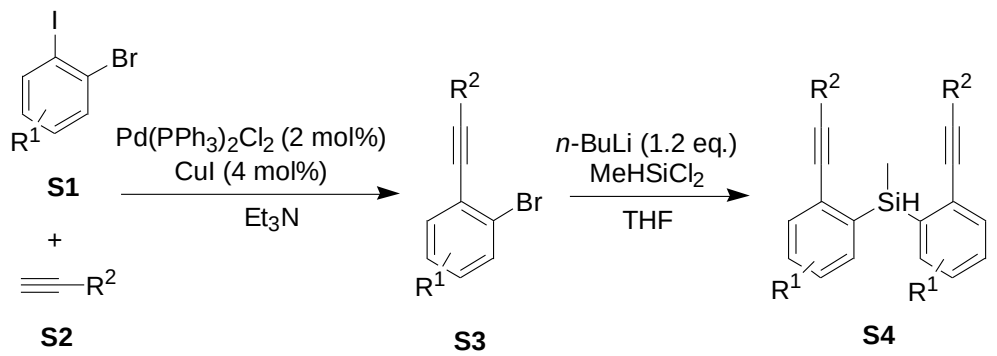

The synthesis of **S3**: A 50 mL single-necked, round-bottomed flask equipped with an egg-shaped magnetic stir bar is flame-dried under vacuum. After cooling to 23 ℃, $Pd(PPh_3)_2Cl_2$ (140 mg, 0.2 mmol, 2 mol %) and CuI (75 mg, 0.4 mmol, 4 mol %) is added, the reaction flask is put under an atmosphere of N_2, and **S1** (10 mmol), Et_3N (18 mL, 120 mmol, 1.8 equiv), and **S2** (10.2 g, 11 mmol, 1.1 equiv) is added via syringe resulting in a clear solution with a brown color. the reaction mixture is stirred at rt for 4 h. The solution was then diluted with EA (20 mL), and washed with water (2 × 20 mL) and brine (2 × 20 mL). The organics were then passed through a hydrophobic frit and concentrated under reduced pressure to give a yellow oil, which was purified by flash chromatography (silica gel, petroleum ether) to afford **S3**.

The synthesis of **S4** (substrate 1 in the text): A 50 mL single-necked, round-bottomed flask equipped with an egg-shaped magnetic stir bar is flame-dried under vacuum. After cooling to 23 ℃, **S3** is added, the reaction flask is put under an atmosphere of N_2, 5 ml (2.5 mmol) of a 2.5 M solution *n*-BuLi in hexanes was added at -78 ℃. The resulting solution was stirred at -78 ^{o}C for 1 h, and then 0.6 mL of $MeHSiCl_2$ (6 mmol, 0.6 equiv) was added slowly to the above mixture at the same temperature. The reaction mixture was stirred for 4 hours at rt. When the reaction is complete, it was quenched with saturated aqueous NH_4Cl (10 mL) and stirred vigorously for 5 minutes. The aqueous phase was extracted with ethyl acetate (3×40 mL). The combined organic layers were dried over Na_2SO_4 and concentrated under reduced pressure. Which was purified by flash chromatography (silica gel, petroleum ether) to afford **S4**.

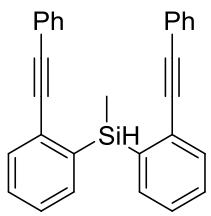

Methylbis(2-(phenylethynyl)phenyl)silane (1a)

White solid. mp 75.4-77.6 ^{o}C.

^{1}H NMR (400 MHz, $CDCl_3$) δ 7.57 (d, J = 7.5 Hz, 3H), 7.42 – 7.32 (m, 6H), 7.32 – 7.22 (m, 9H), 5.36 (q, J = 3.8 Hz, 1H), 0.82 (d, J = 3.8 Hz, 3H).

^{13}C NMR (100 MHz, $CDCl_3$) δ 137.9, 136.2, 132.1, 131.5, 129.6, 129.4, 128.4, 128.3, 127.7, 123.4, 93.0, 90.4, -5.0.

HRMS (ESI-TOF) m/z: $[M+Na]^+$ Calcd for $C_{29}H_{22}NaSi$, 421.1383; found 421.1390.

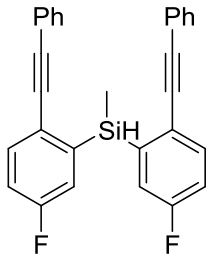

Bis(5-fluoro-2-(phenylethynyl)phenyl)(methyl)silane (1b)

White solid. mp 112.0-112.4 ^{o}C.

^{1}H NMR (400 MHz, $CDCl_3$) δ 7.55 (dd, J = 8.4, 5.2 Hz, 2H), 7.35 (dd, J = 6.7, 3.0 Hz, 4H), 7.30 (d, J = 5.3 Hz, 2H), 7.24 (s, 1H), 7.22 (d, J = 2.6 Hz, 1H), 7.06 (m, J = 8.5, 2.7 Hz, 2H), 5.30 (q, J = 3.6 Hz, 1H), 0.81 (d, J = 3.8 Hz, 3H).

^{13}C NMR (100 MHz, $CDCl_3$) δ 139.5, 136.2, 134.5, 132.7, 131.5, 129.2, 128.67, 128.4, 128.2, 123.6, 92.5, 90.6, 21.4, -4.7.

HRMS (ESI-TOF) m/z: $[M+Na]^+$ Calcd for $C_{29}H_{20}F_2NaSi$, 457.1195; found 457.1215.

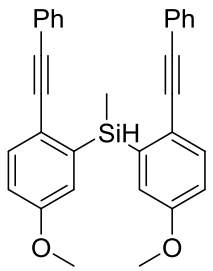

Bis(5-methoxy-2-(phenylethynyl)phenyl)(methyl)silane (1c)

White solid. mp 102.9-104.2 ^{o}C.

^{1}H NMR (400 MHz, $CDCl_3$) δ 7.51 (d, J = 8.5 Hz, 2H), 7.36 – 7.31 (m, 4H), 7.30 – 7.26 (m, 6H), 7.12 (d, J = 2.7 Hz, 2H), 6.88 (dd, J = 8.5, 2.7 Hz, 2H), 5.29 (q, J = 3.8 Hz, 1H), 3.65 (s, 6H), 0.82 (d, J = 3.8 Hz, 3H).

^{13}C NMR (100 MHz, $CDCl_3$) δ 159.0, 139.6, 133.7, 131.4, 128.4, 128.0, 123.7, 121.6, 121.31, 115.3, 91.4, 90.4, 55.2, -5.0.

HRMS (ESI-TOF) m/z: [M+Na]$^+$ Calcd for $C_{31}H_{26}NaO_2Si$, 481.1594; found 481.1611.

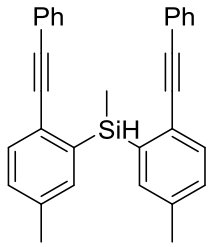

Methylbis(5-methyl-2-(phenylethynyl)phenyl)silane (1d)

Yellow oil.

^{1}H NMR (400 MHz, $CDCl_3$) δ 7.38 (s, 1H), 7.36 (s, 1H), 7.34 (d, J = 1.2 Hz, 2H), 7.28 – 7.24 (m, 3H), 7.22 – 7.20 (m, 3H), 7.19 (s, 4H), 7.08 (dd, J = 7.8, 1.2 Hz, 2H), 5.19 (q, J = 3.8 Hz, 1H), 2.12 (s, 6H), 0.73 (d, J = 3.9 Hz, 3H).

^{13}C NMR (100 MHz, $CDCl_3$) δ 137.8, 137.4, 137.1, 132.0, 131.5, 130.3, 128.3, 128.1, 126.2, 123.7, 92.1, 90.5, 21.5, -5.1.

HRMS (ESI-TOF) m/z: [M+Na]$^+$ Calcd for $C_{31}H_{26}NaSi$, 449.1696; found 449.1868.

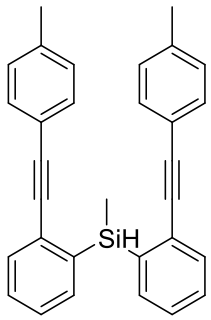

Methylbis(2-(*p*-tolylethynyl)phenyl)silane (1e)

Yellow solid. mp 88.1-92.2 ^{o}C.

^{1}H NMR (400 MHz, $CDCl_3$) δ 7.55 (dd, J = 5.1, 3.6 Hz, 4H), 7.36 (td, J = 7.6, 1.2 Hz, 2H), 7.26 – 7.21 (m, 6H), 7.09 (d, J = 8.0 Hz, 4H), 5.34 (q, J = 3.8 Hz, 1H), 2.34 (s, 6H), 0.81 (d, J = 3.9 Hz, 3H).

^{13}C NMR (100 MHz, $CDCl_3$) δ 138.5, 137.8, 136.2, 131.9, 131.4, 129.6, 129.5, 129.2, 127.5, 120.4, 93.2, 89.8, 21.6, -5.0.

HRMS (ESI-TOF) m/z: $[M+H]^+$ Calcd for $C_{31}H_{27}Si$, 427.1877; found 427.1861.

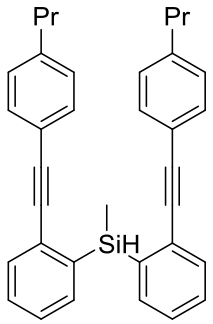

Methylbis(2-((4-propylphenyl)ethynyl)phenyl)silane (1f)

Yellow solid. mp 65.5-68.6 ^{o}C.

^{1}H NMR (400 MHz, $CDCl_3$) δ 7.56 (d, J = 7.9 Hz, 4H), 7.36 (t, J = 7.7 Hz, 2H), 7.26 (t, J = 4.0 Hz, 6H), 7.09 (d, J = 8.1 Hz, 4H), 5.34 (q, J = 3.8 Hz, 1H), 2.61 – 2.52 (m, 4H), 1.62 (dd, J = 15.1, 7.5 Hz, 4H), 0.93 (t, J = 7.3 Hz, 6H), 0.81 (d, J = 3.8 Hz, 3H).

^{13}C NMR (100 MHz, $CDCl_3$) δ 143.2, 137.8, 136.2, 132.0, 131.4, 129.6, 129.5, 128.6, 127.5, 120.6, 93.2, 89.9, 38.1, 24.5, 13.9, -4.9.

HRMS (ESI-TOF) m/z: $[M+H]^+$ Calcd for $C_{35}H_{35}Si$, 483.2503; found 483.2509.

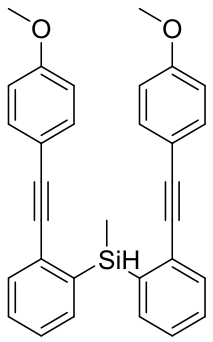

Bis(2-((4-methoxyphenyl)ethynyl)phenyl)(methyl)silane (1g)

White solid. mp 118.5-120.7 ^{o}C.

^{1}H NMR (400 MHz, $CDCl_3$) δ 7.61 – 7.52 (m, 4H), 7.36 (td, J = 7.6, 1.3 Hz, 2H), 7.28 (d, J = 2.0 Hz, 1H), 7.26 (s, 4H), 7.24 (d, J = 1.0 Hz, 1H), 6.81 (d, J = 8.9 Hz, 4H), 5.33 (q, J = 3.8 Hz, 1H), 3.80 (s, 6H), 0.80 (d, J = 3.9 Hz, 3H).

^{13}C NMR (100 MHz, $CDCl_3$) δ 159.7, 137.7, 136.2, 133.0, 131.8, 129.7, 129.5, 127.3, 115.6, 114.1, 93.0, 89.2, 55.4, -5.0.

HRMS (ESI-TOF) m/z: [M+H]$^+$ Calcd for $C_{31}H_{27}O_2Si$, 459.1775; found 459.1781.

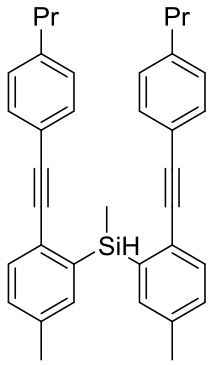

Methylbis(5-methyl-2-((4-propylphenyl)ethynyl)phenyl)silane (1h)

White solid. mp 105.5-106.3 ^{o}C.

^{1}H NMR (400 MHz, $CDCl_3$) δ 7.43 (s, 1H), 7.41 (s, 3H), 7.25 (s, 2H), 7.23 (s, 2H), 7.15 (d, J = 1.5 Hz, 1H), 7.13 (d, J = 1.3 Hz, 1H), 7.09 (d, J = 8.1 Hz, 4H), 5.24 (q, J = 3.8 Hz, 1H), 2.63 – 2.52 (m, 4H), 2.18 (s, 6H), 1.62 (d, J = 7.6 Hz, 4H), 0.93 (t, J = 7.3 Hz, 6H), 0.79 (d, J = 3.8 Hz, 3H).

^{13}C NMR (100 MHz, $CDCl_3$) δ 143.0, 137.7, 137.2, 137.1, 131.9, 131.4, 130.3, 128.5, 126.4, 120.9, 92.3, 89.9, 38.1, 24.5, 21.5, 13.9, -5.0.

HRMS (ESI-TOF) m/z: [M+H]$^+$ Calcd for $C_{37}H_{39}Si$, 511.2816; found 511.2821.

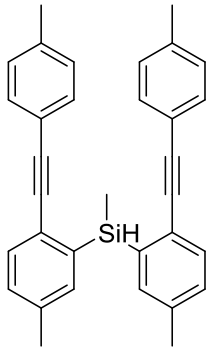

Methylbis(5-methyl-2-(*p*-tolylethynyl)phenyl)silane (1i)

Yellow solid. mp 126.0-130.1 ^{o}C.

^{1}H NMR (400 MHz, $CDCl_3$) δ 7.36 (s, 1H), 7.33 (d, J = 2.4 Hz, 3H), 7.15 (d, J = 8.3 Hz, 4H), 7.10 – 7.03 (m, 2H), 7.01 (d, J = 7.9 Hz, 4H), 5.17 (q, J = 3.7 Hz, 1H), 2.25 (s, 6H), 2.12 (s, 6H), 0.71 (d, J = 3.8 Hz, 3H).

^{13}C NMR (100 MHz, $CDCl_3$) δ 138.2, 138.0, 137.7, 137.6, 137.2, 137.2, 137.0, 135.4, 131.9, 131.8, 131.4, 131.1, 130.3, 130.1, 129.1, 127.2, 126.3, 125.6, 120.6, 96.1, 92.2, 91.6, 89.9, 21.6, 21.6, 21.5, -5.0.

HRMS (ESI-TOF) m/z: [M+Na]$^+$ Calcd for $C_{19}H_{30}N_{12}NaSi$, 477.2378; found 477.2360.

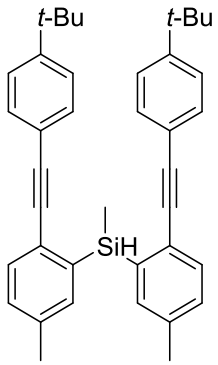

Bis(2-((4-(*tert*-butyl)phenyl)ethynyl)-5-methylphenyl)(methyl)silane (1j)

Yellow solid. mp 116.7-119.1 ^{o}C.

^{1}H NMR (400 MHz, $CDCl_3$) δ 7.44 (s, 1H), 7.42 (s, 1H), 7.40 (s, 2H), 7.29 (q, J = 8.5 Hz, 8H), 7.13 (d, J = 7.8 Hz, 2H), 5.25 (q, J = 3.7 Hz, 1H), 2.16 (s, 6H), 1.30 (s, 18H), 0.80 (d, J = 3.8 Hz, 3H).

^{13}C NMR (100 MHz, $CDCl_3$) δ 151.3, 137.8, 137.2, 137.1, 131.9, 131.3, 130.3, 126.4, 125.3, 120.7, 92.217, 879.927, 34.9, 31.3, 21.5, -5.0.

HRMS (ESI-TOF) m/z: [M+Na]$^+$ Calcd for $C_{39}H_{42}NaSi$, 561.2948; found 561.2960.

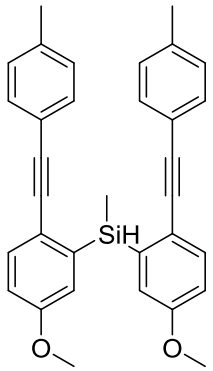

Bis(5-methoxy-2-(*p*-tolylethynyl)phenyl)(methyl)silane (1k)

Yellow solid. mp 117.3-118.1 ^{o}C.

^{1}H NMR (400 MHz, $CDCl_3$) δ 7.39 (s, 1H), 7.36 (s, 1H), 7.14 (s, 2H), 7.12 (s, 2H), 7.02 (d, J = 2.7 Hz, 2H), 6.96 (s, 2H), 6.94 (s, 2H), 6.75 (d, J = 2.7 Hz, 1H), 6.73 (d, J = 2.7 Hz, 1H), 5.20 (q, J = 3.7 Hz, 1H), 3.50 (s, 6H), 2.19 (s, 6H), 0.72 (d, J = 3.8 Hz, 3H).

^{13}C NMR (100 MHz, $CDCl_3$) δ 158.8, 139.5, 138.0, 133.5, 131.2, 129.1, 121.6, 121.5, 120.6, 115.2, 91.6, 89.8, 55.1, 21.5, -5.1.

HRMS (ESI-TOF) m/z: [M+Na]$^+$ Calcd for $C_{33}H_{30}NaO_2Si$, 509.1907; found 509.1920.

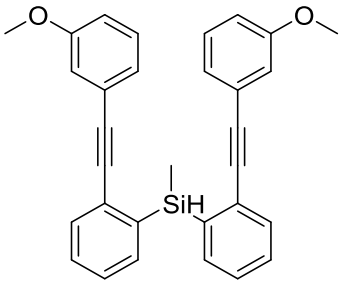

Bis(2-((3-methoxyphenyl)ethynyl)phenyl)(methyl)silane (1l)

Yellow solid. mp 92.9-94.2. ^{o}C.

^{1}H NMR (400 MHz, $CDCl_3$) δ 7.71 – 7.47 (m, 4H), 7.39 (dd, J = 10.6, 4.4 Hz, 2H), 7.33 – 7.27 (m, 2H), 7.24 – 7.17 (m, 2H), 7.03 – 6.93 (m, 2H), 6.92 – 6.82 (m, 4H), 5.38 (dd, J = 7.5, 3.7 Hz, 1H), 3.77 (s, 6H), 0.83 (d, J = 3.9 Hz, 3H).

^{13}C NMR (100 MHz, $CDCl_3$) δ 159.3, 137.8, 136.0, 131.9, 129.5, 129.3, 129.2 127.6, 124.2, 124.0, 115.9, 115.1, 92.8, 90.1, 55.3, -5.1.

HRMS (ESI-TOF) m/z: [M+Na]$^+$ Calcd for $C_{31}H_{26}NaO_2Si$, 481.1594; found 481.1611.

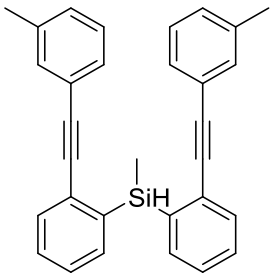

Methylbis(2-(*m*-tolylethynyl)phenyl)silane (1m)

Yellow oil

^{1}H NMR (400 MHz, $CDCl_3$) δ 7.61 (d, J = 7.9 Hz, 4H), 7.41 (td, J = 7.6, 1.1 Hz, 2H), 7.31 (dd, J = 11.0, 3.7 Hz, 2H), 7.21 (d, J = 6.1 Hz, 4H), 7.15 (dd, J = 8.3, 5.8 Hz, 4H), 5.41 (q, J = 3.8 Hz, 1H), 2.34 (s, 6H), 0.85 (d, J = 3.8 Hz, 3H).

^{13}C NMR (100 MHz, $CDCl_3$) δ 138.0, 137.9, 136.2, 132.1, 132.0, 129.6, 129.5, 129.2, 128.55, 128.3, 127.6, 123.2, 93.2, 90.1, 21.3, -5.0.

HRMS (ESI-TOF) m/z: [M+Na]$^+$ Calcd for $C_{31}H_{26}NaSi$, 449.1696; found 449.1710.

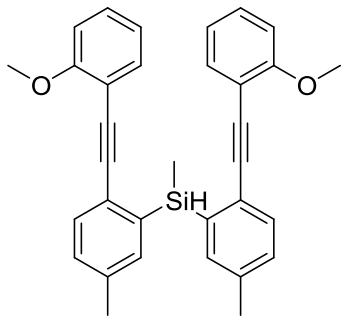

Bis(2-((2-methoxyphenyl)ethynyl)-5-methylphenyl)(methyl)silane (1n)

White solid. mp 102.3-103.8 ^{o}C.

^{1}H NMR (400 MHz, $CDCl_3$) δ 7.72 – 7.52 (m, 4H), 7.41 (d, J = 7.0 Hz, 2H), 7.33 (t, J = 7.3 Hz, 2H), 7.23 (d, J = 7.2 Hz, 2H), 7.05 – 6.85 (m, 4H), 5.88 – 5.02 (m, 1H), 3.90 (s, 6H), 2.27 (s, 6H), 1.02 (d, J = 2.1 Hz, 1H).

^{13}C NMR (100 MHz, $CDCl_3$) δ 159.9, 137.7, 137.1, 133.4, 132.0, 130.1, 129.5, 126.5, 120.4, 112.9, 110.6, 94.5, 88.5, 55.5, 21.3, -5.2.

HRMS (ESI-TOF) m/z: [M+Na]$^+$ Calcd for $C_{33}H_{30}NaO_2Si$, 509.1907; found 509.1919.

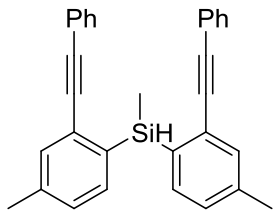

Methylbis(4-methyl-2-(phenylethynyl)phenyl)silane (1o)

Yellow oil.

^{1}H NMR (400 MHz, $CDCl_3$) δ 7.45 (d, J = 7.6 Hz, 2H), 7.42 (s, 2H), 7.35 (dd, J = 6.6, 3.1 Hz, 4H), 7.31 – 7.27 (m, 6H), 7.08 (d, J = 7.5 Hz, 2H), 5.33 (q, J = 3.7 Hz, 1H), 2.34 (s, 6H), 0.79 (d, J = 3.8 Hz, 3H).

^{13}C NMR (100 MHz, $CDCl_3$) δ 139.5, 136.2, 134.5, 132.7, 131.5, 129.2, 128.7, 128.4, 128.2, 123.6, 92.5, 90.6, 21.37, -4.7.

HRMS (ESI-TOF) m/z: [M+Na]$^+$ Calcd for $C_{31}H_{26}NaSi$, 449.1696; found 449.1703.

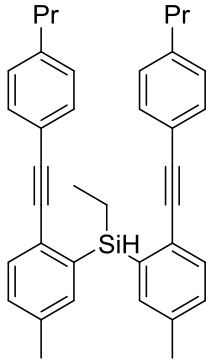

Ethylbis(5-methyl-2-((4-propylphenyl)ethynyl)phenyl)silane (1p)

Yellow oil.

^{1}H NMR (400 MHz, $CDCl_3$) δ 7.35 (s, 1H), 7.18 (d, J = 1.6 Hz, 2H), 7.04 (t, J = 9.5 Hz, 1H), 5.05 (t, J = 3.9 Hz, 1H), 2.58 – 2.44 (m, 1H), 2.10 (s, 1H), 1.54 (dd, J = 12.6, 5.0 Hz, 2H), 1.32 (ddd, J = 11.5, 7.7, 3.8 Hz, 1H), 1.37 – 1.25 (m, 1H), 1.02 (t, J = 7.8 Hz, 1H), 0.87 (dd, J = 9.8, 4.8 Hz, 2H).

^{13}C NMR (100 MHz, $CDCl_3$) δ 143.0, 137.4, 137.1, 137.0, 132.0, 131.4, 130.2, 128.5, 126.5, 120.9, 92.1, 90.0, 38.1, 24.5, 21.5, 13.9, 8.9, 3.6.

HRMS (ESI-TOF) m/z: [M+Na]$^+$ Calcd for $C_{38}H_{40}NaSi$, 547.2791; found 547.2784.

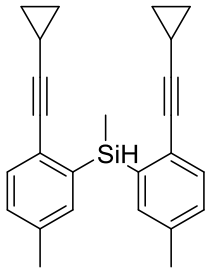

Bis(2-(cyclopropylethynyl)-5-methylphenyl)(methyl)silane (1q)

Yellow oil.

^{1}H NMR (400 MHz, $CDCl_3$) δ 7.22 (d, J = 7.5 Hz, 4H), 7.05 – 7.00 (m, 2H), 4.94 (q, J = 3.8 Hz, 1H), 2.22 (s, 6H), 1.29 – 1.18 (m, 2H), 0.68 – 0.62 (m, 4H), 0.59 (d, J = 3.8 Hz, 3H), 0.55 – 0.48 (m, 2H), 0.48 – 0.41 (m, 2H).

^{13}C NMR (100 MHz, $CDCl_3$) δ 136.7, 135.6, 135.3, 130.8, 129.1, 126.0, 95.2, 20.6, 7.3, 7.3, -0.7, -6.1.

HRMS (ESI-TOF) m/z: $[M+Na]^+$ Calcd for $C_{25}H_{26}NaSi$, 377.1696; found 377.1709.

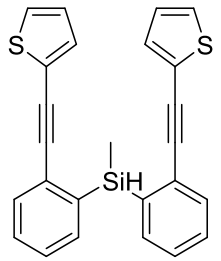

Methylbis(2-(thiophen-2-ylethynyl)phenyl)silane (1r)

White solid. mp 70.5-72.3 ^{o}C.

^{1}H NMR (400 MHz, $CDCl_3$) δ 7.53 (d, J = 7.3 Hz, 2H), 7.45 (d, J = 7.6 Hz, 2H), 7.28 (dd, J = 7.5, 6.7 Hz, 2H), 7.18 (dd, J = 13.9, 6.2 Hz, 4H), 7.03 (d, J = 3.6 Hz, 2H), 6.88 (dd, J = 5.0, 3.7 Hz, 2H), 5.19 (q, J = 3.6 Hz, 1H), 0.73 (d, J = 3.9 Hz, 3H).

^{13}C NMR (100 MHz, $CDCl_3$) δ 137.7, 136.2, 131.8, 129.6, 128.9, 127.8, 127.4, 127.2, 123.4, 94.1, 86.3, -5.1.

HRMS (ESI-TOF) m/z: $[M+Na]^+$ Calcd for $C_{25}H_{18}NaS_2Si$, 433.0511; found 433.0520.

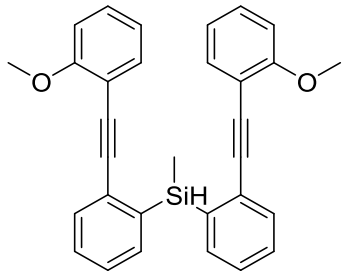

Bis(2-((2-methoxyphenyl)ethynyl)phenyl)(methyl)silane (1s)

Yellow oil.

^{1}H NMR (400 MHz, $CDCl_3$) δ 7.52 (dd, *J* = 14.5, 7.2 Hz, 4H), 7.27 (td, *J* = 7.6, 1.2 Hz, 2H), 7.24 – 7.11 (m, 6H), 6.79 (t, *J* = 8.3 Hz, 4H), 5.31 (q, *J* = 3.8 Hz, 1H), 3.75 (s, 6H), 0.79 (d, *J* = 3.9 Hz, 3H).

^{13}C NMR (100 MHz, $CDCl_3$) δ 160.1, 137.9, 136.3, 133.6, 132.2, 129.8, 129.7, 129.4, 127.4, 120.5, 112.8, 110.7, 94.4, 89.4, 55.7, -5.1.

HRMS (ESI-TOF) m/z: [M+Na]$^{+}$ Calcd for $C_{31}H_{26}NaO_2Si$, 481.1594; found 481.1609.

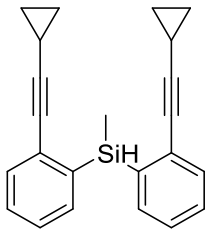

Bis(2-(cyclopropylethynyl)phenyl)(methyl)silane (1t)

Yellow oil.

^{1}H NMR (400 MHz, $CDCl_3$) δ 7.48 (d, *J* = 7.3 Hz, 2H), 7.44 (d, *J* = 7.6 Hz, 2H), 7.34 (td, *J* = 7.5, 1.3 Hz, 2H), 7.29 – 7.22 (m, 2H), 5.11 (q, *J* = 3.8 Hz, 1H), 1.36 (m, *J* = 9.9, 6.6, 4.2 Hz, 2H), 0.78 (m, *J* = 5.8, 3.0 Hz, 4H), 0.73 (d, *J* = 3.9 Hz, 3H), 0.69 – 0.63 (m, 2H), 0.60 – 0.53 (m, 2H).

^{13}C NMR (100 MHz, $CDCl_3$) δ 137.8, 135.8, 131.8, 130.1, 129.3, 126.8, 97.2, 8.4, 0.3, -5.2.

HRMS (ESI-TOF) m/z: [M+Na]$^{+}$ Calcd for $C_{23}H_{22}NaSi$, 349.1383; found 349.1400.

For the chiral Ligand (L8)[3]:

3-(diphenylphosphanyl)-2'-(hydroxy(*o*-tolyl)methyl)-[1,1'-binaphthalen]-2-ol

Colorless solid.

Optical rotation: $[\alpha]_D^{25}$ = +34.5 (c = 0.63, $CHCl_3$).

^{1}H NMR (400 MHz, $CDCl_3$) δ 7.80 (dd, J = 8.3, 3.0 Hz, 2H), 7.60 (t, J = 7.0 Hz, 2H), 7.35 (ddd, J = 22.6, 12.3, 5.7 Hz, 12H), 7.25 (d, J = 8.7 Hz, 1H), 7.22 – 7.14 (m, 4H),

7.10 – 7.00 (m, 3H), 6.84 (dd, J = 13.6, 7.9 Hz, 2H), 6.61 (s, 1H), 5.81 (s, 1H), 1.56 (s, 3H).

^{13}C NMR (100 MHz, $CDCl_3$) δ 153.00, 140.34, 139.76, 134.92, 134.44, 134.33, 134.14, 133.83, 133.64, 133.54, 133.10, 131.58, 130.14, 129.31, 128.82, 128.76, 128.75, 128.69, 128.24, 128.15, 127.27, 126.92, 126.65, 126.40, 126.35, 126.19, 125.94, 125.47, 124.91, 123.95, 71.45, 19.44.

3. General procedure for the synthesis of product 2

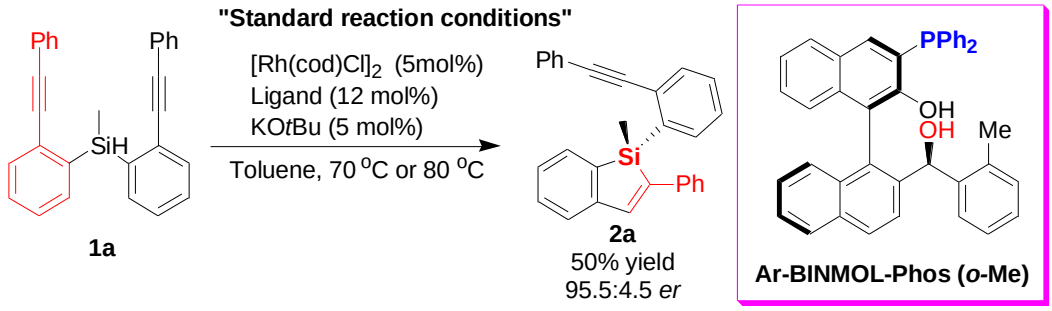

General procedure for the enantioselective synthesis of benzosilole 2 via Rh-catalyzed intramolecular hydrosilylation.A vial was charged with $[Rh(cod)Cl]_2$ (4.9 mg, 5 mol%), **L8** (13.8 mg, 12 mol%), KO*t*Bu (2.7 mg, 12 mol%) and evacuated under high vacuum and backfilled with N_2. Then toluene (1 mL) was added and stirred at room temperature for about 0.5 h. Subsequently, the methylbis(2-(phenylethynyl)phenyl)silane **1a** (79.6 mg, 0.2 mmol) were added to the reaction mixture and was stirred at 70 ℃. Upon reaction completion (72 h, TLC, eluent: hexane), the mixture was filtered over a plug of silica gel (washed with 20 mL EtOAc), and the filtrate was concentrated. The crude was purified by column chromatography to give the products **2**.

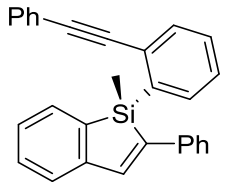

(*S*)-1-methyl-2-phenyl-1-(2-(phenylethynyl)phenyl)-1*H*-benzo[*b*]silole (2a)

The mobile phase for flash chromatography: hexane.Yellow oil. (40.1 mg, 50%).

Optical rotation: $[\alpha]_D^{25}$ = +221.5 (c = 0.63, $CHCl_3$).

^{1}H NMR (400 MHz, $CDCl_3$) δ 7.90 (d, J = 6.9 Hz, 1H), 7.70 (s, 1H), 7.58 (t, J = 7.0 Hz, 3H), 7.51 (dd, J = 6.5, 3.1 Hz, 2H), 7.46 (d, J = 7.4 Hz, 1H), 7.35 (dd, J = 5.0, 1.6 Hz, 3H), 7.33 – 7.30 (m, 3H), 7.29 – 7.20 (m, 3H), 7.19 – 7.11 (m, 2H).

^{13}C NMR (100 MHz, $CDCl_3$) δ 149.1, 143.4, 142.4, 138.8, 137.6, 137.4, 135.6, 132.8, 132.7, 132.6, 131.5, 131.3, 130.2, 129.8, 129.3, 128.8, 128.5, 128.2, 128.1, 127.8, 127.4, 127.2, 127.1, 127.0, 124.6, 123.2, 92.2, 91.3, -3.6.

HRMS: (ESI-TOF) m/z: $[M+H]^+$ Calcd for $C_{29}H_{23}Si$, 399.1564; found 399.1567.

HPLC: Enantiomeric excess was determined by HPLC with a Chiralcel OD-H column and a Phenomenex column (hexanes: 2-propanol = 99.5:0.5, 0.5 mL/min, 330 nm, 95.5:4.5 *er*); major enantiomer t_r = 26.8 min, minor enantiomer t_r = 30.0 min.

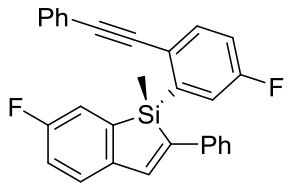

(*R*)-6-fluoro-1-(5-fluoro-2-(phenylethynyl)phenyl)-1-methyl-2-phenyl-1*H*-benzo[*b*]silole (2b)

The mobile phase for flash chromatography: hexane. Yellow oil. (32.1 mg, 37%).

Optical rotation: $[\alpha]_D^{25}$ = +153.6 (c = 0.33, $CHCl_3$).

^{1}H NMR (400 MHz, $CDCl_3$) δ 7.65 (s, 1H), 7.61 – 7.52 (m, 3H), 7.52 – 7.46 (m, 3H), 7.38 (dd, *J* = 5.9, 2.6 Hz, 3H), 7.34 (d, *J* = 7.8 Hz, 2H), 7.21 (dd, *J* = 8.2, 4.8 Hz, 1H), 7.14 (dd, *J* = 8.7, 2.8 Hz, 1H), 7.08 – 6.94 (m, 3H), 0.98 (s, 3H).

^{13}C NMR (100 MHz, $CDCl_3$) δ 163.8, 163.4, 161.3, 160.9, 145.0, 142.4, 141.8, 140.0, 140.0, 139.9, 138.4, 135.0, 134.9, 131.6, 129.0, 128.8, 128.7, 127.6, 126.9, 125.9, 125.9, 125.4, 123.0, 122.5, 122.2, 120.1, 119.9, 117.4, 117.2, 117.0, 116.8, 92.1, 90.0, -3.9.

HRMS (ESI-TOF) m/z: $[M+Na]^+$ Calcd for $C_{29}H_{20}F_2NaSi$, 457.1195; found 457.1120.

HPLC: Enantiomeric excess was determined by HPLC with a Phenomenex column and a Chiralcel OD-H column (hexanes: 2-propanol = 95.5:0.5, 0.5 mL/min, 330 nm, 96.1:3.9 *er*); major enantiomer t_r = 46.6 min, minor enantiomer t_r = 48.5 min.

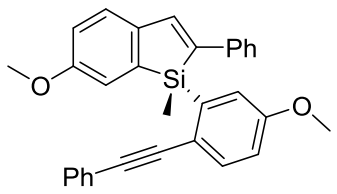

(*S*)-6-methoxy-1-(5-methoxy-2-(phenylethynyl)phenyl)-1-methyl-2-phenyl-1*H*-benzo[*b*]silole (2c)

The mobile phase for flash chromatography: hexane/ethyl acetate = 100:1. White solid. mp 74-76 ^{o}C. (55 mg, 60%).

Optical rotation: $[\alpha]_D^{25}$ = +391.5 (c = 1.63, $CHCl_3$).

^{1}H NMR (400 MHz, $CDCl_3$) δ 7.58 (s, 1H), 7.46 (t, *J* = 8.1 Hz, 6H), 7.24 (dd, *J* = 11.0, 7.3 Hz, 4H), 7.12 (dd, *J* = 7.6, 5.1 Hz, 3H), 6.88 (d, *J* = 2.7 Hz, 1H), 6.73 (ddd, *J* = 13.7, 8.4, 2.6 Hz, 2H), 3.45 (s, 3H), 3.42 (s, 3H), 0.93 (s, 3H).

^{13}C NMR (100 MHz, $CDCl_3$) δ 159.3, 159.0, 142.5, 142.0, 140.0, 140.0, 139.3, 134.3, 131.5, 128.9, 128.6, 128.3, 126.9, 126.9, 125.6, 124.8, 123.6, 121.2, 120.9, 118.4, 116.0, 115.8, 91.8, 90.9, 77.5, 76.8, 55.2, 55.0, -3.3.

HRMS (ESI-TOF) m/z: $[M+Na]^+$ Calcd for $C_{31}H_{26}NaO_2Si$, 481.1592; found 481.1581.

HPLC: Enantiomeric excess was determined by HPLC with a Chiralpak IA column (hexanes: 2-propanol = 99.3:0.7, 0.6 mL/min, 330 nm, 96.7:3.3 *er*); major enantiomer t_r = 19.3 min, minor enantiomer t_r = 26.5 min.

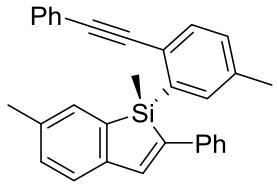

(*R*)-1,6-dimethyl-1-(5-methyl-2-(phenylethynyl)phenyl)-2-phenyl-1*H*-benzo[*b*]silole (2d)

The mobile phase for flash chromatography: hexane. Yellow oil. (34.9 mg, 41%).

Optical rotation: $[\alpha]_D^{25}$ = +223.5 (c = 0.67, $CHCl_3$).

^{1}H NMR (400 MHz, $CDCl_3$) δ 7.63 (s, 1H), 7.58 (s, 1H), 7.49 – 7.37 (m, 5H), 7.28 – 7.16 (m, 5H), 7.06 (ddd, *J* = 22.1, 15.3, 7.3 Hz, 5H), 2.14 (s, 3H), 2.08 (s, 3H), 0.86 (s, 3H).

^{13}C NMR (100 MHz, $CDCl_3$) δ 146.6, 142.5, 142.4, 139.2, 137.9, 137.9, 137.4, 136.8, 136.4, 133.9, 132.8, 131.6, 130.8, 130.7, 128.8, 128.5, 128.4, 127.0, 126.3, 124.5, 123.6, 91.7, 91.6, 21.6, 21.5, -3.5.

HRMS (ESI-TOF) m/z: $[M+Na]^+$ Calcd for $C_{31}H_{26}NaSi$, 449.1696; found 449.1708.

HPLC: Enantiomeric excess was determined by HPLC with a Chiralpak IA column (hexanes: 2-propanol = 99.5:0.5, 0.8 mL/min, 330 nm, 99.3:0.7 *er*); major enantiomer t_r = 10.0 min, minor enantiomer t_r = 11.1 min.

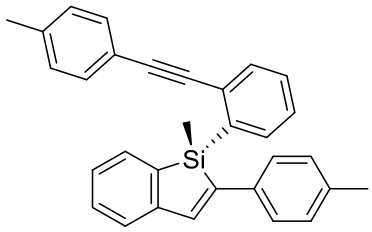

(*S*)-1-methyl-2-(*p*-tolyl)-1-(2-(*p*-tolylethynyl)phenyl)-1*H*-benzo[*b*]silole (2e)

The mobile phase for flash chromatography: hexane. Yellow oil. (34.9 mg, 41%).

Optical rotation: $[\alpha]_D^{25}$ = +321.5 (c = 1.33, $CHCl_3$).

^{1}H NMR (400 MHz, $CDCl_3$) δ 7.83 (d, *J* = 7.0 Hz, 1H), 7.60 (s, 1H), 7.50 (d, *J* = 7.7 Hz, 1H), 7.41 (d, *J* = 8.0 Hz, 2H), 7.36 (d, *J* = 8.1 Hz, 3H), 7.27 – 7.17 (m, 3H), 7.06 (ddd, *J* = 14.5, 9.9, 4.9 Hz, 6H), 2.31 (s, 3H), 2.27 (s, 3H), 0.89 (s, 3H).

^{13}C NMR (100 MHz, $CDCl_3$) δ 149.4, 143.4, 141.5, 138.8, 137.7, 137.5, 137.2, 136.0, 135.7, 132.9, 132.7, 131.6, 130.3, 129.8, 129.6, 129.6, 129.4, 127.8, 127.1, 127.0, 124.5, 120.3, 92.5, 90.9, 21.7, 21.4, -3.5.

HRMS (ESI-TOF) m/z: $[M+Na]^+$ Calcd for $C_{31}H_{26}NaSi$, 449.1686; found 449.1696.

HPLC: Enantiomeric excess was determined by HPLC with a Chiralpak IA column (hexanes: 2-propanol = 99.5:0.5, 0.8 mL/min, 330 nm, 94.6:5.4 *er*); major enantiomer t_r = 10.2 min, minor enantiomer t_r = 21.0 min.

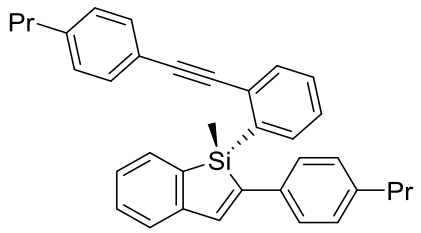

(*S*)-1-methyl-2-(4-propylphenyl)-1-(2-((4-propylphenyl)ethynyl)phenyl)-1*H*-benzo[*b*]silole (2f)

The mobile phase for flash chromatography: hexane. Yellow oil. (64.9 mg, 71%).

Optical rotation: $[\alpha]_D^{25}$ = +232.4 (c = 0.63, $CHCl_3$).

^{1}H NMR (400 MHz, $CDCl_3$) δ 7.83 (d, *J* = 7.0 Hz, 1H), 7.60 (s, 1H), 7.50 (d, *J* = 7.6 Hz, 1H), 7.42 (d, *J* = 8.1 Hz, 2H), 7.37 (t, *J* = 5.9 Hz, 3H), 7.27 – 7.17 (m, 3H), 7.13 – 7.01 (m, 6H), 2.57 – 2.46 (m, 4H), 1.57 (dt, *J* = 14.6, 7.3 Hz, 4H), 0.94 – 0.82 (m, 9H).

^{13}C NMR (100 MHz, $CDCl_3$) δ 149.4, 143.5, 143.4, 142.1, 141.6, 137.7, 137.6, 136.3, 135.8, 132.9, 132.7, 131.6, 130.3, 129.8, 129.6, 129.0, 128.8, 127.7, 127.1, 127.0, 124.5, 120.6, 92.6, 90.9, 38.2, 38.0, 24.6, 24.5, 14.1, 13.9, -3.4.

HRMS (ESI-TOF) m/z: $[M+Na]^+$ Calcd for $C_{35}H_{34}NaSi$, 505.2322; found 505.2313.

HPLC: Enantiomeric excess was determined by HPLC with a Chiralpak IA column (hexanes: 2-propanol = 99.5:0.5, 0.8 mL/min, 330 nm, 93.6:6.5 *er*); major enantiomer t_r = 7.5 min, minor enantiomer t_r = 13.1 min.

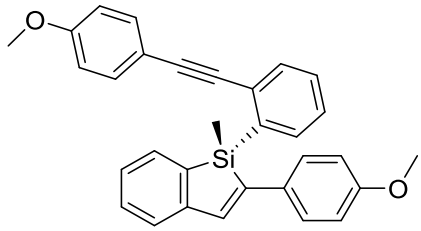

(*S*)-2-(4-methoxyphenyl)-1-(2-((4-methoxyphenyl)ethynyl)phenyl)-1-methyl-1*H*-benzo[*b*]silole (2g)

The mobile phase for flash chromatography: hexane/ethyl acetate = 100:1. Yellow solid. (52.3 mg, 57%).

Optical rotation: $[\alpha]_D^{25}$ = +321.5 (c = 1.67, $CHCl_3$). mp 64.9 ^oC.

^{1}H NMR (400 MHz, $CDCl_3$) δ 7.88 (d, *J* = 6.9 Hz, 1H), 7.61 – 7.41 (m, 8H), 7.33 – 7.24 (m, 2H), 7.17 – 7.09 (m, 2H), 6.89 (t, *J* = 8.7 Hz, 4H), 3.83 (s, 3H), 3.80 (s, 3H), 0.96 (s, 3H).

^{13}C NMR (100 MHz, $CDCl_3$) δ 159.9, 159.1, 149.6, 143.0, 140.3, 137.4, 137.4, 135.8, 135.7, 133.1, 132.9, 132.8, 132.5, 132.5, 131.6, 130.3, 129.8, 129.7, 128.9, 128., 127.6, 127.2, 126.8, 124.3, 92.4, 90.2, 55.5, 55.4, -3.4.

HRMS (ESI-TOF) m/z: [M+Na]$^+$ Calcd for $C_{31}H_{26}NaO_2Si$, 481.1584; found 481.1594.

HPLC: Enantiomeric excess was determined by HPLC with a Chiralpak IA column (hexanes: 2-propanol = 99.5:0.5, 0.8 mL/min, 330 nm, 90.2:9.8 *er*); major enantiomer t_r = 22.2 min, minor enantiomer t_r = 45.0 min.

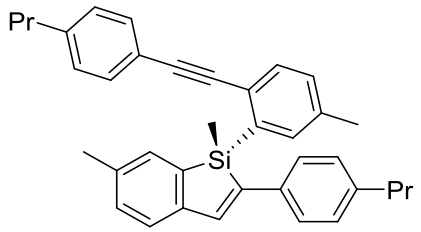

(*R*)-1,6-dimethyl-1-(5-methyl-2-((4-propylphenyl)ethynyl)phenyl)-2-(4-propylphenyl)-1*H*-benzo[*b*]silole (2h)

The mobile phase for flash chromatography: hexane. Yellow oil. (82.7 mg, 81%).

Optical rotation: $[\alpha]_D^{25}$ = +221.5 (c = 0.63, $CHCl_3$).

^{1}H NMR (400 MHz, $CDCl_3$) δ 7.65 (s, 1H), 7.57 (s, 1H), 7.43 – 7.34 (m, 5H), 7.17 (s, 1H), 7.11 – 6.99 (m, 7H), 2.67 – 2.41 (m, 4H), 2.15 (s, 3H), 2.09 (s, 3H), 1.63 – 1.50 (m, 4H), 0.87 (dt, *J* = 7.3, 3.0 Hz, 9H).

^{13}C NMR (100 MHz, $CDCl_3$) δ 146.8, 143.3, 142.4, 141.7, 141.4, 137.9, 137.6, 137.5, 136.6, 136.5, 136.5, 134.0, 132.7, 131.5, 130.8, 130.6, 128.9, 128.7, 127.0, 126.5, 124.3, 120.8, 91.9, 91.1, 38.1, 37.9, 24.6, 24.5, 21.6, 21.5, 14.0, 13.9, -3.4.

HRMS (ESI-TOF) m/z: $[M+Na]^+$ Calcd for $C_{37}H_{38}NaSi$, 533.2635; found 533.2623.

HPLC: Enantiomeric excess was determined by HPLC with a Phenomenex column (hexanes: 2-propanol = 99.5:0.5, 0.6 mL/min, 330 nm, 93.9:6.1 *er*); major enantiomer t_r = 8.6 min, minor enantiomer t_r = 9.6 min.

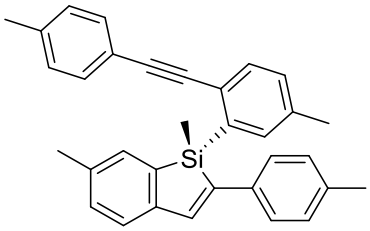

(*R*)-1,6-dimethyl-1-(5-methyl-2-(*p*-tolylethynyl)phenyl)-2-(*p*-tolyl)-1*H*-benzo[*b*]silole (2i)

The mobile phase for flash chromatography: hexane. Yellow oil. (54.5 mg, 60%).

Optical rotation: $[\alpha]_D^{25}$ = +231.1 (c = 1.33, $CHCl_3$).

^{1}H NMR (400 MHz, $CDCl_3$) δ 7.65 (s, 1H), 7.56 (s, 1H), 7.41 – 7.33 (m, 5H), 7.18 (s, 1H), 7.14 – 6.99 (m, 8H), 2.29 (s, 3H), 2.26 (s, 3H), 2.15 (s, 3H), 2.09 (s, 3H), 0.84 (s, 3H).

^{13}C NMR (100 MHz, $CDCl_3$) δ 146.8, 142.3, 141.4, 138.5, 137.9, 137.7, 137.5, 136.9, 136.5, 136.4, 136.3, 134.0, 132.7, 131.5, 130.8, 130.6, 129.5, 129.3, 127.0, 126.5, 124.3, 120.6, 91.8, 91.0, 21.7, 21.6, 21.5, 21.4, -3.5.

HRMS (ESI-TOF) m/z: $[M+Na]^+$ Calcd for $C_{33}H_{30}NaSi$, 477.2009; found 477.2019.

HPLC: Enantiomeric excess was determined by HPLC with a Phenomenex column (hexanes: 2-propanol = 99.5:0.5, 0.6 mL/min, 330 nm, 95.7:4.3 *er*); major enantiomer t_r = 9.7 min, minor enantiomer t_r = 11.2 min.

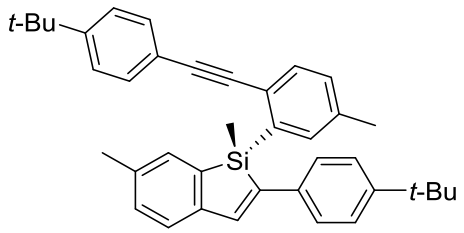

(*R*)-2-(4-(*tert*-butyl)phenyl)-1-(2-((4-(*tert*-butyl)phenyl)ethynyl)-5-methylphenyl)-1,6-dimethyl-1*H*-benzo[*b*]silole (2j)

The mobile phase for flash chromatography: hexane. Yellow oil. (54.8 mg, 51%).

Optical rotation: $[\alpha]_D^{25}$ = +211.9 (c = 0.67, $CHCl_3$).

^{1}H NMR (400 MHz, $CDCl_3$) δ 7.65 (s, 1H), 7.59 (s, 1H), 7.46 – 7.37 (m, 4H), 7.29 (dd, *J* = 15.2, 8.3 Hz, 4H), 7.19 (s, 1H), 7.17 (s, 1H), 7.07 (dt, *J* = 23.2, 7.5 Hz, 3H), 2.17 (s, 3H), 2.11 (s, 3H), 1.26 (s, 9H), 1.24 (s, 9H), 0.85 (s, 3H).

^{13}C NMR (100 MHz, $CDCl_3$) δ 151.6, 150.1, 146.8, 142.4, 141.6, 138.0, 137.7, 137.5, 136.6, 136.4, 136.3, 133.9, 132.7, 131.3, 130.8, 130.6, 126.8, 126.5, 125.7, 125.5, 124.3, 120.6, 91.9, 91.1, 35.9, 34.7, 31.5, 31.4, 21.6, 21.5, -3.4.

HRMS (ESI-TOF) m/z: $[M+Na]^+$ Calcd for $C_{39}H_{42}NaSi$, 561.2948; found 561.2934.

HPLC: Enantiomeric excess was determined by HPLC with a Chiralpak IA column (hexanes: 2-propanol = 99.5:0.5, 0.6 mL/min, 330 nm, 92.4:7.6 *er*); major enantiomer t_r = 7.8 min, minor enantiomer t_r = 8.2 min.

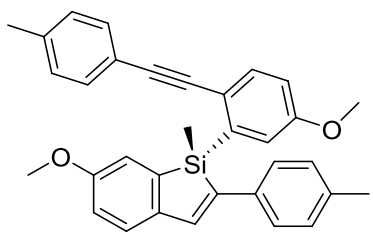

(*R*)-6-methoxy-1-(5-methoxy-2-(*p*-tolylethynyl)phenyl)-1-methyl-2-(*p*-tolyl)-1*H*-benzo[*b*]silole (2k)

The mobile phase for flash chromatography: hexane/ethyl acetate = 100:1. Yellow oil. (38.9 mg, 40%).

Optical rotation: $[\alpha]_D^{25}$ = +158.2 (c = 0.67, $CHCl_3$).

^{1}H NMR (400 MHz, $CDCl_3$) δ 7.56 (s, 1H), 7.49 (d, *J* = 2.6 Hz, 1H), 7.45 (d, *J* = 8.5 Hz, 1H), 7.39 (d, *J* = 1.7 Hz, 2H), 7.37 (d, *J* = 1.7 Hz, 2H), 7.14 – 7.09 (m, 2H), 7.09 – 7.04 (m, 3H), 6.89 (d, *J* = 2.7 Hz, 1H), 6.75 (ddd, *J* = 15.4, 8.4, 2.7 Hz, 2H), 3.49 (s, 3H), 3.46 (s, 3H), 2.30 (s, 3H), 2.27 (s, 3H), 0.91 (s, 3H).

^{13}C NMR (100 MHz, $CDCl_3$) δ 159.1, 158.8, 142.2, 141.5, 140.4, 139.6, 139.6, 138.4, 136.7, 136.4, 134.2, 131.4, 129.6, 129.4, 126.8, 125.4, 121.5, 121.0, 120.6, 118.4, 116.0, 115.7, 91.1, 91.0, 55.2, 55.1, 21.7, 21.3, -3.4.

HRMS (ESI-TOF) m/z: $[M+Na]^+$ Calcd for $C_{33}H_{30}NaO_2Si$, 509.1907; found 509.1905.

HPLC: Enantiomeric excess was determined by HPLC with a Phenomenex column (hexanes: 2-propanol = 99.5:0.5, 0.8 mL/min, 330 nm, 94.0:6.0 *er*); major enantiomer t_r = 19.7 min, minor enantiomer t_r = 25.4 min.

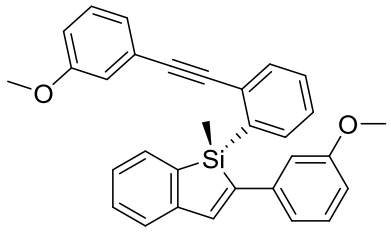

(*S*)-2-(3-methoxyphenyl)-1-(2-((3-methoxyphenyl)ethynyl)phenyl)-1-methyl-1*H*-benzo[*b*]silole (2l)

The mobile phase for flash chromatography: hexane/ethyl acetate = 100:1. Yellow oil. (36.7 mg, 40%).

Optical rotation: $[\alpha]_D^{25}$ = +149.2 (c = 1.33, $CHCl_3$).

^{1}H NMR (400 MHz, $CDCl_3$) δ 7.93 (d, J = 7.0 Hz, 1H), 7.81 – 7.73 (m, 2H), 7.51 (d, J = 7.7 Hz, 1H), 7.42 (dd, J = 7.6, 1.6 Hz, 1H), 7.26 (ddd, J = 9.3, 8.0, 2.4 Hz, 2H), 7.20 – 7.13 (m, 4H), 7.06 – 6.97 (m, 2H), 6.95 – 6.82 (m, 3H), 6.76 (d, J = 7.7 Hz, 1H), 3.80 (s, 3H), 3.38 (s, 3H), 0.87 (s, 3H).

^{13}C NMR (100 MHz, $CDCl_3$) δ 160.2, 156.4, 148.1, 142.8, 140.5, 139.4, 137.3, 134.7, 133.6, 132.8, 132.7, 129.9, 129.6, 128.8, 128.8, 128.5, 127.8, 127.3, 127.1, 126.0, 124.2, 121.0, 120.6, 112.9, 111.0, 110.8, 95.6, 88.3, 55.7, 54.3, -3.3.

HRMS (ESI-TOF) m/z: $[M+Na]^+$ Calcd for $C_{31}H_{26}NaO_2Si$, 481.1594; found 481.1584.

HPLC: Enantiomeric excess was determined by HPLC with a Phenomenex column (hexanes: 2-propanol = 99.6:0.4, 0.8 mL/min, 330 nm, 95.5:4.5 *er*); major enantiomer t_r = 26.2 min, minor enantiomer t_r = 28.7 min.

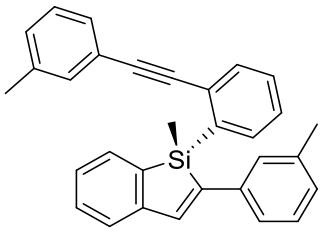

(*S*)-1-methyl-2-(*m*-tolyl)-1-(2-(*m*-tolylethynyl)phenyl)-1*H*-benzo[*b*]silole (2m)

The mobile phase for flash chromatography: hexane. Yellow oil. (46.9 mg, 55%).

Optical rotation: $[\alpha]_D^{25}$ = +272.7 (c = 0.99, $CHCl_3$).

^{1}H NMR (400 MHz, $CDCl_3$) δ 7.90 (d, J = 7.0 Hz, 1H), 7.70 (s, 1H), 7.58 (d, J = 7.6 Hz, 1H), 7.47 – 7.41 (m, 2H), 7.37 – 7.32 (m, 4H), 7.30 – 7.22 (m, 4H), 7.19 – 7.12 (m, 3H), 7.06 (d, J = 7.5 Hz, 1H), 2.36 (s, 3H), 2.34 (s, 3H), 0.98 (s, 3H).

^{13}C NMR (100 MHz, $CDCl_3$) δ 149.3, 143.7, 142.4, 138.9, 138.4, 138.3, 137.8, 137.5, 135.7, 132.9, 132.8, 132.2, 130.3, 129.8, 129.5, 129.5, 128.8, 128.5, 128.2, 127.9, 127.5, 127.1, 124.7, 124.6, 123.2, 92.5, 91.1, 21.7, 21.4, -3.4.

HRMS (ESI-TOF) m/z: $[M+Na]^+$ Calcd for $C_{31}H_{26}NaSi$, 449.1696; found 449.1685.

HPLC: Enantiomeric excess was determined by HPLC with a Chiralpak IA column (hexanes: 2-propanol = 99.5:0.5, 0.6 mL/min, 330 nm, 92.0:8.0 *er*); major enantiomer t_r = 26.0 min, minor enantiomer t_r = 27.8 min.

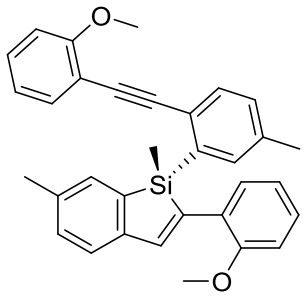

(*R*)-2-(2-methoxyphenyl)-1-(2-((2-methoxyphenyl)ethynyl)-5-methylphenyl)-1,6-dimethyl-1*H*-benzo[*b*]silole (2n)

The mobile phase for flash chromatography: hexane/ethyl acetate = 100:1. Yellow oil. (58.3 mg, 60%).

Optical rotation: $[\alpha]_D^{25}$ = +357.1 (c = 1.33, $CHCl_3$).

^{1}H NMR (400 MHz, $CDCl_3$) δ 7.82 – 7.65 (m, 3H), 7.42 (d, *J* = 8.1 Hz, 2H), 7.24 (td, *J* = 8.3, 1.7 Hz, 1H), 7.19 – 7.10 (m, 1H), 7.07 (d, *J* = 7.6 Hz, 2H), 6.98 (ddd, *J* = 6.7, 4.3, 1.1 Hz, 2H), 6.93 – 6.79 (m, 3H), 6.79 – 6.68 (m, 1H), 3.79 (s, 3H), 3.38 (s, 3H), 2.15 (s, 3H), 2.05 (s, 3H), 0.84 (s, 3H).

^{13}C NMR (100 MHz, $CDCl_3$) δ 160.1, 156.3, 145.6, 142.7, 140.6, 139.3, 137.1, 136.6, 136.4, 135.4, 133.7, 133.5, 132.7, 130.2, 129.7, 129.6, 128.2, 128.1, 126.1, 125.7, 124.0, 120.9, 120.6, 113.1, 110.9, 110.7, 95.9, 87.6, 55.7, 54.3, 21.6, -3.2.

HRMS (ESI-TOF) m/z: $[M+Na]^+$ Calcd for $C_{37}H_{38}NaSi$, 509.1907; found 509.1899.

HPLC: Enantiomeric excess was determined by HPLC with a Phenomenex column (hexanes: 2-propanol = 99.5:0.5, 0.8 mL/min, 330 nm, 92.2:5.8 *er*); major enantiomer t_r = 17.3 min, minor enantiomer t_r = 20.0 min.

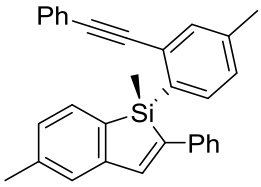

(*S*)-1,5-dimethyl-1-(4-methyl-2-(phenylethynyl)phenyl)-2-phenyl-1*H*-benzo[*b*]silole (2o)

The mobile phase for flash chromatography: hexane. Yellow oil. (41.7 mg, 49%).

Optical rotation: $[\alpha]_D^{25}$ = +201.6 (c = 0.65, $CHCl_3$).

^{1}H NMR (400 MHz, $CDCl_3$) δ 7.76 (d, *J* = 7.2 Hz, 1H), 7.66 (s, 1H), 7.57 (d, *J* = 7.3 Hz, 2H), 7.50 (dd, *J* = 6.6, 3.0 Hz, 2H), 7.43 (s, 1H), 7.36 (dd, *J* = 6.3, 3.4 Hz, 4H), 7.34 – 7.30 (m, 2H), 7.23 (s, 1H), 7.11 (s, 1H), 6.99 (t, *J* = 7.3 Hz, 2H), 2.31 (d, *J* = 4.3 Hz, 6H), 0.94 (s, 3H).

^{13}C NMR (100 MHz, $CDCl_3$) δ 149.6, 144.0, 142.4, 140.3, 139.9, 139.1, 135.8, 134.4, 134.1, 133.5, 132.8, 131.6, 129.3, 128.9, 128.9, 128.5, 128.5, 127.9, 127.2, 127.1, 125.7, 123.5, 91.9, 91.5, 21.7, 21.3, -3.3.

HRMS (ESI-TOF) m/z: $[M+H]^+$ Calcd for $C_{31}H_{27}Si$, 427.1877; found 427.1884.

HPLC: Enantiomeric excess was determined by HPLC with a Chiralpak IA column (hexanes: 2-propanol = 99.5:0.5, 0.5 mL/min, 330 nm, 97.3:2.7 *er*); major enantiomer t_r = 18.4 min, minor enantiomer t_r = 21.9 min.

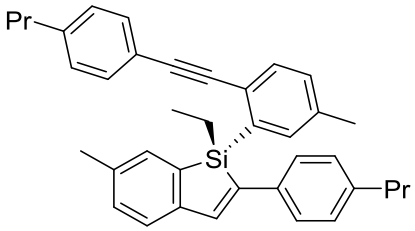

(*R*)-1-ethyl-6-methyl-1-(5-methyl-2-((4-propylphenyl)ethynyl)phenyl)-2-(4-propylphenyl)-1*H*-benzo[*b*]silole (2p)

The mobile phase for flash chromatography: hexane. Yellow oil. (42.0 mg, 41%).

Optical rotation: $[\alpha]_D^{25}$ = +97.8 (c = 0.67, $CHCl_3$).

^{1}H NMR (400 MHz, $CDCl_3$) δ 7.59 (d, J = 14.6 Hz, 1H), 7.40 (d, J = 8.1 Hz, 2H), 7.34 (d, J = 8.1 Hz, 2H), 7.21 – 7.17 (m, 1H), 7.15 (s, 1H), 7.06 (ddd, J = 15.3, 10.1, 4.2 Hz, 6H), 6.97 – 6.91 (m, 1H), 6.88 – 6.81 (m, 1H), 2.57 – 2.45 (m, 4H), 2.16 (s, 3H), 2.10 (s, 2H), 1.56 (dd, J = 15.9, 8.0 Hz, 4H), 1.32 (dd, J = 15.1, 7.8 Hz, 2H), 0.90 – 0.83 (m, 9H).

^{13}C NMR (100 MHz, $CDCl_3$) δ 147.4, 143.2, 142.2, 141.6, 141.5, 137.6, 136.9, 136.9, 136.8, 136.7, 136.4, 134.2, 132.8, 131.5, 130.7, 130.6, 128.9, 128.8, 128.7, 128.6, 127.0, 126.6, 126.6, 124.2, 120.9, 91.6, 91.1, 38.1, 37.9, 24.6, 24.5, 21.6, 21.5, 14.0, 13.9, 7.7, 5.0, 1.2.

HRMS (ESI-TOF) m/z: $[M+Na]^+$ Calcd for $C_{38}H_{40}NaSi$, 547.2791; found 547.2781.

HPLC: Enantiomeric excess was determined by HPLC with a Chiralcel AD-H column (hexanes: 2-propanol = 99.5:0.5, 0.6 mL/min, 330 nm, 97.9:2.1 *er*); major enantiomer t_r = 14.8 min, minor enantiomer t_r = 20.8 min.

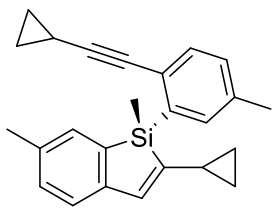

(R)-2-cyclopropyl-1-(2-(cyclopropylethynyl)-5-methylphenyl)-1,6-dimethyl-1*H*-benzo[*b*]silole (2q)

The mobile phase for flash chromatography: hexane. Yellow oil. (31.9 mg, 45%).

Optical rotation: $[\alpha]_D^{25}$ = +162.2 (c = 0.33, $CHCl_3$).

^{1}H NMR (400 MHz, $CDCl_3$) δ 7.42 (s, 1H), 7.28 (dd, J = 1.2, 0.5 Hz, 1H), 7.23 (d, J = 7.8 Hz, 1H), 7.16 (s, 1H), 7.03 – 6.97 (m, 2H), 6.94 (d, J = 7.6 Hz, 1H), 6.84 (s, 1H), 2.22 (s, 3H), 2.19 (s, 3H), 1.79 – 1.69 (m, 1H), 1.42 – 1.30 (m, 1H), 0.81 – 0.69 (m, 6H), 0.61 (s, 3H), 0.59 – 0.43 (m, 2H).

^{13}C NMR (100 MHz, $CDCl_3$) δ 149.2, 147.0, 140.3, 137.2, 137.1, 136.8, 135.9, 135.3, 133.5, 132.6, 130.5, 130.4, 127.0, 122.8, 95.3, 21.6, 21.5, 14.4, 8.6, 8.2, 8.1, 1.2, 0.6, -4.0.

HRMS (ESI-TOF) m/z: $[M+Na]^+$ Calcd for $C_{25}H_{26}NaSi$, 377.1696; found 377.1689.

HPLC: Enantiomeric excess was determined by HPLC with a Phenomenex column (hexanes: 2-propanol = 99.5:0.5, 0.6 mL/min, 330 nm, 92.0:8.0 *er*); major enantiomer t_r = 7.8 min, minor enantiomer t_r = 8.4 min.

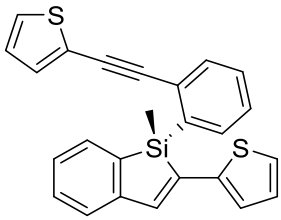

(*R*)-1-methyl-2-(thiophen-2-yl)-1-(2-(thiophen-2-ylethynyl)phenyl)-1*H*-benzo[*b*]silole (2r)

The mobile phase for flash chromatography: hexane. colorless solid. (61.7 mg, 75%).

Optical rotation: $[\alpha]_D^{25}$ = +66.5 (c = 0.33, $CHCl_3$). mp 143.5-146.4 ^oC.

^{1}H NMR (400 MHz, $CDCl_3$) δ 7.77 (d, *J* = 7.0 Hz, 1H), 7.47 (d, *J* = 7.6 Hz, 1H), 7.42 (d, *J* = 5.8 Hz, 2H), 7.26 – 7.14 (m, 5H), 7.12 – 7.09 (m, 2H), 7.04 (d, *J* = 0.7 Hz, 1H), 6.93 (dd, *J* = 5.0, 3.7 Hz, 1H), 6.90 – 6.83 (m, 2H), 0.84 (s, 3H).

^{13}C NMR (100 MHz, $CDCl_3$) δ 149.1, 144.1, 141.3, 137.0, 136.8, 135.7, 133.0, 132.4, 132.2, 130.5, 130.0, 129.0, 128.1, 127.9, 127.8, 127.4, 127.1, 126.7, 124.6, 124.5, 123.3, 94.9, 85.9, -3.8.

HRMS (ESI-TOF) m/z: $[M+H]^+$ Calcd for $C_{25}H_{19}S_2Si$, 411.0692; found 411.0678.

HPLC: Enantiomeric excess was determined by HPLC with a Phenomenex column (hexanes: 2-propanol = 99.5:0.5, 0.6 mL/min, 330 nm, 93.6:6.4 *er*); major enantiomer t_r = 17.9 min, minor enantiomer t_r = 26.1 min.

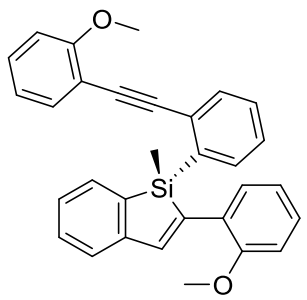

(*R*)-2-(2-methoxyphenyl)-1-(2-((2-methoxyphenyl)ethynyl)phenyl)-1-methyl-1*H*-benzo[*b*]silole (2s)

The mobile phase for flash chromatography: hexane/ethyl acetate = 100:1. Yellow oil. (20.7 mg, 30%).

Optical rotation: $[\alpha]_D^{25}$ = +117.9 (c = 0.67, $CHCl_3$).

^{1}H NMR (400 MHz, $CDCl_3$) δ 7.80 (d, *J* = 7.0 Hz, 1H), 7.60 (s, 1H), 7.51 (d, *J* = 7.4 Hz, 1H), 7.42 – 7.37 (m, 1H), 7.22 (dddd, *J* = 20.7, 10.7, 6.3, 2.1 Hz, 5H), 7.14 – 7.00 (m, 5H), 6.96 – 6.92 (m, 1H), 6.86 – 6.80 (m, 1H), 6.73 (dd, *J* = 8.1, 2.0 Hz, 1H), 3.73 (s, 3H), 3.70 (s, 3H), 0.89 (s, 3H).

^{13}C NMR (100 MHz, $CDCl_3$) δ 160.0, 159.5, 149.1, 143.5, 142.9, 140.4, 137.7, 137.4, 135.8, 132.9, 132.8, 130.3, 129.9, 129.8, 129.6, 129.3, 128.0, 127.3, 124.7, 124.3, 124.2, 120.1, 116.5, 115.1, 113.0, 112.2, 92.3, 91.1, 55.4, 55.3, -3.5.

HRMS (ESI-TOF) m/z: $[M+Na]^+$ Calcd for $C_{31}H_{26}NaO_2Si$, 481.1594; found 481.1609.

HPLC: Enantiomeric excess was determined by HPLC with a Phenomenex column (hexanes: 2-propanol = 99.3:0.7, 0.7 mL/min, 330 nm, 97.2:2.8 *er*); major enantiomer t_r = 21.3 min, minor enantiomer t_r = 24.2 min.

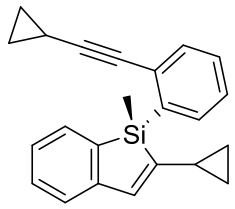

(*R*)-2-cyclopropyl-1-(2-(cyclopropylethynyl)phenyl)-1-methyl-1*H*-benzo[*b*]silole (2t)

The mobile phase for flash chromatography: hexane. Yellow oil. (44.4 mg, 68%).

Optical rotation: $[\alpha]_D^{25}$ = +77.8 (c = 1.33, $CHCl_3$).

^{1}H NMR (400 MHz, $CDCl_3$) δ 7.56 (d, *J* = 6.9 Hz, 1H), 7.46 (dd, *J* = 7.4, 0.8 Hz, 1H), 7.33 (d, *J* = 7.6 Hz, 1H), 7.19 (tdd, *J* = 8.1, 3.7, 1.6 Hz, 2H), 7.10 (td, *J* = 7.4, 1.1 Hz, 1H), 7.03 (t, *J* = 8.0 Hz, 2H), 6.86 (s, 1H), 1.82 – 1.69 (m, 1H), 1.35 (tt, *J* = 8.2, 5.1 Hz, 1H), 0.80 – 0.69 (m, 6H), 0.64 – 0.61 (m, 3H), 0.59 (dd, *J* = 8.9, 4.0 Hz, 1H), 0.50 – 0.44 (m, 1H).

^{13}C NMR (100 MHz, $CDCl_3$) δ 149.6, 148.7, 139.4, 136.1, 135.8, 134.2, 131.7, 131.5, 129.2, 129.1, 128.7, 126.0, 124.9, 122.1, 95.3, 13.5, 7.9, 7.3, 7.2, -0.5, -5.2.

HRMS (ESI-TOF) m/z: $[M+Na]^+$ Calcd for $C_{23}H_{22}NaSi$, 349.1383; found 349.1369.

HPLC: Enantiomeric excess was determined by HPLC with a Phenomenex column (hexanes: 2-propanol = 99.5:0.5, 0.6 mL/min, 330 nm, 93.2:6.8 *er*); major enantiomer t_r = 10.9 min, minor enantiomer t_r = 15.8 min.